DEVELOPMENT OF A TOOLBOX FOR DESIGN FLOOD ESTIMATION: ACCOUNTING FOR NON-STATIONARY DATA IN DESIGN RAINFALL ESTIMATION

KWAZULU-NATAL PILOT STUDY

WRC Project Number C2022/2023-00773

Final Report

KA Johnson, JC Smithers and DV Mukansi
With contributions by
RE Schulze, TR Kjeldsen, S Schütte and JA du Plessis

School of Engineering and Centre for Water Resources Research
College of Agriculture, Engineering and Science
University of KwaZulu-Natal
February 2024

PROJECT ABSTRACT

Most currently used methods for design flood estimation (DFE) in South Africa, required to design hydraulic structures, were developed over 50 years ago and need updating. Standard methods for frequency analysis of extreme events are based on the assumption of a stationary climate. However, this has been challenged due to evidence of a changing climate. This project focussed on the development of toolbox for estimating design rainfalls and floods under non-stationary conditions. The main aims were to investigate trends in rainfall and streamflow data and to investigate potential non-stationarity in the data. The East coast of KwaZulu-Natal was selected for this study based on data availability and accessibility. Results of a trend analysis of annual maximum daily rainfall from 39 observational stations in KwaZulu-Natal showed weak evidence that the annual maximum daily rainfalls have been increasing in magnitude over time. Several non-stationary models, using time and various climate drivers as covariates were developed, and compared to the standard stationary models. Most rainfall records indicate that a stationary behaviour is dominant. Changes in atmospheric CO_2 concentrations explain the largest proportion of changes in the rainfall data relative to other covariates considered in the study. The projected changes in rainfall were analysed using Global Circulation Models (GCMs) to derive possible climate change factors or ratios that could be applied to current design rainfall depths to design for future scenarios. Projected results from this project showed design rainfalls to remain relatively stable compared to present into the near future, with increases of approximately 10%. Projected changes into the distant future show a 10 – 30% increase in design rainfalls in many locations. Results of the trend analysis of the annual maximum streamflow from 19 stations in KwaZulu-Natal indicate that the annual maximum streamflow has been decreasing in magnitude and frequency at the majority of stations. Extreme value analysis was performed using both stationary and non-stationary models using time and rainfall as covariates. Similar to rainfall, the results for the study area show that the stationary models are superior to non-stationary models at most stations with time as a covariate, however, the non-stationary model incorporating observed rainfall as a covariate performed better than the stationary model as well as the non-stationary model with only time as a covariate. These results may differ elsewhere in the country, thus similar analyses in different climatic zones are recommended for further research.

EXECUTIVE SUMMARY

Introduction

Standard methods for frequency analysis of extreme rainfall and flood events assume a stationary climate, i.e., the statistics of the data do not change over time. However, the reported increase in the occurrence of extreme rainfalls leading to catastrophic flood events has raised the questions of whether changes in the magnitude and frequency of observed extreme rainfall events are already evident in South Africa, what the drivers of these changes are, and what the potential impacts on design rainfall estimation and consequently on flood risk assessment could be for in South Africa. Accurate estimations of design floods are required to limit the risk to loss of life and failure of, or over expenditure on, hydraulic structures. The needs to develop methods to account for non-stationary data, and to update design rainfall estimation methods to include possible trends in extreme rainfall events in a changing environment, have been identified as high priority research areas in the National Flood Studies Programme (NFSP) (Smithers *et al.*, 2016). The damage and loss of life caused by recent (2022) flooding across KwaZulu-Natal, and the realisation of possible increased rainfall variability in the future, highlight the fact that Design Flood Estimation (DFE) techniques currently used in South Africa are outdated and need revision.

The impact of a changing climate has become a key concern in South Africa, where temperatures shown a greater increase compared to observed global averages (Ziervogel *et al.*, 2014), and the highest recorded temperatures have been documented in recent years (Moyo and Nyoni, 2021). Generally, heavy rainfalls are related to warmer atmospheric conditions. McBride *et al.* (2022) noted that the probability of significant extreme daily rainfall events occurring has increased for most parts of South Africa. Many observations of global climate trends have raised an increasing concern that the extreme rainfalls, including the Probable Maximum Precipitation (PMP) needed for the design of high-hazard hydraulic infrastructure, will change as a result of the influence of a changing climate (Rouhani, 2016). Johnson and Smithers (2020) revised the 1-day PMPs in South Africa using an updated rainfall database and a modernized methodology and highlighted that many of the extreme events noted in their study occurred after the previously estimated PMPs were published in HRU (1972). Hence, it is critical to update PMP estimates currnetly used in industry, which were derived on the assumption of stationary data, and use this information to estimate the potential impacts of the changing climate on extreme rainfall estimation.

Internationally, numerous research institutions are investigating non-stationarity in flooding using modelled future climate data. With the increasing availability of climate model data through Global Circulation Models (GCMs), there is greater opportunity to use such data to determine the potential impacts of future climate scenarios on extreme rainfall and flood events using advanced statistical techniques, and to develop methods/tools to incorporate these trends in design rainfall and flood estimation.

Given the importance of flood risk management, the shortcomings of the methods currently used by practitioners for DFE and the potential impact of climate change, dealing with a non-stationary climate data series currently requires urgent attention in South Africa (Johnson *et al.*, 2021). A method to account for non-stationary data which incorporates the impacts of a changing climate in extreme design rainfall estimates in South Africa needs to be developed using regional approaches to detect trends in historical data.

Aims of the Project

Given the background provided above, the aims of this project are therefore to undertake the following for South Africa:

(a) To develop and assess the performance of a method to account for the impacts of non-stationary data on design rainfall estimation;
(b) To review and refine the updated 1-day PMP estimates;
(c) To develop and assess the performance of a method to account for the impacts of non-stationary data on PMP estimation; and
(d) To assess the trends in hydrological extremes using regional magnification factors.

Objectives (b) and (c) regarding the PMP were addressed through a report on the update of the 1-day PMP, which was submitted to WRC in February 2023, and a workshop on the use of the revised PMP tools, which was held at Stellenbosch University and online in May 2023.

The outputs of these two deliverables are accessible via the Water Research Observatory website, which is a cloud-based data portal belonging to the Water Research Commission. This final report focusses on assessing trends in hydrological extremes and evaluating the potential impacts of non-stationary data on design rainfall estimation in KwaZulu-Natal (KZN).

Aim (a): Non-stationary Frequency Analysis of Extreme Rainfall Events on the East Coast of KwaZulu-Natal

Extreme flood events can damage hydrological structures such as dam walls, spillways, bridges, and culverts. Therefore, minimising the risk of failure of hydraulic structures requires design floods be estimated accurately. The underestimation of design floods and failure of hydraulic structures can lead to loss of life and significant economic losses, while overestimation may result in over-design which results in excessive construction and maintenance costs. Recent large floods include the events in 2019 and 2022 experienced along the eastern coast of South Africa and have been reported to have resulted in infrastructural damages of billions of Rands, with thousands of people affected (Singh, 2019; Pinto *et al*; 2022).

Traditional methods for frequency analysis of extreme events and most current risk assessment models are based on techniques and concepts developed nearly a century ago (e.g. Fuller, 1914) and are based on the assumption of climate stationarity. However, anthropogenically induced climate change has resulted in changes in extreme weather events, thus questioning the assumption of stationarity (e.g. Vasiliades *et al.*, 2015; Zhou *et al.*, 2016; Demaria *et al.*, 2017; Tan and Gan, 2017; Gao and Zheng, 2018; Ragno *et al.*, 2019a; Ouarda *et al.*, 2020; Song *et al.*, 2020; Hesarkazzazi *et al.*, 2021; Silva *et al.*, 2021). In recent years, the frequency and impacts of extremes have increased substantially in many parts of South Africa (Thoithi *et al.*, 2023). Hence, there is significant interest in understanding how extreme events may change into the future and how frequency analyses should be adapted to account for non-stationary data.

Aim (a) of the study, undertaken as a pilot study on the the East Coast of KwaZulu-Natal, is to determine if any trends exist in observed extreme rainfall events in order to contribute to an understanding of the teleconnection patterns between various climate drivers and the annual maximum daily extreme rainfall and to account for possible non-stationary climate data in the estimation of extreme design rainfall events in South Africa. The objectives of this component of the study were to: (i) investigate trends in annual maximum daily rainfall using parametric and non-parametric statistical tests, (ii) identify potential climate drivers of extreme rainfalls, (iii) perform stationary and non-stationary rainfall frequency analyses, (iv) critically evaluate the stationary vs non-stationary models, and (v) evaluate projected changes in rainfall using GCMs.

In terms of rainfall data analyses undertaken in this study, the annual maximum daily rainfall from 39 observational stations in KwaZulu-Natal, located along the east coast of South Africa, were analysed. The existence of temporal trends in the data series were investigated using non-parametric tests. The results indicate weak evidence that the annual maximum daily rainfalls have been increasing in magnitude over time. The trends detected varied across the sites, with approximately 40 % of sites showing a positive trend, only one of which showed a statistically significant increasing trend. Non-stationary extreme value statistical analysis was used to explore the utility of rainfall relationships in KZN with various potential climate drivers to predict possible future impacts on extreme rainfall. Several non-stationary models, using time and various climate drivers as covariates (Southern Oscillation Index, Dipole Mode Index, CO_2 and Global Mean Temperature), were developed, and compared to the standard stationary models. Most rainfall records indicate that a stationary behaviour is dominant. The variability of the results of the trend and non-stationary analyses highlights the importance of understanding the trends and drivers of extreme rainfalls and the impacts on design rainfall and design flood estimation. To improve the study, the use of other physical covariates, as well as combinations of covariates, should be explored.

Changes in atmospheric CO_2 explain the largest proportion of variability in the rainfall data relative to other covariates considered in the study. The projected changes in rainfall were analysed using Global Circulation Models (GCMs) to derive possible climate change factors, or ratios, that could be applied to current design rainfall depths to design for future scenarios. The ratios of changes from the present to the near future climate periods, and from the present to the distant future climate periods for design rainfall were derived. Design rainfalls are projected to remain stable into the near future compared to the present, with increases of approximately 10%, and ratios increasing with an increase in return period. Projected changes into the distant future show a 10 – 30% increase in design rainfalls in many locations in the study area. These results could vary elsewhere in the country. It is recpommended that the use of projected trends in rainfalls from GCMs should be informed by the considerations based on the observed rainfall data trends.

Aim (d): Detecting Trends in Hydrological Extremes and Non-Stationary Extreme Value Analysis of Flood Data in KwaZulu-Natal

As with rainfall analysis, the current methods and models used to determine design flood estimates from flow data assume that hydrological processes and upstream land uses as well as river and dam abstractions remain stationary (Vogel *et al.*, 2011). However, the magnitude and frequency of extreme flood events is changing in many parts of the world (Vogel *et al.*, 2011; Prosdocimi *et al.*, 2014a; Hesarkazzazi *et al.*, 2021). Therefore, there is a need to investigate, and incorporate if necessary, non-stationary models in DFE in South Africa.

This section includes an analysis of trends in extreme floods along the East Coast of KwaZulu-Natal in South Africa. This study site was selected to complement and correspond to the rainfall analyses. The aims of this component of the study were to determine if any trends exist in observed extreme flood events on the East Coast of KwaZulu-Natal, and to evaluate the possible non-stationarity in observed flow data. The objectives were to: (i) collect, screen, and analyse streamflow data for trends, (ii) perform stationary and non-stationary flood frequency analyses, (iii) critically evaluate the stationary vs non-stationary models, and (iv) investigate regional magnification factors to detect trends.

The annual maximum streamflows from 19 stations in KwaZulu-Natal, along the East Coast of South Africa, were analysed. Non-parametric trends were investigated, and the results indicate that the annual maximum streamflow has been decreasing in magnitude and frequency in the majority of stations. Extreme value analysis was performed using both stationary and non-stationary models using time and rainfall as covariates. Similar to rainfall, the results show that the stationary models are superior to non-stationary models at most stations with time as a covariate. Where possible, streamflow stations were linked with rainfall stations to determine the impact of rainfall on annual maximum streamflow. The results indicate that the non-stationary model incorporating observed rainfall as a covariate performed better than the stationary model as well as the non-stationary model with only time as a covariate. Therefore, incorporation of rainfall in DFE should be considered to account for non-stationary trends and to mitigate the risk of failure of hydraulic structures. Regional magnification factors to account for non-stationarity were thus not investigated further in this study as the majority of the stations showed a negative trend, which means application of a regional magnification factor would result in a reduction of the magnitude of the estimated design floods.

Conclusions

The outcomes presented in this report are sometimes contrary to the outputs from GCMs reported in international studies and to reported increases in extreme events in South Africa. These results may differ elsewhere in the country and this study has highlighted the need to investigate trends and non-stationarity in other parts of the country located in different climate zones and with up-to-date datasets. Further analysis of data for various event durations (e.g. sub-daily or multi-day events) are recommended. Given the generally weak positive trends in rainfall data and negative trends in the annual maximum flow data, alternative more detailed analysis methods, such as the peak over threshold approach, are recommended for future research.

Capacity Building Report

This project has contributed to the support for two postgraduate students. Of these, one student has submitted a PhD thesis for examination, and one student has made progress towards his PhD research. In addition, the project leader is an early career researcher who has gained experience leading this project. This research has been shared at local and international conferences and has been presented at the annual NFSP workshops, attended by practitioners, stakeholders, and researchers.

ACKNOWLEDGEMENTS

The funding of the project by the Water Research Commission and the contribution of the members of the Reference Group members is acknowledged gratefully.

Mr W Nomquphu	Water Research Commission
Mr CJ Brooker	CBA Consulting
Mr E Oakes	DWS
Dr OJ Gericke	CUT
Prof J Ndiritu	University of Witwatersrand
Prof SJ Van Vuuren	University of Stellenbosch
Dr P Wolski	UCT
Dr R Odoulami	UCT
Dr B Abiodun	UCT
Mr M Parak	SANRAL
Mr A Trollip	Anglo American
Prof B Hewitson	UCT
Prof A Gorgens	Zutari

TABLE OF CONTENTS

Page

PROJECT ABSTRACT ii

EXECUTIVE SUMMARY iii

ACKNOWLEDGEMENTS ix

TABLE OF CONTENTS x

LIST OF TABLES xii

LIST OF FIGURES xiii

1. INTRODUCTION 29

2. NON-STATIONARY FREQUENCY ANALYSIS OF EXTREME RAINFALL EVENTS ON THE EAST COAST OF KWAZULU-NATAL 34

 2.1 Introduction 34

 2.2 Materials and Methods 36

  2.2.1 Data sources and case study site selection 36

  2.2.2 Methodology 39

 2.3 Results and Discussion 44

  2.3.1 Trend detection 44

  2.3.2 Analysis of stationary and non-stationary models 47

  2.3.3 Projected changes in rainfall 53

 2.4 Conclusions 56

3. DETECTING TRENDS IN HYDROLOGICAL EXTREMES AND NON-STATIONARY EXTREME VALUE ANALYSIS OF FLOOD DATA IN KWAZULU-NATAL 59

3.1 Introduction 59

3.2 Materials and Methods 60

3.2.1 Data sources and case study site selection 60

3.2.3 Methodology 63

3.3 Results and Discussion 68

3.3.1 Homogeneity test 68

3.3.2 Trend detection 69

3.3.3 Analysis of stationary and non-stationary models 70

3.3.4 Linking rainfall to flow 74

3.4 Conclusions 79

4. DISCUSSIONS, CONCLUSIONS AND RECOMMENDATIONS 81

5. CAPACITY BUILDING 84

6. REFERENCES 85

7. APPENDIX A: Non-stationary Frequency Analysis of Extreme Rainfalls in KwaZulu-Natal 92

8. APPENDIX B: Non-stationary Frequency Analysis of Extreme Floods in KwaZulu-Natal 160

LIST OF TABLES

Page

Table 2.1 Station information for case study sites 38

Table 2.2 Trends in KwaZulu-Natal extreme rainfall using the Mann-Kendall test 46

Table 2.3 The GEV statistical model performance criteria of selected sites in KwaZulu-Natal AMDR for time as a covariate 47

Table 2.4 Summary of best-fit models for all stationary and non-stationary cases 51

Table 3.1 Station information for case study sites along the East Coast of KwaZulu-Natal 62

Table 3.2 Summary of studies that made use of non-stationary models in design flood estimation (after Prosdocimi and Kjeldsen (2021) 67

Table 3.3 Homogenity test of DWS stations in the East Coast of KwaZulu-Natal 68

Table 3.4 Trends in annaul maximum streamflows at stations along the East Coast of KwaZulu-Natal using the Mann-Kendall test 69

Table 3.5 The LP3 statistical model selection criteria of selected sites in the East Coast of KwaZulu-Natal AMS for time as a covariate 70

Table 3.6 Summary of best-fit models for all stationary and non-stationary cases 75

Table 5.1: List of students involved in the project..84

Table 7.1 The GEV statistical model performance criteria of KwaZulu-Natal AMDR for all covariates 98

Table 8.1 The LP3 statistical model performance criteria for all covariates 177

LIST OF FIGURES

Page

Figure 2.1 SASRI stations in KwaZulu-Natal selected for this study 37

Figure 2.2 Stationary and non-stationary design rainfall estimation procedures 40

Figure 2.3 Time series for Station 38 45

Figure 2.4 The GEV (a) stationary model, (b) non-stationary model considering time as a covariate, and (c) effective return period as a function of time for Station 38: Sezela - Illovo Sugar Estate 50

Figure 2.5 Best-fit distribution model, based on the AIC measure 52

Figure 2.6 Best-fit distribution model, based on the BIC measure 52

Figure 2.7 Projected changes from the present to the near future in design rainfalls for 1-day design rainfalls for the 2-, 10-, 50-, and 100-year return periods, derived from outputs from multiple GCMs 55

Figure 2.8 Projected changes from the present to the distant future in design rainfalls for 1-day design rainfalls for the 2-, 10-, 50-, and 100-year return period, derived from outputs from multiple GCMs 56

Figure 3.1 Selected DWS streamflow recording stations along the East Coast of KwaZulu-Natal 62

Figure 3.2 Stationary and non-stationary design flood estimation procedures 64

Figure 3.3 The LP3 (a) stationary model, (b) non-stationary model considering time as a covariate, and (c) effective return period as a function of time for Station W4H012 72

Figure 3.4 Best-fit distribution model, based on the AIC measure 73

Figure 3.5 Best-fit distribution model, based on the BIC measure 73

Figure 3.6 Time series for annual maximum streamflow and rainfall stations in the East Coast of KwaZulu-Natal 77

Figure 3.7 Best-fit distribution model, based on the AIC measure for flow stations linked with a rainfall station 78

Figure 3.8 Best-fit distribution model, based on the BIC measure for flow stations linked with a rainfall station 78

Figure 7.1 Time series of all annual maximum rainfalls at all SASRI stations used in this research 97

Figure 7.2 The GEV (a) stationary model, (b) non-stationary model considering time as a covariate, (c) non-stationary model considering SOI as a covariate, (d) non-stationary model considering DMI as a covariate, (e) non-stationary model considering CO_2 as a covariate, (f) non-stationary model considering GMT as a covariate and (g) effective return period as a function of time for Station 6: Pongola – SASRI 100

Figure 7.3 The GEV (a) stationary model, (b) non-stationary model considering time as a covariate, (c) non-stationary model considering SOI as a covariate, (d) non-stationary model considering DMI as a covariate, (e) non-stationary model considering CO_2 as a covariate, (f) non-stationary model considering GMT as a covariate and (g) effective return period as a function of time for Station 8: Glen Park – St Lucia Farms 101

Figure 7.4 The GEV (a) stationary model, (b) non-stationary model considering time as a covariate, (c) non-stationary model considering SOI as a covariate, (d) non-stationary model considering DMI as a covariate, (e) non-stationary model considering CO_2 as a covariate, (f) non-stationary model considering GMT as a covariate and (g) effective return period as a function of time for Station 9: Mtubatuba – Riverview Sugar Mill 102

Figure 7.5 The GEV (a) stationary model, (b) non-stationary model considering time as a covariate, (c) non-stationary model considering SOI as a covariate, (d) non-stationary model considering DMI as a covariate, (e) non-stationary model considering CO_2 as a covariate, (f) non-stationary model considering GMT as a covariate and (g) effective return period as a function of time for Station 11: Mtunzini – ex SASRI 103

Figure 7.6 The GEV (a) stationary model, (b) non-stationary model considering time as a covariate, (c) non-stationary model considering SOI as a covariate, (d) non-stationary model considering DMI as a covariate, (e) non-stationary model considering CO_2 as a covariate, (f) non-stationary model considering GMT as a covariate and (g) effective return period as a function of time for Station 12: Melmoth – CA Leith & Sons 104

Figure 7.7 The GEV (a) stationary model, (b) non-stationary model considering time as a covariate, (c) non-stationary model considering SOI as a covariate, (d) non-stationary model considering DMI as a covariate, (e) non-stationary model considering CO_2 as a covariate, (f) non-stationary model considering GMT as a covariate and (g) effective return period as a function of time for Station 18: Glendale – Tenrith Farm 105

Figure 7.8 The GEV (a) stationary model, (b) non-stationary model considering time as a covariate, (c) non-stationary model considering SOI as a covariate, (d) non-stationary model considering DMI as a covariate, (e) non-stationary model considering CO_2 as a covariate, (f) non-stationary model considering GMT as a covariate and (g) effective return period as a function of time for Station 20: Tongaat – Klipfontein (THS) 106

Figure 7.9 The GEV (a) stationary model, (b) non-stationary model considering time as a covariate, (c) non-stationary model considering SOI as a covariate, (d) non-stationary model considering DMI as a covariate, (e) non-stationary model considering CO_2 as a covariate, (f) non-stationary model considering GMT as a covariate and (g) effective return period as a function of time for Station 22: Seven Oaks – Saw Mill 107

Figure 7.10 The GEV (a) stationary model, (b) non-stationary model considering time as a covariate, (c) non-stationary model considering SOI as a covariate, (d) non-stationary model considering DMI as a covariate, (e) non-stationary model considering CO_2 as a covariate, (f) non-stationary model considering GMT as a covariate and (g) effective return period as a function of time for Station 23: Noodsberg – Illovo Sugar Mill 108

Figure 7.11 The GEV (a) stationary model, (b) non-stationary model considering time as a covariate, (c) non-stationary model considering SOI as a covariate, (d) non-stationary model considering DMI as a covariate, (e) non-stationary model considering CO_2 as a covariate, (f) non-stationary model considering GMT as a covariate and (g) effective return period as a function of time for Station 26: Illovo – Sugar Estate 109

Figure 7.12 The GEV (a) stationary model, (b) non-stationary model considering time as a covariate, (c) non-stationary model considering SOI as a covariate, (d) non-stationary model considering DMI as a covariate, (e) non-stationary model considering CO_2 as a covariate, (f) non-stationary model considering GMT as a covariate and (g) effective return period as a function of time for Station 27: Vulamehlo – Esperanza 110

Figure 7.13 The GEV (a) stationary model, (b) non-stationary model considering time as a covariate, (c) non-stationary model considering SOI as a covariate, (d) non-stationary model considering DMI as a covariate, (e) non-stationary model considering CO_2 as a covariate, (f) non-stationary model considering GMT as a covariate and (g) effective return period as a function of time for Station 29: Mt Edgecombe – SASRI 111

Figure 7.14 The GEV (a) stationary model, (b) non-stationary model considering time as a covariate, (c) non-stationary model considering SOI as a covariate, (d) non-stationary model considering DMI as a covariate, (e) non-stationary model considering CO_2 as a covariate, (f) non-stationary model considering GMT as a covariate and (g) effective return period as a function of time for Station 38: Sezela – Illovo Sugar Estate 112

Figure 7.15 The GEV (a) stationary model, (b) non-stationary model considering time as a covariate, (c) non-stationary model considering SOI as a covariate, (d) non-stationary model considering DMI as a covariate, (e) non-stationary model considering CO_2 as a covariate, (f) non-stationary model considering GMT as a covariate and (g) effective return period as a function of time for Station 105: Oribi Flats – Minnehaha Farm 113

Figure 7.16 The GEV (a) stationary model, (b) non-stationary model considering time as a covariate, (c) non-stationary model considering SOI as a covariate, (d) non-stationary model considering DMI as a covariate, (e) non-stationary model considering CO_2 as a covariate, (f) non-stationary model considering GMT as a covariate and (g) effective return period as a function of time for Station 110: Renishaw – Crooks Bros Estate 114

Figure 7.17 The GEV (a) stationary model, (b) non-stationary model considering time as a covariate, (c) non-stationary model considering SOI as a covariate, (d) non-stationary model considering DMI as a covariate, (e) non-stationary model considering CO_2 as a covariate, (f) non-stationary model considering GMT as a covariate and (g) effective return period as a function of time for Station 111: Powerscourt – Roseleigh Estate 115

Figure 7.18 The GEV (a) stationary model, (b) non-stationary model considering time as a covariate, (c) non-stationary model considering SOI as a covariate, (d) non-stationary model considering DMI as a covariate, (e) non-stationary model considering CO_2 as a covariate, (f) non-stationary model considering GMT as a covariate and (g) effective return period as a function of time for Station 114: Inanda – Farm 116

Figure 7.19 The GEV (a) stationary model, (b) non-stationary model considering time as a covariate, (c) non-stationary model considering SOI as a covariate, (d) non-stationary model considering DMI as a covariate, (e) non-stationary model considering CO_2 as a covariate, (f) non-stationary model considering GMT as a covariate and (g) effective return period as a function of time for Station 120: Inyaninga – THS 117

Figure 7.20 The GEV (a) stationary model, (b) non-stationary model considering time as a covariate, (c) non-stationary model considering SOI as a covariate, (d) non-stationary model considering DMI as a covariate, (e) non-stationary model considering CO_2 as a covariate, (f) non-stationary model considering GMT as a covariate and (g) effective return period as a function of time for Station 123: Maidstone – Sugar Mill (THS) 118

Figure 7.21 The GEV (a) stationary model, (b) non-stationary model considering time as a covariate, (c) non-stationary model considering SOI as a covariate, (d) non-stationary model considering DMI as a covariate, (e) non-stationary model considering CO_2 as a covariate, (f) non-stationary model considering GMT as a covariate and (g) effective return period as a function of time for Station 125: Sinembe – Spreyton Farm...119

Figure 7.22 The GEV (a) stationary model, (b) non-stationary model considering time as a covariate, (c) non-stationary model considering SOI as a covariate, (d) non-stationary model considering DMI as a covariate, (e) non-stationary model considering CO_2 as a covariate, (f) non-stationary model considering GMT as a covariate and (g) effective return period as a function of time for Station 126: Upper Tongaat – Barwon Farm 120

Figure 7.23 The GEV (a) stationary model, (b) non-stationary model considering time as a covariate, (c) non-stationary model considering SOI as a covariate, (d) non-stationary model considering DMI as a covariate, (e) non-stationary model considering CO_2 as a covariate, (f) non-stationary model considering GMT as a covariate and (g) effective return period as a function of time for Station 129: Kearsney – Ocean Lodge 121

Figure 7.24 The GEV (a) stationary model, (b) non-stationary model considering time as a covariate, (c) non-stationary model considering SOI as a covariate, (d) non-stationary model considering DMI as a covariate, (e) non-stationary model considering CO_2 as a covariate, (f) non-stationary model considering GMT as a covariate and (g) effective return period as a function of time for Station 130: Doornkop – Langespruit Farm...122

Figure 7.25 The GEV (a) stationary model, (b) non-stationary model considering time as a covariate, (c) non-stationary model considering SOI as a covariate, (d) non-stationary model considering DMI as a covariate, (e) non-stationary model considering CO_2 as a covariate, (f) non-stationary model considering GMT as a covariate and (g) effective return period as a function of time for Station 131: Darnall – Sugar Mill (THS) 123

Figure 7.26 The GEV (a) stationary model, (b) non-stationary model considering time as a covariate, (c) non-stationary model considering SOI as a covariate, (d) non-stationary model considering DMI as a covariate, (e) non-stationary model considering CO_2 as a covariate, (f) non-stationary model considering GMT as a covariate and (g) effective return period as a function of time for Station 132: Tugela Mouth – Wetherly Estate 124

Figure 7.27 The GEV (a) stationary model, (b) non-stationary model considering time as a covariate, (c) non-stationary model considering SOI as a covariate, (d) non-stationary model considering DMI as a covariate, (e) non-stationary model considering CO_2 as a covariate, (f) non-stationary model considering GMT as a covariate and (g) effective return period as a function of time for Station 136: Glenside – Misty Krantz Estate 125

Figure 7.28 The GEV (a) stationary model, (b) non-stationary model considering time as a covariate, (c) non-stationary model considering SOI as a covariate, (d) non-stationary model considering DMI as a covariate, (e) non-stationary model considering CO_2 as a covariate, (f) non-stationary model considering GMT as a covariate and (g) effective return period as a function of time for Station 138: Mandini – SAWS 126

Figure 7.29 The GEV (a) stationary model, (b) non-stationary model considering time as a covariate, (c) non-stationary model considering SOI as a covariate, (d) non-stationary model considering DMI as a covariate, (e) non-stationary model considering CO_2 as a covariate, (f) non-stationary model considering GMT as a covariate and (g) effective return period as a function of time for Station 139: Inyoni – Myrln Estate 127

Figure 7.30 The GEV (a) stationary model, (b) non-stationary model considering time as a covariate, (c) non-stationary model considering SOI as a covariate, (d) non-stationary model considering DMI as a covariate, (e) non-stationary model considering CO_2 as a covariate, (f) non-stationary model considering GMT as a covariate and (g) effective return period as a function of time for Station 142: Eshowe – Brocklee Farm 128

Figure 7.31 The GEV (a) stationary model, (b) non-stationary model considering time as a covariate, (c) non-stationary model considering SOI as a covariate, (d) non-stationary model considering DMI as a covariate, (e) non-stationary model considering CO_2 as a covariate, (f) non-stationary model considering GMT as a covariate and (g) effective return period as a function of time for Station 143: Nkwaleni – Zigagazi 129

Figure 7.32 The GEV (a) stationary model, (b) non-stationary model considering time as a covariate, (c) non-stationary model considering SOI as a covariate, (d) non-stationary model considering DMI as a covariate, (e) non-stationary model considering CO_2 as a covariate, (f) non-stationary model considering GMT as a covariate and (g) effective return period as a function of time for Station 144: Felixton – Sugar Mill (THS) 130

Figure 7.33 The GEV (a) stationary model, (b) non-stationary model considering time as a covariate, (c) non-stationary model considering SOI as a covariate, (d) non-stationary model considering DMI as a covariate, (e) non-stationary model considering CO_2 as a covariate, (f) non-stationary model considering GMT as a covariate and (g) effective return period as a function of time for Station 146: Kulu Halt – Honey Farm 131

Figure 7.34 The GEV (a) stationary model, (b) non-stationary model considering time as a covariate, (c) non-stationary model considering SOI as a covariate, (d) non-stationary model considering DMI as a covariate, (e) non-stationary model considering CO_2 as a covariate, (f) non-stationary model considering GMT as a covariate and (g) effective return period as a function of time for Station 147: Ukulu Properties – Crystal Holdings 132

Figure 7.35 The GEV (a) stationary model, (b) non-stationary model considering time as a covariate, (c) non-stationary model considering SOI as a covariate, (d) non-stationary model considering DMI as a covariate, (e) non-stationary model considering CO_2 as a covariate, (f) non-stationary model considering GMT as a covariate and (g) effective return period as a function of time for Station 148: Mposa – Redcroft Farm 133

Figure 7.36 The GEV (a) stationary model, (b) non-stationary model considering time as a covariate, (c) non-stationary model considering SOI as a covariate, (d) non-stationary model considering DMI as a covariate, (e) non-stationary model considering CO_2 as a covariate, (f) non-stationary model considering GMT as a covariate and (g) effective return period as a function of time for Station 149: Kwambonambi – Mondi Forestry....... 134

Figure 7.37 The GEV (a) stationary model, (b) non-stationary model considering time as a covariate, (c) non-stationary model considering SOI as a covariate, (d) non-stationary model considering DMI as a covariate, (e) non-stationary model considering CO_2 as a covariate, (f) non-stationary model considering GMT as a covariate and (g) effective return period as a function of time for Station 151: ULOA – Mark & Ross Sugar Estate....... 135

Figure 7.38 The GEV (a) stationary model, (b) non-stationary model considering time as a covariate, (c) non-stationary model considering SOI as a covariate, (d) non-stationary model considering DMI as a covariate, (e) non-stationary model considering CO_2 as a covariate, (f) non-stationary model considering GMT as a covariate and (g) effective return period as a function of time for Station 152: Mtubatuba – Nyalazi River....... 136

Figure 7.39 The GEV (a) stationary model, (b) non-stationary model considering time as a covariate, (c) non-stationary model considering SOI as a covariate, (d) non-stationary model considering DMI as a covariate, (e) non-stationary model considering CO_2 as a covariate, (f) non-stationary model considering GMT as a covariate and (g) effective return period as a function of time for Station 154: Mkuze – Mkuze Estate....... 137

Figure 7.40 The GEV (a) stationary model, (b) non-stationary model considering time as a covariate, (c) non-stationary model considering SOI as a covariate, (d) non-stationary model considering DMI as a covariate, (e) non-stationary model considering CO_2 as a covariate, (f) non-stationary model considering GMT as a covariate and (g) effective return period as a function of time for Station 155: Pongola – Impala Irrigation Board 138

Figure 7.41 Time series of annual maximum rainfall for SASRI station 6 and 6 GCMs for corresponding years 139

Figure 7.42 Time series of annual maximum rainfall for SASRI station 8 and 6 GCMs for corresponding years 139

Figure 7.43 Time series of annual maximum rainfall for SASRI station 9 and 6 GCMs for corresponding years 139

Figure 7.44 Time series of annual maximum rainfall for SASRI station 11 and 6 GCMs for corresponding years 140

Figure 7.45 Time series of annual maximum rainfall for SASRI station 12 and 6 GCMs for corresponding years 140

Figure 7.46 Time series of annual maximum rainfall for SASRI station 18 and 6 GCMs for corresponding years 140

Figure 7.47 Time series of annual maximum rainfall for SASRI station 20 and 6 GCMs for corresponding years 141

Figure 7.48 Time series of annual maximum rainfall for SASRI station 22 and 6 GCMs for corresponding years 141

Figure 7.49 Time series of annual maximum rainfall for SASRI station 23 and 6 GCMs for corresponding years 141

Figure 7.50 Time series of annual maximum rainfall for SASRI station 26 and 6 GCMs for corresponding years 142

Figure 7.51 Time series of annual maximum rainfall for SASRI station 27 and 6 GCMs for corresponding years......142

Figure 7.52 Time series of annual maximum rainfall for SASRI station 29 and 6 GCMs for corresponding years......142

Figure 7.53 Time series of annual maximum rainfall for SASRI station 38 and 6 GCMs for corresponding years......143

Figure 7.54 Time series of annual maximum rainfall for SASRI station 105 and 6 GCMs for corresponding years......143

Figure 7.55 Time series of annual maximum rainfall for SASRI station 110 and 6 GCMs for corresponding years......143

Figure 7.56 Time series of annual maximum rainfall for SASRI station 111 and 6 GCMs for corresponding years......144

Figure 7.57 Time series of annual maximum rainfall for SASRI station 114 and 6 GCMs for corresponding years......144

Figure 7.58 Time series of annual maximum rainfall for SASRI station 120 and 6 GCMs for corresponding years......144

Figure 7.59 Time series of annual maximum rainfall for SASRI station 123 and 6 GCMs for corresponding years......145

Figure 7.60 Time series of annual maximum rainfall for SASRI station 125 and 6 GCMs for corresponding years......145

Figure 7.61 Time series of annual maximum rainfall for SASRI station 126 and 6 GCMs for corresponding years......145

Figure 7.62 Time series of annual maximum rainfall for SASRI station 129 and 6 GCMs for corresponding years......146

Figure 7.63 Time series of annual maximum rainfall for SASRI station 130 and 6 GCMs for corresponding years......146

Figure 7.64 Time series of annual maximum rainfall for SASRI station 131 and 6 GCMs for corresponding years......146

Figure 7.65 Time series of annual maximum rainfall for SASRI station 132 and 6 GCMs for corresponding years......147

Figure 7.66 Time series of annual maximum rainfall for SASRI station 136 and 6 GCMs for corresponding years......147

Figure 7.67 Time series of annual maximum rainfall for SASRI station 138 and 6 GCMs for corresponding years......147

Figure 7.68 Time series of annual maximum rainfall for SASRI station 139 and 6 GCMs for corresponding years......148

Figure 7.69 Time series of annual maximum rainfall for SASRI station 142 and 6 GCMs for corresponding years......148

Figure 7.70 Time series of annual maximum rainfall for SASRI station 143 and 6 GCMs for corresponding years......148

Figure 7.71 Time series of annual maximum rainfall for SASRI station 146 and 6 GCMs for corresponding years......149

Figure 7.72 Time series of annual maximum rainfall for SASRI station 144 and 6 GCMs for corresponding years......149

Figure 7.73 Time series of annual maximum rainfall for SASRI station 147 and 6 GCMs for corresponding years......149

Figure 7.74 Time series of annual maximum rainfall for SASRI station 148 and 6 GCMs for corresponding years......150

Figure 7.75 Time series of annual maximum rainfall for SASRI station 149 and 6 GCMs for corresponding years....150

Figure 7.76 Time series of annual maximum rainfall for SASRI station 151 and 6 GCMs for corresponding years....150

Figure 7.77 Time series of annual maximum rainfall for SASRI station 152 and 6 GCMs for corresponding years....151

Figure 7.78 Time series of annual maximum rainfall for SASRI station 154 and 6 GCMs for corresponding years....151

Figure 7.79 Time series of annual maximum rainfall for SASRI station 155 and 6 GCMs for corresponding years....151

Figure 7.80 Projected changes from the present to the near future in design rainfalls for the 1-day 2-year Return Period derived from outputs from multiple GCMs......152

Figure 7.81 Projected changes from the present to the distant future in design rainfalls for the 1-day 2-year Return Period derived from outputs from multiple GCMs......153

Figure 7.82 Projected changes from the present to the near future in design rainfalls for the 1-day 10-year Return Period derived from outputs from multiple GCMs....154

Figure 7.83 Projected changes from the present to the distant future in design rainfalls for the 1-day 10-year Return Period derived from outputs from multiple GCMs....155

Figure 7.84 Projected changes from the present to the near future in design rainfalls for the 1-day 50-year Return Period derived from outputs from multiple GCMs....156

Figure 7.85 Projected changes from the present to the distant future in design rainfalls for the 1-day 50-year Return Period derived from outputs from multiple GCMs....157

Figure 7.86 Projected changes from the present to the near future in design rainfalls for the 1-day 100-year Return Period derived from outputs from multiple GCMs 158

Figure 7.87 Projected changes from the present to the distant future in design rainfalls for the 1-day 100-year Return Period derived from outputs from multiple GCMs 159

Figure 8.1 Time series of annual streamflows at stations along the East Coast of KwaZulu-Natal.......162

Figure 8.2 The LP3 (a) stationary model, (b) non-stationary model considering time as a covariate, and (c) effective return period as a function of time for Station: T5H012 163

Figure 8.3 LP3 (a) stationary model, (b) non-stationary model considering time as a covariate, and (c) effective return period as a function of time for Station: U2H001.......164

Figure 8.4 LP3 (a) stationary model, (b) non-stationary model considering time as a covariate, and (c) effective return period as a function of time for Station: U2H006.......165

Figure 8.5 LP3 (a) stationary model, (b) non-stationary model considering time as a covariate, and (c) effective return period as a function of time for Station: U2H048.......166

Figure 8.6 LP3 (a) stationary model, (b) non-stationary model considering time as a covariate, (c) non-stationary model considering rainfall as a covariate, and (d) effective return period as a function of time for Station:U3H001 167

Figure 8.7 LP3 (a) stationary model, (b) non-stationary model considering time as a covariate, (c) non-stationary model considering rainfall as a covariate, and (d) effective return period as a function of time for Station:U3H005 168

Figure 8.8 LP3 (a) stationary model, (b) non-stationary model considering time as a covariate, and (c) effective return period as a function of time for Station: U4H002.......169

Figure 8.9 LP3 (a) stationary model, (b) non-stationary model considering time as a covariate, and (c) effective return period as a function of time for Station: U6H003 170

Figure 8.10 LP3 (a) stationary model, (b) non-stationary model considering time as a covariate, (c) non-stationary model considering rainfall as a covariate, and (d) effective return period as a function of time for Station:V5H002 171

Figure 8.11 LP3 (a) stationary model, (b) non-stationary model considering time as a covariate, and (c) effective return period as a function of time for Station: W1H004 172

Figure 8.12 LP3 (a) stationary model, (b) non-stationary model considering time as a covariate, (c) non-stationary model considering rainfall as a covariate, and (d) effective return period as a function of time for Station:W1H009 173

Figure 8.13 LP3 (a) stationary model, (b) non-stationary model considering time as a covariate, and (c) effective return period as a function of time for Station: W2H005 174

Figure 8.14 LP3 (a) stationary model, (b) non-stationary model considering time as a covariate, and (c) effective return period as a function of time for Station: W3H022 175

Figure 8.15 LP3 (a) stationary model, (b) non-stationary model considering time as a covariate, (c) non-stationary model considering rainfall as a covariate, and (d) effective return period as a function of time for Station:W4H012 176

1. INTRODUCTION

Estimates of extreme design rainfall are needed routinely for Design Flood Estimation (DFE) to design and assess the flood risk of hydraulic structures such as dam spillways, culverts and stormwater drains. Standard methods for frequency analysis of extreme events are based on the assumption of a stationary climate (Prosdocimi *et al.*, 2014b), i.e. that the long-term attributes of climate do not change over time. However, it is postulated that anthropogenically induced climate change has resulted in changes in extreme weather events, thus questioning the assumption of stationarity (Serinaldi and Kilsby, 2015). As a consequence of a projected changing climate, the frequency and magnitude of extreme rainfall events is expected to increase in the future (Bates *et al.*, 2008), thus further exacerbating flood risk exposure of already vulnerable communities and hydraulic infrastructure. The possible non-stationarity in climate is projected to result in changes in rainfall and runoff characteristics, with potential impacts on the accuracy of current estimates of design rainfall and on the estimation of extreme rainfall quantities such as the Probable Maximum Precipitation (PMP). This may have significant consequences for the flood risk profiles of existing hydraulic infrastructure and on the design of new hydraulic infrastructure, and consequently also for the South African economy (Cullis *et al.*, 2015). It is therefore essential to account for possible trends and associated uncertainties associated with non-stationary climate data in the analysis of extreme rainfall events (Yilmaz *et al.*, 2014) in support of more reliable design of critical infrastructure and credible flood management interventions.

The damage and loss of life caused by recent (2022) flooding across the East Coast regions of KwaZulu-Natal, and the realisation of possible increased rainfall variability in the future, highlight the fact that DFE techniques currently used South Africa are outdated and need revision. As a consequence, a National Flood Studies Programme (NFSP) has been initiated to overhaul and modernise DFE procedures used in South Africa (Smithers *et al.*, 2016). The NFSP is a comprehensive plan covering all approaches to DFE, which includes updating and modernisations of the estimation of design rainfalls and floods under non-stationary climate conditions in South Africa. The need to develop methods to account for non-stationary data, and to update design rainfall estimation methods to include possible trends in extreme rainfall events in a changing environment, have been identified as high priority research areas in the NFSP.

The impact of a changing climate has become a key concern in South Africa (e.g. Department of Environmental Affairs, 2014a; Department of Environmental Affairs, 2014b; Department of Environmental Affairs, 2017). In South Africa, over the past five decades the mean annual temperatures have increased by more than 1.5 times the observed global average increase (Ziervogel *et al.*, 2014). The Department of Environmental Affairs (2017) noted that the highest recorded temperatures up to that year since 1951 occurred in 2015. Moyo and Nyoni (2021) noted that South Africa is likely to be at least 3ºC warmer by 2050 than the period from 1961-2000 under a "business-as-usual" scenario in greenhouse gas emissions. The Intergovernmental Panel on Climate Change (IPCC) note that severe and widespread impacts associated with such temperature increases are attributable to climate change (IPCC, 2018). Changes in temperature have a significant impact on extreme weather events (Pfahl *et al.*, 2017; IPCC, 2018) and, generally, warmer atmospheric conditions are more conducive to heavy rainfall events (IPCC, 2017a; Pfahl *et al.*, 2017). Over parts of South Africa, it has been noted that the frequency of extreme rainfall events has increased (Ziervogel *et al.* (2014).

The estimation of design floods is impacted by changes in rainfall and runoff distribution characteristics (Smithers, 2012b). Many observations of global climate trends have raised an increasing concern that the extreme rainfalls, including the PMP, needed for the design of high-hazard hydraulic infrastructure, will change due to the influence of a changing climate (Rouhani, 2016). The potential influences of climate change on key variables for PMP estimation, such as maximum moisture and precipitation efficiency, have been studied in some detail (Clark, 1987; Rastogi *et al.*, 2017). Results of that research suggest that changes in both atmospheric temperature and the maximum atmospheric moisture that can be held may increase PMP estimates by approximately 20% due to climate change (Clark, 1987; Rastogi *et al.*, 2017).

Johnson and Smithers (2020) revised the 1-day PMPs in South Africa using an updated rainfall database and a modernized methodology and highlighted that many of the extreme events noted in their study occurred after the previously estimated PMPs published in HRU (1972). This indicates that there has been an increase in extreme rainfall events recorded compared to previous years. Hence it is critical to publish the updated PMP estimates, derived on the assumption of stationary data, and use this information to estimate the potential impacts of the changing climate on extreme rainfall estimation.

Dam safety management has conventionally been carried out assuming stationary climatic conditions (Ehsani *et al.*, 2017). However, researchers are increasingly taking the non-stationarity hypothesis in rainfall and flood frequency analysis into account to cater for the effects of climate change (Gregersen *et al.*, 2017; Sarhadi and Soulis, 2017; Fluixá-Sanmartín *et al.*, 2019; Pedretti and Irannezhad, 2019; Hesarkazzazi *et al.*, 2021). Moyo and Nyoni (2021) warn that most climate change scenarios for South Africa show potential detrimental impacts on dams and flood risk management. Warmer and drier climate is linked to increased risk of droughts which adversely impact on the reliability of water supply systems and the structural integrity of dams. Warmer and wetter scenarios are characterized by more frequent and severe extreme flood events which are directly linked to dam safety concerns as well as to increased sedimentation. Ultimately, any climate change scenario is highly likely to have an adverse impact on dam safety and flood risk management. Luxford and Faulkner (2020) recommend the development of a practical method of non-stationary flood frequency estimation in the UK, that includes investigating trends in extreme rainfall and incorporating non-stationarity and integrates the modelling of past trends and future expected climate change.

The importance of this research has recently been highlighted by the Water Research Commission (WRC) through a Webinar titled "Roadshow: Advancing Dam Safety in The Context of Climate Change in South Africa" held in May 2021. Dams are strategic assets for storing water to support life and socio-economic development. Their failure often results in the loss of life, extensive downstream damage to the environment and impacts on economic activities. In South Africa the Dam Safety Office, located within the Department of Water and Sanitation (DWS), is responsible for ensuring the safety of dams. In addition to normal ageing-related deterioration of dams, their safety is likely threatened by climate change. According to the erstwhile Department of Environmental Affairs (now DEFF), the biggest cost increase associated with climate change in the water sector will be in infrastructure damage due to flooding, projected to rise from about R670 million per year to R3.5 billion per year (WRC, 2021).

Given the importance of flood risk management, the shortcomings of the methods currently used by practitioners for DFE and the potential impact of climate change, dealing with a non-stationary climate data series currently requires urgent attention in South Africa (Johnson *et al.*, 2021). Hattingh (2021) noted that to address the challenge of climate change and its impacts on dams, risk-based approaches need to be developed to account for uncertainty associated with a non-stationary climate, further highlighting the importance of this research in the South African context. With the increasing availability of climate model data through Global Circulation Models (GCMs), there is greater opportunity to use such data to determine the potential impacts of future climate scenarios on extreme rainfall and flood events using advanced statistical techniques, and to develop methods/tools to incorporate these trends in design rainfall and flood estimation. For example, numerous research institutions in the UK are involved in research on non-stationarity in flooding using climate model data (Luxford and Faulkner, 2020).

All DFE methods currently used in South Africa are based on the assumption of a stationary climate. The concept of regionally derived "magnification" adjustment factor to account for non-stationarity is a convenient method for linking trends due to non-stationary frequency analysis to estimates from methods based on the assumption of stationarity, as well as providing an intuitive means of communicating the effects of change on design floods. While many of the climate modelling studies reported in the literature indicate changes in the frequency and magnitude of extreme flood events, there does not seem to be consensus in the literature on the detection of trends in the observed data. This disparity could be attributed to the relatively short periods of observations available. Kjeldsen and Prosdocimi (2021a) presented a regional approach to magnification factors to allow a statistical assessment of the impact of non-stationary data on design floods in both gauged and ungauged locations, regardless of the causes (e.g. climate change, increased abstractions, changes in land cover) of non-stationary data. This approach can be used to allow more robust assessment of trends in regional series of hydrological extremes and changes in design rainfalls and floods across a specified region or pooling group in South Africa.

Given the above, a method to account for non-stationary data which incorporates the impacts of a changing climate in extreme design rainfall estimates in South Africa needs to be developed using regional approaches to detect trends in historical data.

Given the background provided above, the aims of this project are therefore to undertake the following for South Africa:

(a) To develop and assess the performance of a method to account for the impacts of non-stationary data on design rainfall estimation;
(b) To review and refine the updated 1-day PMP estimates;
(c) To develop and assess the performance of a method to account for the impacts of non-stationary data on PMP estimation; and
(d) To assess the trends in hydrological extremes using regional magnification factors.

Objectives regarding the PMP were addressed through Deliverable 3, a report on the update of the 1-day PMP which was submitted to WRC in February 2023, and Deliverable 4, a workshop on the use of the revised PMP tools which was held at Stellenbosch University and online in May 2023. The outputs of these two deliverables are accessible via the Water Research Observatory website, which is a cloud-based data portal belonging to the Water Research Commission. This report focusses on assessing trends in hydrological extremes and the impacts of possible non-stationary data on design rainfall estimation in KwaZulu-Natal.

The structure of this document is as follows:
Detecting trends in rainfall extremes and non-stationary extreme value analysis of rainfall data in KwaZulu-Natal are presented in Chapter 2 and detecting trends in flood extremes and non-stationary extreme value analysis of peak discharge data is covered in Chapter 3. Chapter 4 contains discussion and conclusions on this study. Chapter 5 presents a summary of the capacity building through the project. Chapter 6 lists the references used and Chapters 7 and 8 contain the appendices.

2. NON-STATIONARY FREQUENCY ANALYSIS OF EXTREME RAINFALL EVENTS ON THE EAST COAST OF KWAZULU-NATAL

KA Johnson, JC Smithers, RE Schulze, TR Kjeldsen and S Schütte

2.1 Introduction

Extreme hydrological events such as floods are one of the deadliest hazards in South Africa (Pinto *et al.*, 2022). Extreme floods events can damage hydrological structures such as dams, spillways, bridges and culverts. Therefore, minimising the risk of failure of hydraulic structures requires design floods be accurately estimated. The underestimation of design floods and failure of hydraulic structures can lead to loss of life and significant economic losses, while overestimation may result in over-design which results in excessive construction and maintenance costs. The trade-off between safety and costs is a delicate balancing act, especially for emerging economies with public budgets under pressure from competing demands. The South African Government has reported that the most common weather-related catastrophes in South Africa between the period 1900 to 2014 were floods, droughts and large storms (DFFE, 2016). Recent large floods include the event on the April 2022 experienced along the eastern coast of South Africa which was reported to have resulted in infrastructural damages to the value of 17 billion Rands and 435 casualties, 55 injured, and 54 people missing (Pinto *et al.*, 2022). Similarly, for an event in the same region in April 2019, Singh (2019) reported 650 million Rands damages to infrastructure and 60 deaths. These reported losses highlight the critical importance of flood management in the region and the absolute need for risk analysis to be supported by the best available information, data and methods. This is particularly important as the magnitude and frequency of extreme weather events is expected to increase over time, combined with an increase in social vulnerability resulting from growing populations and associated economic activity.

Traditional methods for frequency analysis of extreme events and most current risk assessment models are based on techniques and concepts developed around a century ago (e.g. Fuller, 1914) and are based on the assumption of climate stationarity, i.e. that no temporal change is evident in the statistics of extreme events (Prosdocimi *et al.*, 2014; Ragno *et al.*, 2019b). However, anthropogenically induced climate change has resulted in changes in extreme weather events, thus questioning the assumption of stationarity (Serinaldi and Kilsby, 2015). In recent years, the frequency and impacts of extremes have increased substantially in many parts of South Africa (Thoithi *et al.*, 2023). Hence, there is significant interest in understanding how extreme events may change into the future and how frequency analyses should be adapted to account for non-stationary data.

Statistical models used to analyse extreme events can be broadly categorised into two groups: stationary and non-stationary. In a stationary model, the observations are assumed to be drawn from a static/non-varying probability distribution function, which is assumed to represent the entire population of data, with constant parameters. Hence, the statistics of extreme events are assumed to not change over time or with respect to another variable or covariate. However, in a non-stationary model, the parameters of the underlying probability distribution function change over time or due to a selected covariate (Sadegh *et al.*, 2015). Several studies have promoted the idea of moving away from stationary models to ensure that the changing properties of extreme hydrological events are captured and accounted for in design estimates (e.g. Vasiliades *et al.*, 2015; Zhou *et al.*, 2016; Demaria *et al.*, 2017; Tan and Gan, 2017; Gao and Zheng, 2018; Ragno *et al.*, 2019a; Ouarda *et al.*, 2020; Song *et al.*, 2020; Hesarkazzazi *et al.*, 2021; Silva *et al.*, 2021).

Moyo and Nyoni (2021) warned that most climate change scenarios in South Africa show detrimental impacts on dams and flood risk management. Warmer and drier climate is linked to increased risk of droughts which adversely impact on the reliability of water supply systems and the structural integrity of dams. Warmer and wetter scenarios are characterised by more frequent and severe extreme flood events which are directly linked to dam safety concerns as well as to increased sedimentation. McBride *et al.* (2022) noted that, despite the total number of observed rain days having remained relatively constant over the past century, the probability of significant extreme daily rainfall events occurring has increased for most parts of South Africa. Ultimately, many climate change scenarios are highly likely to have an adverse impact on dam safety and flood risk management. The impacts of climate change can be modelled using outputs from GCMs. These models can be used at a global scale or can be downscaled, and bias corrected for application at local scales.

Given the importance of water resources and flood risk management, the potential impact of climate change on the magnitude and frequency of extreme events requires urgent attention in South Africa to ensure that the best possible science is supporting operational hydrological decision-making and risk assessments (Smithers *et al.*, 2014; Johnson *et al.*, 2021). This urgency is supported by Hattingh (2021), who highlighted the need to address the challenge of climate change and its impacts on dams, including risk-based approaches, in order to account for uncertainty associated with a non-stationary climate, with this further highlighting the importance of this research in the South African context.

The aims of the study reported in this chapter are to determine if any trends exist in observed extreme rainfall events along the East Coast of KwaZulu-Natal, to contribute an understanding of the teleconnection patterns between various climate drivers and the annual maximum daily extreme rainfall and to account for possible non-stationarity in climate data in the estimation of extreme design rainfall events in South Africa. The objectives of this chapter are to: (i) investigate trends in annual maximum daily rainfall using parametric and non-parametric statistical tests, (ii) identify potential climate drivers of extreme rainfalls, (iii) perform stationary and non-stationary rainfall frequency analyses, (iv) critically evaluate the stationary vs non-stationary models, and (v) evaluate projected changes in rainfall using GCMs.

2.2 Materials and Methods

2.2.1 Data sources and case study site selection

Given the lack of access to concurrent and up-to-date rainfall data at a national scale from the South African Weather Services (SAWS), the east coast of KwaZulu-Natal (KZN) in South Africa was selected for a case study to investigate how extreme rainfalls may have changed over time, as data were available for this region. Daily rainfall data were obtained from the South African Sugarcane Research Institute (SASRI), which provides open access to up-to-date climate data over the sugarcane production region within South Africa. Approximately 100 stations with rainfall data up to the year 2020 were extracted from the SASRI database. The rainfall data were screened according to the following criteria:

a) the record length must be at least 40 years,
b) the record should be the most up-to-date, and
c) no more than three months of data should be missing.

The daily rainfall time series from each site was checked for missing data. To construct a time series of the Annual Maximum Daily Rainfall (AMDR) it is important that each year of the records be sufficiently complete so that the largest rainfall totals are likely to have been captured and to prevent seasonal bias. Based on the selection criteria, 39 sites were selected for this study. Figure 2.1 depicts the SASRI station numbers and locations of the stations used in the study and Table 2.1 contains a summary of the station information.

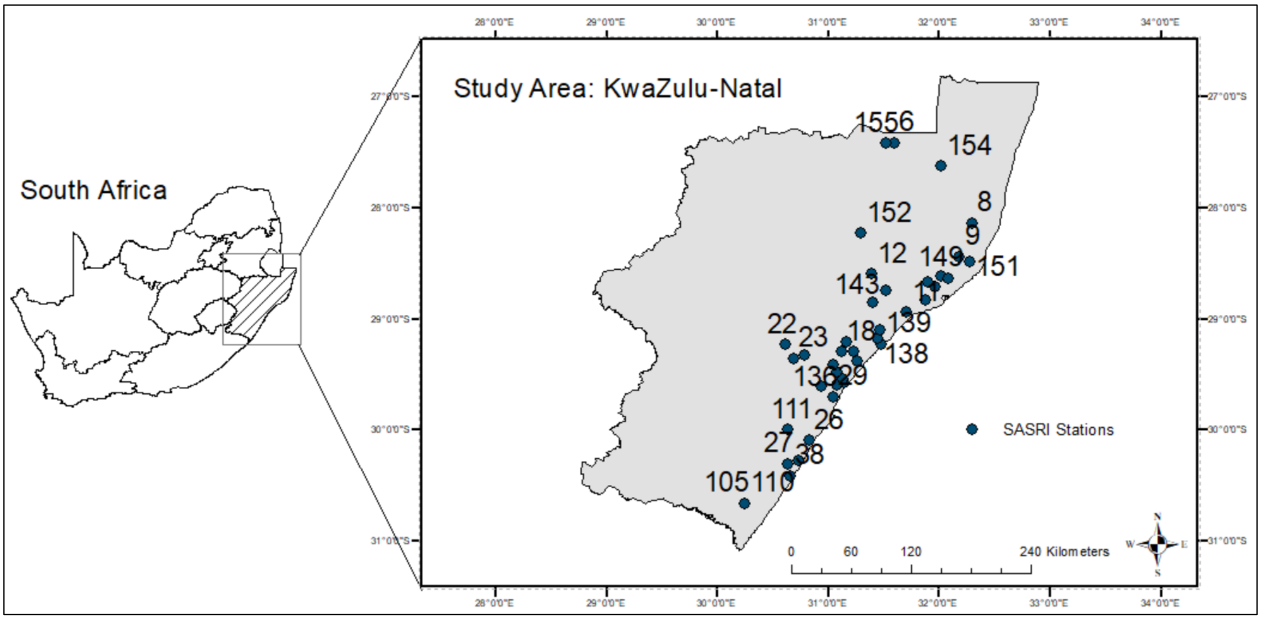

Figure 2.1 SASRI stations in KwaZulu-Natal selected for this study

Table 2.1 Station information for case study sites

Station Name	SASRI Station Number	Altitude (m)	Start Year	End Year	Total Years
Pongola – SASRI	6	308	1966	2014	48
Glen Park – St Lucia Farms	8	35	1966	2020	54
Mtubatuba – Riverview Sugar Mill	9	46	1966	2020	54
Mtunzini – ex SASRI	11	36	1966	2020	54
Melmoth – CA Leith & Sons	12	790	1967	2020	53
Glendale – Tenrith Farm	18	129	1966	2020	54
Tongaat – Klipfontein (THS)	20	72	1965	2020	55
Seven Oaks – Saw Mill	22	1067	1966	2020	54
Noodsberg – Illovo Sugar Mill	23	1008	1971	2020	49
Illovo – Sugar Estate	26	15	1966	2020	54
Vulamehlo – Esperanza	27	195	1968	2015	47
Mt Edgecombe – SASRI	29	96	1927	2020	93
Sezela – Illovo Sugar Estate	38	90	1976	2020	44
Oribi Flats - Minnehaha Farm	105	520	1965	2020	55
Renishaw – Crooks Bros Estate	110	61	1957	2020	63
Powerscourt – Roseleigh Estate	111	637	1957	2020	63
Inanda – Farm	114	556	1957	2020	63
Inyaninga – THS	120	107	1957	2019	62
Maidstone – Sugar Mill (THS)	123	46	1957	2020	63
Sinembe – Spreyton Farm	125	237	1957	2020	63
Upper Tongaat – Barwon Farm	126	457	1957	2020	63
Kearsney – Ocean Lodge	129	277	1957	2020	63
Doornkop – Langespruit Farm	130	545	1957	2020	63
Darnall – Sugar Mill (THS)	131	142	1957	2020	63
Tugela Mouth – Wetherly Estate	132	114	1957	2015	58
Glenside – Misty Krantz Estate	136	997	1974	2017	43
Mandini – SAWS	138	99	1957	2020	63
Inyoni – Myrln Estate	139	107	1957	2020	63
Eshowe – Brocklee Farm	142	549	1957	2020	63
Nkwaleni – Zigagazi	143	137	1957	2019	62
Felixton – Sugar Mill (THS)	144	46	1957	2020	63
Kulu Halt - Honey Farm	146	61	1957	2020	63
Ukulu Properties – Crystal Holdings	147	152	1957	2020	63

Station Name	SASRI Station Number	Altitude (m)	Start Year	End Year	Total Years
Mposa – Redcroft Farm	148	91	1957	2020	63
Kwambonambi – Mondi Forestry	149	30	1957	2020	63
ULOA – Mark & Ross Sugar Estate	151	15	1957	2015	58
Mtubatuba – Nyalazi River	152	34	1957	2015	58
Mkuze – Mkuze Estate	154	150	1957	2020	63
Pongola – Impala Irrigation Board	155	290	1957	2020	63

2.2.2 Methodology

The basic methodology applied in this study to determine extreme rainfall quantities at a given location, and how they may vary with respect to a selected covariate, is detailed in the following sections. The main steps involved in this approach are summarised in Figure 2.2.

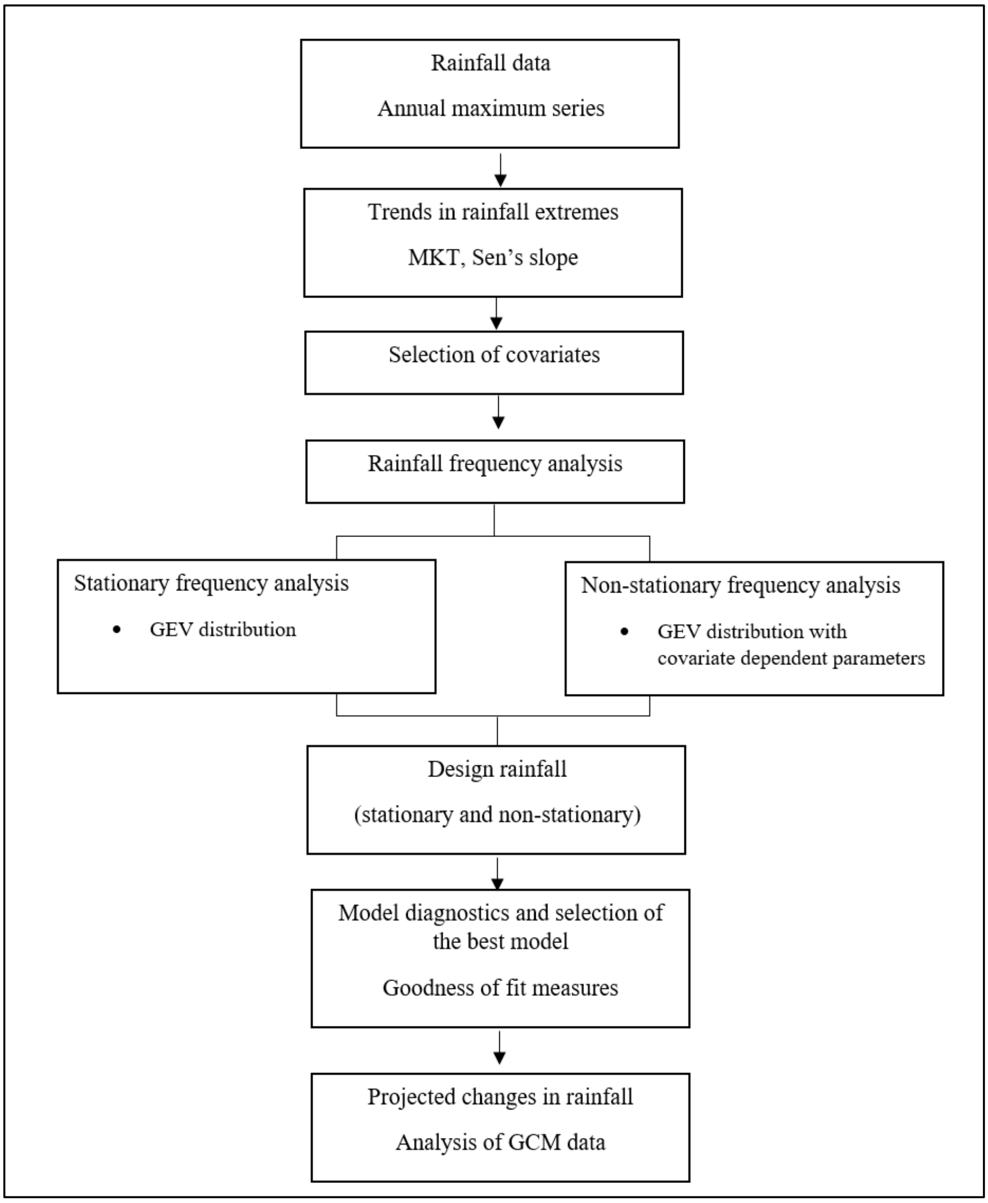

Figure 2.2 Stationary and non-stationary design rainfall estimation procedures

2.2.2.1 Trends in rainfall extremes

The existence or not of trends in hydrological extremes can be investigated using parametric or non-parametric methods. Parametric methods include using simple linear regression to investigate how annual maximum rainfall changes over time. However, this method can only be used on data that are normally distributed (Kundzewicz, 2019). The Mann-Kendall Test, MKT, (Mann, 1945; Kendall, 1962) is a non-parametric test often used to detect trends in hydrological extremes (Cheng *et al.*, 2014; Yilmaz and Perera, 2015; Agilan and Umamahesh, 2018; Ragno *et al.*, 2019a; Hesarkazzazi *et al.*, 2021). The term 'non-parametric' refers to the absence of assumptions about the distribution of the data in the method (Mathivha *et al.*, 2021). The MKT does not provide information on the magnitude of a trend, it only provides details about the existence, significance, and direction of a trend (Mangini *et al.*, 2018). In addition, the Sen's slope is a non-parametric method used to evaluate the linear trend of the data series (Sen, 1968). Hence, the MKT and Sen's slope were selected to detect trends in the AMDR data.

2.2.2.2 Frequency distribution and non-stationary models

The three-parameter Generalised Extreme Value (GEV) distribution is commonly applied to Annual Maximum Series (AMS) of rainfall data. The GEV has been determined to be a suitable distribution for design rainfall estimation in South Africa (Smithers, 1996; Smithers and Schulze, 2000b) and it allows the incorporation of non-stationarity through varying parameters. The GEV distribution was thus selected for use in this research to evaluate the non-stationarity of rainfall data over time.

The GEV distribution function is used to model time series of annual maximum series data or block maxima. The GEV cumulative distribution function is given as (Coles, 2001):

$$\Psi_{GEV}(x) = \exp\left\{-\left(1 + \xi \cdot \left(\frac{x-\mu}{\sigma}\right)\right)^{-\frac{1}{\xi}}\right\} \tag{2.1}$$

for $1 + \xi \cdot ((x - \mu)/\sigma) > 0. \mu, \sigma,$ and ξ are the parameters of the distribution: μ is the location parameter, $\sigma > 0$ is the scale parameter, and ξ is the shape parameter which defines the tail behaviour of the distribution. The stationary GEV model can be extended for dependent series by letting the parameters of the distribution be a function of a general covariate x_c, i.e., $\mu(x_c), \sigma(x_c), \xi(x_c)$ (Coles, 2001). Hence, the non-stationary form of Eq. (2.1) is described as:

$$\Psi_{GEV}(x \mid x_c) = \exp\left\{-\left(1 + \xi(x_c) \cdot \left(\frac{x-\mu(x_c)}{\sigma(x_c)}\right)\right)^{-\frac{1}{\xi(x_c)}}\right\} \tag{2.2}$$

The concept of effective return period or effective design value is defined as q-quantile, Q, varying as a function of a given covariate, e.g., temporal and/or physical. Therefore, for a constant value of $RP = 1/q$, where q is the annual exceedance probability, the effective return period is defined as:

$$\left(\left(x_c, Q_q(x_c)\right),\ q \in [0,1]\right) \tag{2.3}$$

where

x_c = the covariate, and

$Q_q(x_c)$ = the q-quantile.

The Process-informed Non-stationary Extreme Value Analysis (ProNEVA) is a tool in MATLAB developed by Ragno *et al.* (2019b) in which the non-stationary component is defined by a temporal or physical driver. This tool has been used to perform stationary and non-stationary rainfall frequency analysis for this study.

2.2.2.3 Selection of covariates

According to Agilan and Umamahesh (2017), the most suitable covariates for short-duration rainfall events (less than 24 hours) are local processes, e.g. local temperature changes and urbanisation, whilst the most suitable covariates for long-duration (1-day and greater) rainfall events are global processes, such as global temperature change, the El Niño-Southern Oscillation (ENSO) cycle, and the Indian Ocean Dipole (IOD) cycle. ENSO and IOD are significant drivers of the southern African climate during the austral summer rainy season, and have thus been used in numerous studies to predict the occurrence of extremes (Gaughan *et al.*, 2016; Hoell *et al.*, 2021; Lüdecke *et al.*, 2021).

ENSO and IOD are related to sea surface variations and air pressure across the world, based on observed data. ENSO is represented by the Southern Oscillation Index (SOI), which is associated with warm Sea Surface Temperatures (SST) and is characterised by the variations between the Indonesian Low pressure system and the South Pacific Tropical High pressure system (de Silva and Hornberger, 2019). The IOD is an oscillation of SST in the equatorial Indian Ocean and is considered relevant to the climate of countries surrounded by the Indian Ocean. It is represented by the Dipole Mode Index (DMI). The effects of ENSO and IOD are considered to be independent (de Silva and Hornberger, 2019), hence both phenomena are considered as potential significant covariates for this study.

As changes in temperature are linked to increased greenhouse gas concentrations (IPCC, 2017), and these climate process behaviours and their associations are potentially non-stationary (Endris *et al.*, 2019), CO_2 concentrations for South Africa and Global Mean Temperatures (GMT) were included as potential significant covariates for this study.

The main purpose of this chapter is to contribute to an understanding of the teleconnection patterns between the Southern Oscillation Index (SOI), Dipole Mode Index (DMI), Carbon Dioxide (CO_2), and Global Mean Temperature (GMT) and annual maximum daily extreme rainfall in KZN, in identifying non-stationary patterns in the data. Data used for the analyses are SOI and DMI monthly data from 1928 – 2020 (Bureau of Meteorology, 2023), annual global carbon emissions data ($MtCO_2$) from 1960 – 2020 (Global Carbon Atlas, 2023), and global mean temperature data from 1928 – 2020 (National Aeronautics and Space Administration, 2023).

2.2.2.4 Model diagnostics and selection of the best model

The purpose of fitting a statistical model, whether it is stationary or non-stationary, is to characterise the population from which the data were drawn for further analysis. Hence, it is necessary to check the performance of the fitted model to the data (Coles, 2001). Several metrics are implemented to assess the Goodness of Fit (GOF) and support model selection, including: (1) the Akaike Information Criterion (AIC), (2) the Bayesian Information Criterion (BIC), and (3) the Root Mean Square Error (RMSE).

The Akaike Information Criterion, (AIC) (Akaike, 1974), is a GOF measure that compares the frequency models and represents how well each model fits the data relative to other models. The lower the AIC value, the better the model performance, in comparison to other models. The AIC is computed as follows:

$$AIC = 2 \cdot (D - \hat{L}) \tag{2.4}$$

where D is the number of parameters of the statistical model and $\hat{L}$ is the log-likelihood function which is a measure of how well a particular model fits the data using the probability density of observed data viewed as a function of the parameters of a statistical model.

The Bayesian Information Criterion (BIC) (Schwarz, 1978) is defined as:

$$BIC = D \cdot \ln(N) - 2 \cdot \hat{L}, \tag{2.5}$$

where N is the length of records. As with AIC, the model with lower BIC yields the best fit. The Root Mean Square Error (RMSE) is widely used in hydrology and climatology as a GOF measurement, and is given by

$$RMSE = \sqrt{\frac{\sum_{i=1}^{n}(y_i - Y_i)^2}{n}} \tag{2.6}$$

where

y_i = the actual value for the ith observation,

Y_i = the predicted value for the ith observation, and

n = the number of observations.

A perfect fit is associated with $RMSE = 0$, given $RMSE \in [0, \infty)$.

2.3 Results and Discussion

2.3.1 Trend detection

Table 2.2 contains a summary of results for the analyses of the AMS from 39 stations subjected to the MKT and Sen's slope test. The MKT was evaluated at the 5% significance level. Figure 7.1 in Appendix A contains the graphs depicting the time series plot for each station assessed. Based on the MKT and Sen's test, the results indicate that for the majority of the stations in the

KZN study region no significant upward trend over time was detected, with approximately 40% of stations showing a positive trend and only one station (Station 38: Sezela - Illovo Sugar Estate), located on the south coast of the province, showing a significant positive trend, as shown in Figure 2.3. It is noteworthy that this station has one of the shortest record lengths, which could influence the results. These results highlight the difficulties in detecting significant trends in relatively short and highly variable at-site hydro-meteorological series, especially when using non-parametric tests with relatively low statistical power. The results are similar to those found by Kibii (2021), who assessed seasonal and annual rainfall trends in South Africa and found that daily rainfall reflected insignificant trends.

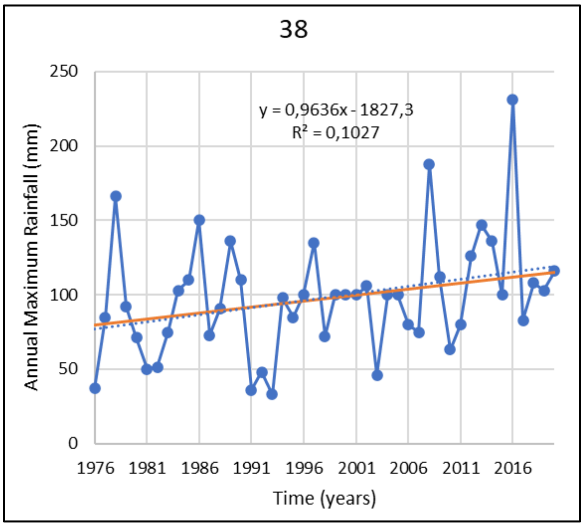

Figure 2.3 Time series for Station 38

Table 2.2 Trends in KwaZulu-Natal extreme rainfall using the Mann-Kendall test

Station Name	SASRI Station Number	p-value	Sen's Slope	Interpretation of Test
Pongola – SASRI	6	0.088	0.426	Insignificant positive trend
Glen Park – St Lucia Farms	8	0.147	-0.367	Insignificant negative trend
Mtubatuba – Riverview Sugar Mill	9	0.092	-0.609	Insignificant negative trend
Mtunzini – ex SASRI	11	0.674	-0.150	Insignificant negative trend
Melmoth – CA Leith & Sons	12	0.747	0.070	Insignificant positive trend
Glendale – Tenrith Farm	18	0.165	-0.396	Insignificant negative trend
Tongaat – Klipfontein (THS)	20	0.472	-0.244	Insignificant negative trend
Seven Oaks – Saw Mill	22	0.983	0.000	Insignificant trend
Noodsberg – Illovo Sugar Mill	23	0.604	0.073	Insignificant positive trend
Illovo – Sugar Estate	26	0.389	0.333	Insignificant positive trend
Vulamehlo – Esperanza	27	0.985	0.000	Insignificant positive trend
Mt Edgecombe – SASRI	29	0.075	0.250	Insignificant positive trend
Sezela – Illovo Sugar Estate	38	**0.023***	**0.810***	**Significant positive trend***
Oribi Flats – Minnehaha Farm	105	0.539	0.255	Insignificant positive trend
Renishaw – Crooks Bros Estate	110	0.070	0.613	Insignificant positive trend
Powerscourt – Roseleigh Estate	111	0.147	-0.344	Insignificant negative trend
Inanda – Farm	114	0.835	-0.062	Insignificant negative trend
Inyaninga – THS	120	0.585	-0.121	Insignificant negative trend
Maidstone – Sugar Mill (THS)	123	0.509	0.167	Insignificant positive trend
Sinembe – Spreyton Farm	125	0.138	0.323	Insignificant positive trend
Upper Tongaat – B rwon Farm	126	0.354	0.208	Insignificant positive trend
Kearsney – Ocean Lodge	129	0.461	-0.081	Insignificant negative trend
Doornkop – Langespruit Farm	130	0.780	-0.033	Insignificant negative trend
Darnall – Sugar Mill (THS)	131	0.672	0.092	Insignificant negative trend
Tugela Mouth – Wetherly Estate	132	0.468	-0.191	Insignificant negative trend
Glenside – Misty Krantz Estate	136	0.100	-0.448	Insignificant negative trend
Mandini – SAWS	138	0.206	0.401	Insignificant positive trend
Inyoni – Myrln Estate	139	0.147	0.359	Insignificant positive trend
Eshowe – Brocklee Farm	142	0.404	-0.195	Insignificant negative trend
Nkwaleni – Zigagazi	143	0.826	-0.039	Insignificant negative trend
Felixton – Sugar Mill (THS)	144	0.631	-0.136	Insignificant negative trend
Kulu Halt – Honey Farm	146	0.516	-0.176	Insignificant negative trend
Ukulu Properties – Crystal Holdings	147	0.655	-0.129	Insignificant negative trend
Mposa – Redcroft Farm	148	0.972	0.007	Insignificant positive trend
Kwambonambi – Mondi Forestry	149	0.242	-0.257	Insignificant negative trend
ULOA – Mark & Ross Sugar Estate	151	0.517	-0.203	Insignificant negative trend
Mtubatuba - Nyalazi River	152	0.367	-0.230	Insignificant negative trend
Mkuze – Mkuze Estate	154	0.839	-0.023	Insignificant negative trend
Pongola – Impala Irrigation Board	155	0.235	0.249	Insignificant positive trend

***Significant trends at 5% level identified**

2.3.2 Analysis of stationary and non-stationary models

Both stationary and non-stationary frequency analyses were undertaken using the GEV distribution for all stations in the study area. For the non-stationary frequency analysis, the location and scale parameters of the GEV distribution were modelled as linear functions of the selected covariates and the shape parameter was kept constant.

Firstly, the non-stationary models considering time as a covariate were compared to the stationary models for each station. Table 2.3 contains a summary of results for the AIC, BIC and RMSE tests considering time as a covariate at the 39 stations used in the study. The AIC and BIC and RMSE values of the stationary model are lower than those of the non-stationary model for most stations. Based on the AIC, the results indicate that 35 out of 39 stations in the KZN region are better modelled through the stationary model, as lower AIC, BIC, and RMSE values indicate a superior performing model (Ragno *et al.*, 2019b). The non-stationary models provided a better fit than the corresponding stationary model at only four stations (38, 136, 138 and 152). Using the BIC measure, the non-stationary models for only one station (138) were found to give a better fit of the data. Ouarda *et al.* (2020) found similar results considering time as covariate in the non-stationary model.

Table 2.3 The GEV statistical model performance criteria of selected sites in KwaZulu-Natal AMDR for time as a covariate

Station Name	SASRI Station Number	Stationary			Non-Stationary		
		AIC	**BIC**	**RMSE**	**AIC**	**BIC**	**RMSE**
Pongola - SASRI	6	460.81	466.49	1.62	462.90	474.25	1.29
Glen Park - St Lucia Farms	8	558.34	564.36	1.55	562.22	574.27	1.27
Mtubatuba - Riverview Sugar Mill	9	575.74	581.70	1.82	579.30	591.24	1.60
Mtunzini - ex SASRI	11	580.81	586.83	1.32	587.07	599.11	1.41
Melmoth - CA Leith & Sons	12	524.07	529.98	2.01	530.18	542.00	2.18
Glendale - Tenrith Farm	18	538.31	544.27	1.24	542.06	553.99	1.63

Station Name	SASRI Station Number	Stationary			Non-Stationary		
		AIC	BIC	RMSE	AIC	BIC	RMSE
Tongaat - Klipfontein (THS)	20	549.95	555.97	1.24	553.22	565.27	1.66
Seven Oaks - Saw Mill	22	493.72	499.74	4.30	495.97	508.02	3.57
Noodsberg - Illovo Sugar Mill	23	433.83	439.57	2.60	440.31	451.78	2.73
Illovo - Sugar Estate	26	531.30	537.10	1.76	536.26	547.85	1.35
Vulamehlo - Esperanza	27	504.05	509.60	1.88	508.19	519.30	1.58
Mt Edgecombe - SASRI	29	954.38	961.98	1.45	956.19	971.39	1.16
Sezela - Illovo Sugar Estate	38	449.01	454.36	1.79	**447.38***	456.30	**1.71***
Oribi Flats - Minnehaha Farm	105	597.12	603.20	1.22	600.91	613.06	0.99
Renishaw - Crooks Bros Estate	110	678.80	685.27	1.18	681.18	694.14	0.97
Powerscourt - Roseleigh Estate	111	650.68	657.16	1.71	654.17	667.12	1.47
Inanda - Farm	114	654.36	660.84	1.68	660.62	673.57	1.49
Inyaninga - THS	120	638.31	644.73	1.12	641.61	654.47	0.97
Maidstone - Sugar Mill (THS)	123	644.55	651.02	1.53	649.04	662.00	1.39
Sinembe - Spreyton Farm	125	646.42	652.90	1.87	647.89	660.84	2.15
Upper Tongaat - Barwon Farm	126	650.56	657.04	1.75	655.20	668.15	1.57
Kearsney - Ocean Lodge	129	624.55	631.03	2.60	627.67	640.62	2.11
Doornkop - Langespruit Farm	130	633.31	639.74	1.45	639.00	651.86	1.15
Darnall - Sugar Mill (THS)	131	644.40	650.87	1.62	650.88	663.84	1.88
Tugela Mouth - Wetherly Estate	132	582.99	589.23	1.38	587.49	599.96	0.96
Glenside - Misty Krantz Estate	136	449.30	454.65	5.50	**441.49***	450.41	**4.77***
Mandini - SAWS	138	669.56	676.04	3.14	**663.81***	**674.60***	**2.37***
Inyoni - Myrln Estate	139	655.28	661.76	1.53	658.52	671.47	1.26

Station Name	SASRI Station Number	Stationary			Non-Stationary		
		AIC	BIC	RMSE	AIC	BIC	RMSE
Eshowe - Brocklee Farm	142	649.98	656.46	1.43	653.17	666.12	1.03
Nkwaleni - Zigagazi	143	639.43	645.91	1.86	644.96	657.91	1.61
Felixton - Sugar Mill (THS)	144	658.45	664.92	1.53	662.85	675.80	1.41
Kulu Halt - Honey Farm	146	674.01	680.48	1.63	679.81	692.77	1.53
Ukulu Properties - Crystal Holdings	147	672.21	678.69	1.42	677.51	690.46	2.02
Mposa - Redcroft Farm	148	658.21	664.68	1.61	664.53	677.49	1.64
Kwambonambi - Mondi Forestry	149	656.35	662.82	2.01	664.71	677.66	2.00
ULOA - Mark & Ross Sugar Estate	151	639.67	645.90	3.13	645.48	657.94	2.83
Mtubatuba - Nyalazi River	152	578.80	585.03	2.13	**578.77***	591.24	**1.31***
Mkuze - Mkuze Estate	154	612.12	618.59	2.37	617.67	630.62	1.14
Pongola - Impala Irrigation Board	155	615.82	622.30	2.09	618.61	631.57	2.37

*** Non-stationary model performs better than stationary model overall**

Station 38 (Sezela - Illovo Sugar Estate) in Figure 2.4 was the only station to show a significant increase in rainfall over time and have the non-stationary time-model outperform the stationary model. This station also showed an increase in the effective return period of rainfall, which summarizes the impact of time on rainfall by describing return periods as functions of time (x-axis). Although Station 38 showed a positive trend in data and a corresponding increase in overall effective return periods, the trends of effective return periods vary for each station and a positive trend does not necessarily correlate to an increasing effective return period.

The effective return period for Station 38 is shown to increase as a function of time for all return periods. Figure 6.3 depicts the GEV for the: (a) stationary model, (b) non-stationary model, and (c) effective return period as a function of time for Station 38: Sezela (Illovo Sugar Estate). Appendix A (Figure 7.2 to Figure 7.40) contains the plots for the stationary and non-stationary frequency analyses for all covariates and effective return periods for all stations.

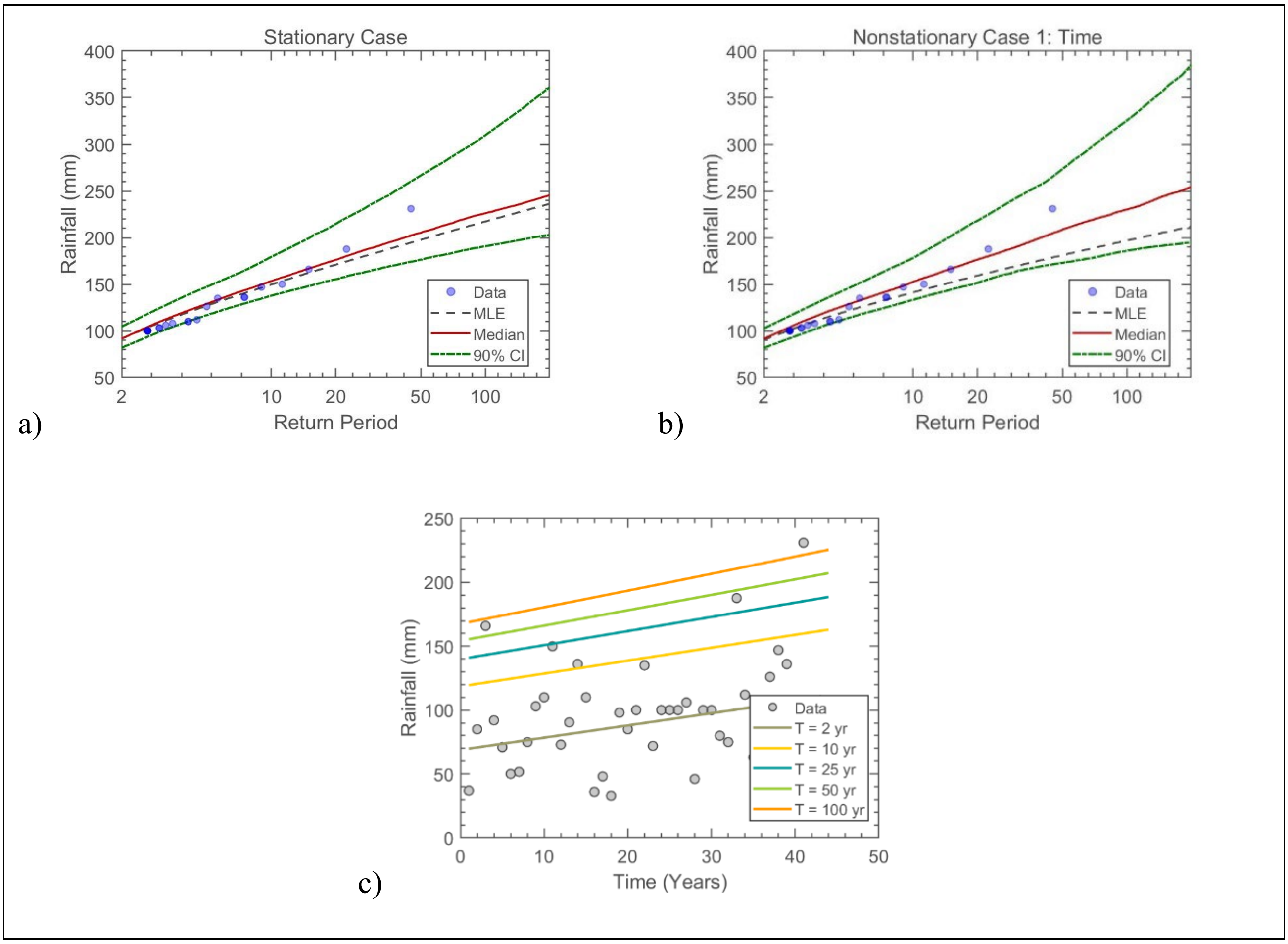

Figure 2.4 The GEV (a) stationary model, (b) non-stationary model considering time as a covariate, and (c) effective return period as a function of time for Station 38: Sezela - Illovo Sugar Estate

Secondly, the non-stationary models considering SOI, DMI, CO_2 and GMT as covariates were compared to the stationary models for each station. Table 2.4 summarises the best-fit models for the stationary and non-stationary cases based on AIC and BIC measures. The detailed results are presented in Table 7.1 in Appendix A. The stationary models perform better than the non-stationary models at 56 % and 36 % of stations, based on the AIC and BIC measures, respectively. Some non-stationarity is noted with respect to time; however, very little impact due to SOI and DMI is evident.

Most often the stations where the non-stationary CO_2 model outperformed the other models resulted in consistent trends for both AIC and BIC tests. This indicates that it may be argued that climate driving factors, such as CO_2 changes, largely influence extreme rainfalls in KZN. None of the non-stationary models considering GMT as a covariate outperformed any other model.

Table 2.4 Summary of best-fit models for all stationary and non-stationary cases

AIC		**BIC**	
Model	**Number of best-fit models**	**Model**	**Number of best-fit models**
Stationary	22 (56 %)	Stationary	14 (36 %)
Non-stationary - Time	4 (10 %)	Non-stationary - Time	2 (5 %)
Non-stationary - SOI	4 (10 %)	Non-stationary - SOI	0 (0 %)
Non-stationary - DMI	1 (3 %)	Non-stationary - DMI	0 (0 %)
Non-stationary - CO_2	8 (21 %)	Non-stationary - CO_2	23 (59 %)
Non-stationary - GMT	0 (0 %)	Non-stationary - GMT	0 (0 %)

Figure 2.5 and Figure 2.6 show the locations of which models best fit the data based on AIC and BIC, respectively. No spatial patterns are evident based on the location of the best-fit non-stationary models.

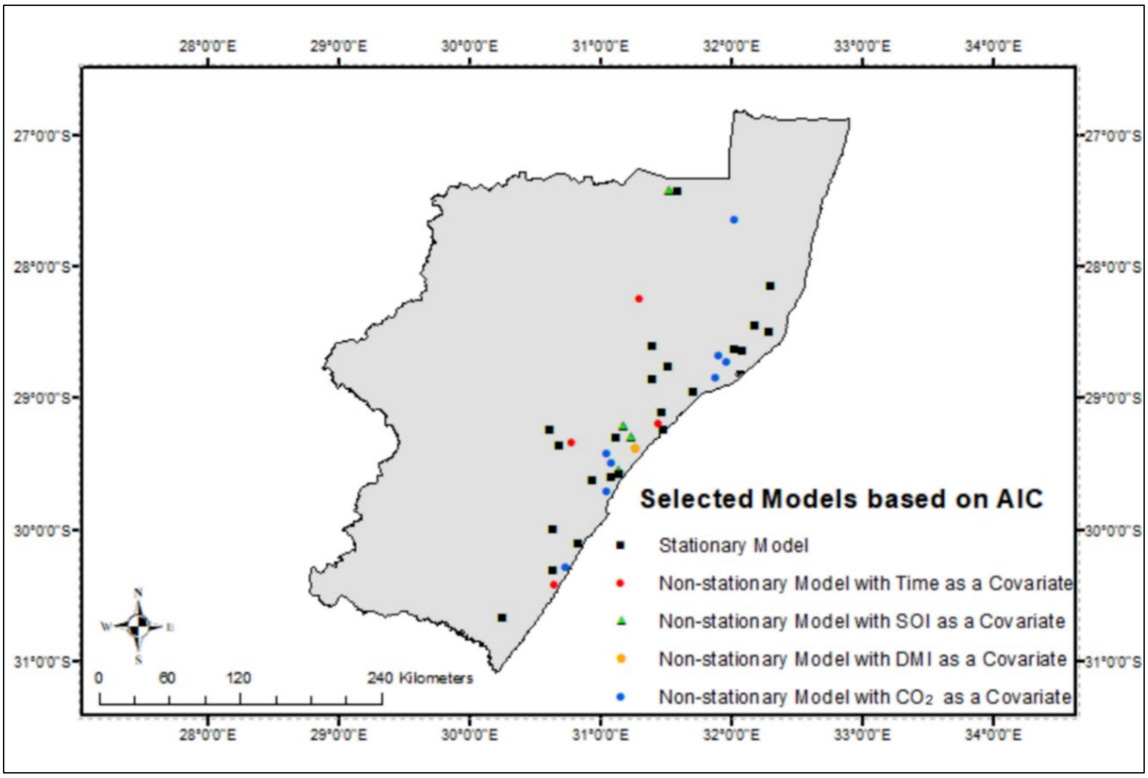

Figure 2.5 Best-fit distribution model, based on the AIC measure

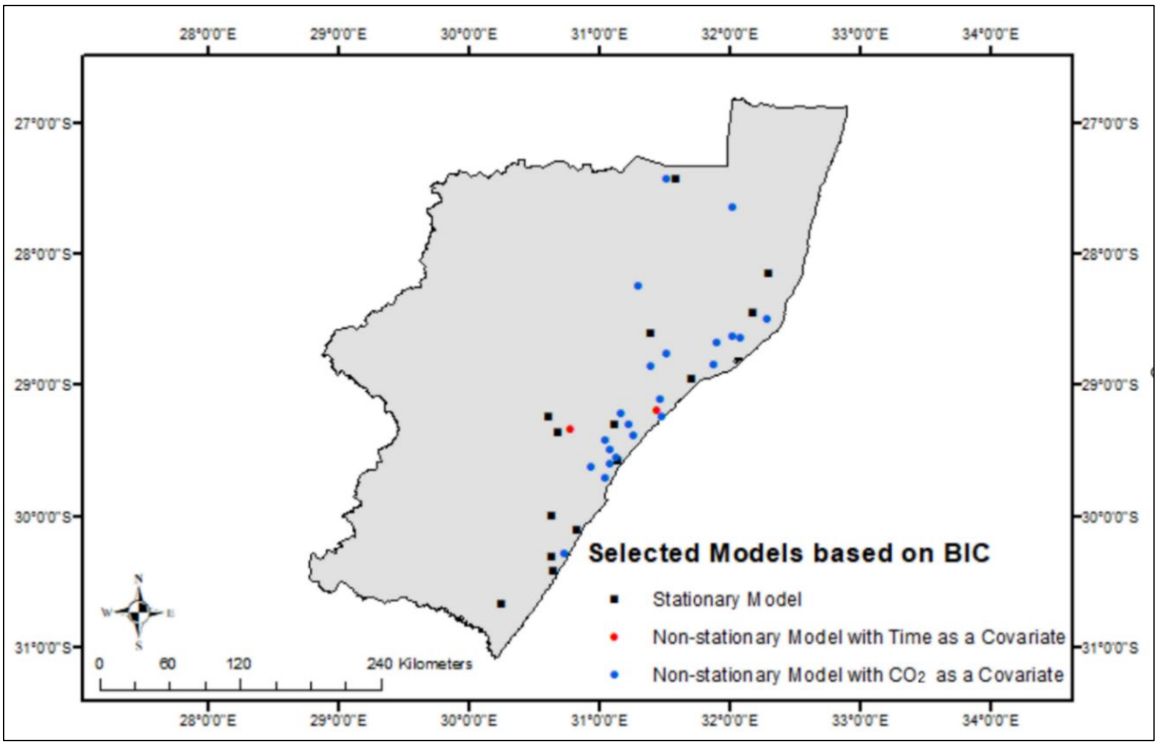

Figure 2.6 Best-fit distribution model, based on the BIC measure

2.3.3 Projected changes in rainfall

The results of the analysis of observed data in the previous sections mostly show insignificant changes in historical extreme rainfalls and design rainfalls. However, there is still a need to understand possible future scenarios for design purposes. To consider the projected changes in rainfall and the possible climate change factors, or ratios, that could be applied to current design rainfall depths to estimate design for future scenarios, an ensemble of very high-resolution climate model simulations of present-day climate as well as projections of future climate changes over South Africa was selected. These projections were produced by the CSIR using the CCAM regional climate model and were further bias-corrected to local observed temperature and rainfall data by Schütte *et al*. (2023). The data used in this study were sourced from Schütte *et al.* (2023) and contains outputs from six GCMs from the CMIP5 archive based on the Representative Concentration Pathway (RCP) Scenarios 8.5, i.e. the "business as usual" scenario of Greenhouse Gas emissions into the future. The simulations span the period 1961-2100.

The six GCMs are the:

- Australian Community Climate and Earth System Simulator (ACCESS1-0),
- Community Climate System Model (CCSM4),
- National Center for Meteorological Research Coupled Global Climate Model, v5 (CNRM-CM5),
- Geophysical Fluid Dynamics Laboratory Coupled Model (GFDL-CM3),
- Max Planck Institute Coupled Earth System Model (MPI-ESM-LR), and
- Norwegian Earth System Model (NorESM1-M).

Schütte *et al.* (2023) bias corrected the daily rainfall to the spatial resolution of the Quinary catchments, where the bias correction involved matching the GCM output with observations for an identical historical period. To verify whether the GCM output captured the observed record for the SASRI stations, the annual maximum rainfalls derived from the 6 GCMs were plotted against those from the SASRI station AMDRs (Figure 7.41 to Figure 7.79 in Appendix A). Generally, the GCMs' annual maximum rainfalls were found to be greater than the observed values. It is noteworthy that the GCMs' outputs cannot be expected to have the maximum rainfalls at the same time period as the observed values, but are rather useful for evaluating future trends. Therefore, the GCMs were used to analyse the projected rainfall for the region.

Using the annual maximum rainfall from the GCMs, design rainfalls were calculated for the 1-day event for the 2-, 10-, 50- and 100-year return periods. The ratios of changes from the GCMs' present (1961-1990) to the near future (2015-2044) and from the present to the distant future (2070-2099) for design rainfalls were calculated. The average projected changes from the 'present to near future' and the 'present to distant future' for the ensemble mean of the 6 GCMs are shown in Figure 2.7 and Figure 2.8, respectively. The ratios for each GCM for each return period are presented in Appendix A (Figure 7.80 to Figure 7.87).

The majority of sites along the coastline show no increase in 1-day design rainfall for the near future. Slight increases are notable further inland, with the ratios increasing with an increase in return period. Projected changes into the distant future show a 10 – 30% increase in 1-day design rainfalls in many locations.

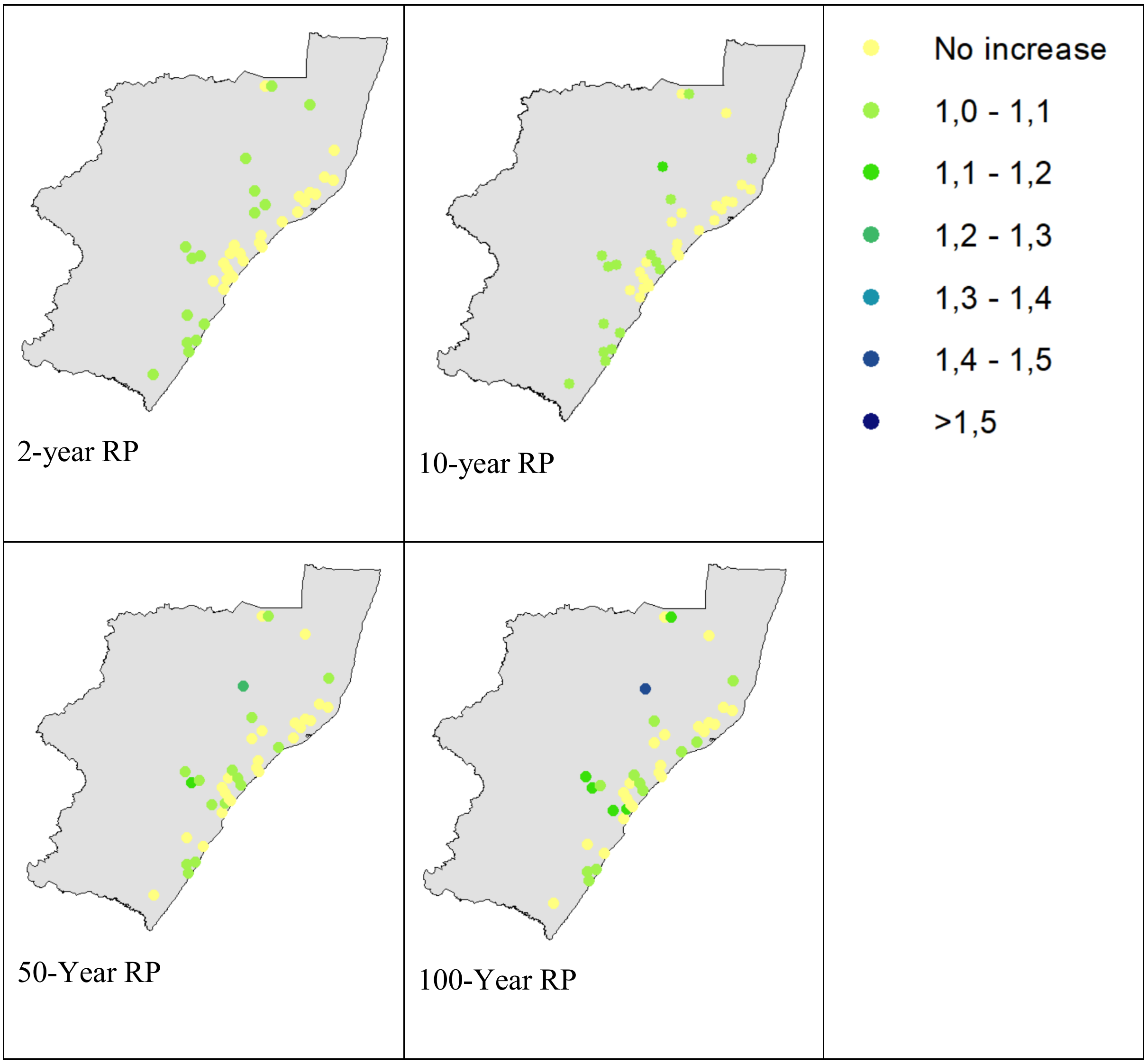

Figure 2.7 Projected changes from the present to the near future in design rainfalls for 1-day design rainfalls for the 2-, 10-, 50-, and 100-year return periods, derived from outputs from multiple GCMs

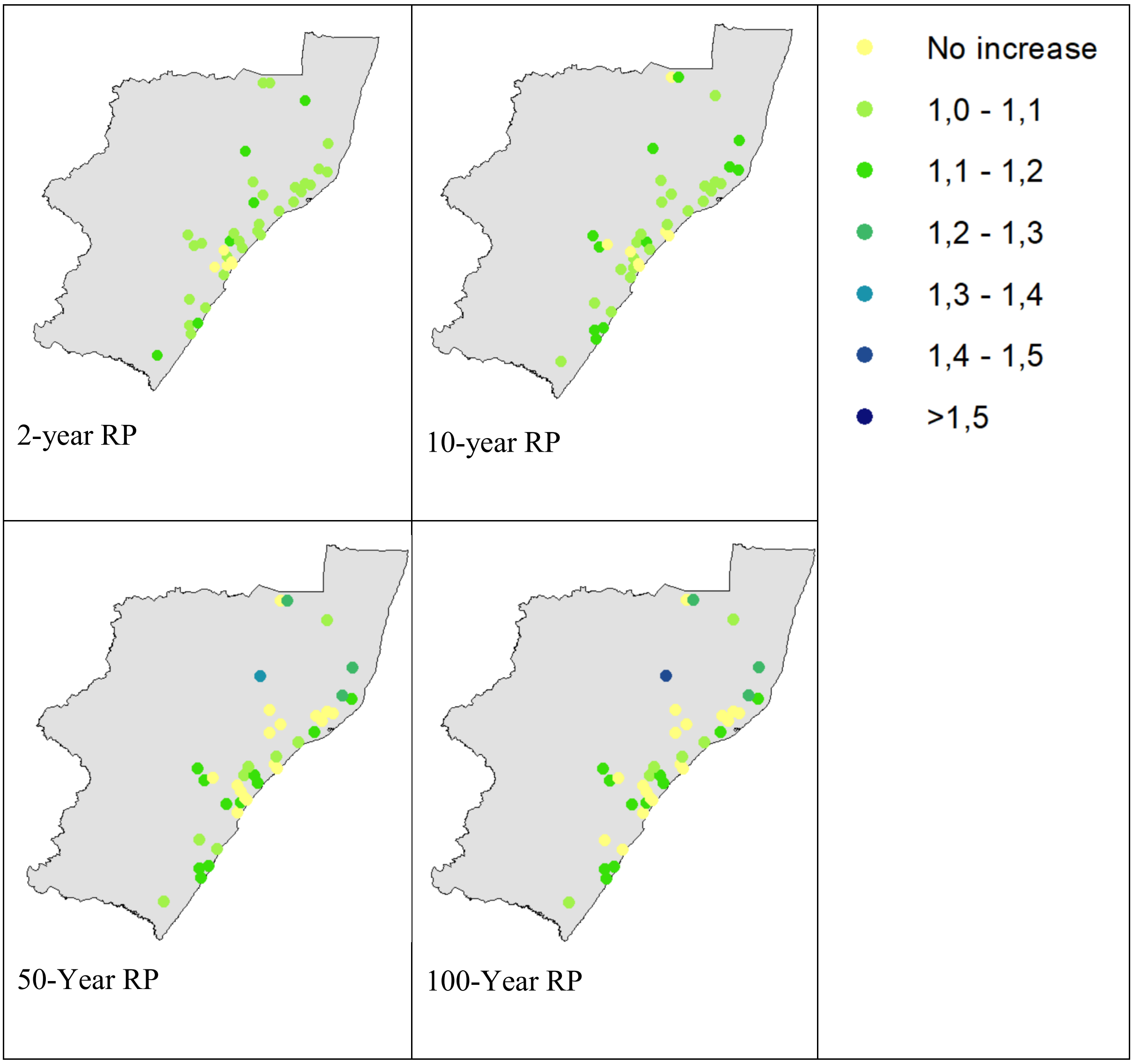

Figure 2.8 Projected changes from the present to the distant future in design rainfalls for 1-day design rainfalls for the 2-, 10-, 50-, and 100-year return period, derived from outputs from multiple GCMs

2.4 Conclusions

The reported increases in extreme rainfall events and their impacts reported from around the world, and particularly the east coast of South Africa in recent years, have motivated a move towards a non-stationary approach to frequency analysis to ensure that the changing properties of extremes are accounted for in design rainfall estimation, and consequently, in the design and flood risk assessent of hydraulic infrastructure.

This chapter investigated the presence of non-stationarity in the annual maximum values of extreme daily rainfalls in KwaZulu-Natal along the east coast of South Africa. The location of the study was chosen based on data availability from SASRI as no data were accessible through SAWS for use in this study. A total of 39 daily rainfall stations with record lengths of at least 40 years were analysed to investigate trends in the occurrences of extreme rainfalls. The MKT and Sen's slope were used to determine the trends in the AMDR, and results indicate that only one station (No. 38) out of 39 showed a significant increasing trend in annual maximum rainfall occurrences. Frequency analysis was performed using both stationary and non-stationary models using time, SOI, DMI, CO_2 and GMT as covariates and the results show that the stationary models are superior to non-stationary models at most stations when using the model diagnostic and selection methods such as AIC, BIC and RMSE. Only changes in the CO_2 covariate were shown to significantly impact the extreme rainfalls. Investigation of trends at other sites in the country located in various climate zones is recommended.

Endris *et al.* (2019) note that although SOI may not exhibit significant changes, the long-term trend in SST and the corresponding changes in atmospheric circulations may influence SOI related teleconnections. This means that if the conditions associated with SOI change, even if the SOI characteristics do not change, then rainfall characteristics can possibly change in regions that respond to SOI. Therefore, investigating future changes in rainfall associated with SOI and other indices driven by SST changes is crucial in understanding the changing vulnerability to extreme events. Further research into understanding the frequency distributions of the actual covariates, and how they are projected to change, is recommended.

With the increasing availability of projected climate information through GCMs, there is greater opportunity to use such data to determine the potential impacts of future climate scenarios on extreme rainfall and flood events using advanced statistical techniques, and to develop methods/tools to incorporate these trends into design rainfall and flood estimation. This study investigated the projected changes in design rainfalls using data from downscaled

GCMs and noted that rainfalls are not projected to change significantly into the near future in the study area. Increases into the distant future along the KZN coastal region are expected to be around 10 – 30% for many parts. The use of projected rainfalls from GCMs should be well guided by the considerations based on the observed rainfall data trends. However, for other parts of the country, these changes could be greater as was found, for example, by Schütte *et al.*, (2022).

The variability of the results of the non-stationary analysis highlights the importance of understanding the trends and drivers of extreme rainfalls and the impacts on design rainfall and design flood estimation. The results of the non-stationary analysis can be improved by investigating the use of other physical covariates or climate drivers, e.g., large weather systems such as Cut-off Lows, as well as combinations of covariates.

The annual maximum series is widely adopted in rainfall frequency analyses, as the sampling process is straightforward. However, using a peaks-over-threshold (POT) model is an alternative approach used to represent the behaviour of exceedances above a selected threshold, and which offers the opportunity to include more observations in the dataset and hence, more flexibility when compared to the use of annual maxima (Pan *et al.*, 2022). Despite the theoretical advantages, the POT is underutilised internationally due to the complexity in the selection of appropriate thresholds. It is recommended that the POT approach be investigated for detecting non-stationarity in extreme rainfall data in South Africa.

This study analysed the 1-day rainfall event. However, in KZN coastal areas extremes are frequently associated with multi-day events. Therefore, the non-stationary analysis of short duration (< 24h), required for DFE in most urban catchments, and multi-day extreme event data is recommended for future research.

3. DETECTING TRENDS IN HYDROLOGICAL EXTREMES AND NON-STATIONARY EXTREME VALUE ANALYSIS OF FLOOD DATA IN KWAZULU-NATAL

D Mukansi, JC Smithers and KA Johnson

3.1 Introduction

In order to minimise the risk of failure of hydrological structures it is vital to ensure that design floods be adequately estimated. The underestimation of design floods can lead to loss of life and significant economic losses, while overestimation may result in over-design which results in adverse economic impacts. The South African Government has reported that the most common weather-related catastrophe in South African between the period 1900 to 2014 were floods, droughts and large storms (DFFE, 2016). Socio-economic losses due to such disasters can be minimised by adequate Design Flood Estimation (DFE).

As with rainfall analysis, the current methods and models used to determine design flood estimates from flow data assume that hydrological outputs remain stationary (Vogel *et al.*, 2011). However, the magnitude and frequency of extreme flood events is changing in many parts of the world (Vogel *et al.*, 2011; Prosdocimi *et al.*, 2014a; Hesarkazzazi *et al.*, 2021). Therefore, there is a need to investigate, and to incorporate if necessary, non-stationary models in DFE in South Africa.

Where observed data are available, frequency analysis of the data is the recommend approach for design rainfall and flood estimation when there is adequate record length and good quality observed data (Smithers, 2012a). The quality of observed flow data is influenced by hydrometrics such as incorrect manual capturing of data, malfunctioning of measuring instruments, poor maintenance of the gauging site and exceedance of the rating table (Nathanael, 2015). Smithers *et al.* (2015) highlighted that South Africa has relatively few streamflow gauging stations which have more than 50 years of good quality data. However, it is important that data are adequately screened to prevent incorrect estimations of design floods (Calitz, 2020).

This chapter includes an analysis of trends in extreme floods along the East Coast of KwaZulu-Natal in South Africa. This study site was selected to complement and correspond to the rainfall analyses conducted in Chapter 2. The aims of the study reported in this chapter are to determine if any trends exist in observed extreme flood events along the East Coast of KwaZulu-Natal, and to evaluate the possible non-stationarity in observed flow data. The objectives are to: (i) collect, screen, and analyse the streamflow data for trends, (ii) perform stationary and non-stationary rainfall frequency analyses, (iii) critically evaluate the stationary vs non-stationary models, and (iv) investigate regional magnification factors to detect trends.

3.2 Materials and Methods

3.2.1 Data sources and case study site selection

The Annual Maximum Series (AMS) streamflow data were obtained from the Department of Water and Sanitation (DWS) website, which provides open access of up-to-date flow data for South Africa. Approximately 90 stations with flow data up to the year 2023 were extracted from the DWS database for stations located in the East Coast region of KwaZulu-Natal.

3.2.2 Data screening and assessment

The flow data were then screened according to the criteria and methods described in Sections 2.2.1. In addition to the criteria used in Section 2.2.1, the data were screened based on the recorded depth of flow. If the recorded depth of flow exceeded the maximum rating table depth, the data were extended by a maximum of 20%. However, the percentage of rating table exceedances recorded in the AMS should be less than 20% of the total record length (Nathanael, 2015).

3.2.2.1 Rating table exceedance

Most streamflow gauging stations do not measure the discharge directly; rather, the stations record the stage height which is correlated with discharge (Petersen-Øverleir and Reitan, 2009). Rating table exceedance refers to an occurrence where the maximum stage rating is exceeded. In this case the discharge associated with the maximum stage rating is recorded by DWS for the observations which exceed the maximum rated stage (Nathanael, 2015). The DWS codes this error with "A", which means that some of the potential high flows are not captured and should be extrapolated (Calitz, 2020).

There are various methods used to extrapolate the rating curve, including the extension of the fitted regression line and the hydraulic analysis which requires additional data (Haddad *et al.*, 2010). The various methods contain uncertainty in the estimation of the extrapolated discharge (Petersen-Øverleir and Reitan, 2009). The challenge with extension of the rating curve using a regression approach is that the larger the extension the greater the uncertainty in the estimated flow (Calitz, 2020). Haddad *et al.* (2010) used the rating ratio approach, which is the ratio of estimated flow to the maximum observed flow to determine the maximum allowable extrapolation. Nathanael (2015), Gericke and Smithers (2018), and Calitz (2020) adopted 20% to be the maximum allowable increase in flow discharge. Based on the selection criteria described in Section 2.2.1 and the rating exceedance criteria, 19 sites were selected for this study. Figure 3.1 shows the locations and Table 3.1 contains a summary of the stations selected.

Figure 3.1 Selected DWS streamflow recording stations along the East Coast of KwaZulu-Natal

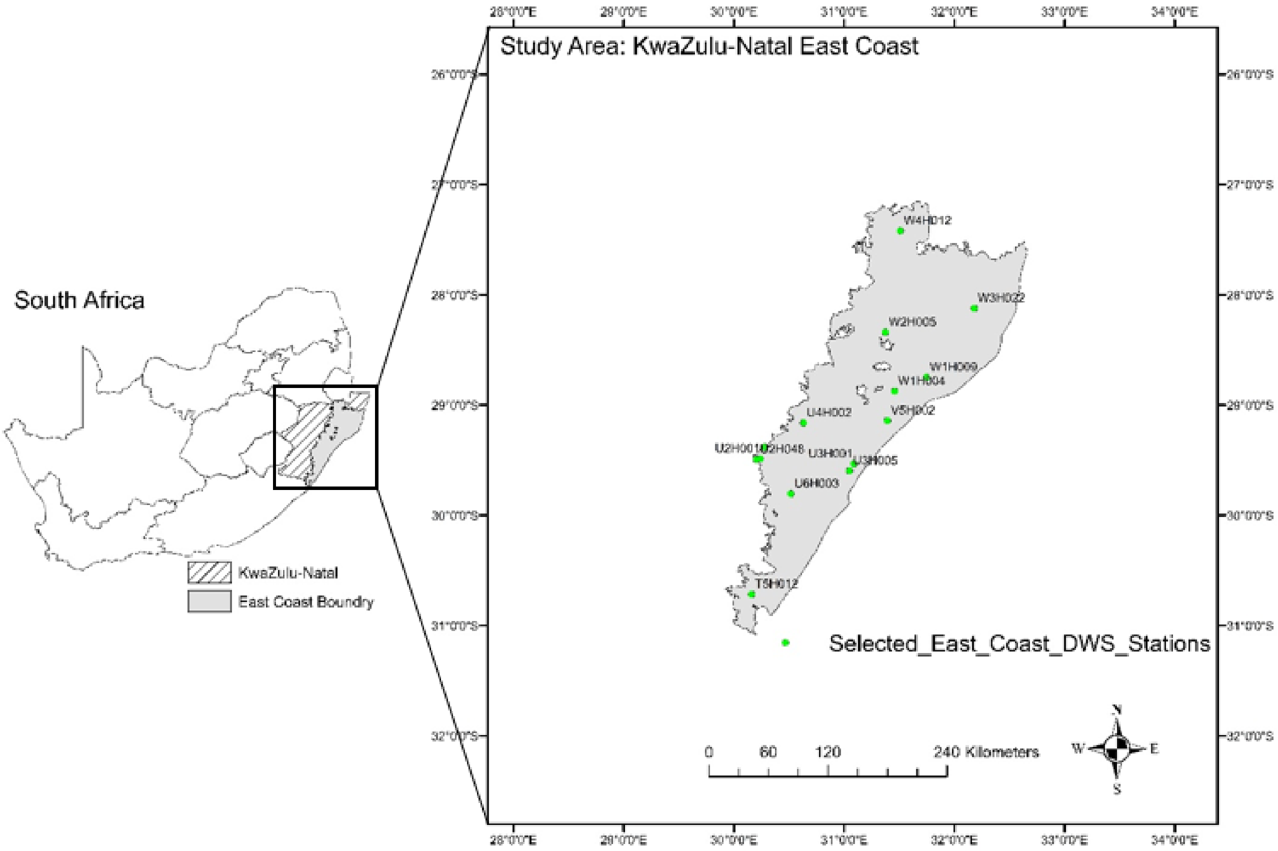

Table 3.1 Station information for case study sites along the East Coast of KwaZulu-Natal

Station Name	DWS Station Number	Start Year	End Year	Record Length (years)
Mzimkhulwana River-Horseshoe	T5H012	1970	2023	53
Mgeni River-Howick	U2H001	1948	1993	45
Mgeni River-Table Mountain	U2H005	1950	2023	73
Karkloof River-Shafton	U2H006	1954	2023	69
Sterk River-Groothoek	U2H012	1960	2023	63
Mgeni River-Albert Falls	U2H014	1964	2023	59
Mgeni River-Midmar	U2H048	1968	2023	55
Mdloti River-Cotton Lands	U3H005	1975	2023	48

Mvoti River-Mistley	U4H002	1949	2023	74
Mlazi River-Umlaas	U6H003	1981	2023	42
Lovu River-Beaulieu Estate	U7H007	1964	2023	59
Tugela River-Mandini	V5H002	1956	2023	67
Mlalazi River-Eshowe	W1H004	1948	2023	75
Mhlatuze-Riverview	W1H009	1960	2023	63
Mhlatuze River-Mhlatuze	W1H028	1979	2023	44
White Mfolozi-Over	W2H005	1960	2020	60
Hluhluwe River-Farm 3/7638	W3H022	1964	2023	59
Right Canal from Phongolo River-The Bokfontein	W4H012	1950	2023	73
Mkuze River @ Rietboklaagte	W3H001	1966	2023	57

3.2.3 Methodology

The basic methodology applied in this study to determine extreme streamflow quantities at a given location, and how they may vary with respect to a selected covariate, are detailed in the following sections. The main steps involved in this approach are summarised in Figure 3.2.

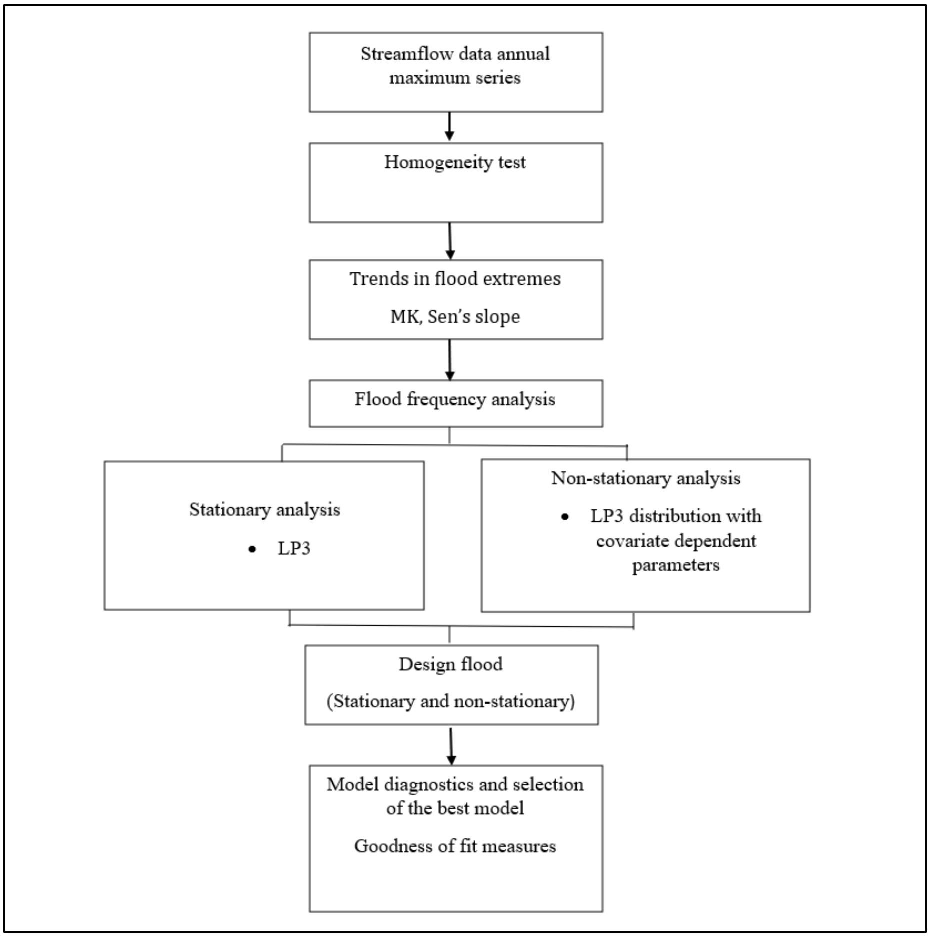

Figure 3.2 Stationary and non-stationary design flood estimation procedures

3.2.3.1 Testing for homogeneity

When performing a trend test it is important that the results reflect only actual changes in the non-stationarity of the hydrological process and not inconsistencies in the measuring system (Xiong and Guo, 2004). There are common measurement errors that occur when data are recorded, such as movement of the gauging station, changes in measurement structures and rating/calibration equations (Mallakpour and Villarini, 2016). A homogeneity test can be used to determine the point/s at which change occur in a data set.

The Pettitt test is a non-parametric method that is used to detect a sudden change in the data set (Conte *et al.*, 2019). A change point is defined as point in the data set where there is a sudden change in the mean, median, and variance. The change may be due to natural or anthropogenic changes in the data set (Scott and Chandler, 2011). The non-parametric method outputs the time of the change and its associated probability (Rougé *et al.*, 2013). The null hypothesis (H_o) of the method is that there is no change in trend, while the alternative hypothesis (H_a) is that there is a trend. The analysis is performed by rejecting the H_o if the probability of the change is greater than the significance level chosen to perform the analysis (Faulkner *et al.*, 2020b). The disadvantage of the method is that it only detects a change at a single point, and that the method categorises gradual trends as sudden changes (Rougé *et al.*, 2013).

3.2.3.2 Trends in flood extremes

The non-parametric Mann-Kendall test and Sen's slope test, as described in Section 2.2.2.1, were used to determine trends in streamflow.

3.2.3.3 Frequency distribution and non-stationary models

Process-informed Nonstationary Extreme Value Analysis (ProNEVA) in MATLAB was used to analyse stationary and non-stationary models. The tool allows the user to incorporate different types of physical drivers and it can be used to model the Log-Pearson Type III (LP3), GEV and Grand Pareto (GPA) distributions. ProNEVA makes use of a newly developed hybrid evolution Markov Chain Monte Carlo approach for uncertainty assessment and numerical parameters estimation (Ragno *et al.*, 2019a). Details of the LP3 methods were reported by Griffis and Stedinger (2007) and Singo *et al.* (2012). Kjeldsen *et al.* (2002) analysed annual maximum floods in KwaZulu-Natal and concluded that the Log-normal, LP3, and GPA distributions were the most suitable models. Görgens (2007) recommended the use of the LP3 and GEV to model floods in South Africa. The LP3 was chosen in this study as it was found to be suitable for floods analysis in most design flood estimation studies in South Africa.

3.2.3.4 Selection of covariates

Time is often used as a proxy for the identification of physical drivers that vary with time such as land use and land cover changes (Hesarkazzazi *et al.*, 2021). These physical drivers are responsible for the change in the annual flood series. In other studies by Villarini *et al.* (2009) and Prosdocimi *et al.* (2014a), extreme rainfall was used as a covariate. Table 3.2 contains a summary of studies that make use of different covariates such as time, population, and rainfall. In a study by Hesarkazzazi *et al.* (2021), rainfall, time and temperature were used as covariates of annual floods and the study concluded that the best model often includes rainfall as a covariate. Owing to the limitation on the availability of data, only time and rainfall were used as covariates in this study.

Table 3.2 Summary of studies that made use of non-stationary models in design flood estimation (after Prosdocimi and Kjeldsen (2021)

Distribution	Variable	Model	Covariate	Reference
Log-Normal LN(μ,σ)	River discharge	Location: $\mu = \mu_0 + \mu_1 x$ scale: $\sigma = \sigma_0$ (constant)	Time	(Vogel *et al.*, 2011)
Gumbel(μ,σ)	River discharge	Location: $\mu = g(x)$ (non-parametric) scale: $\sigma = g(x)$ (non-parametric)	Time, population, and rainfall	(Villarini *et al.*, 2009)
Log-Normal LN(μ,σ)	River discharge	Location: $\mu = \mu_0 + \mu_1 x + \mu_{12} r$ scale: $\sigma = \sigma_0$ (constant)	Time and 99th rainfall	(Prosdocimi *et al.*, 2014a)
Log-Normal LN(μ,σ)	River discharge	Location: $\mu = \mu_0 + \mu_1 x$ scale: $\sigma = \sigma_0$ (constant)	Time	(Zhang *et al.*, 2015)
GEV(μ,σ,ξ)	River discharge	Location: $\mu = \mu_0 + \mu_1 x$ scale: $\exp(\sigma = \sigma_0 + \sigma_1 x)$ (constant) shape: $\xi = \xi_0$ (constant)	Time and rainfall	(Šraj *et al.*, 2016)
Log-Normal LN(μ,σ) and GEV(μ,σ,ξ)	Rainfall or River discharge	Location: $\mu = \mu_0 + \mu_1 x$ scale: $\sigma = \sigma_0$ (constant) shape: $\xi = \xi_0$ (constant)	Time	(Salas *et al.*, 2018)
Log-Normal LN(μ,σ)	River discharge	Location: $\mu = \mu_0 + \mu_1 x$ scale: $\sigma = \sigma_0$ (constant)	Time	(Kjeldsen and Prosdocimi, 2021b)

3.2.3.5 Linking streamflow to rainfall

In order to investigate the relationship between flow and rainfall, flow stations were linked to rainfall stations that fall within the same Quinary catchment. These stations were then used to perform stationary and non-stationary flood frequency analysis with time and rainfall as covariates.

3.2.3.6 Model diagnostics and selection of the best model

The AIC, BIC, and RMSE that as described in detail in Section 2.2.2.4 were used to select the best model.

3.3 Results and Discussion

3.3.1 Homogeneity test

Table 3.3 contains a summary of results of the AMS for 19 stations subjected to the Petit homogeneity test to detect a split in the data, which refers to a point at which there is change in the data set. The results show that six stations (T5H012, U2H005, U2H012, U2H014, U7H007 and W1H028) have a split and are therefore not homogenous. However, Station T5H012 was included in further analysis because the period of data after the split was more than 40 years. Thus 14 stations were retained for further analyses.

Table 3.3 Homogenity test of DWS stations in the East Coast of KwaZulu-Natal

Station Number	Pettit test p value	Interpretation
T5H012	< 0.0001	Not homogenous
U2H001	0.931	Homogenous
U2H005	0.003	Not homogenous
U2H006	0.937	Homogenous
U2H012	0.008	Not homogenous
U2H014	0.046	Not homogenous
U2H048	0.194	Homogenous
U3H005	0.069	Homogenous

U4H002	0.145	Homogenous
U6H003	0.739	Homogenous
U7H007	<0.0001	Not homogenous
V5H002	0.008	Homogenous
W1H004	0.722	Homogenous
W1H009	0.261	Homogenous
W1H028	0.015	Not homogenous
W2H005	0.399	Homogenous
W3H022	0.274	Homogenous
W4H012	0.101	Homogenous
W3H001	0.166	Homogenous

3.3.2 Trend detection

Table 3.4 contains a summary of results of the trend analyses in the AMS for the 14 stations subjected to the MKT and Sen's slope test. The test was performed using the 5% significance level. Based on the tests, the results indicate that majority of the stations along the East Coast of KwaZulu-Natal experienced an insignificant trend, with approximately 21% of stations showing a positive trend and only one station (W4H012), showing a significant positive trend. The Sen's slopes for 79% of the stations are negative, which indicates that even though the trend is not significant at the majority of the stations, the direction of the trend is negative. Figure 8.1 (a-n) in Appendix B contains graphs depicting the time series plot for each station assessed. The linear trend lines in most of the time series graphs are negative, which is consistent with the result of the Mann-Kendall test which resulted in a negative trend for 79% of the stations analysed.

Table 3.4 Trends in annaul maximum streamflows at stations along the East Coast of KwaZulu-Natal using the Mann-Kendall test

Station Number	p-value	Sen's slope	Interpretation of Test
T5H012	0.831	0.182	insignificant positive trend
U2H001	0.688	0.056	insignificant positive trend
U2H006	0.239	-0.099	insignificant negative trend
U2H048	0.099	-0.306	insignificant negative trend
U3H005	**0.012***	**-1.069***	**significant negative trend***
U4H002	0.086	-0.004	insignificant negative trend

Station Number	p-value	Sen's slope	Interpretation of Test
U6H003	0.0452	-0.146	insignificant negative trend
V5H002	**0.00001***	**-25.847***	**significant negative trend***
W1H004	0.819	-0.003	insignificant negative trend
W1H009	0.086	-1.148	insignificant negative trend
W2H005	0.599	-0.033	insignificant negative trend
W3H022	0.306	-0.077	insignificant negative trend
W4H012	**<0.0001***	**0.102***	**significant positive trend***
W3H001	0.078	-0.236	insignificant negative trend

***Significant trends at 5% level identified**

3.3.3 Analysis of stationary and non-stationary models

Both stationary and non-stationary frequency analyses were undertaken using the LP3 distribution for the 14 stations in the study area. For the non-stationary frequency analysis, the location parameter of the LP3 distribution were modelled as linear functions of the selected covariate. The scale and shape parameters were kept constant. The plots, as shown in Figure 8.2 to Figure 8.15 in Appendix B, show no significant differences between the stationary and non-stationary models as both models are under-simulating the high flows.

Table 3.5 contains a summary of results for the AIC, BIC and RMSE tests considering time as a covariate at the 14 stations used in the study. In the majority of the stations AIC and BIC and RMSE values of the stationary model are lower than those of the non-stationary model. The non-stationary models provide a better fit than the corresponding stationary model at only five stations (U3H001, U3H005, V5H002, W1H009 and W4H012). Based on the AIC, the results indicate that 6 out of 14 stations (43%) along the East Coast are better modelled through the stationary model, as low values of AIC and BIC from the same data indicate a better performing model (Faulkner *et al.*, 2020a). Using the BIC measure, the non-stationary models for only one station (U3H005) was found to give a better fit of the data.

Table 3.5 The LP3 statistical model selection criteria of selected sites in the East Coast of KwaZulu-Natal AMS for time as a covariate

Station Number	Stationary			Non-Stationary		
	AIC	**BIC**	**RMSE**	**AIC**	**BIC**	**RMSE**
T5H012	168.38	174.24	21.94	170.24	178.04	**19.25***
U2H001	138.91	144.19	38.25	140.85	147.89	**29.08***
U2H006	185.00	191.75	12.10	186.16	195.15	13.24
U2H048	207.09	213.16	34.94	**206.50***	214.57	40.36
U3H001	107.06	112.16	19.71	**106.37***	113.12	**15.17***
U3H005	176.15	181.37	9782.30	**168.51***	**175.45***	**404.24***
U4H002	167.92	174.15	14.02	168.48	176.79	**13.75***
U6H003	167.27	172.48	24.84	169.36	176.31	31.58
V5H002	122.90	128.58	29.43	**108.19***	**115.76***	**11.72***
W1H004	299.17	305.95	25.47	301.55	310.60	66.88
W1H009	168.59	174.44	32.37	**164.98***	**172.80***	**25.28***
W2H005	123.26	129.28	32.81	123.91	131.94	**32.22***
W3H022	249.08	254.94	64.95	251.06	258.86	**47.91***
W4H012	19.89	26.28	22.27	**-78.60***	**-70.09***	32.32

*** Non-stationary model performs better than stationary model**

Station W4H012 was the only station to show a significant increase in streamflow. This station also showed an increase in the effective return period of streamflow. Figure 3.3 depicts the LP3 for the: (a) stationary model, (b) non-stationary model, and (c) effective return period as a function of time for Station W4H012. The effective return period for Station W4H012 is shown to increase as a function of time for all return periods. Appendix B (Figure 8.2 to Figure 8.15) contains the plots for the stationary and non-stationary frequency analyses for all covariates and effective return periods for all stations.

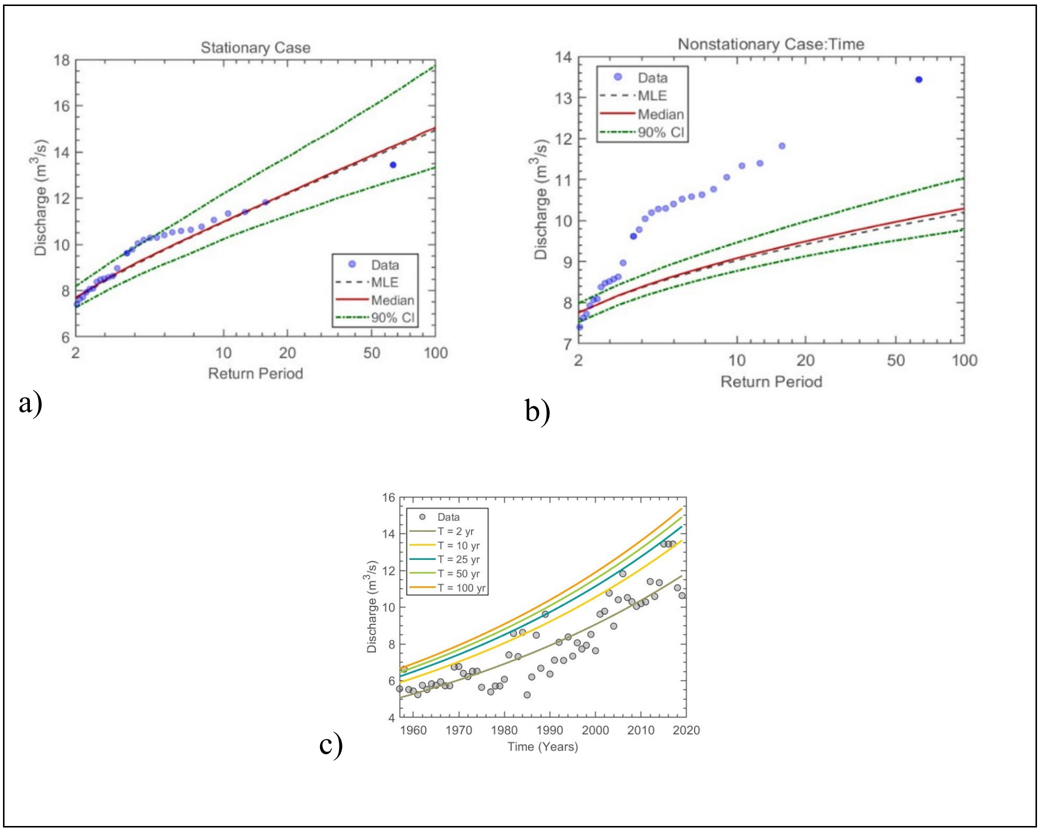

Figure 3.3 The LP3 (a) stationary model, (b) non-stationary model considering time as a covariate, and (c) effective return period as a function of time for Station W4H012

Figure 3.4 and Figure 3.5 show the locations of which models best fit the data based on AIC and BIC, respectively. No spatial patterns are evident based on the location of the best-fit stationary models.

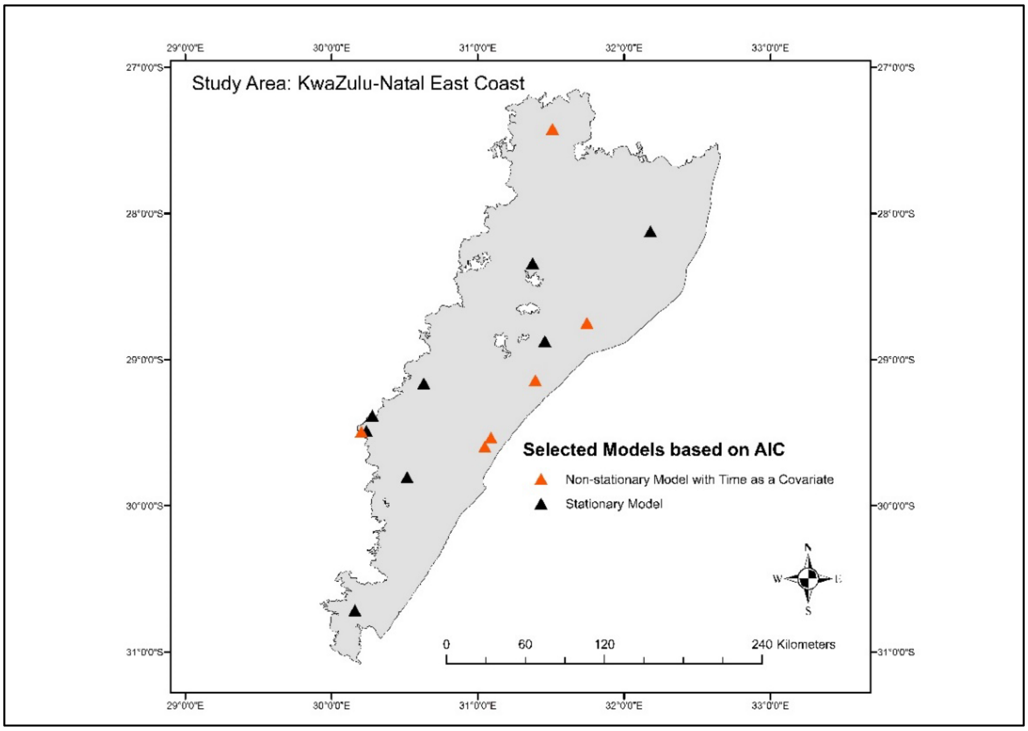

Figure 3.4 Best-fit distribution model, based on the AIC measure

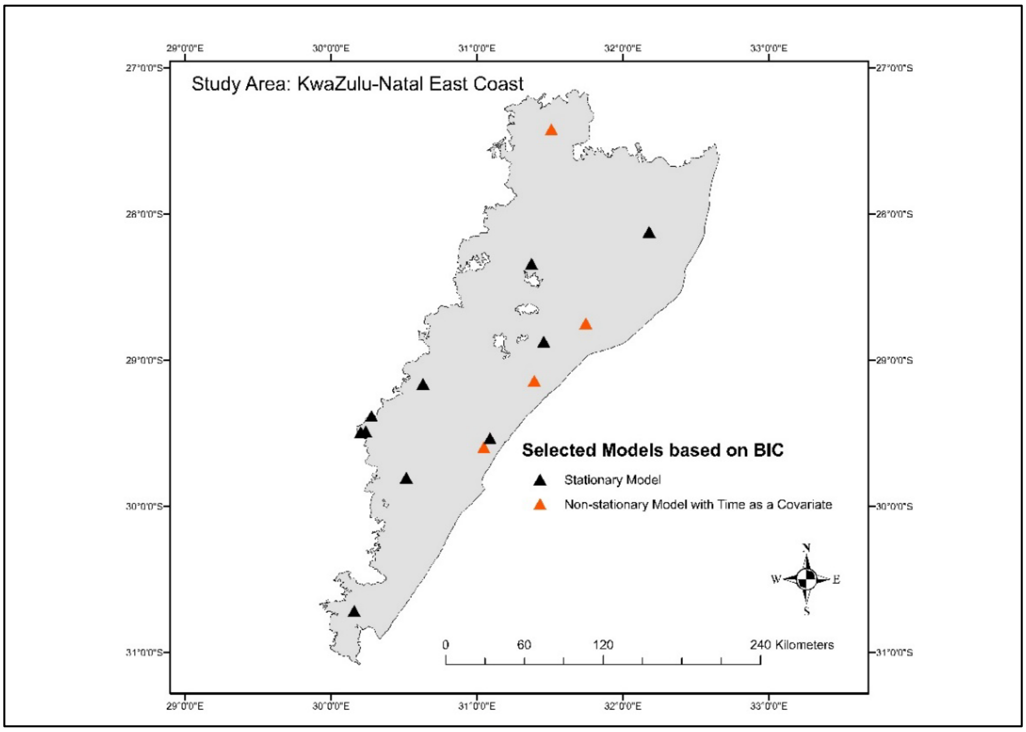

Figure 3.5 Best-fit distribution model, based on the BIC measure

3.3.4 Linking rainfall to flow

Figure 3.6 depicts the time series for annual maximum streamflow and annual maximum rainfall for stations along the East Coast of KwaZulu-Natal. Figure 3.6 (b, c, d, e, and h) show the stations that have a relation between streamflow and rainfall. However, Figure 3.6 (a, f, g, and h) depict the stations (U2H003, W3H008,W4H003, and W3H015) that could not be used for further analysis as there was no correlation between streamflow and rainfall. This could be for a number of reasons, not limited to the location of the raingauges within the catchments, antecedent soil water conditions, and land use change. These stations had more than 20% of the AMS data exceeding the rating table and therefore, did not meet the screening method described in Section 3.2.2 and were discarded from further analyses.

Table 3.6 contains a summary of the best-fit models for the stationary and non-stationary cases based on AIC and BIC measures. The non-stationary models considering time and rainfall as covariates were compared to the stationary models for each station. The detailed results are presented in Table 8.1 in Appendix B. The non-stationary models perform better than the stationary models at 100% and 80% of stations based on the AIC and BIC measures, respectively. Non-stationary model with rainfall as covariate performed better than time as a covariate at 60% of the stations based on AIC, but performed similarly at 40% of the stations with respect to BIC.

The results of this study indicate that the best model of non-stationarity includes rainfall as a covariate. The same conclusion was established by Hesarkazzazi *et al.* (2021) for floods in the northwest of England.

Figure 3.7 and Figure 3.8 show the locations of which models best fit the data based on AIC and BIC, respectively, for those flow stations that are linked to a rainfall station. No spatial patterns are evident based on the location of the best-fit models.

Table 3.6 Summary of best-fit models for all stationary and non-stationary cases

AIC		BIC	
Model	**Number of best-fit models**	**Model**	**Number of best-fit models**
Stationary	0 (0 %)	Stationary	1(20 %)
Non-stationary – Time	2(40 %)	Non-stationary – Time	2 (40 %)
Non-stationary – Rainfall	3 (60 %)	Non-stationary – Rainfall	2 (40 %)

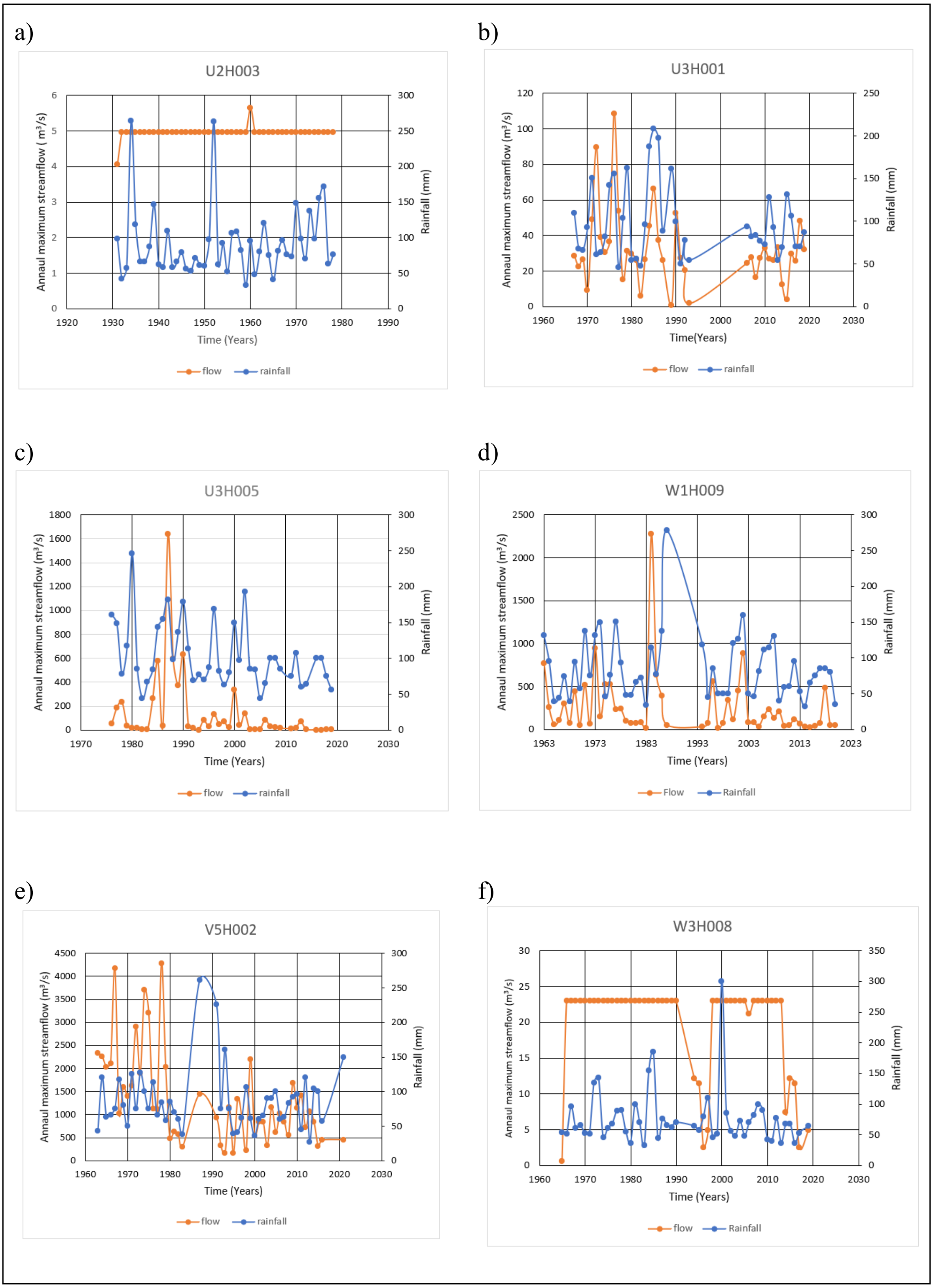
a)
U2H003
Annaul maximum streamflow (m³/s)
Rainfall (mm)
Time (Years)
flow
rainfall
b)
U3H001
Annaul maximum streamflow (m³/s)
Rainfall (mm)
Time(Years)
flow
rainfall
c)
U3H005
Annaul maximum streamflow (m³/s)
Rainfall (mm)
Time (Years)
flow
rainfall
d)
W1H009
Annaul maximum streamflow (m³/s)
Rainfall (mm)
Time (Years)
Flow
Rainfall
e)
V5H002
Annaul maximum streamflow (m³/s)
Rainfall (mm)
Time (Years)
flow
rainfall
f)
W3H008
Annaul maximum streamflow (m³/s)
Rainfall (mm)
Time (Years)
flow
Rainfall

g)

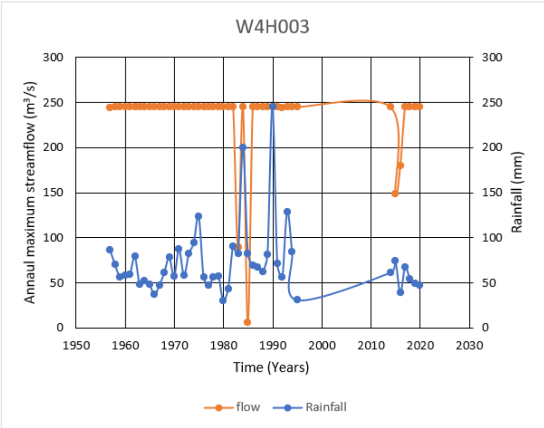

h)

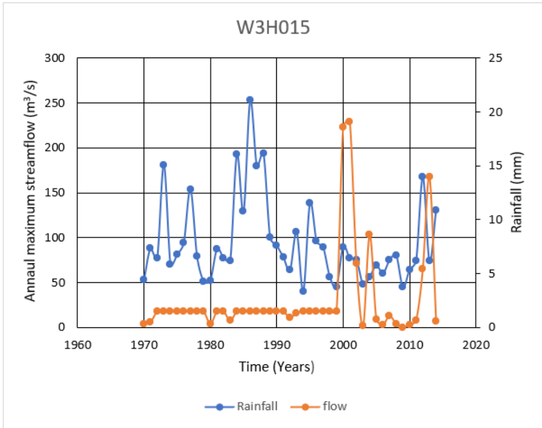

i)

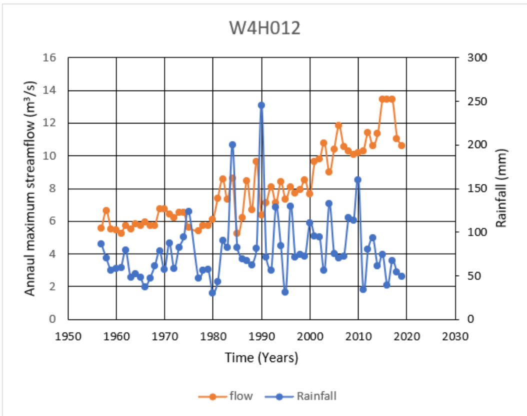

Figure 3.6 Time series for annual maximum streamflow and rainfall stations in the East Coast of KwaZulu-Natal

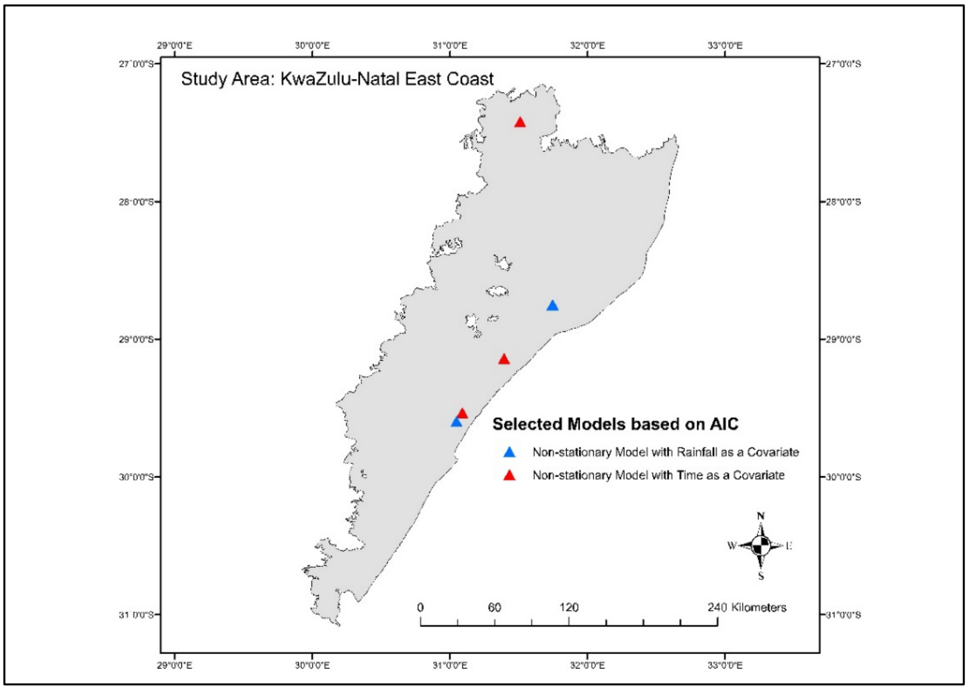

Figure 3.7 Best-fit distribution model, based on the AIC measure for flow stations linked with a rainfall station

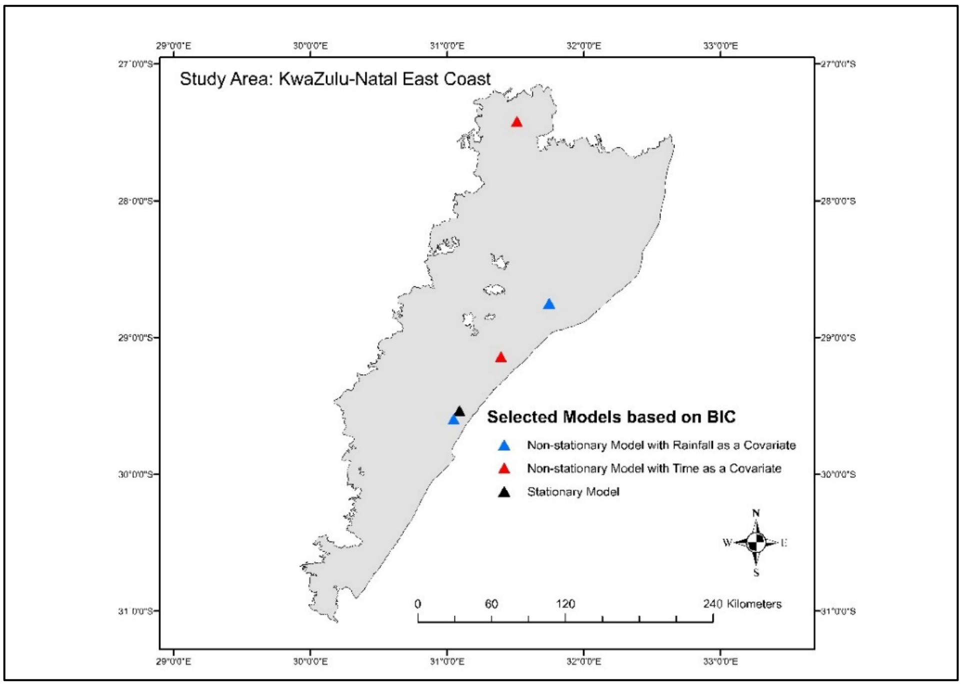

Figure 3.8 Best-fit distribution model, based on the BIC measure for flow stations linked with a rainfall station

3.4 Conclusions

DFE is vital to ensure adequate design and flood rsik assessment of hydraulic structures and to minimise failure due to floods. However, as with rainfall, the current methods used to estimate design floods using streamflow data assume that hydrological conditions remain stationary over time. Studies reported in the literature are challenging this assumption as the frequency and magnitude of extremes are reported to be increasing as consequence of anthropogenic factors such as land use and climate change. Despite advances reported in the international literature, no studies from South Africa have reported the use of non-stationary models in DFE.

The accuracy of the DFE is based on the quality of data used. This chapter details the criteria used to screen and select stations for use in this study and the methodology adopted to determine trends in hydrological extremes of streamflow data. The study area had a total of approximately 90 stations with flow data up to the year 2023 which are available from the DWS website. After screening the data and performing a homogeneity test using the Pettit test, 14 stations were found suitable for further analysis.

The 14 streamflow stations with record lengths of at least 40 years were analysed to detect trends in the occurrences of extreme floods. Trends in annual maximum streamflow data were analysed using the non-parametric Man-Kendall Test. The results showed that approximately 79% of the analysed stations in the East Coast of KwaZulu-Natal had negative trends with approximately 18% of the negative trends being significant ($p < 0.05$). Only one station (W4H012) out of the 14 showed a significant increase in the trend of annual maximum streamflow.

Flood frequency analysis was performed using both stationary and non-stationary models using time and rainfall as covariates. The graphical approach between the different models was similar because the models could not accurately model the high flows for all return periods. This may be attributed to the model failing to model potential outlier events. For non-stationary analysis, the skewness can be varied as a function of a covariate which may be used to improve the simulation in future studies.

The non-stationary analysis was also able to determine the changes in magnitude of floods associated with a particular return period. The results also show that the stationary models are superior to non-stationary models at most stations with time as a covariate when using the model diagnostic and selection methods such as AIC, BIC and RMSE. At selected stations where flow was linked with rainfall, the non-stationary model with rainfall as a covariate performed better than both the stationary model and non-stationary model with time as a covariate. Therefore, further research of trends at other sites in the country located in various climate zones is recommended with rainfall being used as a covariate. Other recommendations include varying the other parameters of the probability distribution as a function of rainfall, especially the skewness as the LP3 disrtirbution.

Regional magnification factors both at site and at regional level were not pursued further in this study as regional magnification factors are dependent on the general direction of the trend of the observed data. Since approximately 79% of the stations analysed in this study showed a negative trend, the magnification factors that would be calculated would results in a decrease in the DFE as these factors would be lower than one. It is recommended that future research investigate the causes of the negative trends in the annual maximum flow data, and more in-depth investigation into trends in the flow which may not be evident in the annual maximum flow data.

4. DISCUSSIONS, CONCLUSIONS AND RECOMMENDATIONS

The ability to reliably estimate the expected magnitude and frequency of extreme rainfall and flood events is fundamental for improving design concepts and risk assessment methods. This is particularly important for extreme events that have significant impacts on society, infrastructure, and human lives, such as extreme precipitation events causing flooding and landslides.

The assumption that hydrological processes remain stationary is still applied for DFE in South Africa. However, several studies have challenged this assumption as the hydrological conditions change due to anthropogenic factors such as climate change, land cover changes, and land use changes. This project aimed to contribute new knowledge on a method to account for non-stationary data, which incorporates the impacts of a changing climate in extreme design rainfall and flood estimates in South Africa. Therefore, the pilot undertaken in this study focussed on investigating trends in extreme rainfall and floods, incorporating non-stationarity in frequency analysis on annual maximum rainfall and streamflow data, and investigating the use of magnification factors to account for trends in varying hydrological conditions.

The results of the trend analysis of rainfall data show weak evidence that the annual maximum daily rainfalls in the study region have been increasing in magnitude over time. In addition, non-stationary analysis of rainfall considering various climate drivers as covariates show that most rainfall records exhibit a stationary behaviour. Results of the analysis of annual maximum streamflow show decreasing trends in magnitude and frequency at the majority of stations. As with rainfall, at most streamflow stations, the stationary models are superior to the non-stationary models when considering changes over time. However, non-stationary models considering rainfall as a covariate were found to often be superior to the corresponding stationary models. Despite the majority of the stations showing an insignificant negative trend, the presence of the trend can be used to challenge the assumption of stationarity.

The outcomes presented in this report are sometimes contrary to the outputs from GCMs reported in international studies, and to reported increases in extreme events in South Africa. This may be due to the limited study area, the limited spatial density and record length of stations, the selected duration of events, and high upstream abstraction of streamflow that cannot be accounted for when performing extreme value analysis. The results may differ in other parts of the country and further analysis on a national scale covering different climatic zones is recommended. Furthermore, the sampling uncertainty of projections from GCMs used to investigate potential future changes in extreme events should be investigated.

The annual maximum series approach, which is widely adopted in rainfall frequency analyses, was used in this study. This approach has the limitation that only the highest event is used per year and thus, other large events within the same year are not captured in the analyses. However, using a peaks-over-threshold (POT) approach is an alternative to the annual maxima approach, which can be used to represent the behaviour of exceedances above a selected threshold. A POT approach offers the opportunity to include more observations in the dataset and hence, more flexibility when compared to the use of only annual maxima (Pan *et al.*, 2022). It is recommended that the POT approach be investigated for detecting non-stationarity in extreme rainfall data in South Africa in future studies.

The identification and analysis of climate drivers of extreme events is vital to understanding the trends of the driving mechanisms of extreme rainfalls and floods. The results of the non-stationary analysis can be improved by investigating the use of other physical covariates or climate drivers, e.g., large weather systems such as Cut-off Lows, as well as combinations of covariates. Rainfall was incorporated in the non-stationary streamflow models as a covariate. However, to link specific rainfall and flood events, rainfall and streamflow should be linked through a hydrological model, e.g. rainfall-runoff model, in future research. Furthermore, catchment rainfall, time of concentration, and flood peaks should be considered in non-stationary rainfall-runoff relationships in future research.

This study analysed the 1-day rainfall and flood events. However, in KZN coastal areas extremes are often associated with multi-day events. Furthermore, extreme events in other parts of the country may be driven by shorter, more intense events occurring within a single day. Therefore, the non-stationary analysis of short duration (< 24h) and multi-day extreme event data is recommended for future research. Given the genrally negative trends in annual maximum flood data, it is recommended that future research investigate the causes of the negative trends in the annual maximum flow data, and more in-depth investigation into trends in the flow which may not be evident in the annual maximum flow data.

Regional magnification factors were not investigated further in this study as the majority of the stations within the study area showed a negative trend, which would mean the application of a regional magnification factor would result in a reduction of the design floods estimated using non-stationary-based methods. However, it is recommended that further investigation into the use of regional magnification factors in other parts of South Africa should be undertaken.

5. CAPACITY BUILDING

The students involved in the project and their roles are summarised in Table 5.1

Table 5.1: List of students involved in the project

Name	Degree	Role	Comment
Ms KA Johnson	PhD Engineering	Project leader, PhD Candidate	Completed research towards doctoral degree with PhD Submitted in December 2023.
Mr DV Mukansi	PhD Engineering	PhD Candidate	Continuing with doctoral degree with intention to submit in 2025.
Mr MS Nyathi	BSc Engineering (Civil)	Undergraduate student	Completed degree and final year research dissertation project in 2022.
Mr N Singh	BSc Engineering (Civil)	Undergraduate student	Completed final year research dissertation project in 2022.

This research has been shared at the South African Hydrological Society Conference in October 2022 and at the International Association of Hydrological Sciences Assembly in Germany in July 2023, and presented at the annual NFSP workshop in May 2024 at Stellenbosch University. These events were attended by practitioners, stakeholders and academic researchers.

6. REFERENCES

Agilan, V and Umamahesh, NV. 2017. Modelling nonlinear trend for developing non-stationaryrainfall intensity–duration–frequency curve. *International Journal of Climatology* 37 (2017): 1265–1281.

Agilan, V and Umamahesh, NV. 2018. Covariate and parameter uncertainty in non-stationary rainfall IDF curve. *International Journal of Climatology* 38 365–383.

Akaike, H. 1974. A new look at the statistical model identification. *IEEE Transactions on Automatic Control* 19 (6): 716 - 723.

Bates, B, Kundzewicz, ZW, Wu, S and Palutikof, J. 2008. *Climate Change and Water. Technical Paper of the Intergovernmental Panel on Climate Change*. IPCC Secretariat, Geneva, Switzerland.

Bureau of Meteorology. 2023. Forcast & Drivers: Climate Driver Update - Climate drivers in the Pacific, Indian and Southern oceans and the Tropics. [Internet]. Available from: http://www.bom.gov.au/climate/enso/. [Accessed: 18 April].

Calitz, JP. 2020. Development and assessment of regionalised approaches to design flood estimation in South Africa. Unpublished PhDEng thesis, School of Engineering, University of KwaZulu-Natal, Pietermaritzburg, South Africa

Cheng, L, AghaKouchak, A, Gilleland, E and Katz, RW. 2014. Non-stationary extreme value analysis in a changing climate. *Climatic Change* 127 (2): 353–369.

Clark, RA.1987. Hydrologic design criteria and climate variability. *Tlie Influence of Climate Change and Climatic Variability on the Hydrologic Regime and Water Resources*, IAHS, Vancouver Symposium.

Coles, S. 2001. *An Introduction to modelling of extreme values*. Springer, London, UK.

Conte, LC, Bayer, DM and Bayer, FM. 2019. Bootstrap Pettitt test for detecting change points in hydroclimatological data: case study of Itaipu Hydroelectric Plant, Brazil. *Hydrological Sciences Journal* 64 (11): 1312-1326.

Cullis, J, Alton, T, Arndt, C, Cartwright, A, Chang, A, Gabriel, S, Gebretsadik, Y, Hartley, F, de Jager, G, Makrelov, K, Robertson, G, Schlosser, CA, Strzepek, K and Thurlow, J. 2015. *An uncertainty approach to modelling climate change risk in South Africa.* WIDER Working Paper 2015/045. World Institute for Development Economics Research, Finland.

de Silva, MT and Hornberger, GM. 2019. Identifying El Niño–Southern Oscillation influences on rainfall with classification models: implications for water resource management of Sri Lanka. *Hydrology and Earth System Sciences* 23 (4): 1905-1929.

Demaria, EMC, Goodrich, D and Keefer, T. 2017. Frequency Analysis of Extreme Sub-Daily Precipitation under Stationary and Non-Stationary Conditions across Two Contrasting Hydroclimatic Environments. *Hydrology and Earth System Sciences*

Department of Environmental Affairs. 2014a. *Climate change adaptation: Perspectives for disaster risk reduction and management in South Africa*. Provisional modelling of drought, flood and sea level rise impacts and a description of adaptation responses, Report no 3 for the Long Term Adaptation Scenarios Research Flagship Program (LTAS) (Draft). Department of Environmental Affairs, Pretoria.

Department of Environmental Affairs. 2014b. *National climate change repsonse: White paper*. Department of Environmental Affairs Pretoria.

Department of Environmental Affairs. 2017. *South Africa's 2nd Annual Climate Change Report 2016*. Department of Environmental Affairs, Pretoria.

DFFE. 2016. Climate information and early warning systems for supporting the Disaster Risk Reduction and Management Sector in South Africa. [Internet]. Department of Environmental Affiars South Africa, Pretoria, South Africa. Available from: https://www.dffe.gov.za/sites/default/files/reports/ltasbook2of7_climateinformationandearlywarningsystemsforsupportingtheDRR.pdf. [Accessed: 09 Novemeber 2022].

Ehsani, N, Vörösmarty, CJ, Fekete, BM and Stakhiv, EZ. 2017. Reservoir operations under climate change: Storage capacity options to mitigate risk. *Journal of Hydrology* 555 (2017): 435–446.

Endris, HS, Lennard, C, Hewitson, BC, Dosio, A, Nikulin, G and Artan, GA. 2019. Future changes in rainfall associated with ENSO, IOD and changes in the mean state over Eastern Africa. *Climate Dynamics* 52 2029–2053.

Faulkner, D, Griffin, A, Hannaford, J, Sharkey, P, Warren, S and Shelton, K. 2020a. b Development of Interim National Guidance on Non-stationary Fluvial Flood Frequency Estimation. *Science Report FRS18087/IG* 1

Faulkner, D, Griffin, A, Hannaford, J, Sharkey, P, Warren, S and Shelton, K. 2020b. b Development of Interim National Guidance on Non-stationary Fluvial Flood Frequency Estimation. *Science Report FRS18087/IG* 1 (1): 1-232.

Faulkner, D, Griffin, A, Hannaford, J, Sharkey, P, Warren, S and Shelton, K. 2020c. *Development of interim national guidance on non-stationary fluvial flood frequency estimation – science report*. FRS18087/IG/R1. Environment Agency, Horizon House, Deanery Road, Bristol, UK.

Fluixá-Sanmartín, J, Morales-Torres, A, Escuder-Bueno, I and Paredes-Arquiola, J. 2019. Quantification of climate change impact on dam failure risk under hydrological scenarios: a case study from a Spanish dam. *Natural Hazards and Earth System Sciences* 19 (2019): 2117–2139.

Fuller, WE. 1914. Flood flows. *Transactions of the American Society of Civil Engineers* 77: 564-617.

Gao, M and Zheng, H. 2018. Nonstationary extreme value analysis of temperature extremes in China. *Stochastic Environmental Research and Risk Assessment* 32 1299–1315.

Gaughan, AE, Staub, CG, Hoell, A, Weaver, A and Waylen, PR. 2016. Inter- and Intra-annual precipitation variability and associated relationships to ENSO and the IOD in southern Africa. *International Journal of Climatology* 36 1643–1656.

Gericke, O and Smithers, J. 2018. An improved and consistent approach to estimate catchment response time parameters: Case study in the C5 drainage region, South Africa. *Journal of Flood Risk Management* 11 S284-S301.

Global Carbon Atlas. 2023. Global carbon Atlas - Emissions. [Internet]. Available from: https://globalcarbonatlas.org/emissions/carbon-emissions/. [Accessed: 23 June].

Görgens, A. 2007. *Joint peak-volume (JPV) design flood hydrographs for South Africa*. Water Research Commission Pretoria, South Africa.

Gregersen, IB, Madsen, H, Rosbjerg, D and Arnbjerg-Nielsen, K. 2017. A regional and nonstationary model for partial duration series of extreme rainfall. *Water Resources Research* 53 2659–2678.

Griffis, V and Stedinger, J. 2007. Log-Pearson type 3 distribution and its application in flood frequency analysis. I: Distribution characteristics. *Journal of Hydrologic Engineering* 12 (5): 482-491.

Haddad, K, Rahman, A, Weinmann, PE, Kuczera, G and Ball, J. 2010. Streamflow data preparation for regional flood frequency analysis: Lessons from southeast Australia. *Australasian Journal of Water Resources* 14 (1): 17-32.

Hao, Z and Singh, VP. 2013. Entropy-based method for extreme rainfall analysis in Texas. *Journal of geophysical research: atmospheres* 118 263–273.

Hattingh, L.2021. Surveillance and climate change. In: ed. WRC, *Roadshow: Advancing Dam Safety in The Context of Climate Change in South Africa*, Water Research Commission, RSA

Hesarkazzazi, S, Arabzadeh, R, Hajibabaei, M, Rauch, W, Kjeldsen, TR, Prosdocimi, I, Castellarin, A and Sitzenfrei, R. 2021. Stationary vs non-stationary modelling of flood frequency distribution across northwest England. *Hydrological Sciences Journal* 66 (4): 729-744.

Hoell, A, Gaughan, AE, Magadzire, T and Harrison, L. 2021. The Modulation of Daily Southern Africa Precipitation by El Niño–Southern Oscillation across the Summertime Wet Season. *Journal of Climate* 34 (3): 1115–1134.

HRU. 1972. *Design flood determination in South Africa*. 1/72. Hydrological Research Institute, University of the Witwatersrand, Johannesburg, RSA.

IPCC. 2017a. *Climate updates.* The Royal Society, London, United Kingdoms.

IPCC. 2017b. *Climate updates. What have we learnt since the IPCC 5th Assessment Report*. The Royal Society, London.

IPCC. 2018. Summary for Policymakers. In: eds. Masson-Delmotte, V, Pörtner, H-O, Skea, J, Zhai, P, Roberts, D, Shukla, PR, A. Pirani, W. Moufouma-Okia, C. Péan, R. Pidcock, S. Connors, J. B. R. Matthews, Y. Chen, X. Zhou, M. I. Gomis, E. Lonnoy, T. Maycock, M. Tignor and Waterfield, T, *Global warming of 1.5°C. An IPCC Special Report on the impacts of global warming of 1.5°C above pre-industrial levels and related global greenhouse gas emission pathways, in the context of strengthening the global response to the threat of climate change, sustainable development, and efforts to eradicate poverty*. World Meteorological Organization, Geneva, Switzerland.

Johnson, K, Smithers, J and Schulze, R. 2021. A review of methods to account for impacts of non-stationary climate data on extreme rainfalls for design rainfall estimation in South Africa. *Journal of the South African Institution of Civil Engineering* 63 (3): 55-61.

Johnson, KA and Smithers, JC. 2020. Updating the estimation of 1-day probable maximum precipitation in South Africa. *Journal of Hydrology: Regional Studies* 32 (2020): 1-15.

Kendall, M. 1962. *Rank CorrelationMethods*. Hafner Publishing Company, New York, NY. USA.

Kibii, J. 2021. Assesment of Seasonal and Annual Trends and Variability in South Africa. Unpublished thesis, Faculty of Engineering, Stellenbosch Uninversity, South Africa.

Kjeldsen, T and Prosdocimi, I. 2021a. Assessment of trends in hydrological extremes using regional magnification factors. *Advances in Water Resources* 149 (2021): 103852.

Kjeldsen, TR and Prosdocimi, I. 2021b. Assessment of trends in hydrological extremes using regional magnification factors. *Advances in Water Resources* 149 103852.

Kjeldsen, TR, Smithers, J and Schulze, R. 2002. Regional flood frequency analysis in the KwaZulu-Natal province, South Africa, using the index-flood method. *Journal of hydrology* 255 (1-4): 194-211.

Kundzewicz, ZW. 2019. *Changes in flood risk in Europe*. CRC Press, Postdam, Germany.

Lüdecke, H-J, Müller-Plath, G, Wallace, MG and Lüning, S. 2021. Decadal and multidecadal natural variability of African rainfall. *Journal of Hydrology: Regional Studies* 34 (2021): 100795.

Luxford, F and Faulkner, D. 2020. *Recommendations for future research and practice on non-stationarity in UK flooding*. Report FRS18087/REA/R2. Bristol, UK.

Mallakpour, I and Villarini, G. 2016. A simulation study to examine the sensitivity of the Pettitt test to detect abrupt changes in mean. *Hydrological Sciences Journal* 61 (2): 245-254.

Mangini, W, Viglione, A, Hall, J, Hundecha, Y, Ceola, S, Montanari, A, Rogger, M, Salinas, JL, Borzì, I and Parajka, J. 2018. Detection of trends in magnitude and frequency of flood peaks across Europe. *Hydrological Sciences Journal* 63 (4): 493-512.

Mann, HB. 1945. Nonparametric tests against trend. *Econometrica* 13 (3): 245–259.

Mathivha, F, Nkosi, M and Mutoti, M. 2021. Evaluating the relationship between hydrological extremes and groundwater in Luvuvhu River Catchment, South Africa. *Journal of Hydrology: Regional Studies* 37 100897.

McBride, C, Kruger, AC and L.Dyson. 2022. Changes in extreme daily rainfall characteristics in South Africa: 1921–2020. *Weather and Climate Extremes* 38 100517.

Moyo, P and Nyoni, B.2021. Impact of Climate on the Safety of Concrete Arch Dams. In: ed. WRC, *Roadshow: Advancing Dam Safety in The Context of Climate Change in South Africa*,

Nathanael, J, Jonathan. 2015. Assessing the performance of regional flood frequency analysis methods in South Africa. Unpublished MSc thesis, School of Hydrology University of KwaZulu-Natal, Pietermaritzburg, South Africa

National Aeronautics and Space Administration. 2023. Global Climate Change: Vital Signs - Global Temperature. [Internet]. Available from: https://climate.nasa.gov/vital-signs/global-temperature/. [Accessed: 23 July].

Ouarda, TBMJ, Charron, C and St-Hilaire, A. 2020. Uncertainty of stationary and nonstationary models for rainfall frequency analysis. *International Journal of Climatology* 40 2373–2392.

Pan, X, Rahman, A, Haddad, K and Ouarda, TBMJ. 2022. Peaks-over-threshold model in flood frequency analysis: a scoping review. *Stochastic Environmental Research and Risk Assessment* 36 (2022): 2419–2435.

Pedretti, D and Irannezhad, M. 2019. Non-stationary peaks-over-threshold analysis of extreme precipitation events in Finland, 1961–2016. *International Journal of Climatology* 39 1128–1143.

Petersen-Øverleir, A and Reitan, T. 2009. Accounting for rating curve imprecision in flood frequency analysis using likelihood-based methods. *Journal of Hydrology* 366 (1-4): 89-100.

Pfahl, S, O'Gorman, PA and Fischer, EM. 2017. Understanding the regional pattern of projected future changes in extreme precipitation. *Nature Climate Change*

Pinto, I, Zachariah, M, Wolski, P, Landman, S, Phakula, V, Maluleka, W, Bopape, M, Engelbrecht, C, Jack, C, McClure, A, Bonnet, R, Vautard, R, Philip, S, Kew, S, Heinrich, D, Vahlberg, M, Singh, R, Arrighi, J, Thalheimer, L, Van Aalst, M, Li, S, Sun, J, Vecchi, G, Yang, W, Tradowsky, J, Otto, F and Dipura, R. 2022. Climate change exacerbated rainfall causing devastating flooding in Eastern South Africa. *World weather attribution intiative* 1 (1): 1-31.

Prosdocimi, I, Kjeldsen, T and Svensson, C. 2014a. Non-stationarity in annual and seasonal series of peak flow and precipitation in the UK. *Natural Hazards and Earth System Sciences* 14 (5): 1125-1144.

Prosdocimi, I, Kjeldsen, TR and Svensson, C. 2014b. Non-stationarity in annual and seasonal series of peak flow and precipitation in the UK. *Natural Hazards and Earth Systems Sciences* 14 1125–1144.

Ragno, E, AghaKouchak, A, Cheng, L and Sadegh, M. 2019a. A generalized framework for process-informed nonstationary extreme value analysis. *Advances in Water Resources* 130 270-282.
Ragno, E, AghaKouchak, A, Cheng, L and Sadegh, M. 2019b. A generalized framework for process-informed nonstationary extreme value analysis. *Advances in Water Resources* 130 (2019): 270–282.
Ragno, E, AghaKouchak, A, Cheng, L and Sadegh, M. 2019c. Process-informed Nonstationary Extreme Value Analysis (ProNEVA) User Manual.
Rastogi, D, Kao, S-C, Ashfaq, M, Mei, R, Kabela, ED, Gangrade, S, Naz, BS, Preston, BL, Singh, N and Anantharaj, VG. 2017. Effects of climate change on probable maximum precipitation: A sensitivity study over the Alabama-Coosa-Tallapoosa River Basin. *Journal of geophysical research: atmospheres* 122 4808–4828.
Rougé, C, Ge, Y and Cai, X. 2013. Detecting gradual and abrupt changes in hydrological records. *Advances in Water Resources* 53 33-44.
Rouhani, H. 2016. Climate change impact on probable maximum precipitation and probable maximum flood in Québec. Unpublished thesis, Department of Civil Engineering, University of Sherbrooke, Québec, Canada.
Sadegh, M, Vrugt, JA, Xu, C and Volpi, E. 2015. The stationarity paradigm revisited: hy- pothesis testing using diagnostics, summary metrics, and DREAM(ABC). *Water Resources Research* 51 (11): 9207–9231.
Salas, J, Obeysekera, J and Vogel, R. 2018. Techniques for assessing water infrastructure for nonstationary extreme events: a review. *Hydrological Sciences Journal* 63 (3): 325-352.
Sarhadi, A and Soulis, ED. 2017. Time-varying extreme rainfall intensity-duration-frequency curves in a changing climate,. *Geophysical Research Letters* 44 2454–2463.
Schütte S, Schulze RE, Clark DJ, , Kunz, RP, Wolski, P, Lumsden, T, Smithers, JC, Stuart-Hill, SI, Thornton-Dibb, SLC, Horan, MJC, Toucher, ML and Jele, Z (2023). A *national assessment of potential climate change impacts on the hydrological yield of different hydro-climatic zones of South Africa: Report 1 - methodology and results*. in Eds Schütte S, Schulze RE, Clark DJ, WRC Report No. 2833/1/22, Water Research Commission, Pretoria, South Africa.
Schwarz, G. 1978. Estimating the dimension of a model. *The Annals of Statistics* 6 (2): 461-464.
Scott, M and Chandler, R. 2011. *Statistical methods for trend detection and analysis in the environmental sciences*. John Wiley & Sons, London, United Kingdom.
Sen, PK. 1968. Estimates of the Regression Coefficient based on Kendall's Tau. *Journal of the American Statistical Association* 63 (324): 1379-1389.
Serinaldi, F and Kilsby, CG. 2015. Stationarity is undead: Uncertainty dominates the distribution of extremes. *Advances in Water Resources* 77 17-36.
Silva, DF, Simonovic, SP, Schardong, A and Goldenfum, AV. 2021. Assessment of non-stationary IDF curves under a changing climate: Case study of different climatic zones in Canada. *Journal of Hydrology: Regional Studies* 36 (2021): 100870.
Singh, K. 2019. Durban floods damage estimated at over R650m. [Internet]. News24, Durban, South Africa. Available from: https://www.news24.com/News24/durban-floods-damage-estimated-at-over-r650m-20190426. [Accessed: 09 November 2022].
Singo, L, Kundu, P, Odiyo, J, Mathivha, F and Nkuna, T. 2012. Flood frequency analysis of annual maximum stream flows for Luvuvhu river catchment, Limpopo province, South Africa.
Smithers, J. 2012a. Methods for design flood estimation in South Africa. *Water SA* 38 (4): 633-646.
Smithers, J, Streatfield, J, Gray, R and Oakes, E. 2015. Performance of regional flood frequency analysis methods in KwaZulu-Natal, South Africa. *Water SA* 41 (3): 390-397.

Smithers, JC. 1996. Short-duration rainfall frequency model selection in Southern Africa. *Water SA* 22 (3): 211-217.
Smithers, JC. 2012b. Review of methods for design flood estimation in South Africa. *Water SA* 38 (4): 633-646.
Smithers, JC, Görgens, A, Gericke, J, Jonker, V and Roberts, CPR. 2014. *The initiation of a national flood studies programme for South Africa*. RSA.
Smithers, JC, Görgens, A, Gericke, J, Jonker, V and Roberts, CPR. 2016. *The Initiation of a National Flood Studies Programme for South Africa*. South African National Committee on Large Dams (SANCOLD), Pretoria, South Africa.
Smithers, JC and Schulze, RE. 2000. *Long duration design rainfall estimates for South Africa*. 811/1/00. Water Research Commission, Pretoria, RSA.
Song, X, Zou, X, Mo, Y, Zhang, J, Zhang, C and Tian, Y. 2020. Nonstationary bayesian modeling of precipitation extremes in the Beijing-Tianjin-Hebei Region, China. *Atmospheric Research* 242
Šraj, M, Viglione, A, Parajka, J and Blöschl, G. 2016. The influence of non-stationarity in extreme hydrological events on flood frequency estimation. *J. Hydrol. Hydromech* 64 (4): 426-437.
Tan, X and Gan, TY. 2017. Non-stationary analysis of the frequency and intensity of heavy precipitation over Canada and their relations to large-scale climate patterns. *Climate Dynamics* 48 2983–3001.
Thoithi, W, Blamey, RC and Reason, CJC. 2023. April 2022 Floods over East Coast South Africa: Interactions between a Mesoscale Convective System and a Coastal Meso-Low. *Atmosphere* 14 (78): 1-23.
Vasiliades, L, Galiatsatou, P and Loukas, A. 2015. Nonstationary frequency analysis of annual maximum rainfall using climate covariates. *Water Resource Management* 29 339–358.
Villarini, G, Smith, JA, Serinaldi, F, Bales, J, Bates, PD and Krajewski, WF. 2009. Flood frequency analysis for nonstationary annual peak records in an urban drainage basin. *Advances in water resources* 32 (8): 1255-1266.
Vogel, RM, Yaindl, C and Walter, M. 2011. Nonstationarity: flood magnification and recurrence reduction factors in the United States 1. *JAWRA Journal of the American Water Resources Association* 47 (3): 464-474.
WRC. 2021. Roadshow: Advancing Dam Safety in The Context of Climate Change in South Africa. [Internet]. Available from: https://wrc.org.za/?mdocs-file=61565. [Accessed: 12 May].
Xiong, L and Guo, S. 2004. Trend test and change-point detection for the annual discharge series of the Yangtze River at the Yichang hydrological station/Test de tendance et détection de rupture appliqués aux séries de débit annuel du fleuve Yangtze à la station hydrologique de Yichang. *Hydrological sciences journal* 49 (1): 99-112.
Yilmaz, AG, Hossain, I and Perera, BJC. 2014. Effect of climate change and variability on extreme rainfall intensity–frequency–duration relationships: A case study of Melbourne. *Hydrology and Earth System Sciences* 18 4065–4076.
Yilmaz, AG and Perera, BJC. 2015. Spatiotemporal Trend Analysis of Extreme Rainfall Events in Victoria, Australia. *water Resource Management* 29 (2015): 4465–4480.
Zhang, Q, Gu, X, Singh, VP, Xiao, M and Xu, CY. 2015. Flood frequency under the influence of trends in the Pearl River basin, China: changing patterns, causes and implications. *Hydrological Processes* 29 (6): 1406-1417.

Zhou, C, R, Chen, Y, F, Gu, S, H, Huang, Q, Yuan, J, C and Yu, S, N. 2016. A new threshold selection method for peak over for non-stationary time series. *IOP Conference Series: Earth and Environmental Science* 39

Ziervogel, G, New, M, Archer van Garderen, E, Midgley, G, Taylor, A, Hamann, R, Stuart-Hill, S, Myers, J and Warburton, M. 2014. Climate change impacts and adaptation in South Africa. *WIREs Climate Change* 5 605–620.

7. APPENDIX A: Non-stationary Frequency Analysis of Extreme Rainfalls in KwaZulu-Natal

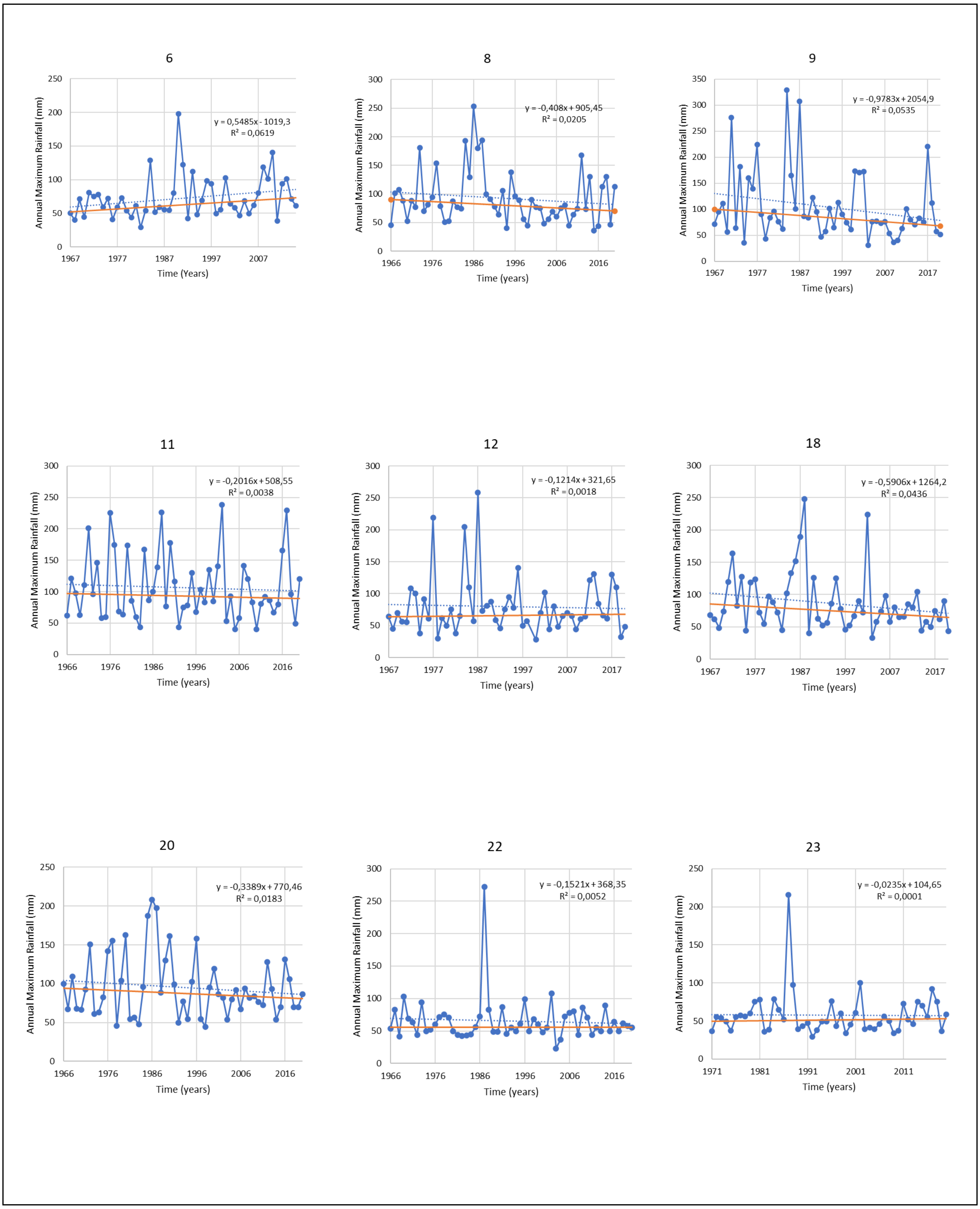
6
y = 0,5485x - 1019,3
R² = 0,0619
Annual Maximum Rainfall (mm)
Time (Years)
8
y = -0,408x + 905,45
R² = 0,0205
Annual Maximum Rainfall (mm)
Time (years)
9
y = -0,9783x + 2054,9
R² = 0,0535
Annual Maximum Rainfall (mm)
Time (years)
11
y = -0,2016x + 508,55
R² = 0,0038
Annual Maximum Rainfall (mm)
Time (years)
12
y = -0,1214x + 321,65
R² = 0,0018
Annual Maximum Rainfall (mm)
Time (years)
18
y = -0,5906x + 1264,2
R² = 0,0436
Annual Maximum Rainfall (mm)
Time (years)
20
y = -0,3389x + 770,46
R² = 0,0183
Annual Maximum Rainfall (mm)
Time (years)
22
y = -0,1521x + 368,35
R² = 0,0052
Annual Maximum Rainfall (mm)
Time (years)
23
y = -0,0235x + 104,65
R² = 0,0001
Annual Maximum Rainfall (mm)
Time (years)

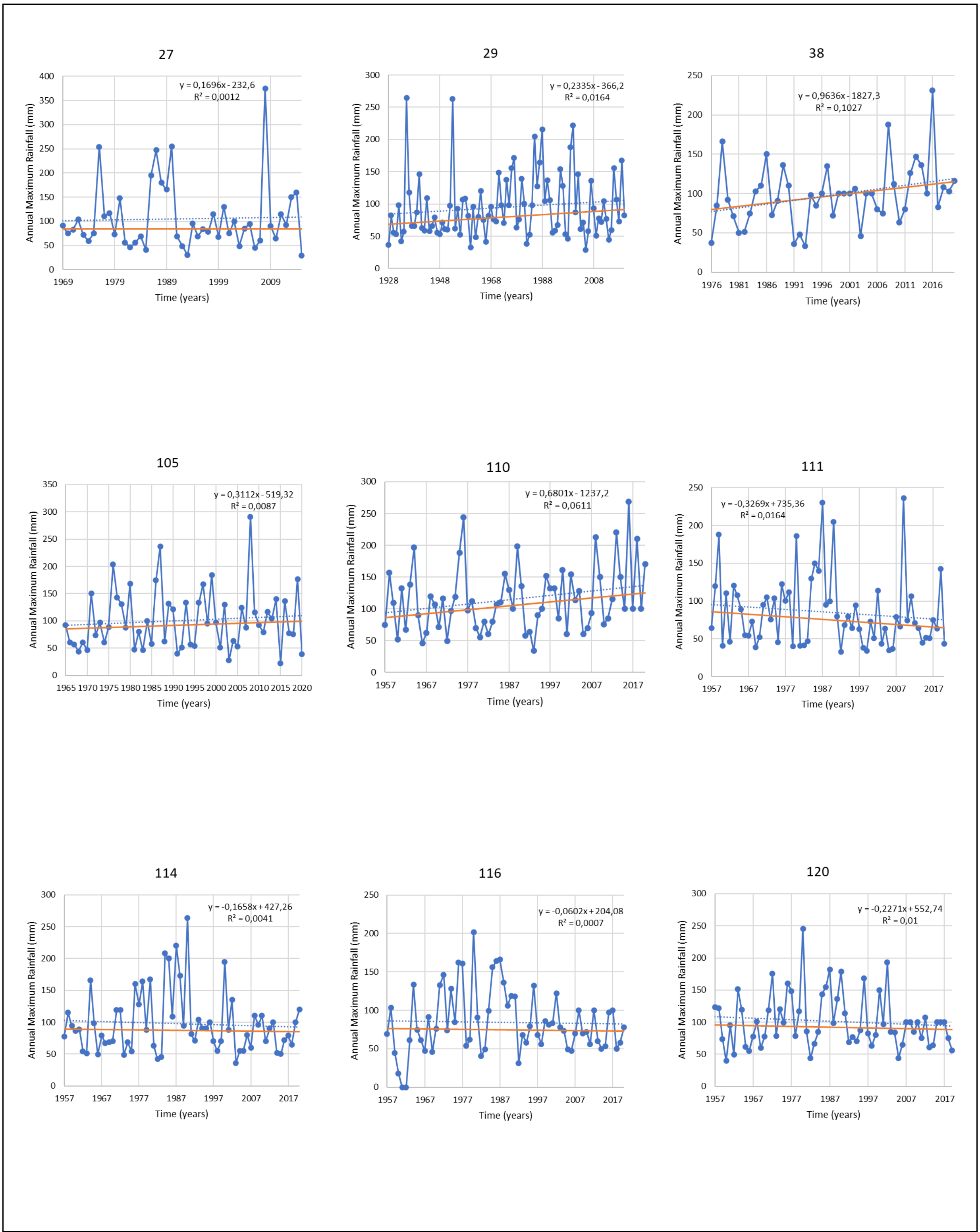
27
y = 0,1696x - 232,6
R² = 0,0012
Annual Maximum Rainfall (mm)
Time (years)
29
y = 0,2335x - 366,2
R² = 0,0164
Annual Maximum Rainfall (mm)
Time (years)
38
y = 0,9636x - 1827,3
R² = 0,1027
Annual Maximum Rainfall (mm)
Time (years)
105
y = 0,3112x - 519,32
R² = 0,0087
Annual Maximum Rainfall (mm)
Time (years)
110
y = 0,6801x - 1237,2
R² = 0,0611
Annual Maximum Rainfall (mm)
Time (years)
111
y = -0,3269x + 735,36
R² = 0,0164
Annual Maximum Rainfall (mm)
Time (years)
114
y = -0,1658x + 427,26
R² = 0,0041
Annual Maximum Rainfall (mm)
Time (years)
116
y = -0,0602x + 204,08
R² = 0,0007
Annual Maximum Rainfall (mm)
Time (years)
120
y = -0,2271x + 552,74
R² = 0,01
Annual Maximum Rainfall (mm)
Time (years)

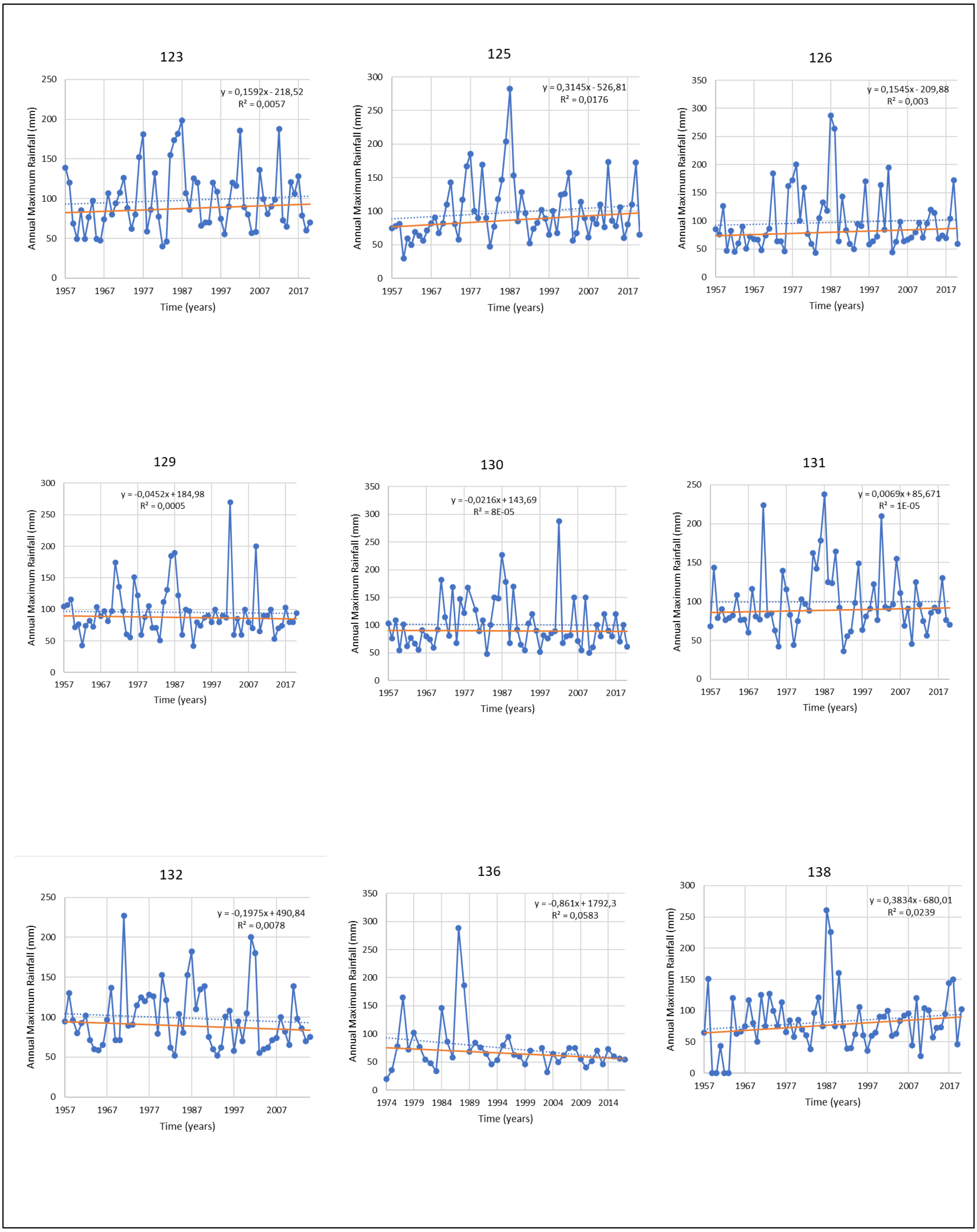
123
y = 0,1592x - 218,52
R² = 0,0057
125
y = 0,3145x - 526,81
R² = 0,0176
126
y = 0,1545x - 209,88
R² = 0,003
129
y = -0,0452x + 184,98
R² = 0,0005
130
y = -0,0216x + 143,69
R² = 8E-05
131
y = 0,0069x + 85,671
R² = 1E-05
132
y = -0,1975x + 490,84
R² = 0,0078
136
y = -0,861x + 1792,3
R² = 0,0583
138
y = 0,3834x - 680,01
R² = 0,0239
Annual Maximum Rainfall (mm)
Time (years)

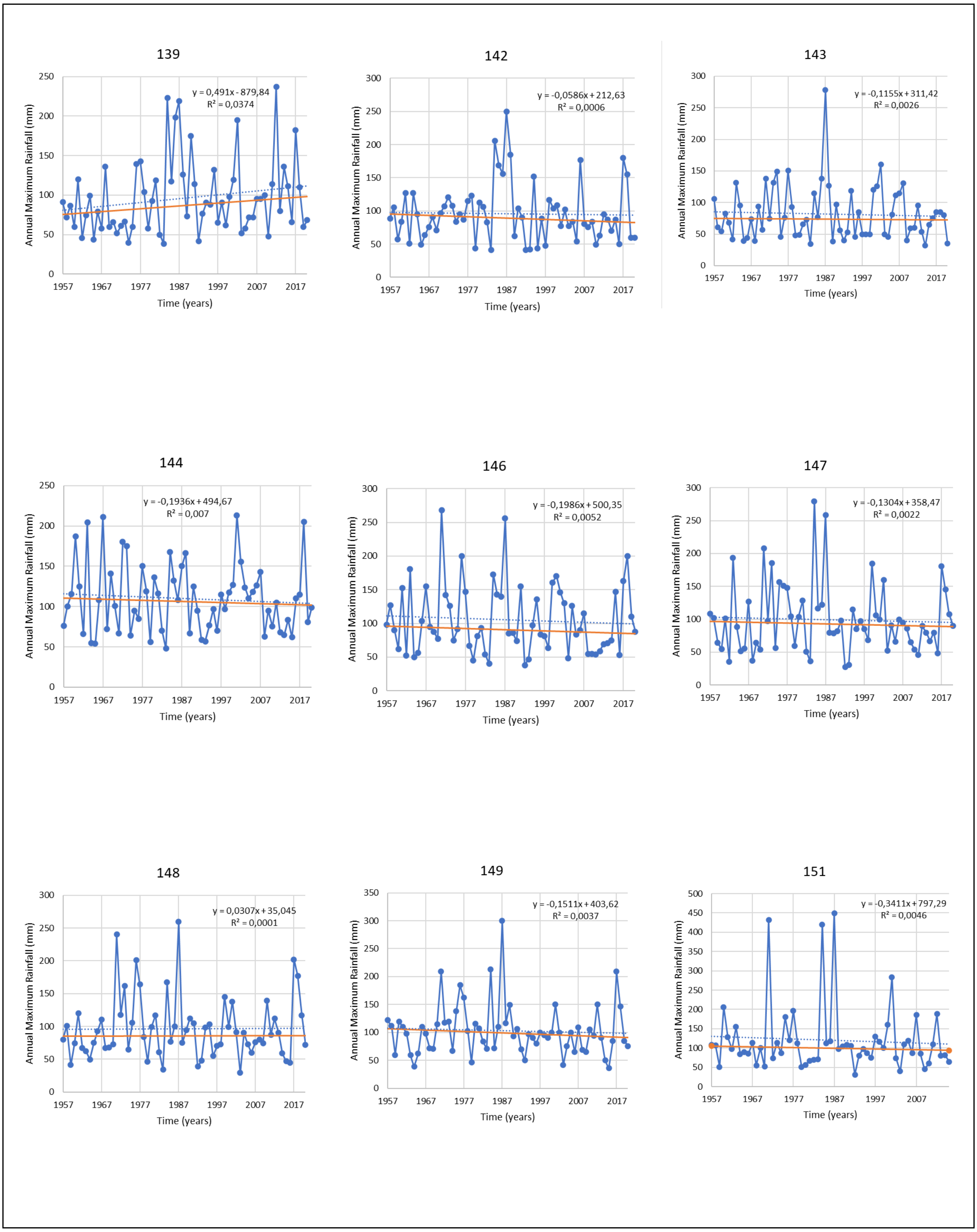
139
y = 0,491x - 879,84
R² = 0,0374
142
y = -0,0586x + 212,63
R² = 0,0006
143
y = -0,1155x + 311,42
R² = 0,0026
144
y = -0,1936x + 494,67
R² = 0,007
146
y = -0,1986x + 500,35
R² = 0,0052
147
y = -0,1304x + 358,47
R² = 0,0022
148
y = 0,0307x + 35,045
R² = 0,0001
149
y = -0,1511x + 403,62
R² = 0,0037
151
y = -0,3411x + 797,29
R² = 0,0046
Annual Maximum Rainfall (mm)
Time (years)

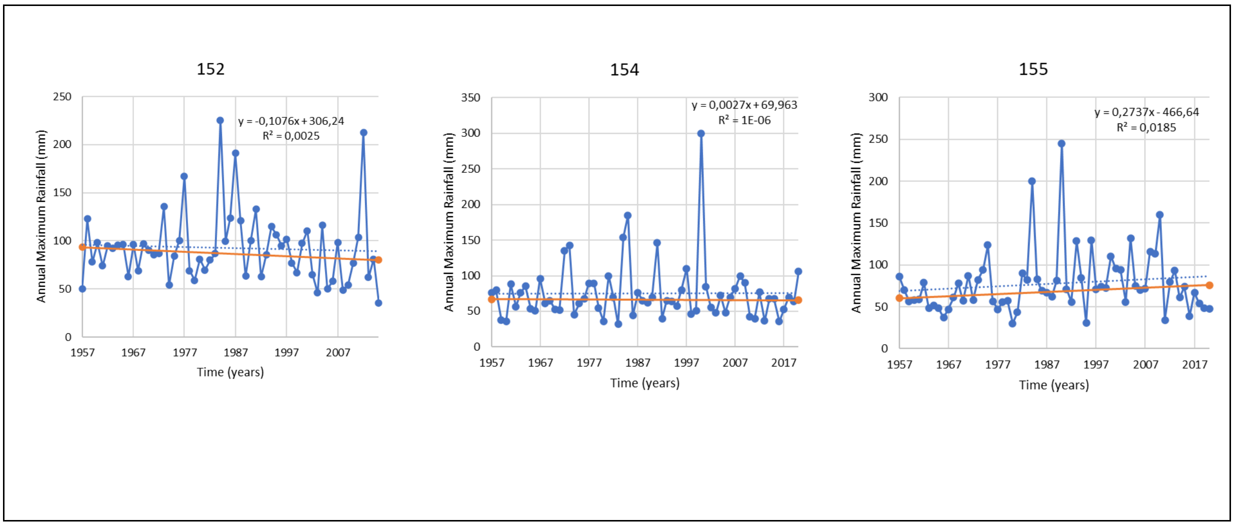

Figure 7.1 Time series of all annual maximum rainfalls at all SASRI stations used in this research

Table 7.1 The GEV statistical model performance criteria of KwaZulu-Natal AMDR for all covariates

Station	Stationary			Time			SOI			DMI			CO_2			GMT		
	AIC	**BIC**	**RMSE**	**AIC**	**BIC**	**RMSE**	**AIC**	**BIC**	**RMSE**	**AIC**	**BIC**	**RMSE**	**AIC**	**BIC**	**RMSE**	**AIC**	**BIC**	**RMSE**
6	**460.81***	**466.49***	1.62	462.90	474.25	1.29	466.03	477.38	1.99	467.20	478.55	1.29	462.24	473.59	1.80	464.75	476.10	2.19
8	**558.34***	**564.36***	1.55	562.22	574.27	1.27	564.37	576.41	1.72	565.59	577.63	1.95	563.35	575.40	1.48	568.60	580.65	2.76
9	**575.74***	**581.70***	1.82	579.30	591.24	1.60	581.04	592.97	2.18	578.66	590.59	2.87	578.19	590.13	1.55	582.89	594.83	2.07
11	**580.81***	**586.83***	1.32	587.07	599.11	1.41	588.62	600.67	0.81	588.92	600.96	2.03	587.58	599.63	1.31	591.74	603.79	2.19
12	**524.07***	**529.98***	2.01	530.18	542.00	2.18	528.74	540.56	2.26	531.72	543.54	2.54	530.49	542.31	1.99	532.85	544.67	3.09
18	**538.31***	**544.27***	1.24	542.06	553.99	1.63	543.78	555.71	1.70	545.74	557.68	1.39	543.40	555.34	0.69	543.70	555.64	1.32
20	**549.95***	**555.97***	1.24	553.22	565.27	1.66	552.50	564.55	1.35	557.23	569.28	2.11	555.74	567.79	1.25	557.10	569.14	1.33
22	**493.72***	**499.74***	4.30	495.97	508.02	3.57	493.85	505.89	3.47	498.92	510.96	4.52	498.78	510.82	5.28	503.65	515.69	3.39
23	**433.83***	**439.57***	2.60	440.31	451.78	2.73	440.62	452.09	2.55	441.10	452.57	3.89	439.35	450.83	1.89	440.19	451.66	3.48
26	**531.30***	**537.10***	1.76	536.26	547.85	1.35	534.84	546.43	1.96	537.86	549.45	1.85	535.87	547.47	1.45	538.18	549.77	1.61
27	**504.05***	**509.60***	1.88	508.19	519.30	1.58	508.46	519.56	2.44	512.28	523.38	2.82	508.10	519.20	1.89	511.83	522.93	1.81
29	954.38	961.98	1.45	956.19	971.39	1.16	958.87	974.07	1.60	959.00	974.19	1.42	**643.43***	**656.10***	1.50	961.56	976.75	1.38
38	449.01	**454.36***	1.79	**447.38***	456.30	1.71	461.64	472.48	1.85	463.70	474.54	1.66	458.18	469.02	1.85	459.78	470.62	1.32
105	**597.12***	**603.20***	1.22	600.91	613.06	0.99	604.05	616.20	1.61	603.70	615.86	0.91	600.57	612.72	1.21	605.83	617.98	0.91
110	678.80	685.27	1.18	681.18	694.14	0.97	683.75	696.70	1.71	683.33	696.28	1.14	**650.71***	**663.37***	1.08	683.65	696.60	1.10
111	**650.68***	**657.16***	1.71	654.17	667.12	1.47	655.94	668.89	1.49	657.11	670.06	2.04	650.80	663.46	1.29	656.77	669.73	2.39
114	**654.36***	660.84	1.68	660.62	673.57	1.49	658.41	669.20	1.75	662.80	675.75	2.06	**633.35***	**646.01***	1.70	662.84	675.80	1.99
120	**638.31***	644.73	1.12	641.61	654.47	0.97	640.56	653.42	1.97	644.34	657.20	1.54	**612.32***	**624.89***	1.25	644.00	656.86	1.82
123	644.55	651.02	1.53	649.04	662.00	1.39	**642.21***	655.17	1.41	651.48	664.43	1.58	**618.31***	**630.98***	1.32	650.09	663.05	1.57
125	646.42	652.90	1.87	647.89	660.84	2.15	647.01	659.96	1.66	650.52	663.48	1.87	**620.45***	**633.11***	1.49	649.62	662.57	1.53
126	650.56	657.04	1.75	655.20	668.15	1.57	656.14	669.09	1.93	657.72	670.67	2.10	**626.12***	**638.78***	2.00	658.26	671.21	2.70

Station	Stationary			Time			SOI			DMI			CO_2			GMT		
	AIC	**BIC**	**RMSE**	**AIC**	**BIC**	**RMSE**	**AIC**	**BIC**	**RMSE**	**AIC**	**BIC**	**RMSE**	**AIC**	**BIC**	**RMSE**	**AIC**	**BIC**	**RMSE**
129	624.55	631.03	2.60	627.67	640.62	2.11	**622.30***	635.25	1.66	631.82	644.77	2.37	**600.28***	**612.94***	2.06	630.02	642.97	2.21
130	633.31	639.74	1.45	639.00	651.86	1.15	**628.60***	641.46	1.39	641.77	654.62	2.33	**611.81***	**624.38***	0.97	641.73	654.59	1.63
131	644.40	650.87	1.62	650.88	663.84	1.88	650.17	663.12	1.75	**642.24***	655.19	2.44	**621.77***	**634.43***	1.92	653.09	666.04	2.61
132	**582.99***	589.23	1.38	**587.49***	599.96	0.96	589.90	602.36	1.06	592.20	604.67	0.83	**559.93***	**572.08***	0.99	588.75	601.21	1.46
136	449.30	454.65	5.50	**441.49***	**450.41***	4.77	451.62	462.33	4.52	457.21	467.91	6.41	**445.74***	456.45	4.92	449.28	459.98	6.54
138	669.56	676.04	3.14	**663.81**	**674.60**	2.37	677.33	690.28	3.75	679.25	692.20	2.71	633.86	**646.53***	2.44	669.05	682.00	2.74
139	**655.28***	661.76	1.53	658.52	671.47	1.26	659.45	672.41	1.19	663.34	676.29	1.30	629.94	**642.60***	1.54	661.57	674.52	1.22
142	**649.98***	656.46	1.43	653.17	666.12	1.03	655.72	668.68	1.65	656.72	669.67	1.73	626.53	**639.19***	1.14	654.73	667.69	2.10
143	**639.43***	645.91	1.86	644.96	657.91	1.61	645.66	658.62	2.57	646.46	659.41	2.48	617.40	**630.07***	1.64	649.00	661.96	1.43
144	658.45	664.92	1.53	662.85	675.80	1.41	665.18	678.13	1.15	664.23	677.19	1.39	**633.52***	**646.18***	1.67	666.58	679.54	1.29
146	674.01	680.48	1.63	679.81	692.77	1.53	674.94	687.90	1.56	679.88	692.83	1.71	**650.45***	**663.11***	1.54	681.38	694.34	1.73
147	672.21	678.69	1.42	677.51	690.46	2.02	676.90	689.86	2.11	679.51	692.47	1.83	**647.37***	**660.03***	0.97	678.23	691.18	1.52
148	**658.21***	664.68	1.61	664.53	677.49	1.64	665.19	678.15	1.37	665.33	678.29	1.87	635.96	**648.63***	1.15	668.46	681.41	2.32
149	**656.35***	662.82	2.01	664.71	677.66	2.00	661.89	674.84	2.43	663.86	676.81	1.94	632.88	**645.55***	1.88	666.08	679.03	1.90
151	**639.67***	645.90	3.13	645.48	657.94	2.83	646.86	659.32	3.32	641.45	653.91	3.53	616.16	**628.31***	2.22	648.76	661.23	4.23
152	578.80	585.03	2.13	578.77	591.24	1.31	583.30	595.76	2.11	588.86	601.33	3.06	546.38	**558.53***	1.62	578.97	591.44	3.86
154	612.12	618.59	2.37	617.67	630.62	1.14	615.03	627.98	2.03	618.64	631.59	2.38	**590.86***	**603.53***	2.42	621.78	634.73	3.37
155	615.82	622.30	2.09	618.61	631.57	2.37	**615.63***	628.58	2.16	617.83	630.79	2.07	**591.24***	**603.90***	1.38	621.73	634.68	3.17

***Best-fit model based on AIC and BIC**

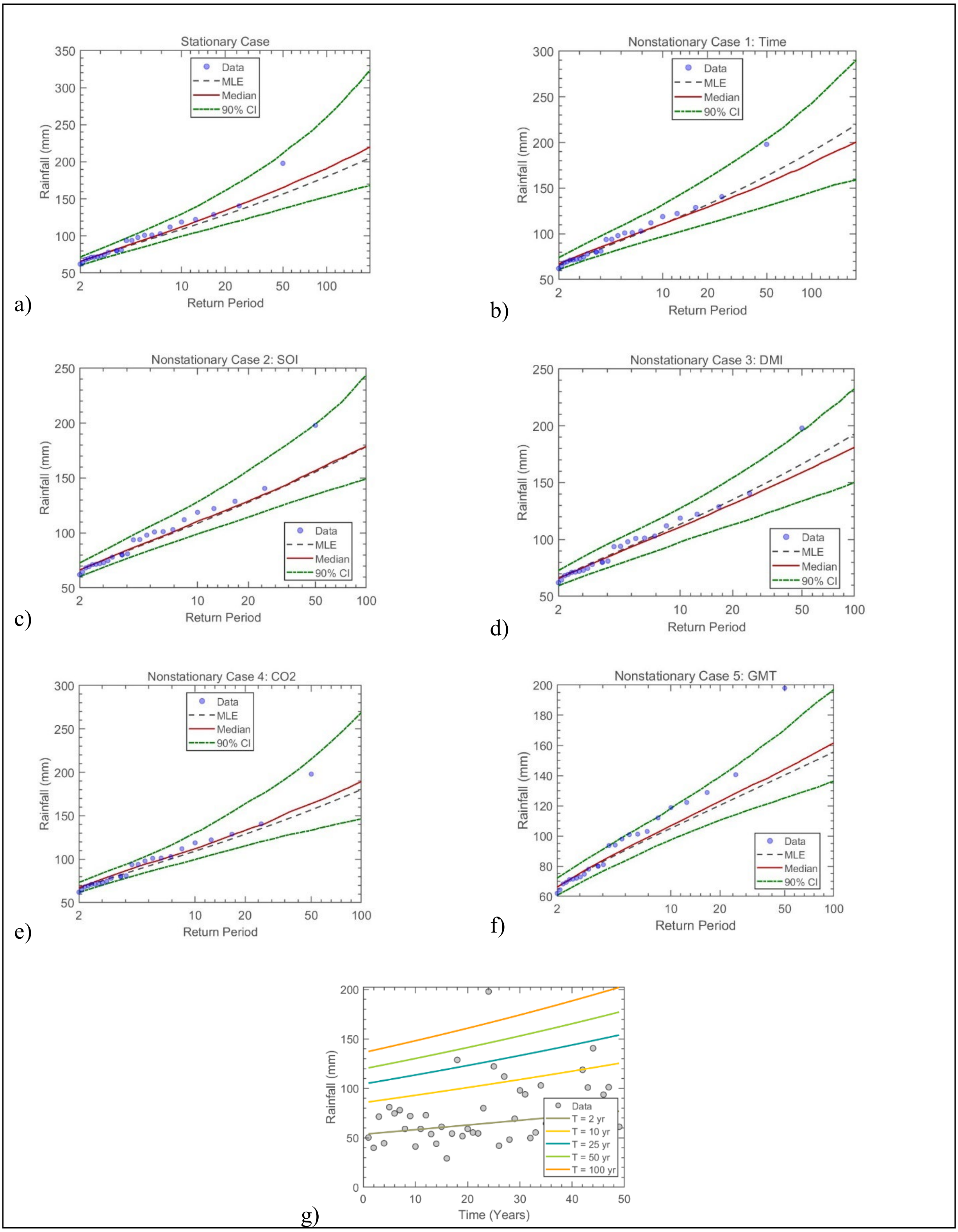

Figure 7.2 The GEV (a) stationary model, (b) non-stationary model considering time as a covariate, (c) non-stationary model considering SOI as a covariate, (d) non-stationary model considering DMI as a covariate, (e) non-stationary model considering CO_2 as a covariate, (f) non-stationary model considering GMT as a covariate and (g) effective return period as a function of time for Station 6: Pongola – SASRI

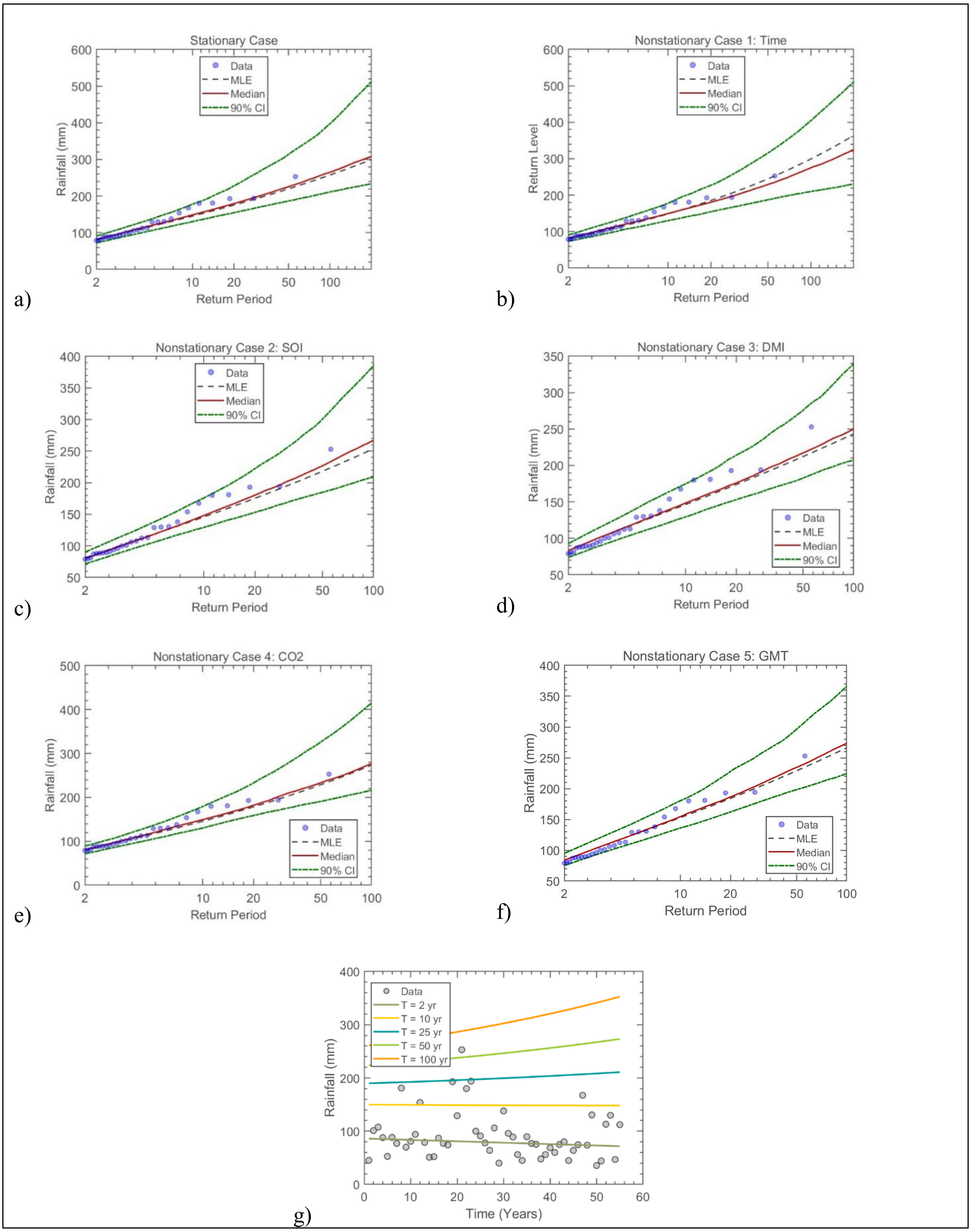

Figure 7.3 The GEV (a) stationary model, (b) non-stationary model considering time as a covariate, (c) non-stationary model considering SOI as a covariate, (d) non-stationary model considering DMI as a covariate, (e) non-stationary model considering CO_2 as a covariate, (f) non-stationary model considering GMT as a covariate and (g) effective return period as a function of time for Station 8: Glen Park – St Lucia Farms

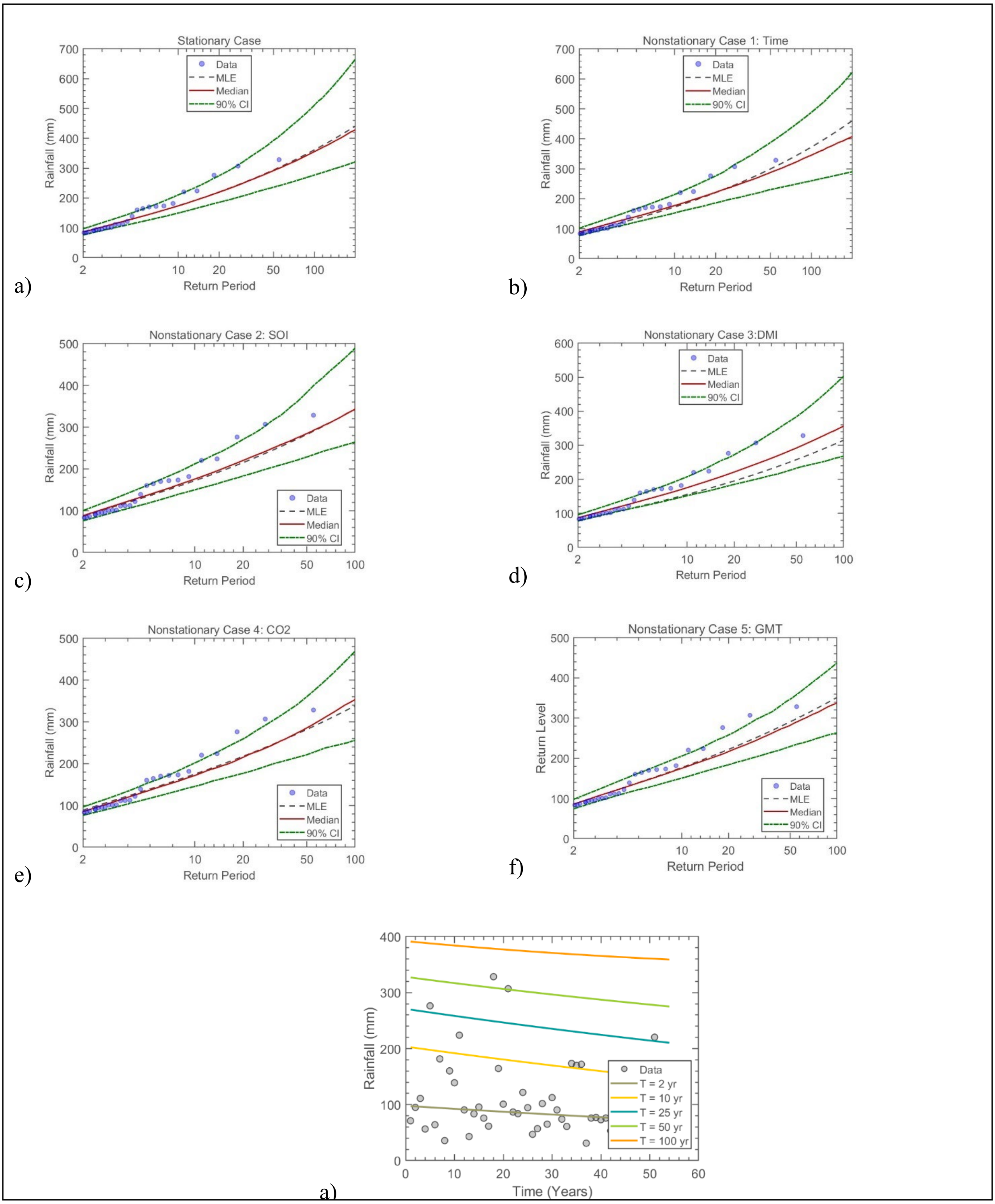

Figure 7.4 The GEV (a) stationary model, (b) non-stationary model considering time as a covariate, (c) non-stationary model considering SOI as a covariate, (d) non-stationary model considering DMI as a covariate, (e) non-stationary model considering CO_2 as a covariate, (f) non-stationary model considering GMT as a covariate and (g) effective return period as a function of time for Station 9: Mtubatuba – Riverview Sugar Mill

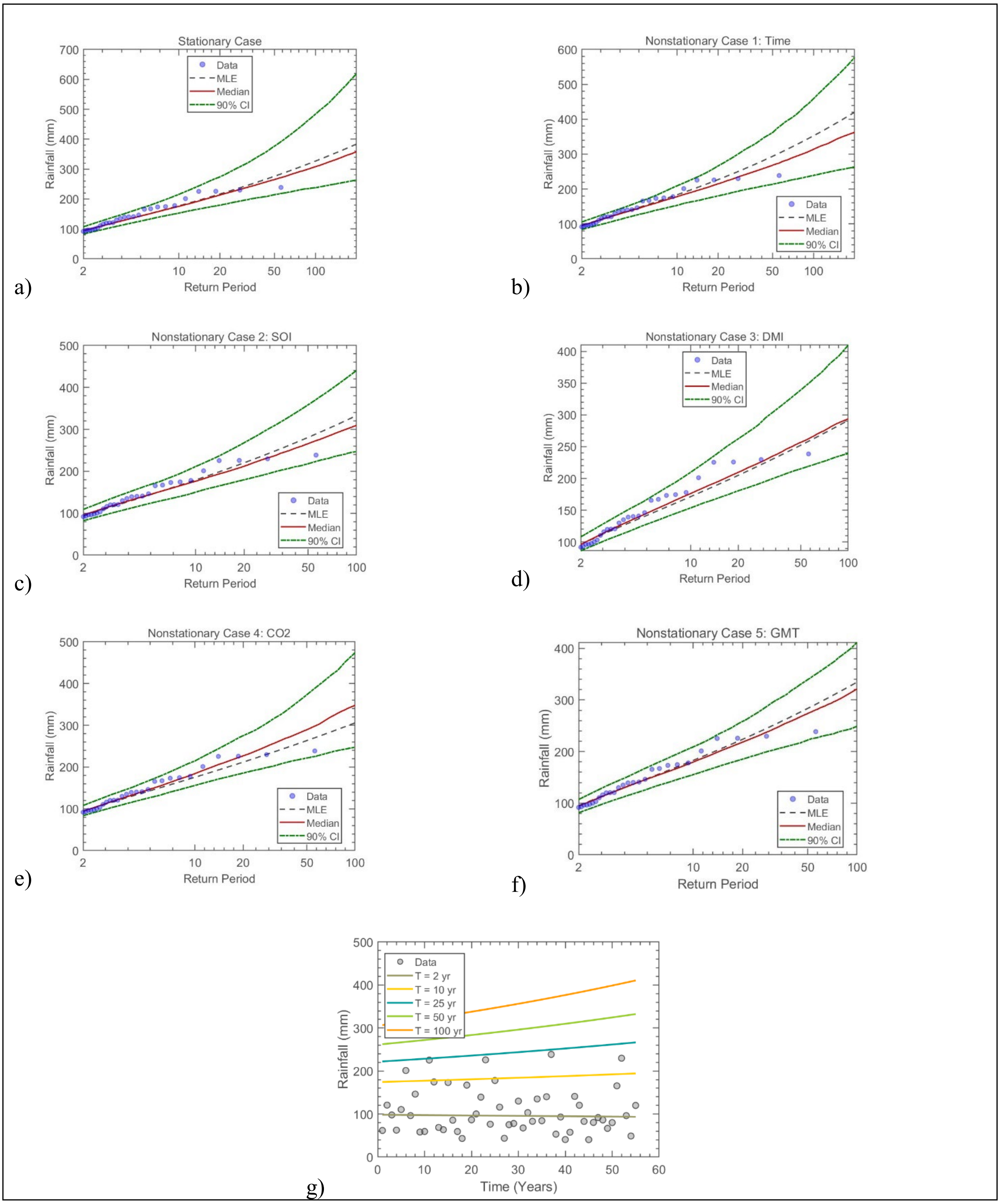

Figure 7.5 The GEV (a) stationary model, (b) non-stationary model considering time as a covariate, (c) non-stationary model considering SOI as a covariate, (d) non-stationary model considering DMI as a covariate, (e) non-stationary model considering CO_2 as a covariate, (f) non-stationary model considering GMT as a covariate and (g) effective return period as a function of time for Station 11: Mtunzini – ex SASRI

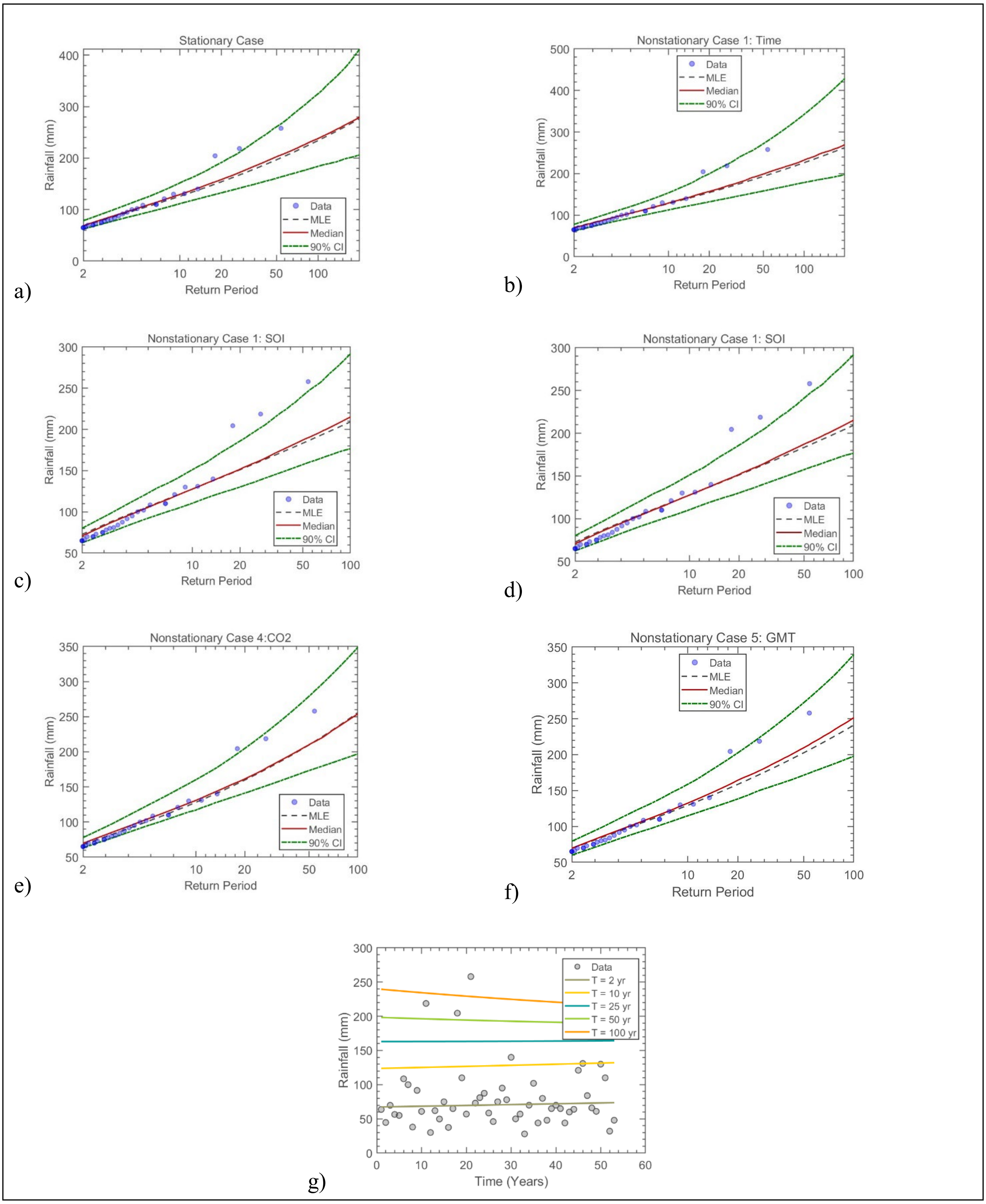

Figure 7.6 The GEV (a) stationary model, (b) non-stationary model considering time as a covariate, (c) non-stationary model considering SOI as a covariate, (d) non-stationary model considering DMI as a covariate, (e) non-stationary model considering CO_2 as a covariate, (f) non-stationary model considering GMT as a covariate and (g) effective return period as a function of time for Station 12: Melmoth – CA Leith & Sons

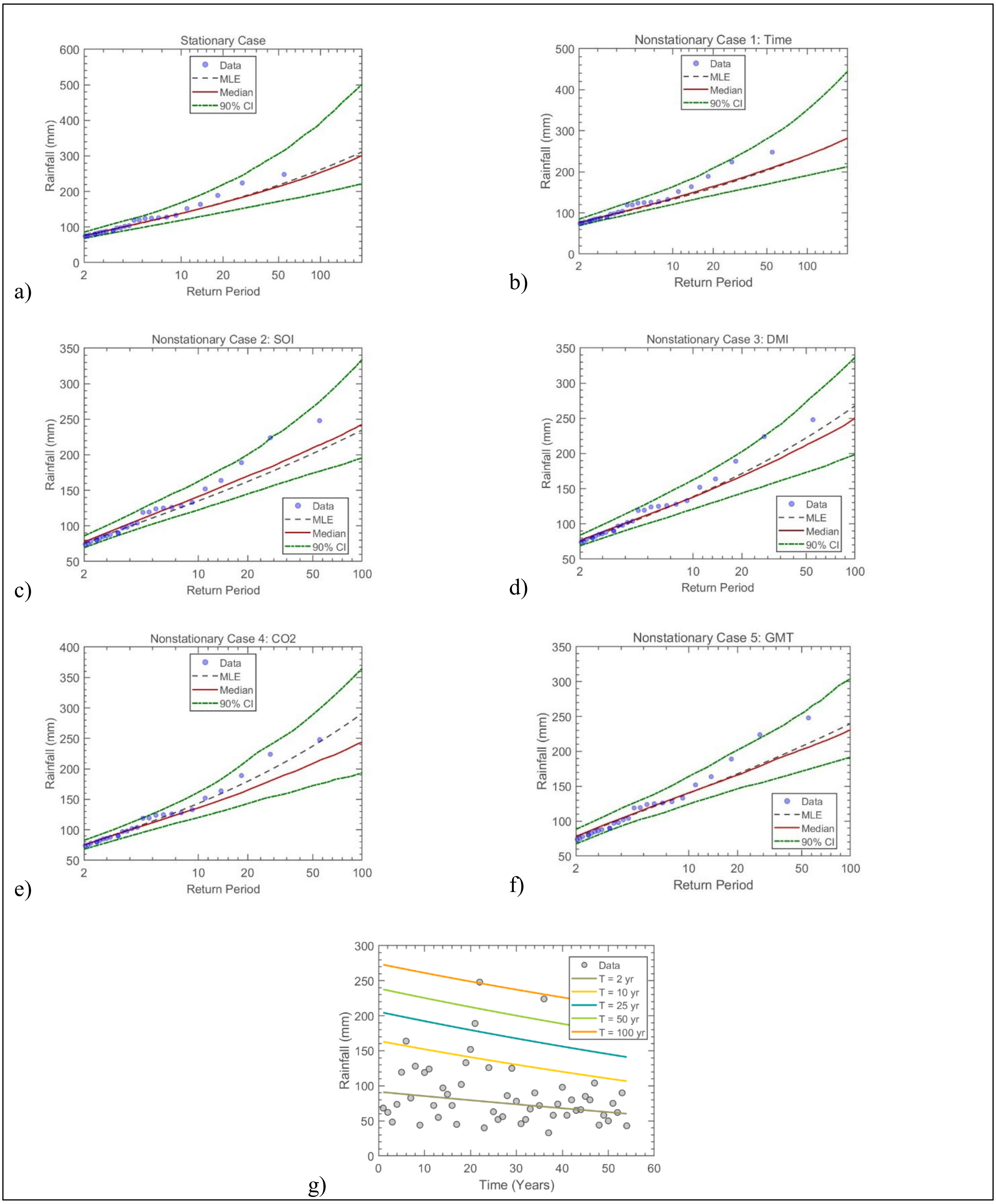

Figure 7.7 The GEV (a) stationary model, (b) non-stationary model considering time as a covariate, (c) non-stationary model considering SOI as a covariate, (d) non-stationary model considering DMI as a covariate, (e) non-stationary model considering CO_2 as a covariate, (f) non-stationary model considering GMT as a covariate and (g) effective return period as a function of time for Station 18: Glendale – Tenrith Farm

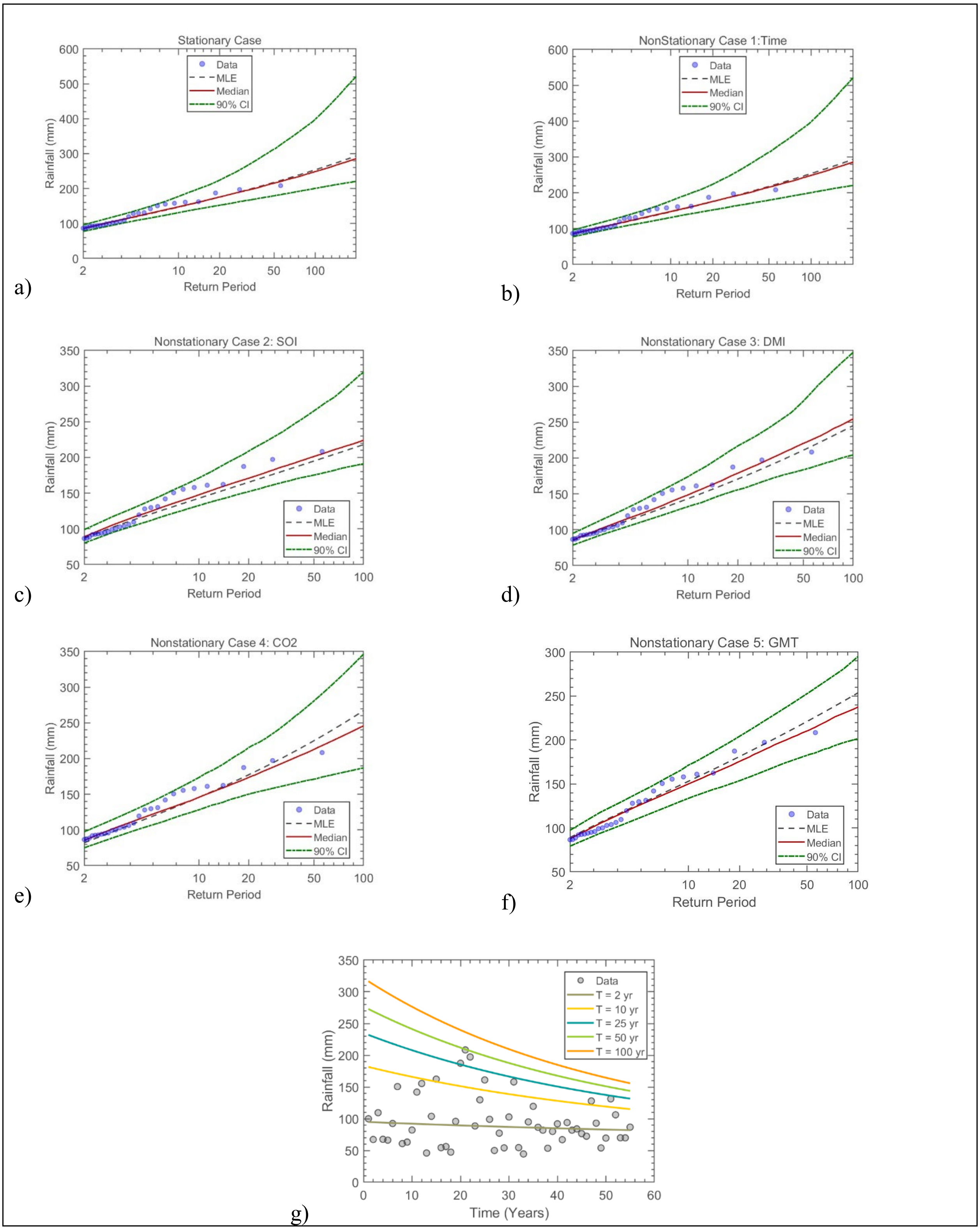

Figure 7.8 The GEV (a) stationary model, (b) non-stationary model considering time as a covariate, (c) non-stationary model considering SOI as a covariate, (d) non-stationary model considering DMI as a covariate, (e) non-stationary model considering CO_2 as a covariate, (f) non-stationary model considering GMT as a covariate and (g) effective return period as a function of time for Station 20: Tongaat – Klipfontein (THS)

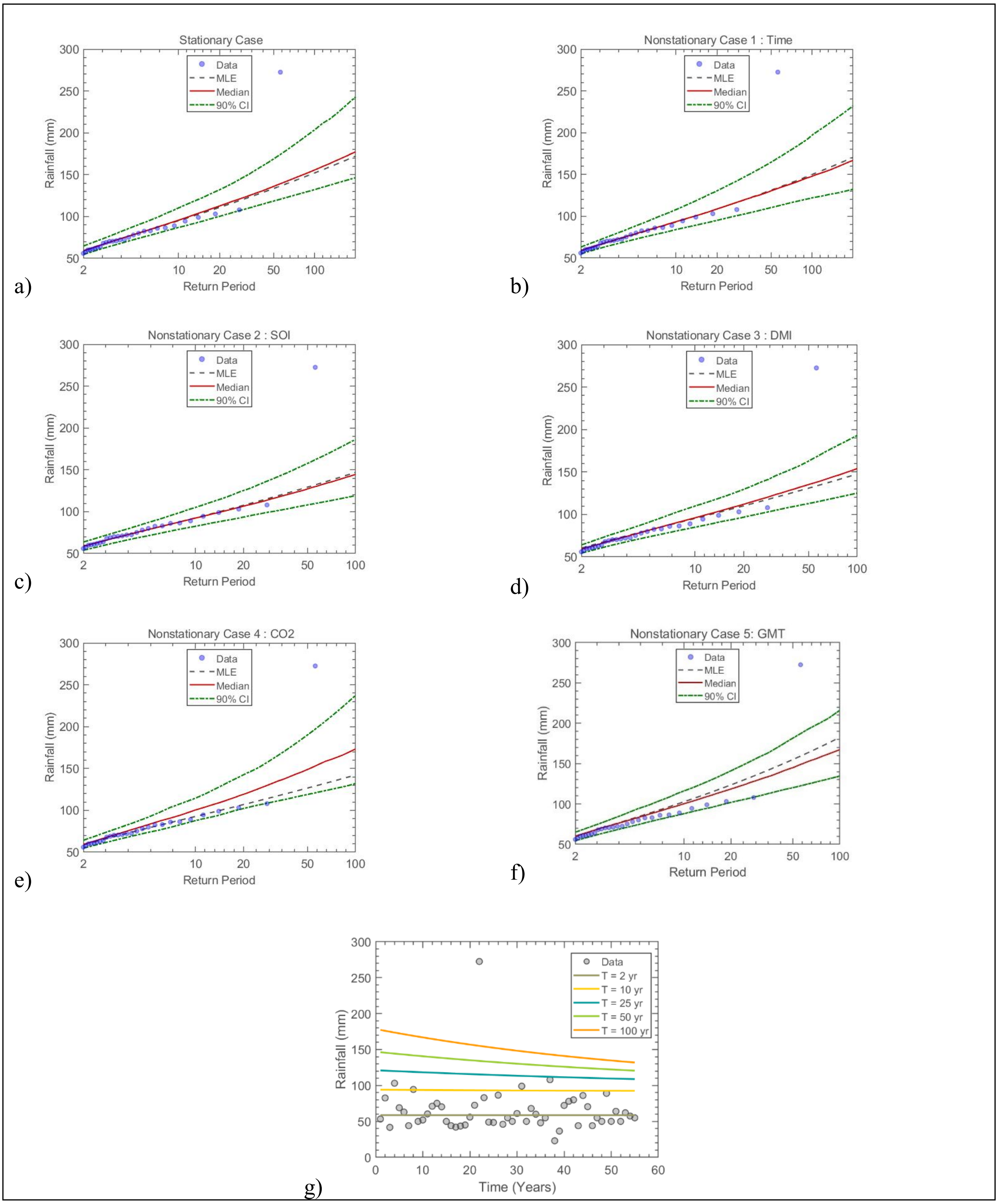

Figure 7.9 The GEV (a) stationary model, (b) non-stationary model considering time as a covariate, (c) non-stationary model considering SOI as a covariate, (d) non-stationary model considering DMI as a covariate, (e) non-stationary model considering CO_2 as a covariate, (f) non-stationary model considering GMT as a covariate and (g) effective return period as a function of time for Station 22: Seven Oaks – Saw Mill

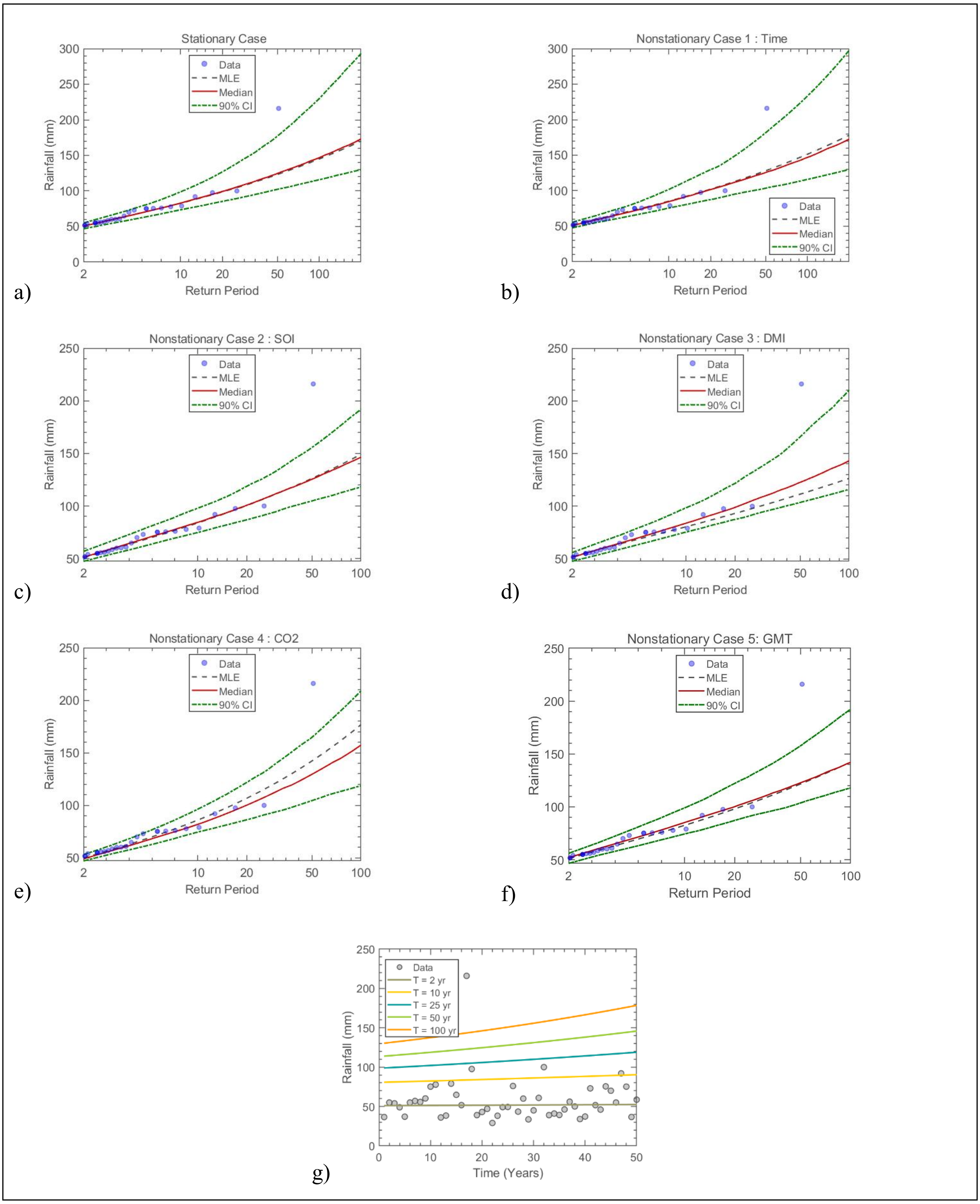

Figure 7.10 The GEV (a) stationary model, (b) non-stationary model considering time as a covariate, (c) non-stationary model considering SOI as a covariate, (d) non-stationary model considering DMI as a covariate, (e) non-stationary model considering CO_2 as a covariate, (f) non-stationary model considering GMT as a covariate and (g) effective return period as a function of time for Station 23: Noodsberg – Illovo Sugar Mill

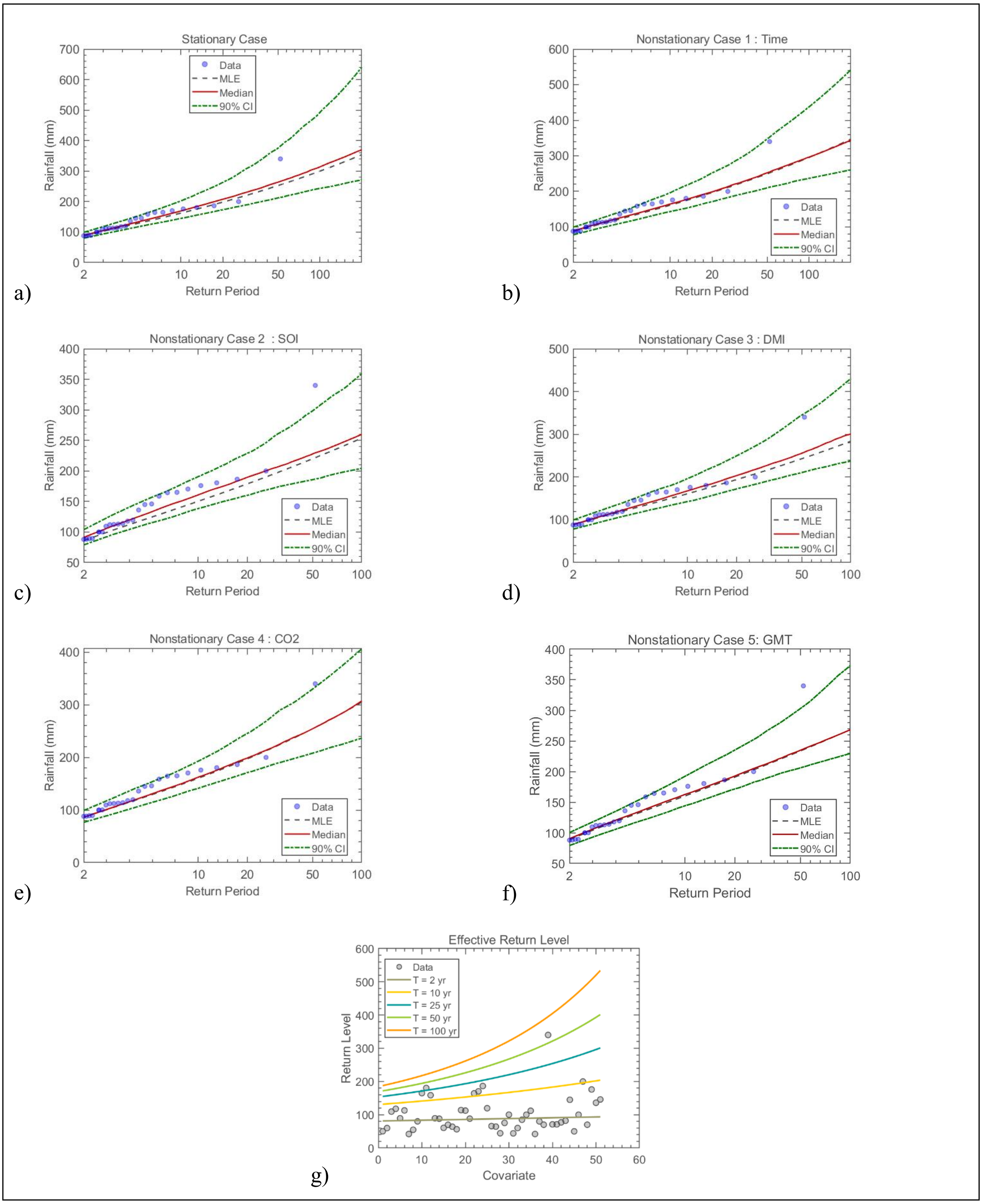

Figure 7.11 The GEV (a) stationary model, (b) non-stationary model considering time as a covariate, (c) non-stationary model considering SOI as a covariate, (d) non-stationary model considering DMI as a covariate, (e) non-stationary model considering CO_2 as a covariate, (f) non-stationary model considering GMT as a covariate and (g) effective return period as a function of time for Station 26: Illovo – Sugar Estate

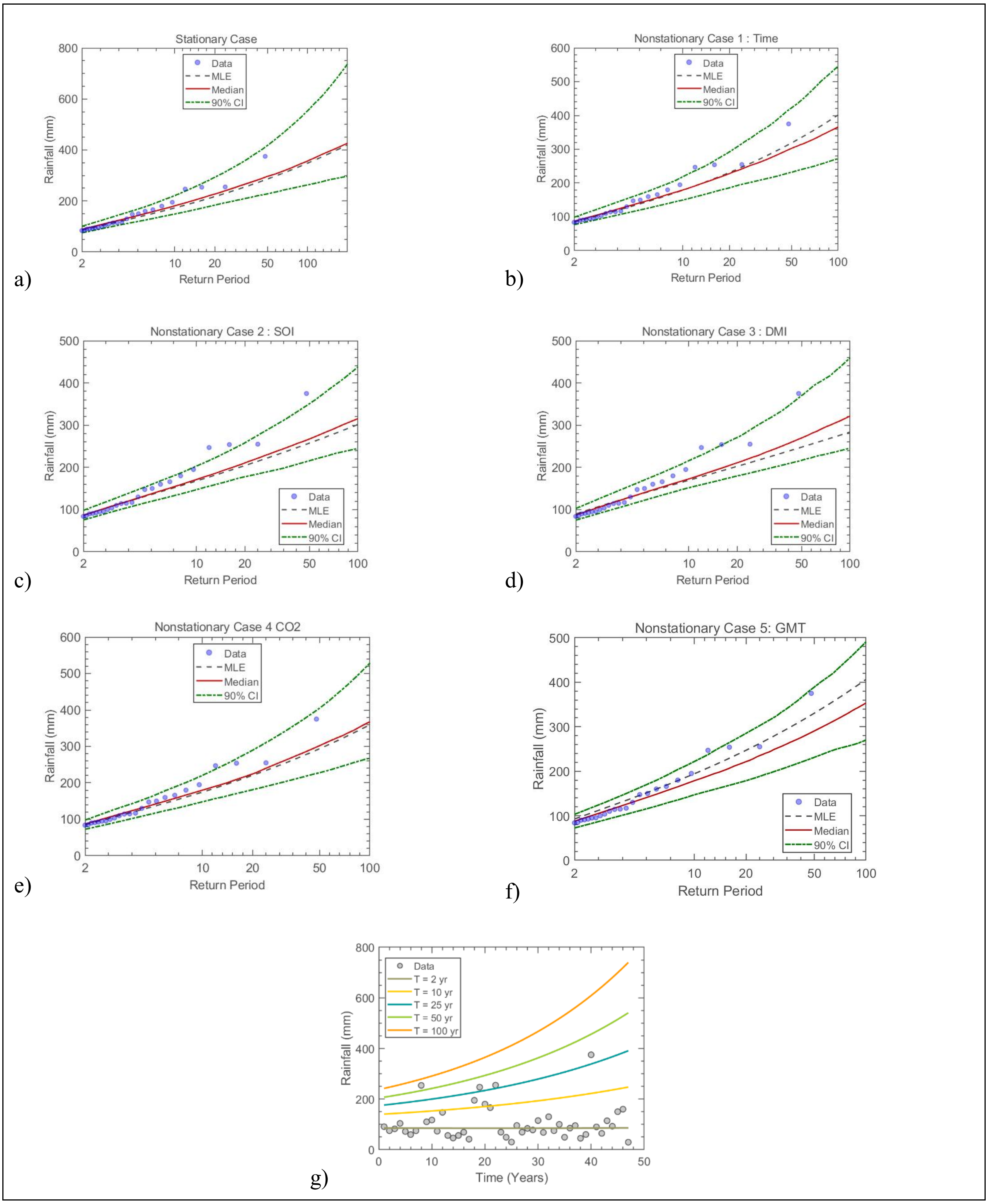

Figure 7.12 The GEV (a) stationary model, (b) non-stationary model considering time as a covariate, (c) non-stationary model considering SOI as a covariate, (d) non-stationary model considering DMI as a covariate, (e) non-stationary model considering CO_2 as a covariate, (f) non-stationary model considering GMT as a covariate and (g) effective return period as a function of time for Station 27: Vulamehlo – Esperanza

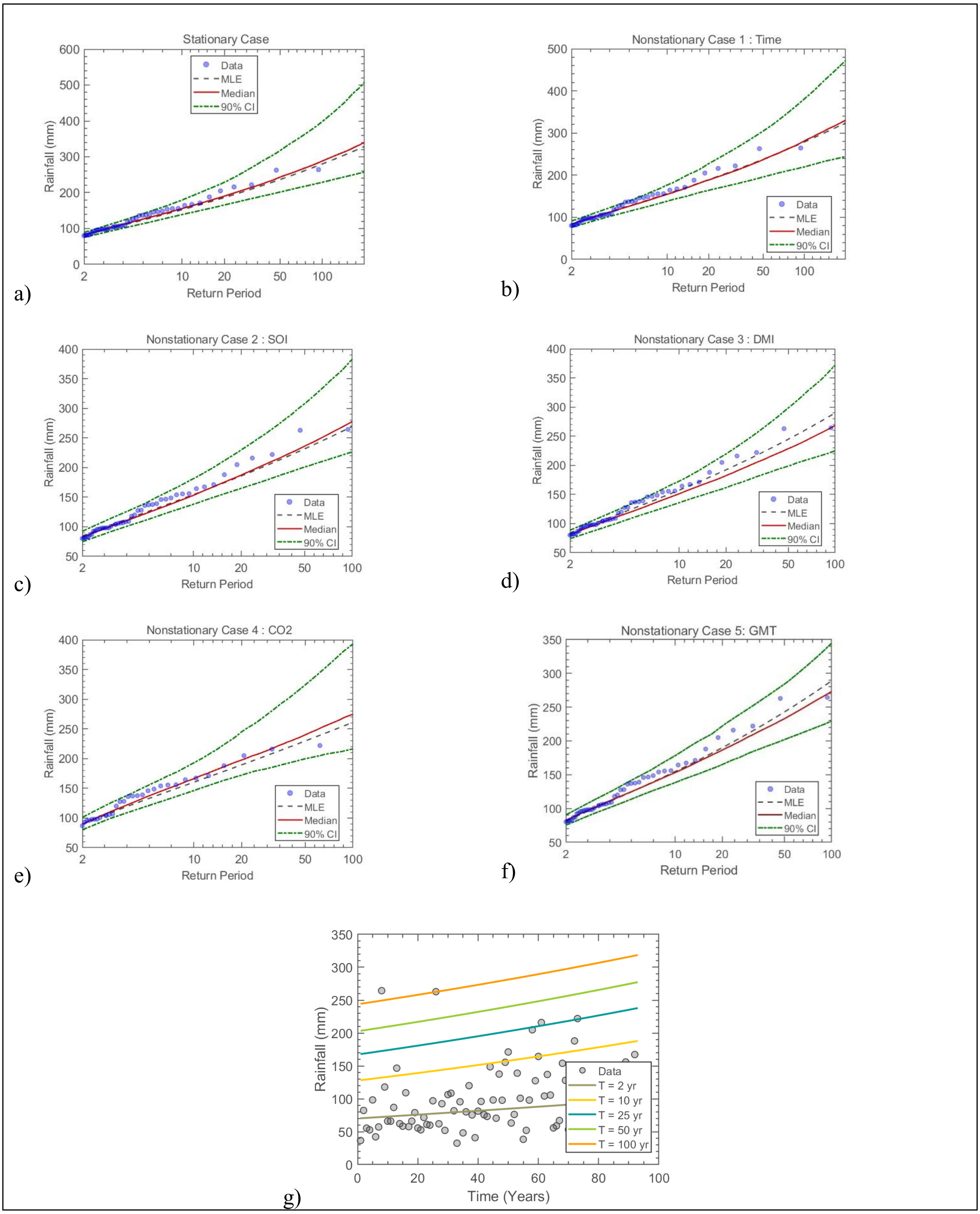

Figure 7.13 The GEV (a) stationary model, (b) non-stationary model considering time as a covariate, (c) non-stationary model considering SOI as a covariate, (d) non-stationary model considering DMI as a covariate, (e) non-stationary model considering CO_2 as a covariate, (f) non-stationary model considering GMT as a covariate and (g) effective return period as a function of time for Station 29: Mt Edgecombe – SASRI

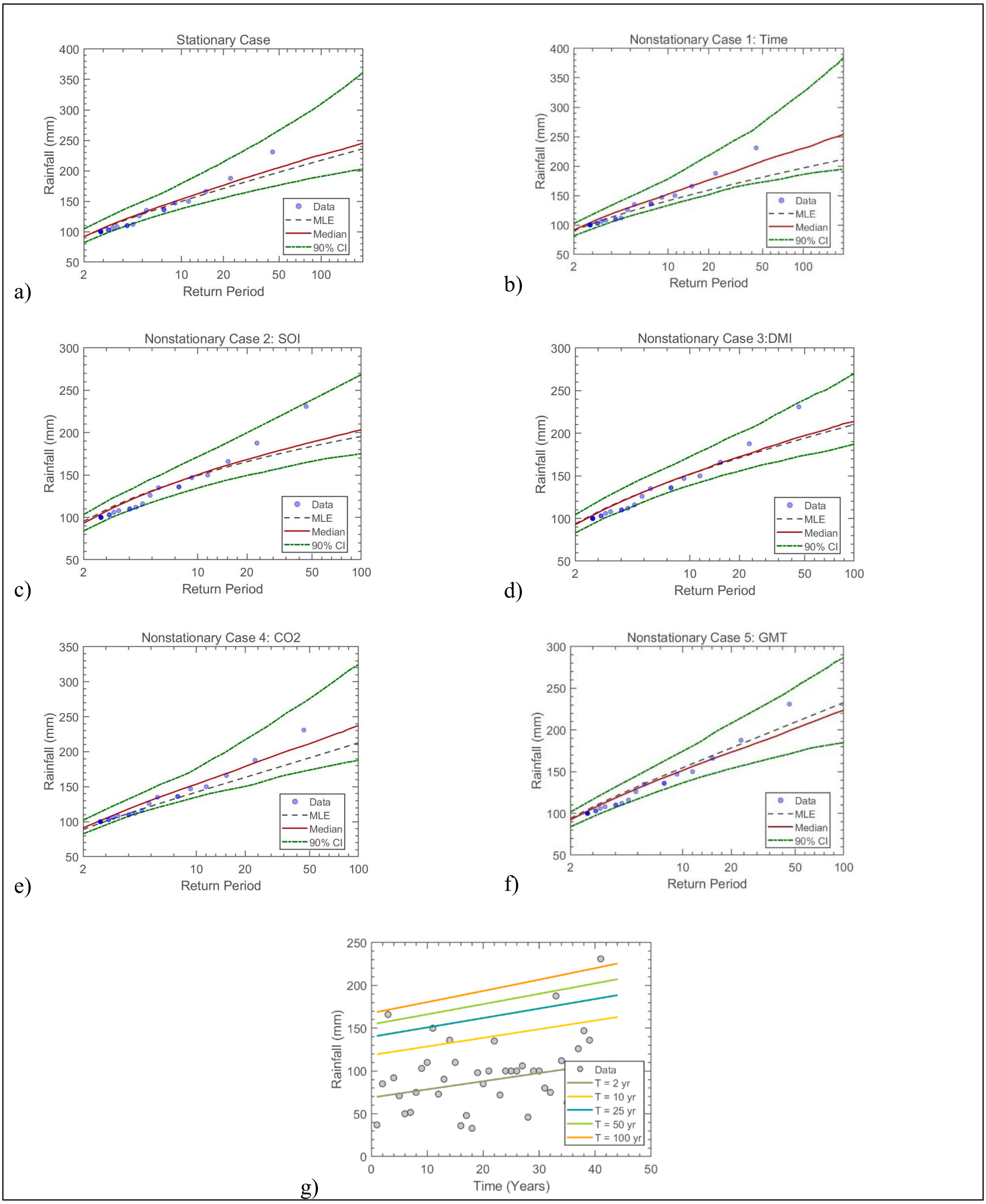

Figure 7.14 The GEV (a) stationary model, (b) non-stationary model considering time as a covariate, (c) non-stationary model considering SOI as a covariate, (d) non-stationary model considering DMI as a covariate, (e) non-stationary model considering CO_2 as a covariate, (f) non-stationary model considering GMT as a covariate and (g) effective return period as a function of time for Station 38: Sezela – Illovo Sugar Estate

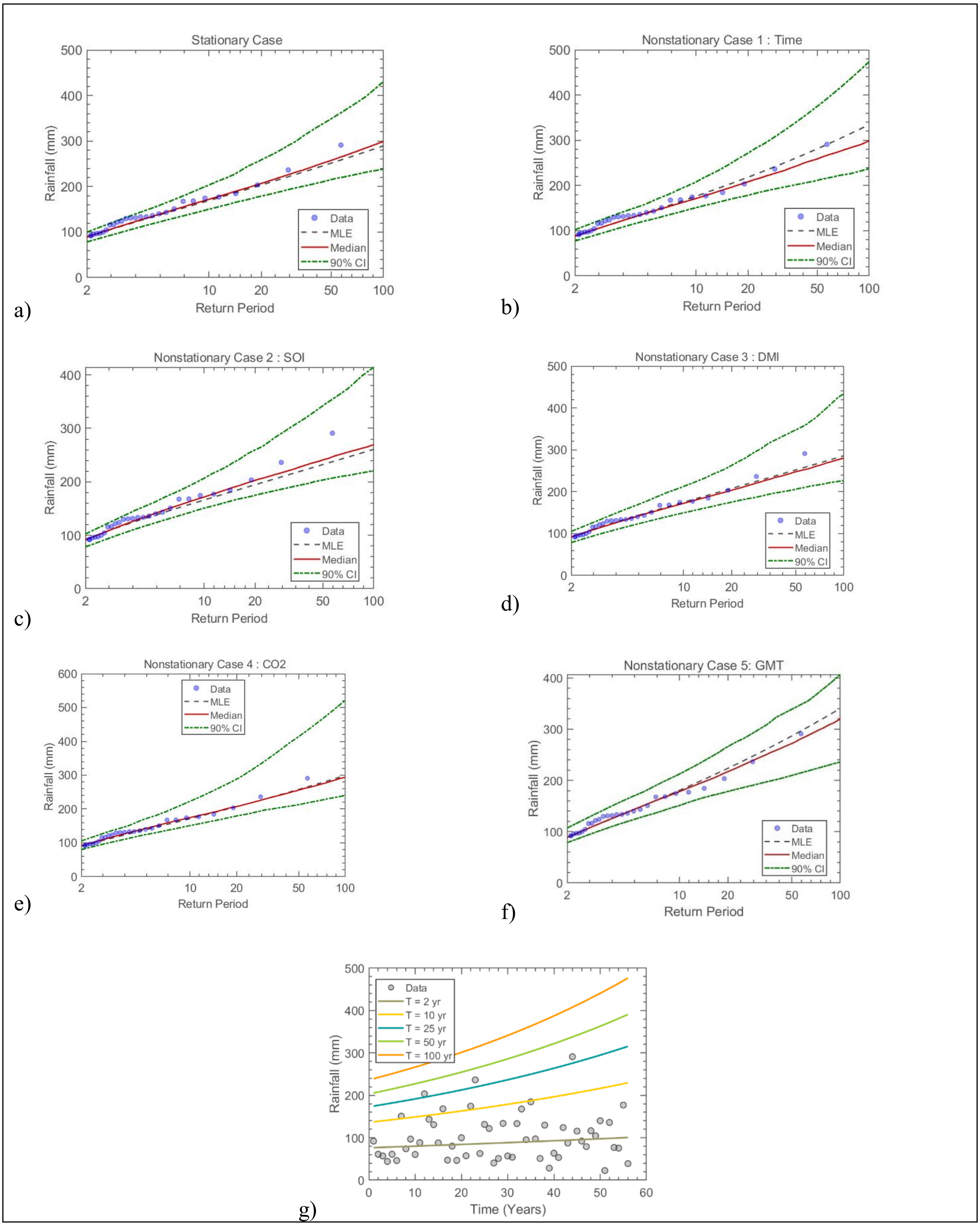

Figure 7.15 The GEV (a) stationary model, (b) non-stationary model considering time as a covariate, (c) non-stationary model considering SOI as a covariate, (d) non-stationary model considering DMI as a covariate, (e) non-stationary model considering CO_2 as a covariate, (f) non-stationary model considering GMT as a covariate and (g) effective return period as a function of time for Station 105: Oribi Flats – Minnehaha Farm

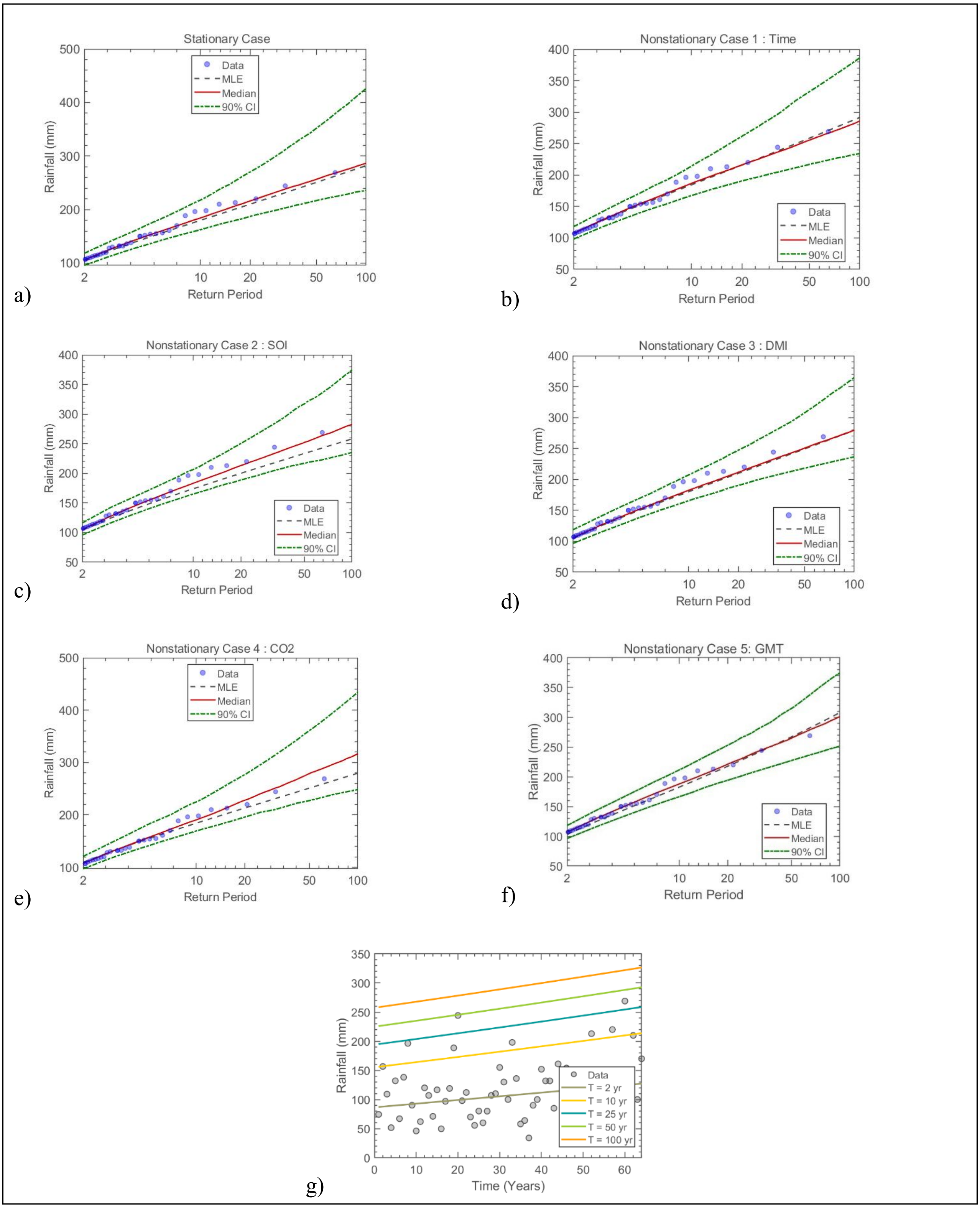

Figure 7.16 The GEV (a) stationary model, (b) non-stationary model considering time as a covariate, (c) non-stationary model considering SOI as a covariate, (d) non-stationary model considering DMI as a covariate, (e) non-stationary model considering CO_2 as a covariate, (f) non-stationary model considering GMT as a covariate and (g) effective return period as a function of time for Station 110: Renishaw – Crooks Bros Estate

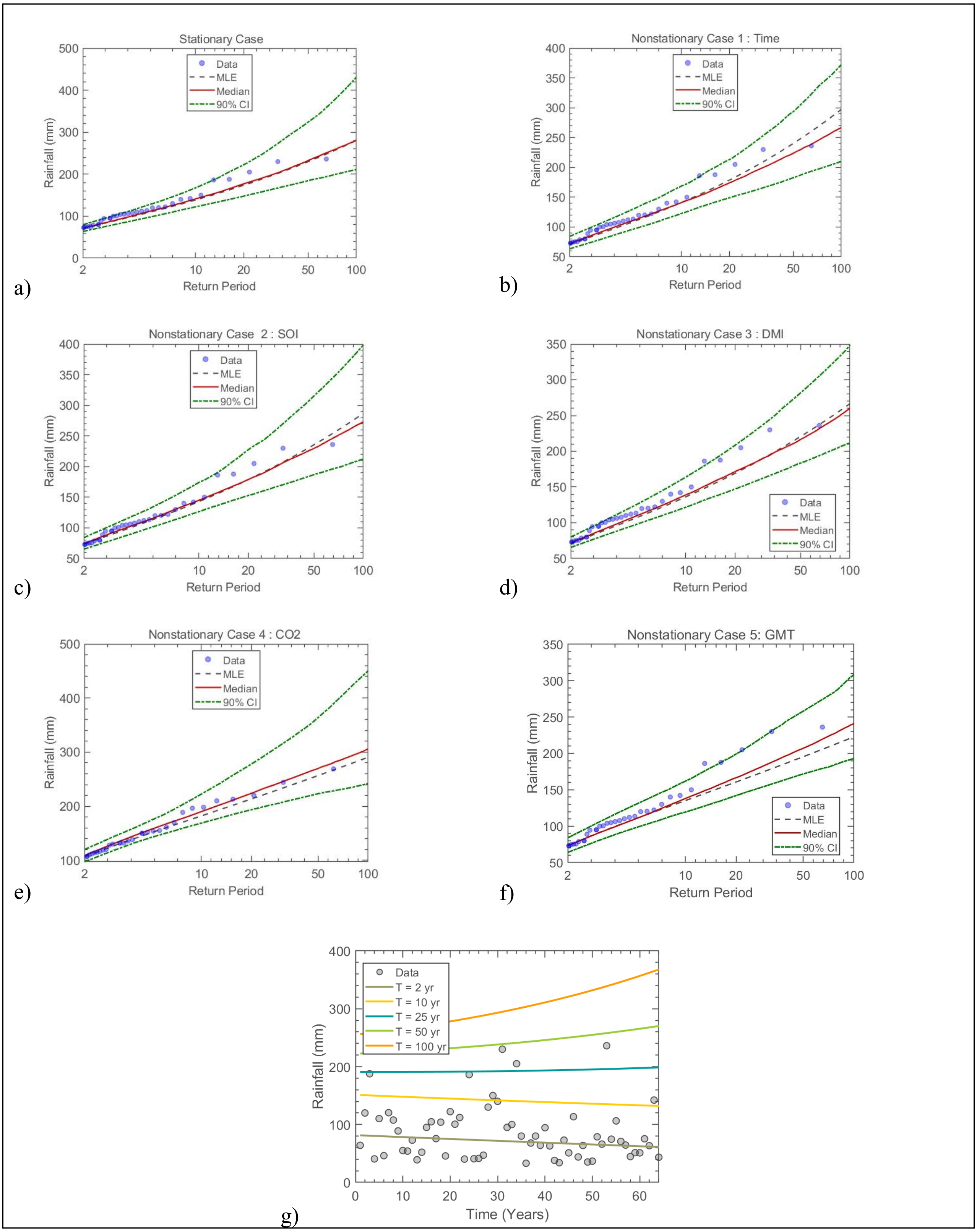

Figure 7.17 The GEV (a) stationary model, (b) non-stationary model considering time as a covariate, (c) non-stationary model considering SOI as a covariate, (d) non-stationary model considering DMI as a covariate, (e) non-stationary model considering CO_2 as a covariate, (f) non-stationary model considering GMT as a covariate and (g) effective return period as a function of time for Station 111: Powerscourt – Roseleigh Estate

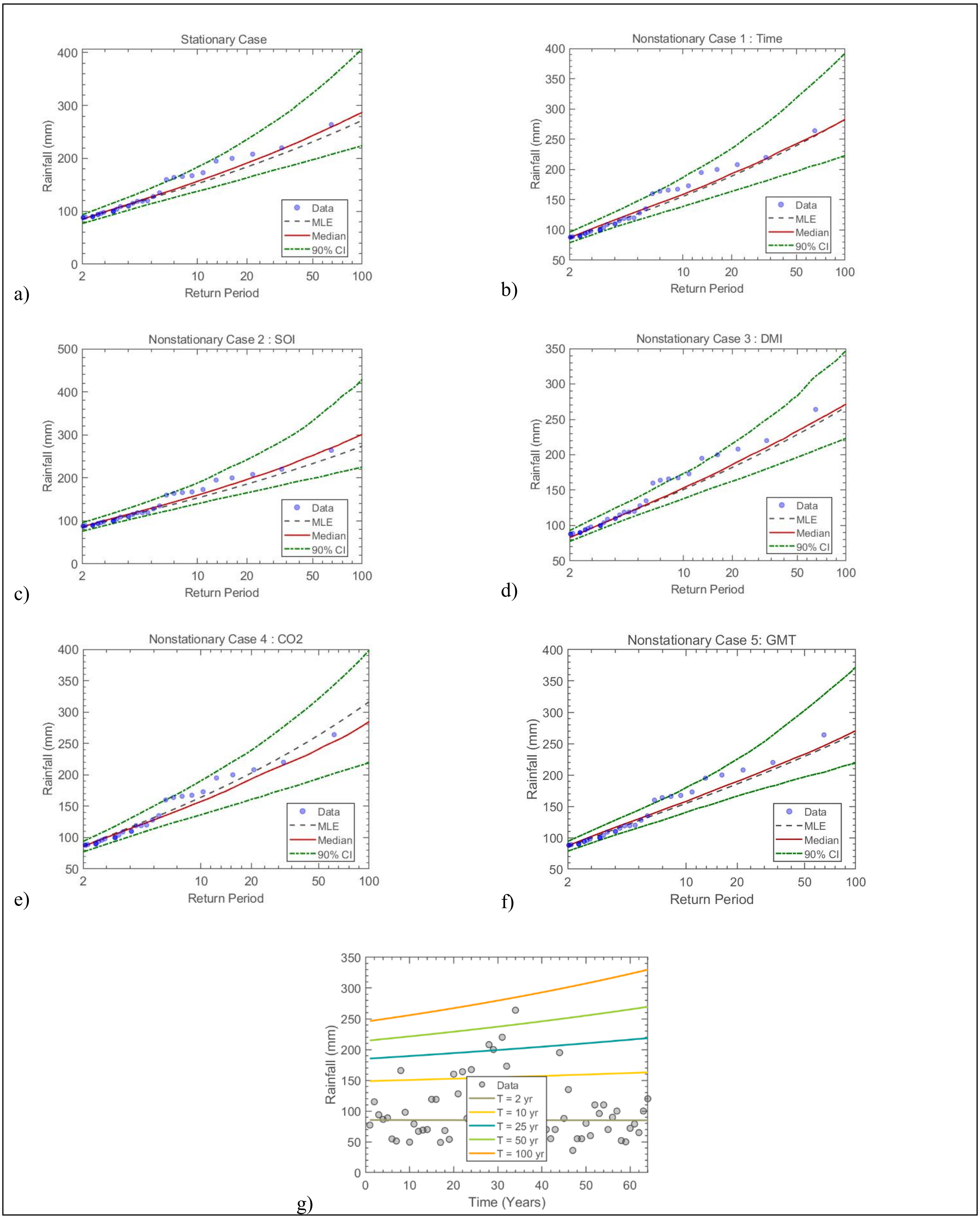

Figure 7.18 The GEV (a) stationary model, (b) non-stationary model considering time as a covariate, (c) non-stationary model considering SOI as a covariate, (d) non-stationary model considering DMI as a covariate, (e) non-stationary model considering CO_2 as a covariate, (f) non-stationary model considering GMT as a covariate and (g) effective return period as a function of time for Station 114: Inanda – Farm

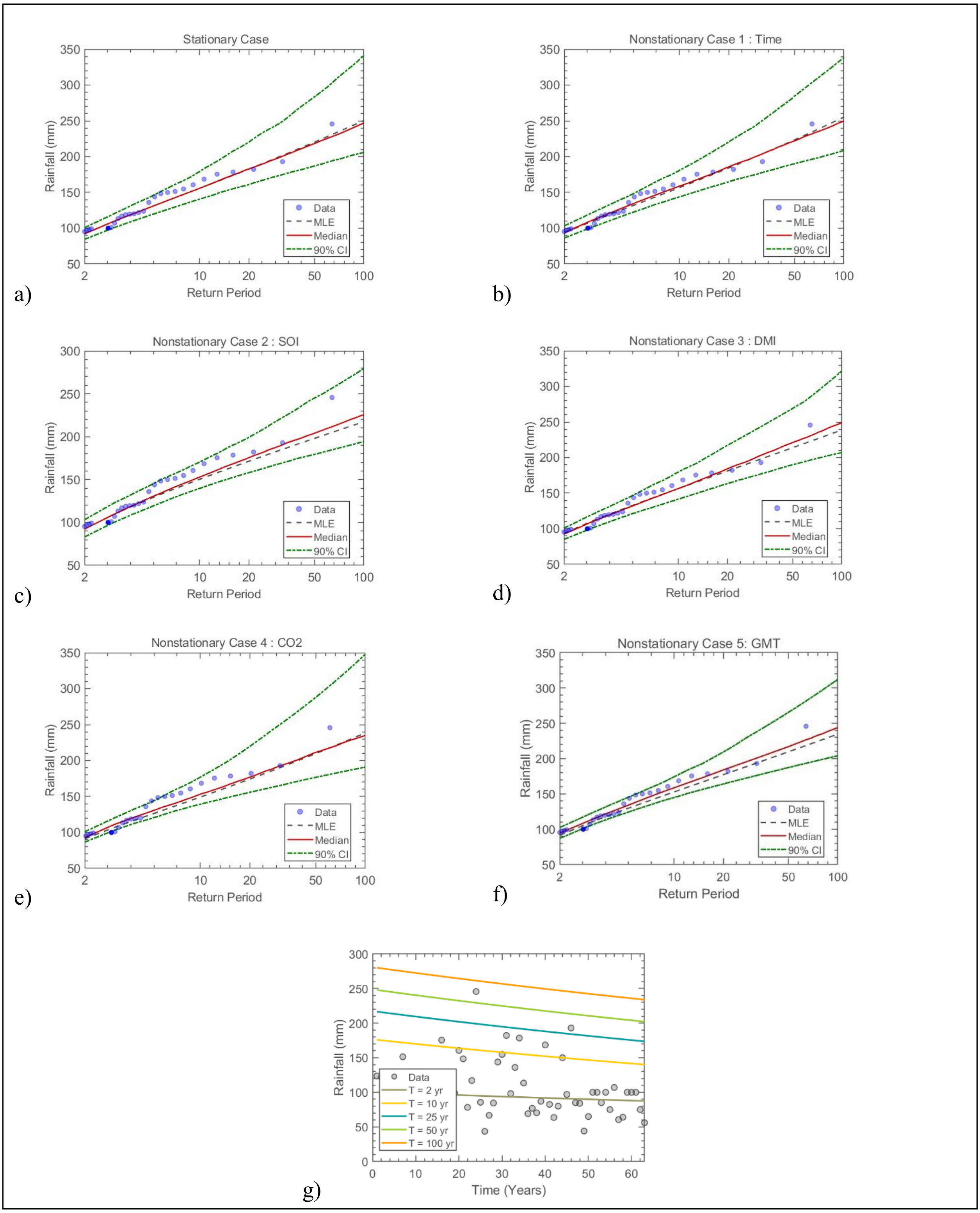

Figure 7.19 The GEV (a) stationary model, (b) non-stationary model considering time as a covariate, (c) non-stationary model considering SOI as a covariate, (d) non-stationary model considering DMI as a covariate, (e) non-stationary model considering CO_2 as a covariate, (f) non-stationary model considering GMT as a covariate and (g) effective return period as a function of time for Station 120: Inyaninga – THS

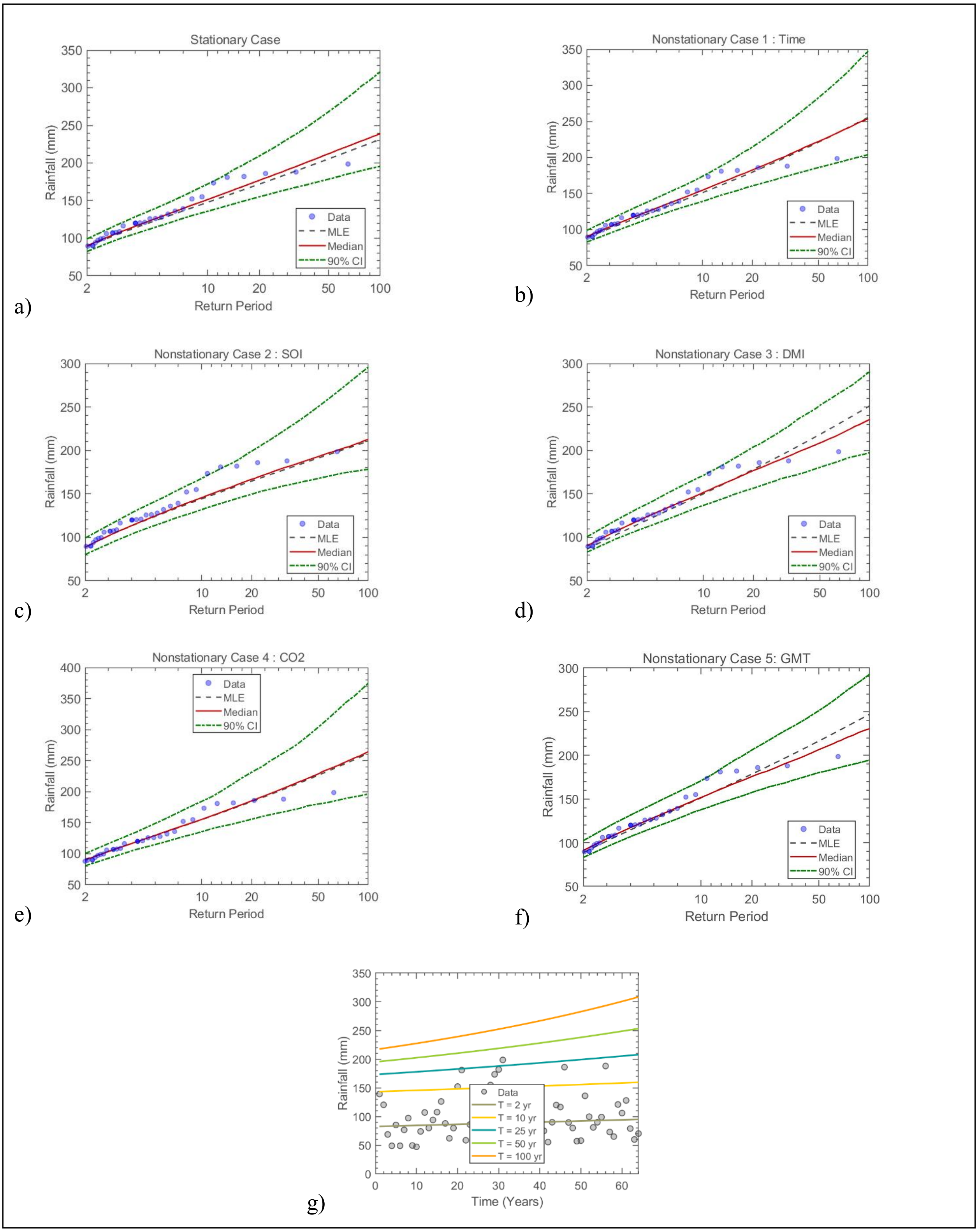

Figure 7.20 The GEV (a) stationary model, (b) non-stationary model considering time as a covariate, (c) non-stationary model considering SOI as a covariate, (d) non-stationary model considering DMI as a covariate, (e) non-stationary model considering CO_2 as a covariate, (f) non-stationary model considering GMT as a covariate and (g) effective return period as a function of time for Station 123: Maidstone – Sugar Mill (THS)

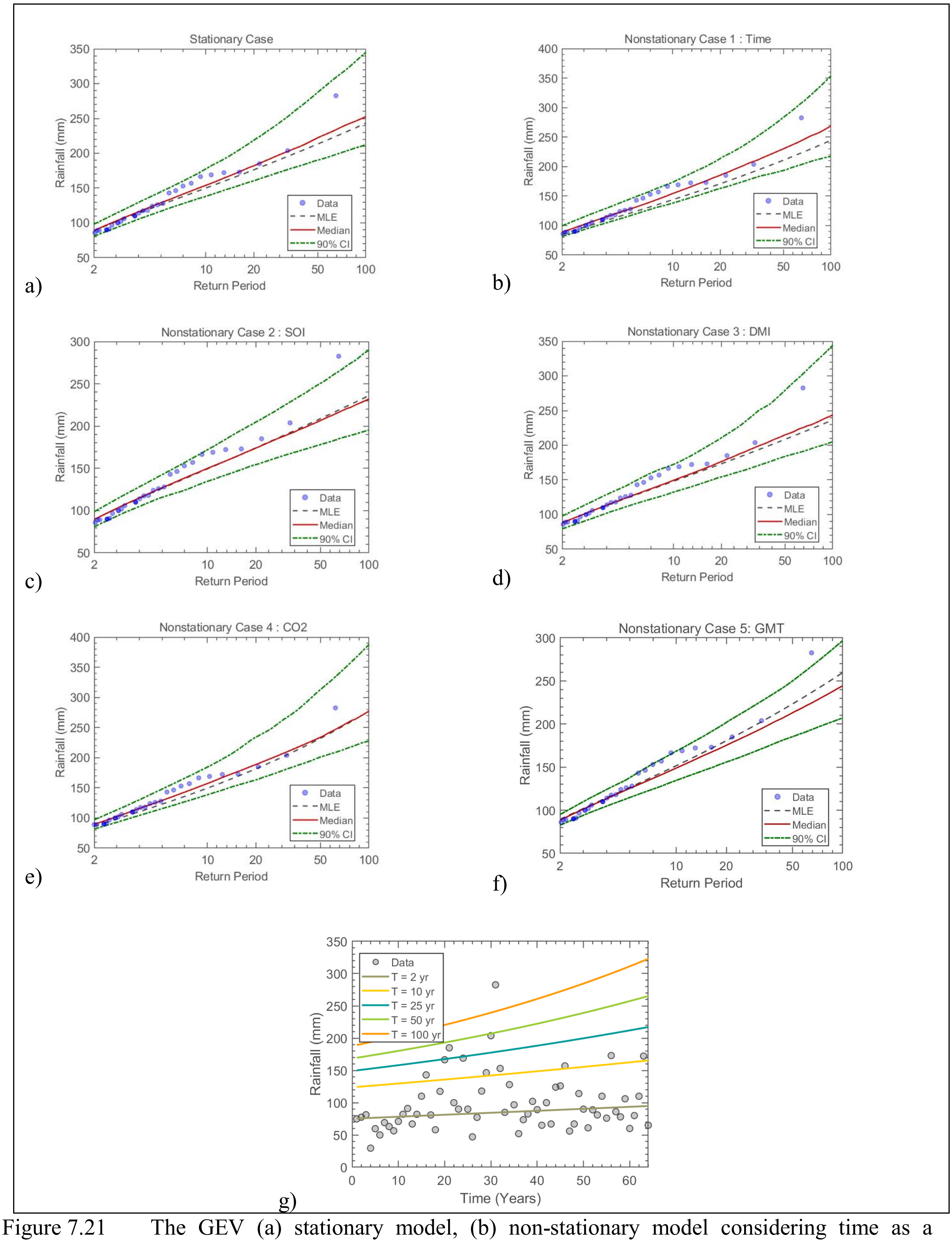

Figure 7.21 The GEV (a) stationary model, (b) non-stationary model considering time as a covariate, (c) non-stationary model considering SOI as a covariate, (d) non-stationary model considering DMI as a covariate, (e) non-stationary model considering CO_2 as a covariate, (f) non-stationary model considering GMT as a covariate and (g) effective return period as a function of time for Station 125: Sinembe – Spreyton Farm

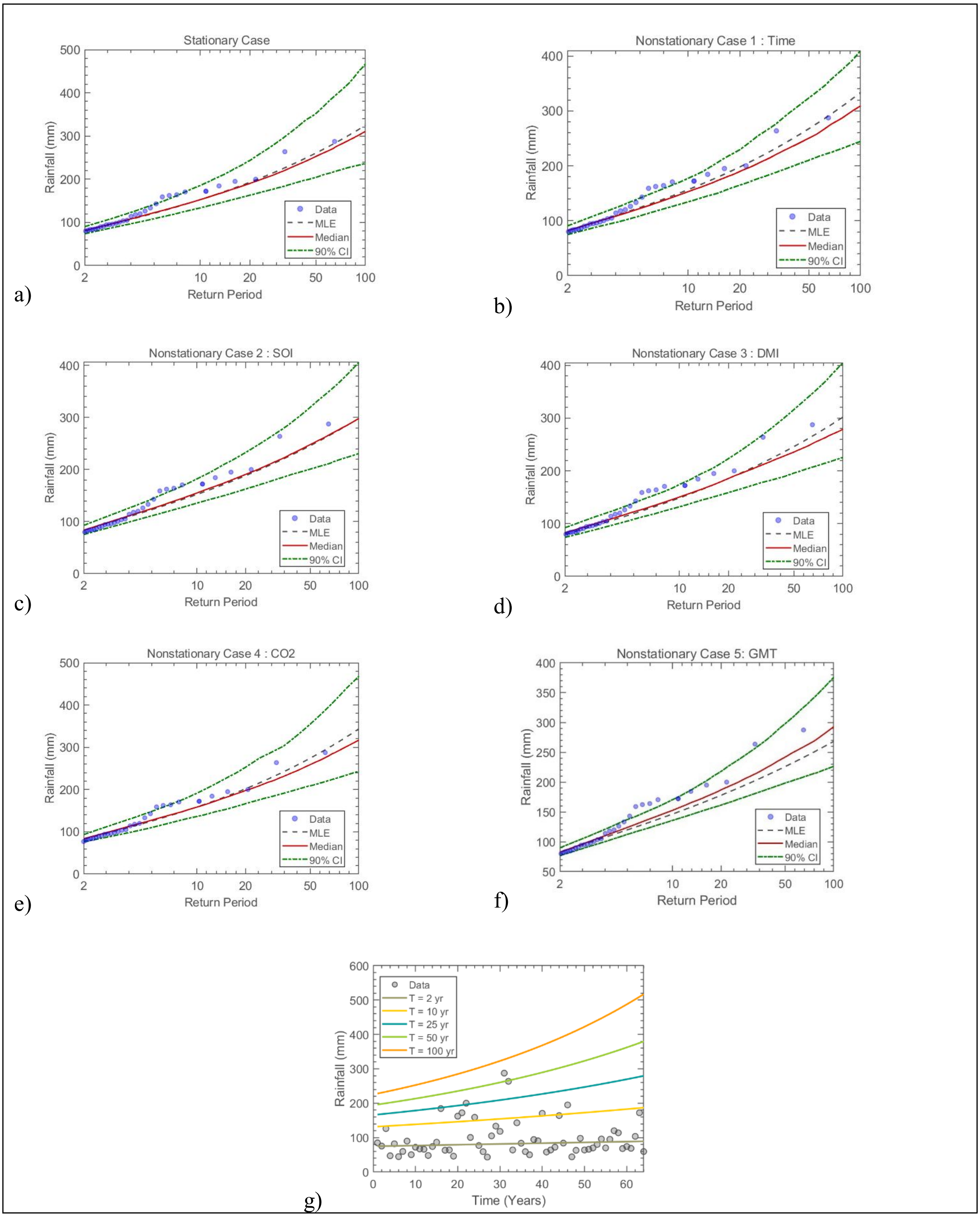

Figure 7.22 The GEV (a) stationary model, (b) non-stationary model considering time as a covariate, (c) non-stationary model considering SOI as a covariate, (d) non-stationary model considering DMI as a covariate, (e) non-stationary model considering CO_2 as a covariate, (f) non-stationary model considering GMT as a covariate and (g) effective return period as a function of time for Station 126: Upper Tongaat – Barwon Farm

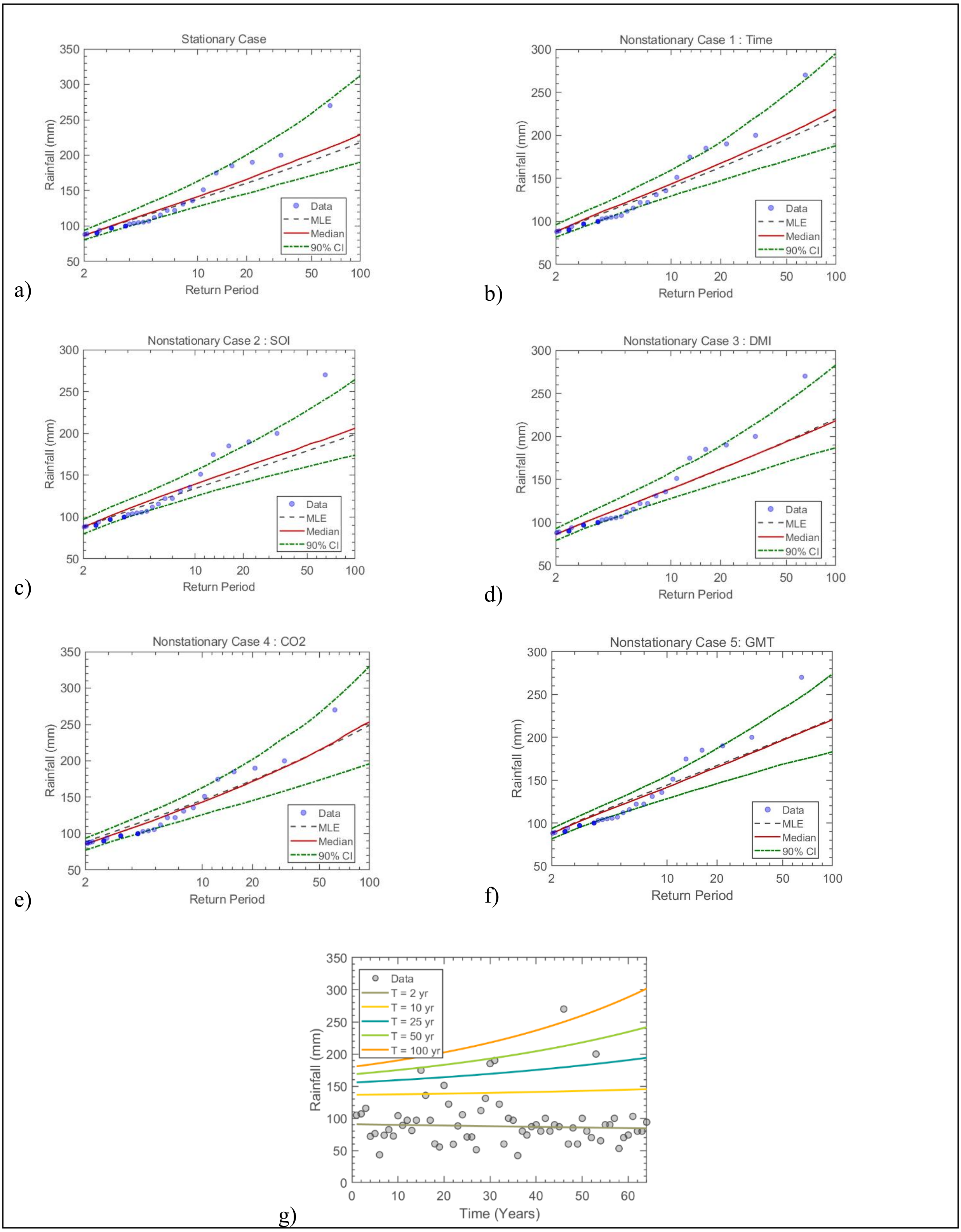

Figure 7.23 The GEV (a) stationary model, (b) non-stationary model considering time as a covariate, (c) non-stationary model considering SOI as a covariate, (d) non-stationary model considering DMI as a covariate, (e) non-stationary model considering CO_2 as a covariate, (f) non-stationary model considering GMT as a covariate and (g) effective return period as a function of time for Station 129: Kearsney – Ocean Lodge

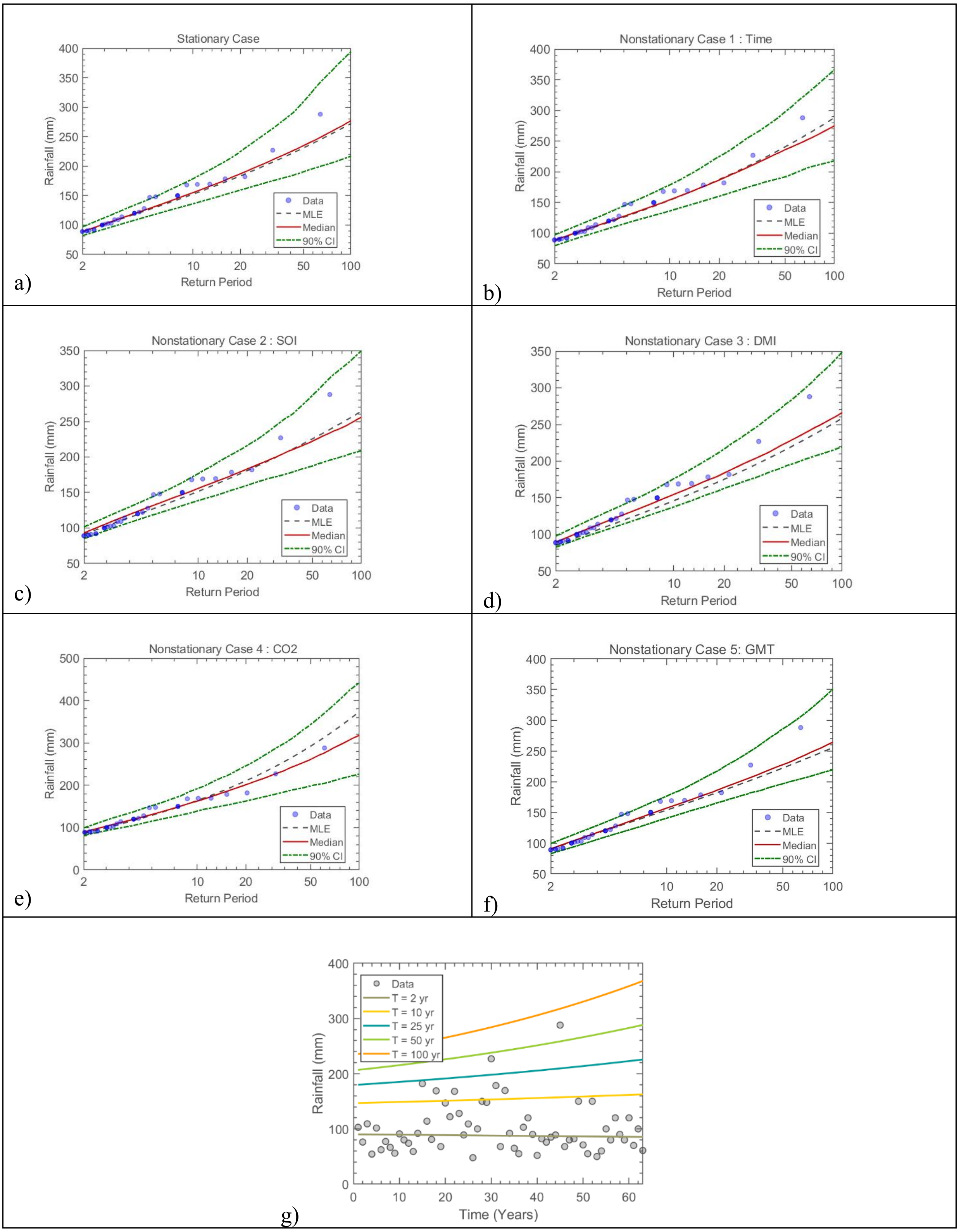

Figure 7.24 The GEV (a) stationary model, (b) non-stationary model considering time as a covariate, (c) non-stationary model considering SOI as a covariate, (d) non-stationary model considering DMI as a covariate, (e) non-stationary model considering CO_2 as a covariate, (f) non-stationary model considering GMT as a covariate and (g) effective return period as a function of time for Station 130: Doornkop – Langespruit Farm

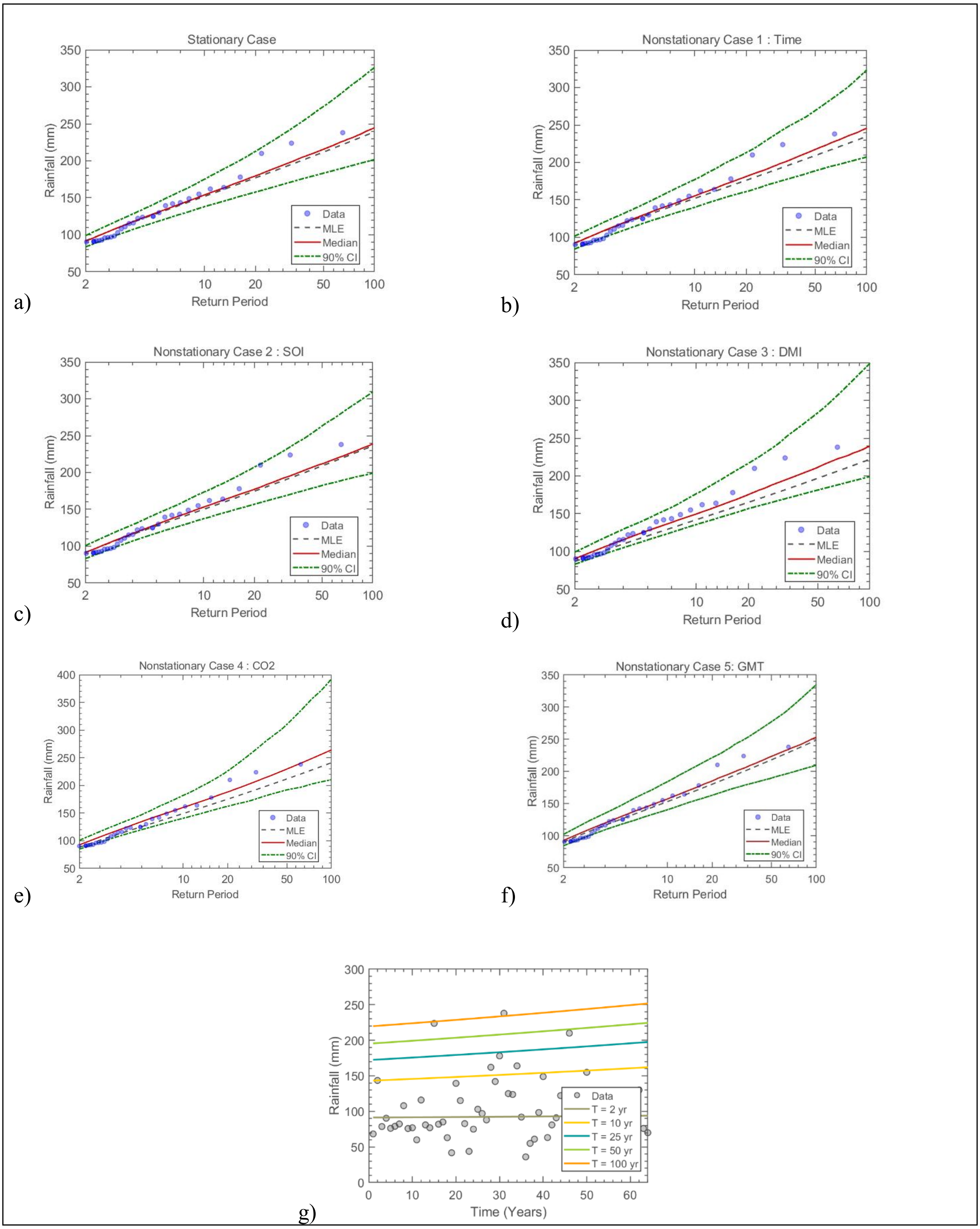

Figure 7.25 The GEV (a) stationary model, (b) non-stationary model considering time as a covariate, (c) non-stationary model considering SOI as a covariate, (d) non-stationary model considering DMI as a covariate, (e) non-stationary model considering CO_2 as a covariate, (f) non-stationary model considering GMT as a covariate and (g) effective return period as a function of time for Station 131: Darnall – Sugar Mill (THS)

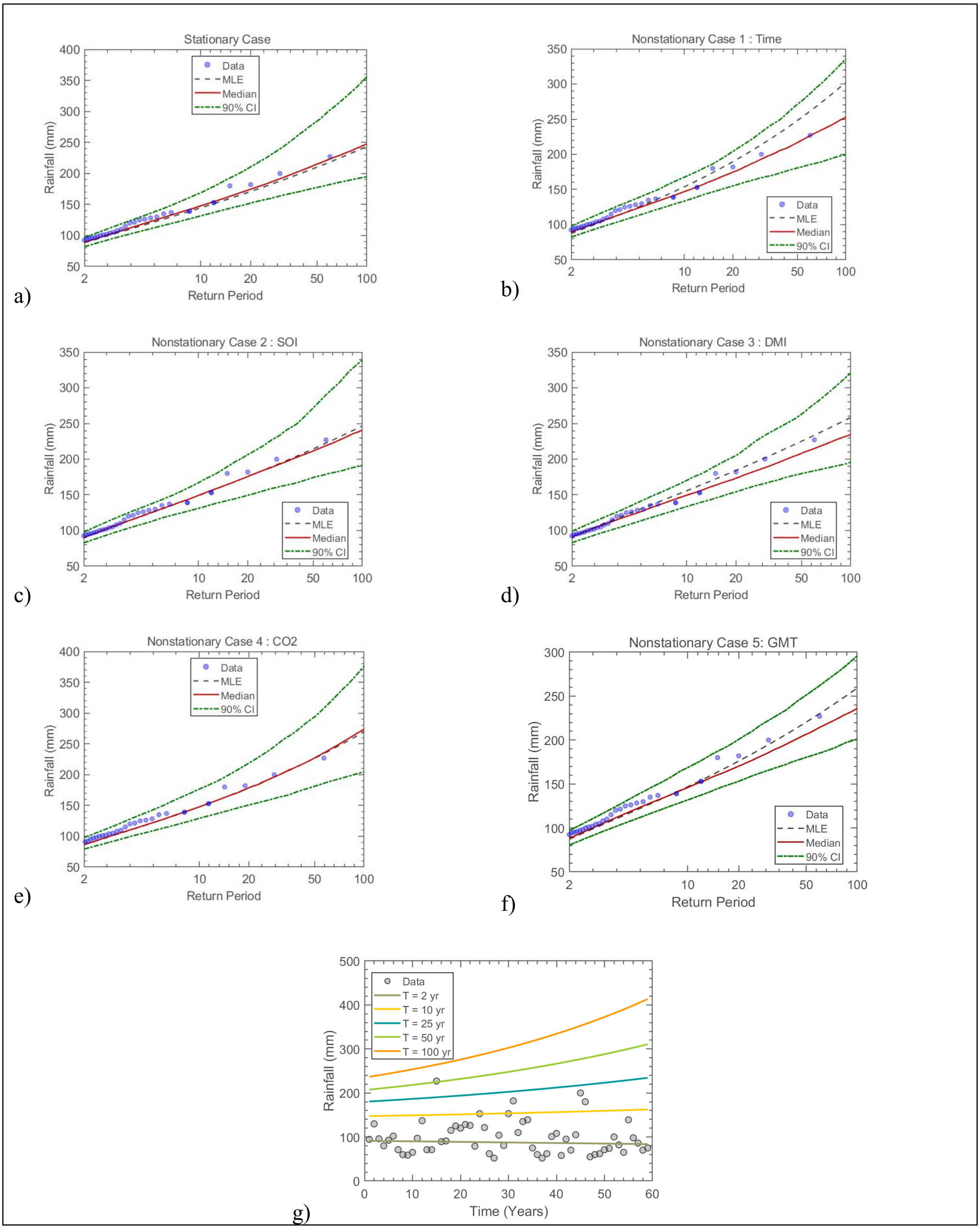

Figure 7.26 The GEV (a) stationary model, (b) non-stationary model considering time as a covariate, (c) non-stationary model considering SOI as a covariate, (d) non-stationary model considering DMI as a covariate, (e) non-stationary model considering CO_2 as a covariate, (f) non-stationary model considering GMT as a covariate and (g) effective return period as a function of time for Station 132: Tugela Mouth – Wetherly Estate

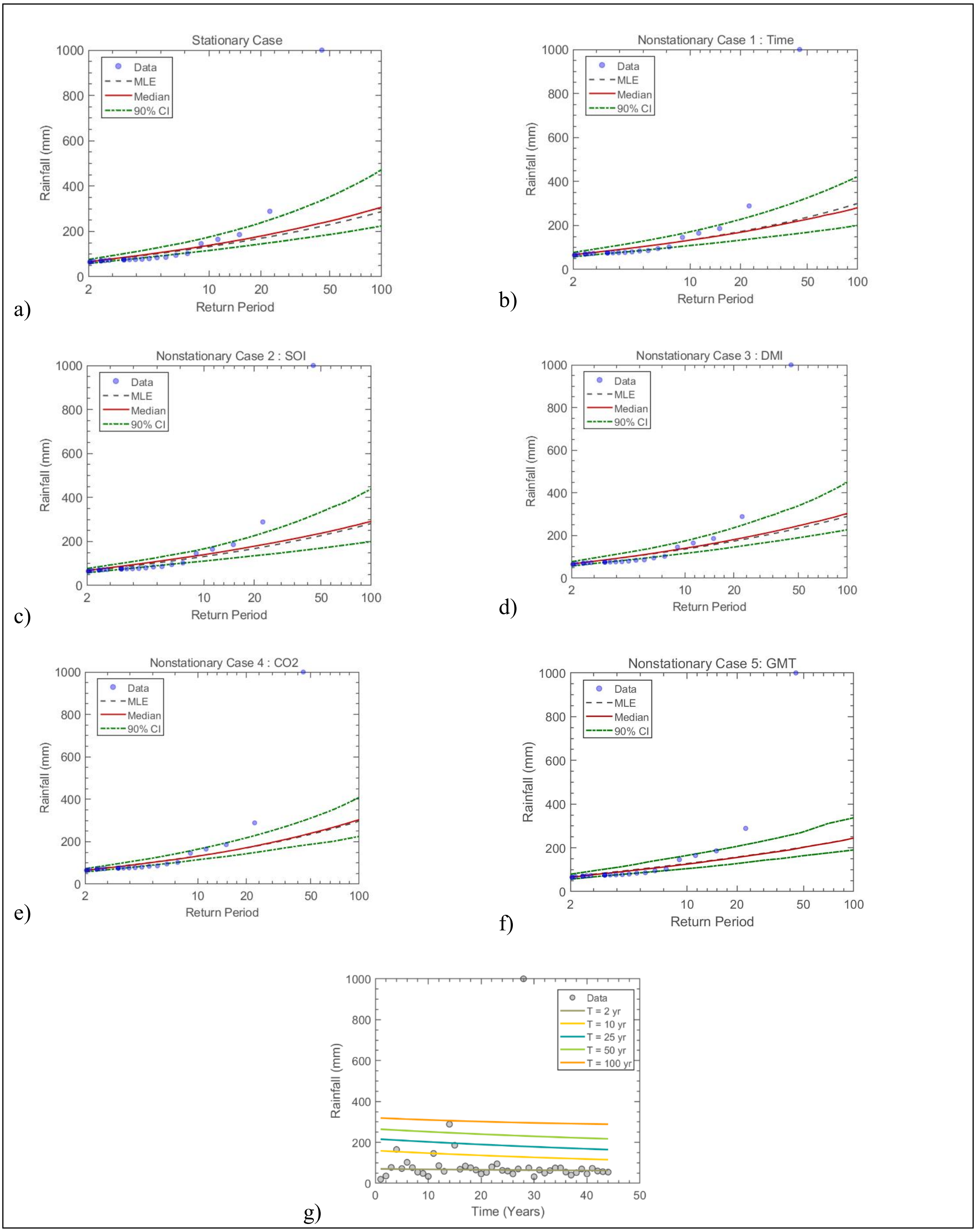

Figure 7.27 The GEV (a) stationary model, (b) non-stationary model considering time as a covariate, (c) non-stationary model considering SOI as a covariate, (d) non-stationary model considering DMI as a covariate, (e) non-stationary model considering CO_2 as a covariate, (f) non-stationary model considering GMT as a covariate and (g) effective return period as a function of time for Station 136: Glenside – Misty Krantz Estate

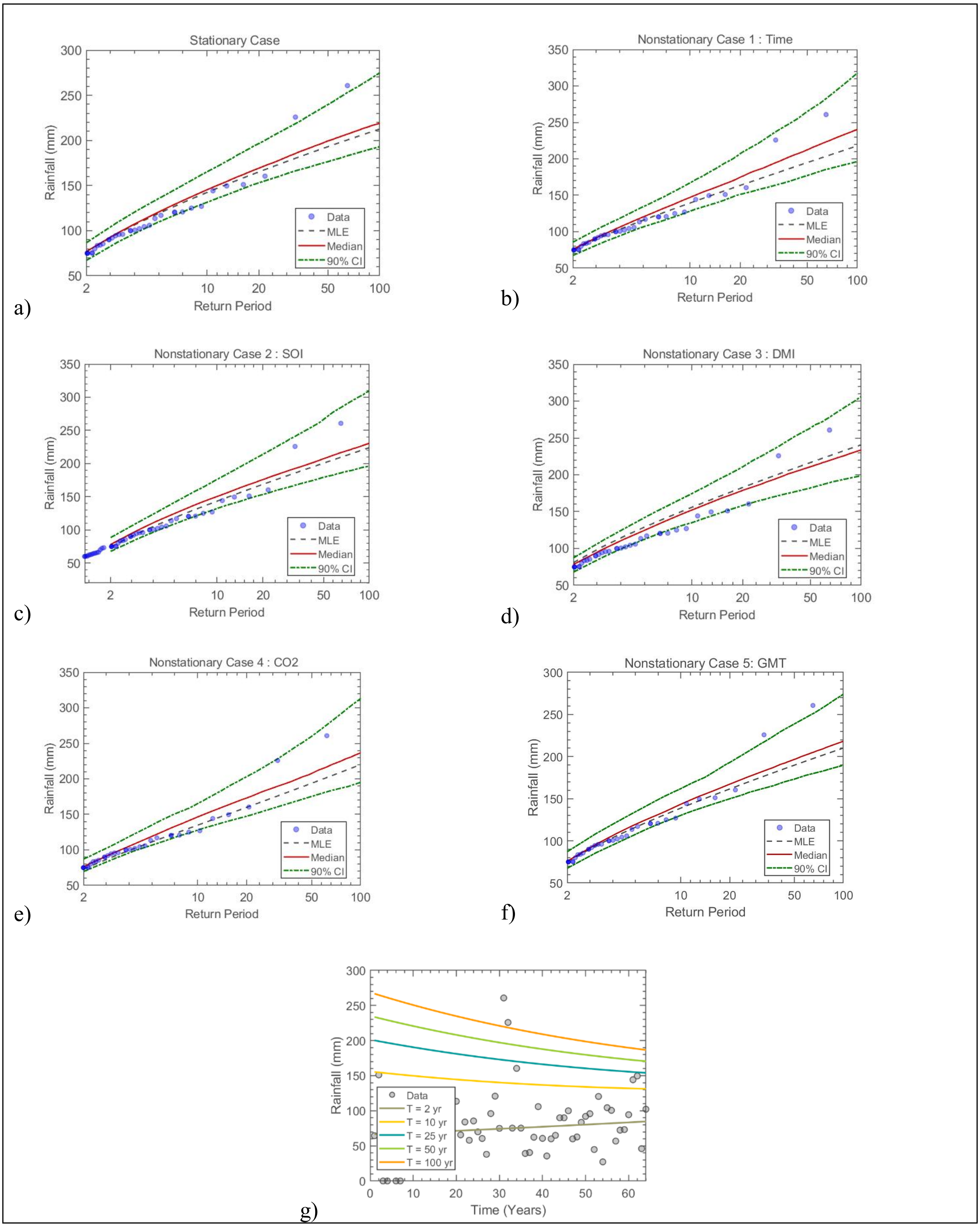

Figure 7.28 The GEV (a) stationary model, (b) non-stationary model considering time as a covariate, (c) non-stationary model considering SOI as a covariate, (d) non-stationary model considering DMI as a covariate, (e) non-stationary model considering CO_2 as a covariate, (f) non-stationary model considering GMT as a covariate and (g) effective return period as a function of time for Station 138: Mandini – SAWS

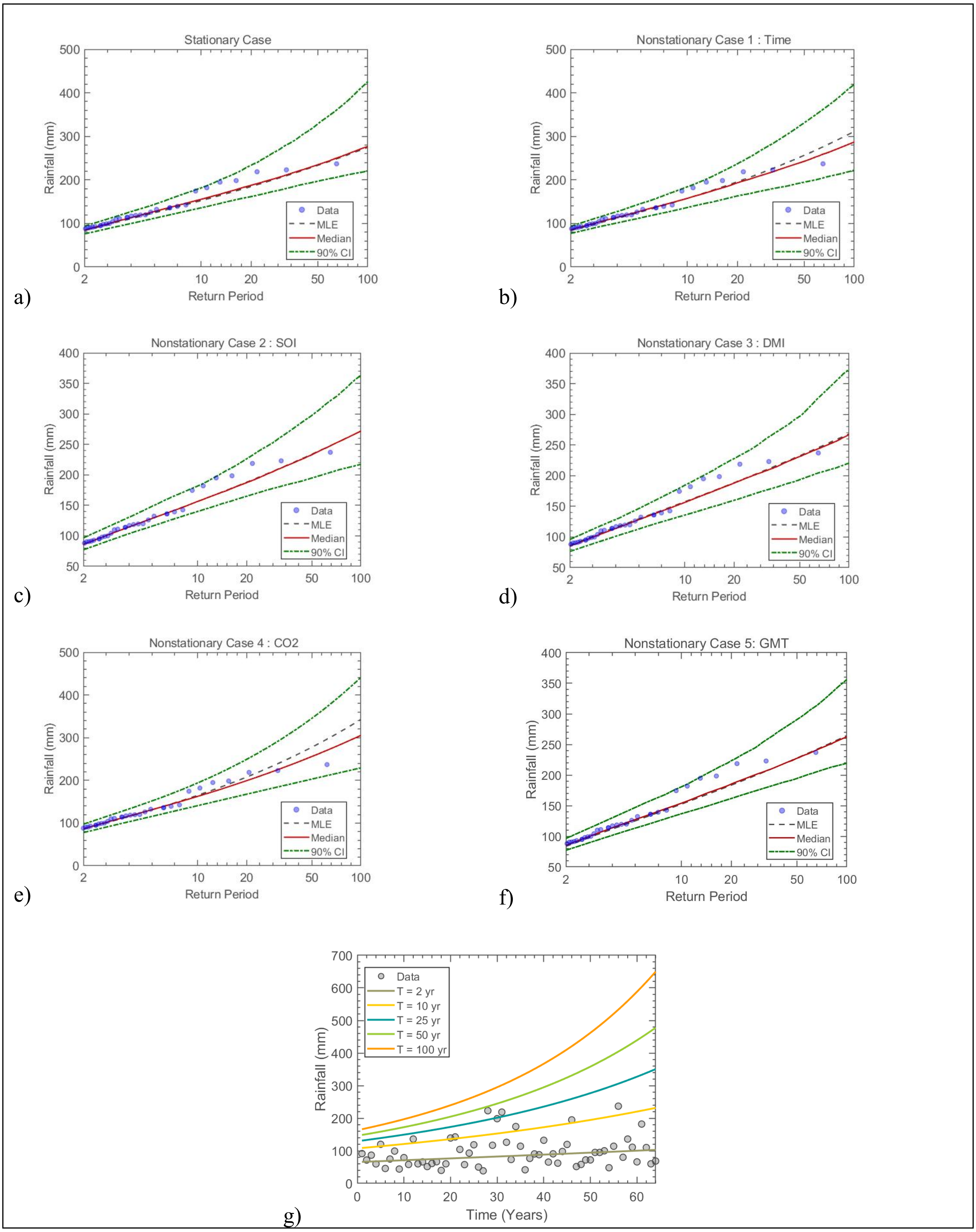

Figure 7.29 The GEV (a) stationary model, (b) non-stationary model considering time as a covariate, (c) non-stationary model considering SOI as a covariate, (d) non-stationary model considering DMI as a covariate, (e) non-stationary model considering CO_2 as a covariate, (f) non-stationary model considering GMT as a covariate and (g) effective return period as a function of time for Station 139: Inyoni – Myrln Estate

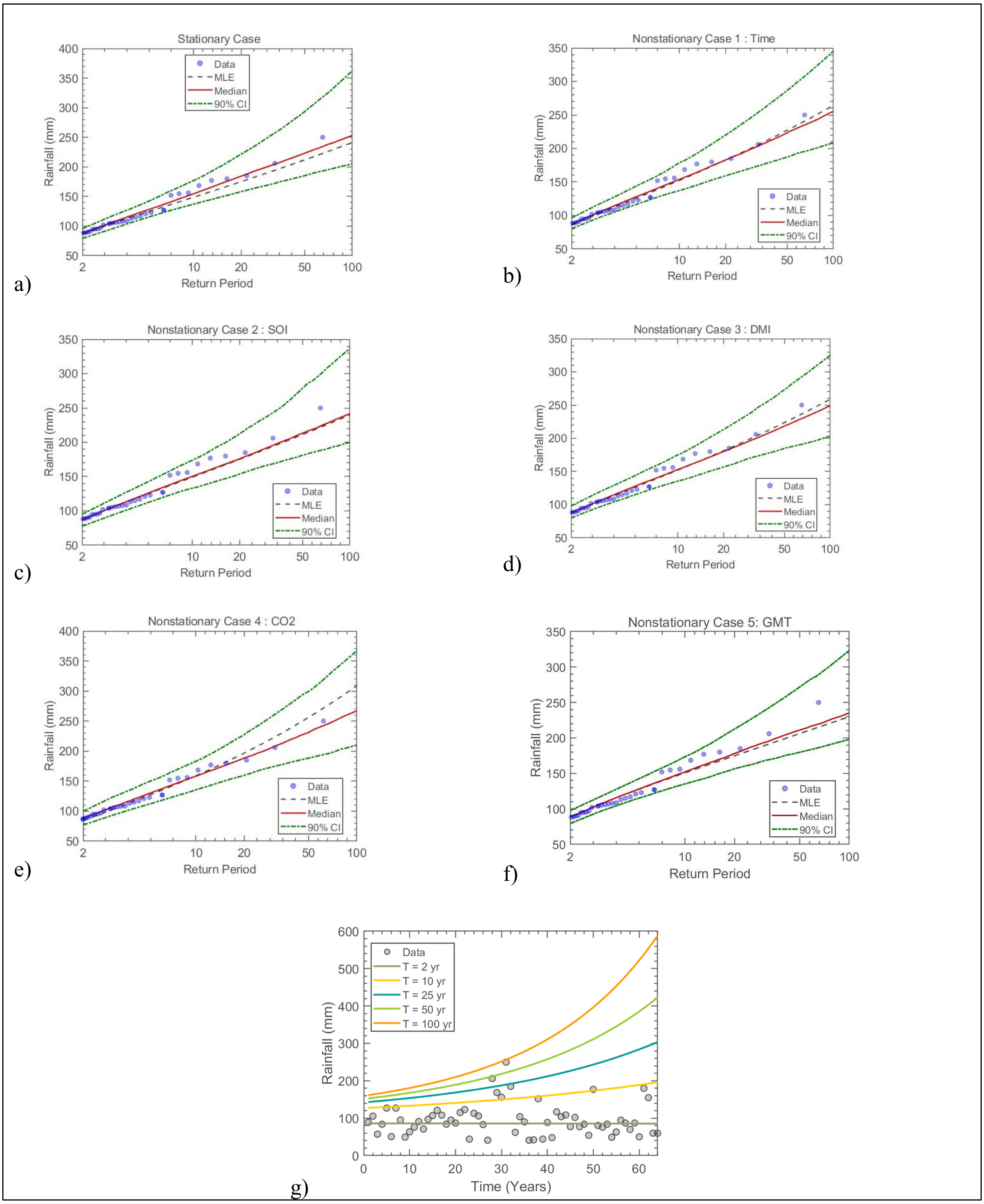

Figure 7.30 The GEV (a) stationary model, (b) non-stationary model considering time as a covariate, (c) non-stationary model considering SOI as a covariate, (d) non-stationary model considering DMI as a covariate, (e) non-stationary model considering CO_2 as a covariate, (f) non-stationary model considering GMT as a covariate and (g) effective return period as a function of time for Station 142: Eshowe – Brocklee Farm

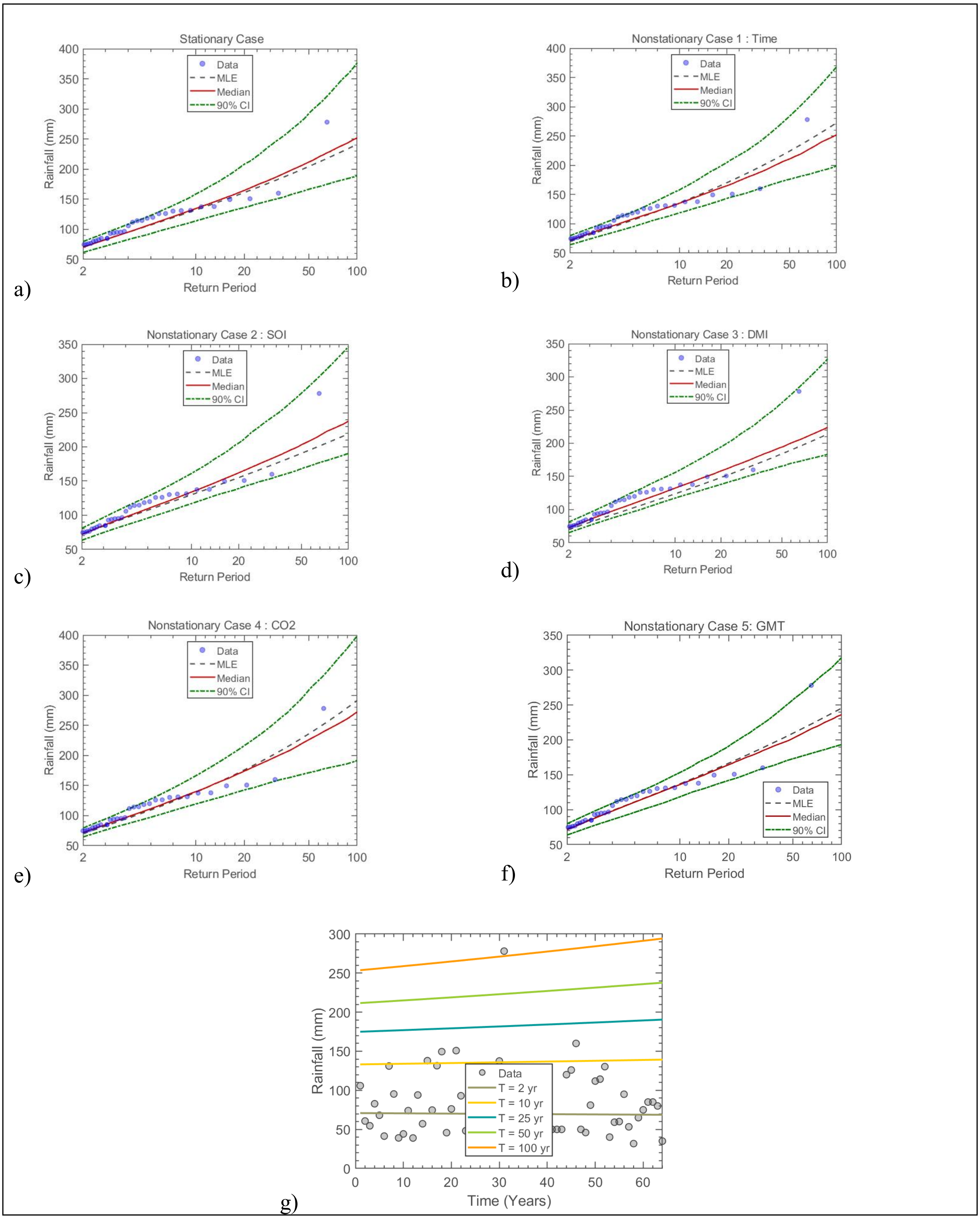

Figure 7.31 The GEV (a) stationary model, (b) non-stationary model considering time as a covariate, (c) non-stationary model considering SOI as a covariate, (d) non-stationary model considering DMI as a covariate, (e) non-stationary model considering CO_2 as a covariate, (f) non-stationary model considering GMT as a covariate and (g) effective return period as a function of time for Station 143: Nkwaleni – Zigagazi

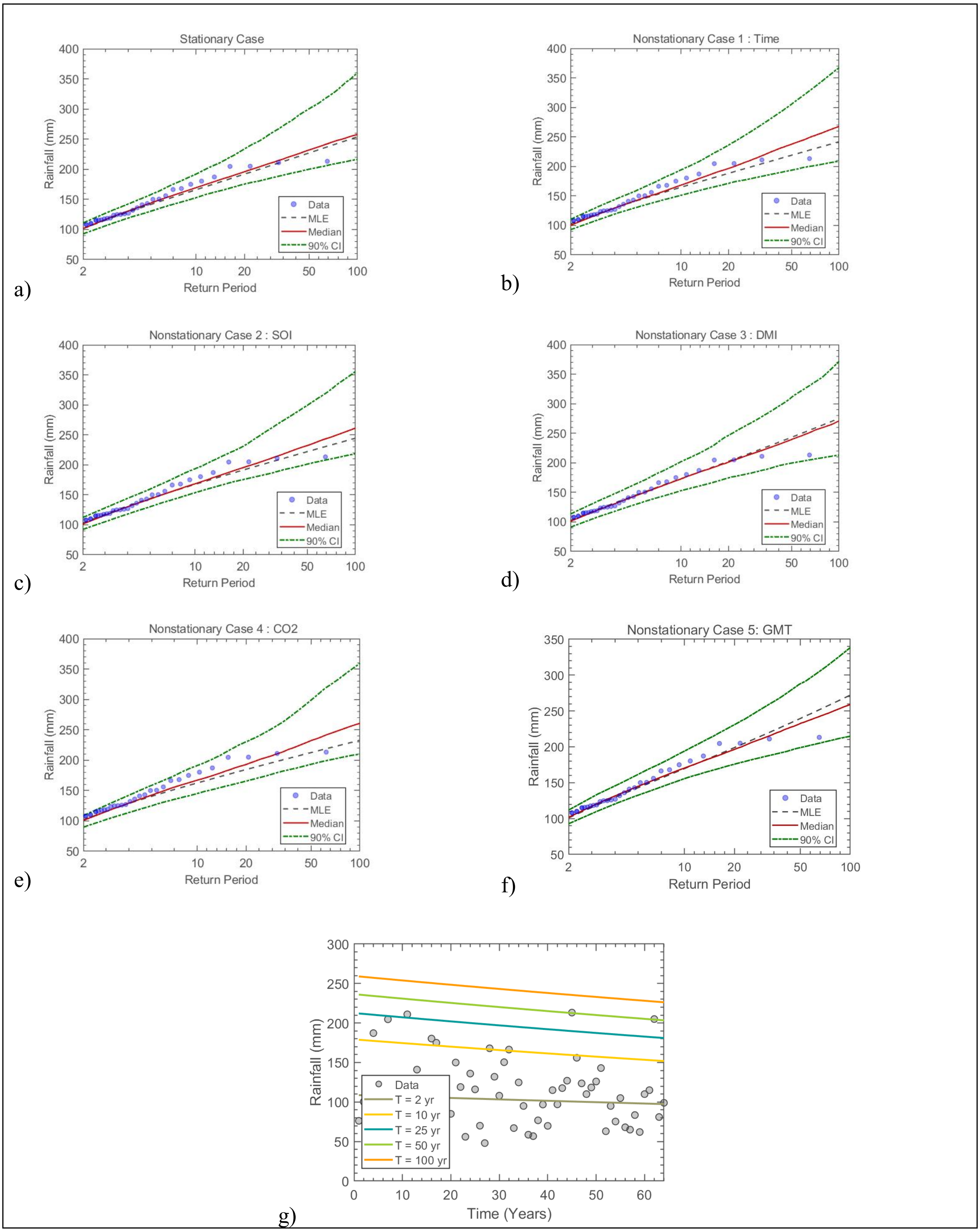

Figure 7.32 The GEV (a) stationary model, (b) non-stationary model considering time as a covariate, (c) non-stationary model considering SOI as a covariate, (d) non-stationary model considering DMI as a covariate, (e) non-stationary model considering CO_2 as a covariate, (f) non-stationary model considering GMT as a covariate and (g) effective return period as a function of time for Station 144: Felixton – Sugar Mill (THS)

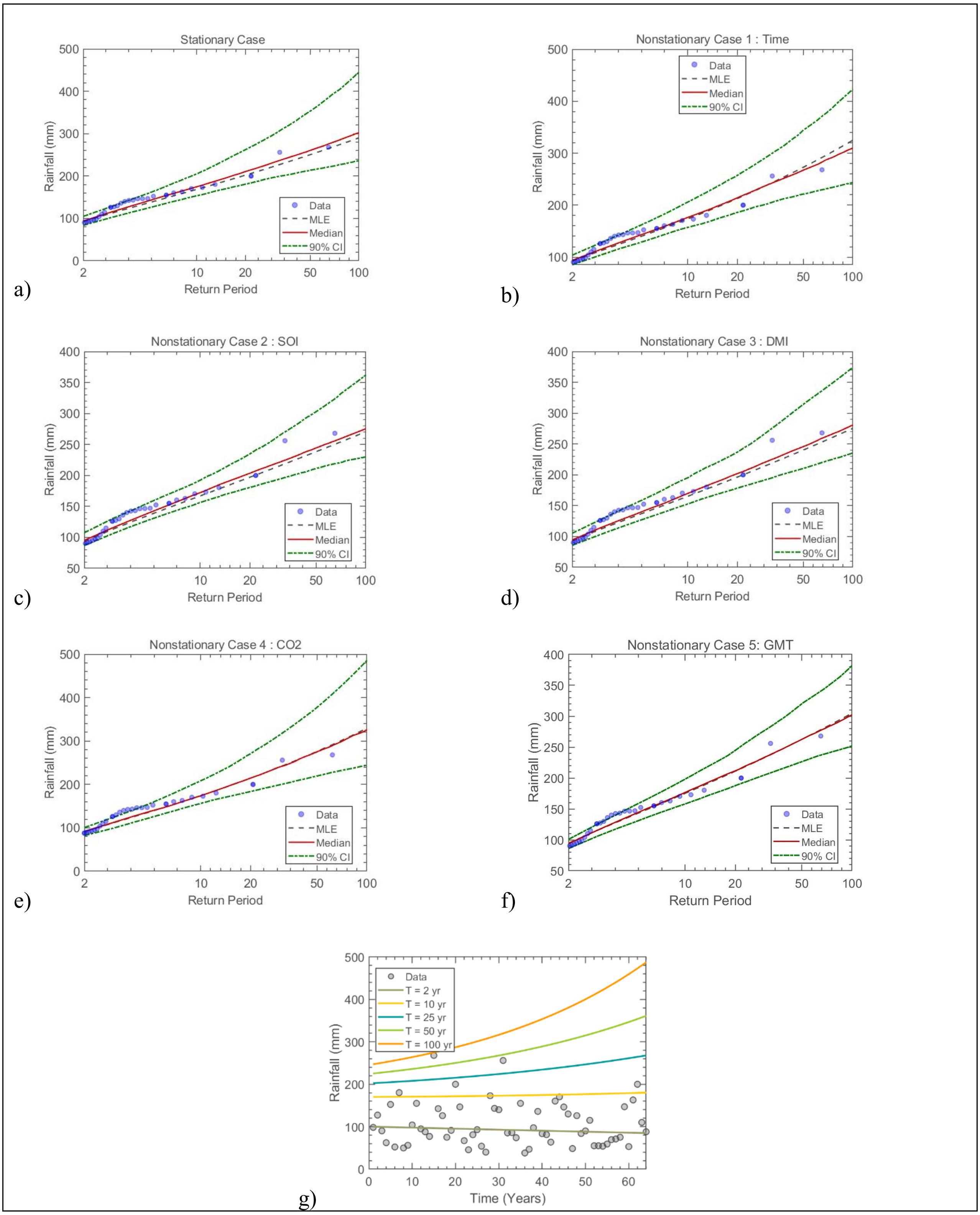

Figure 7.33 The GEV (a) stationary model, (b) non-stationary model considering time as a covariate, (c) non-stationary model considering SOI as a covariate, (d) non-stationary model considering DMI as a covariate, (e) non-stationary model considering CO_2 as a covariate, (f) non-stationary model considering GMT as a covariate and (g) effective return period as a function of time for Station 146: Kulu Halt – Honey Farm

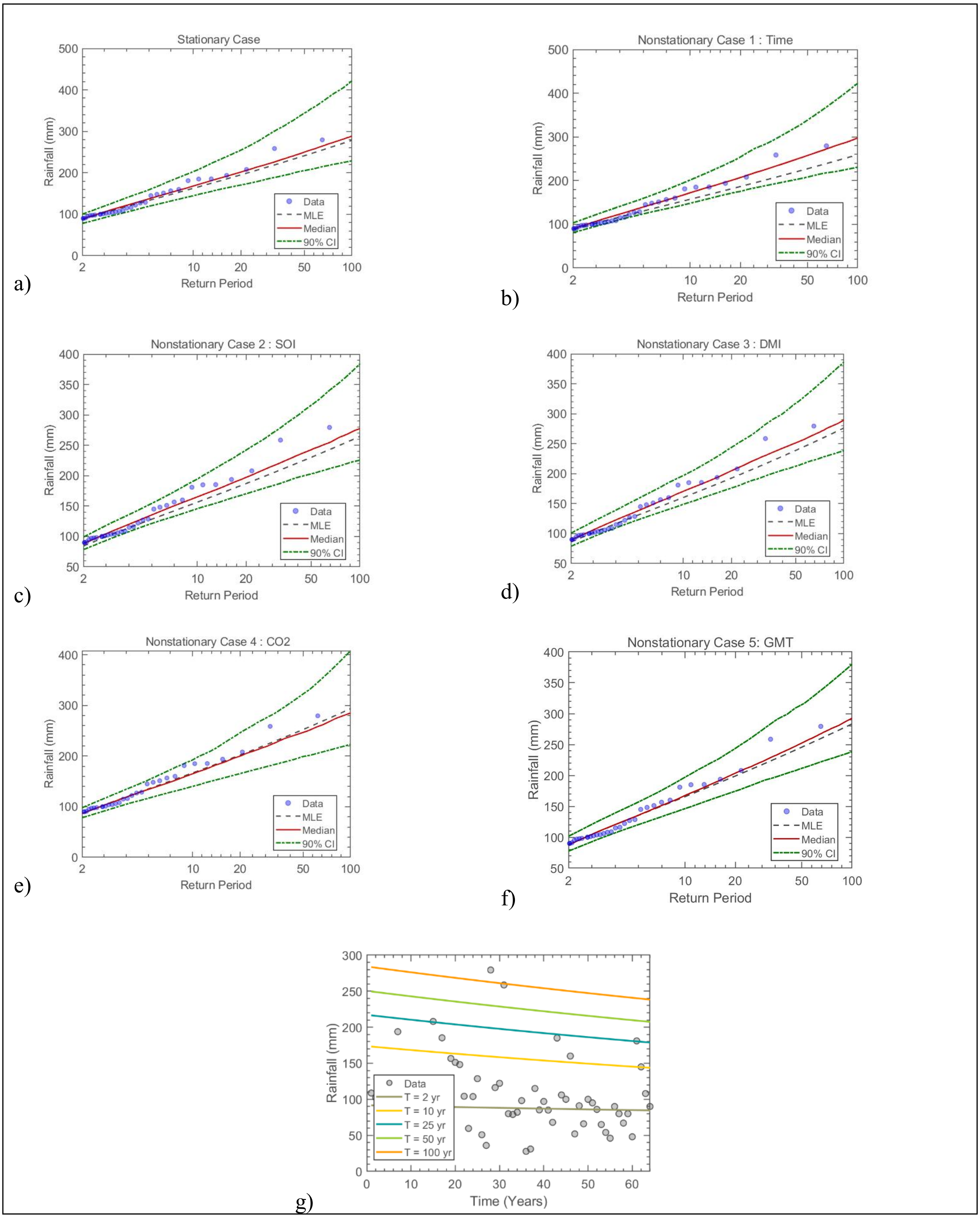

Figure 7.34 The GEV (a) stationary model, (b) non-stationary model considering time as a covariate, (c) non-stationary model considering SOI as a covariate, (d) non-stationary model considering DMI as a covariate, (e) non-stationary model considering CO_2 as a covariate, (f) non-stationary model considering GMT as a covariate and (g) effective return period as a function of time for Station 147: Ukulu Properties – Crystal Holdings

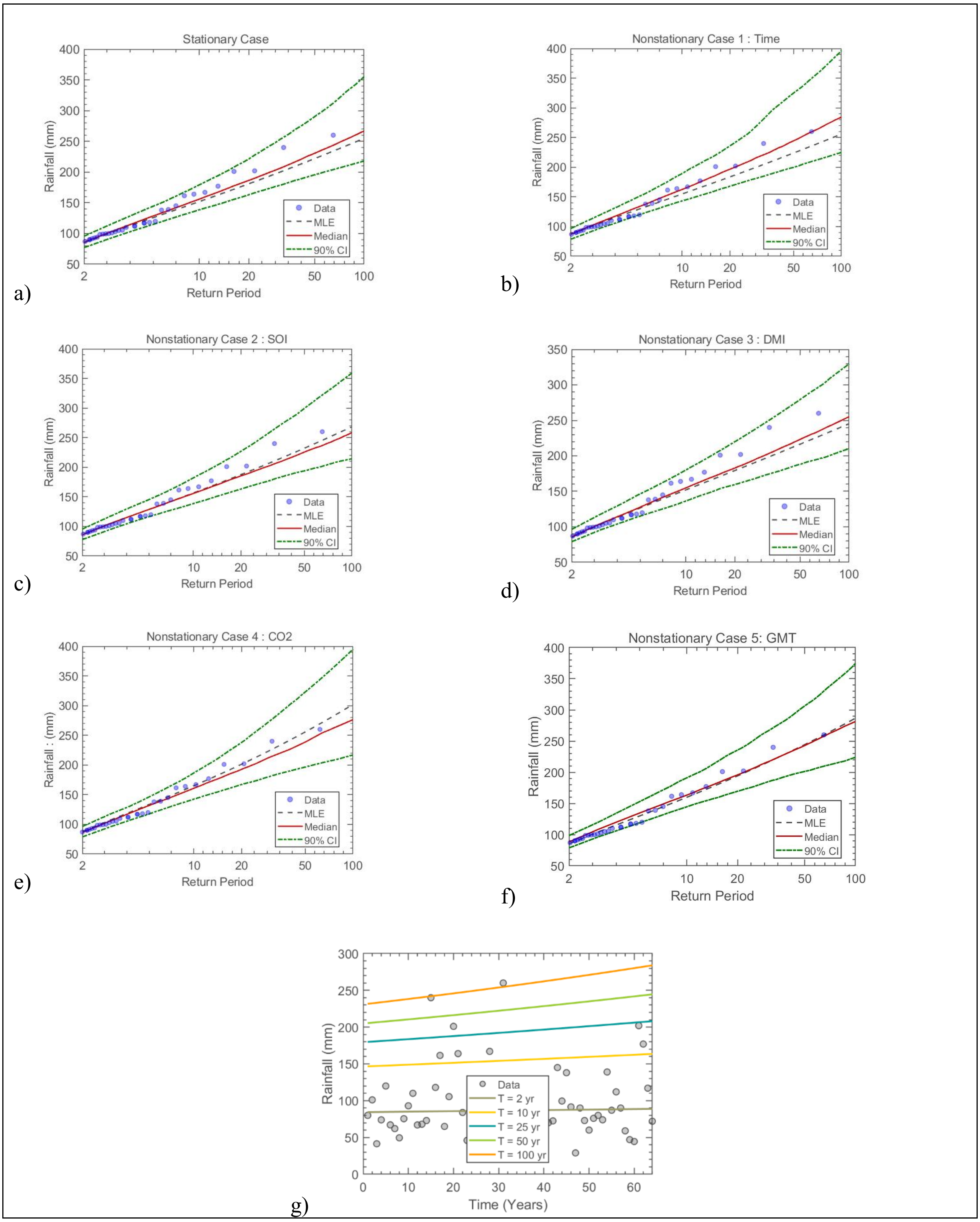

Figure 7.35 The GEV (a) stationary model, (b) non-stationary model considering time as a covariate, (c) non-stationary model considering SOI as a covariate, (d) non-stationary model considering DMI as a covariate, (e) non-stationary model considering CO_2 as a covariate, (f) non-stationary model considering GMT as a covariate and (g) effective return period as a function of time for Station 148: Mposa – Redcroft Farm

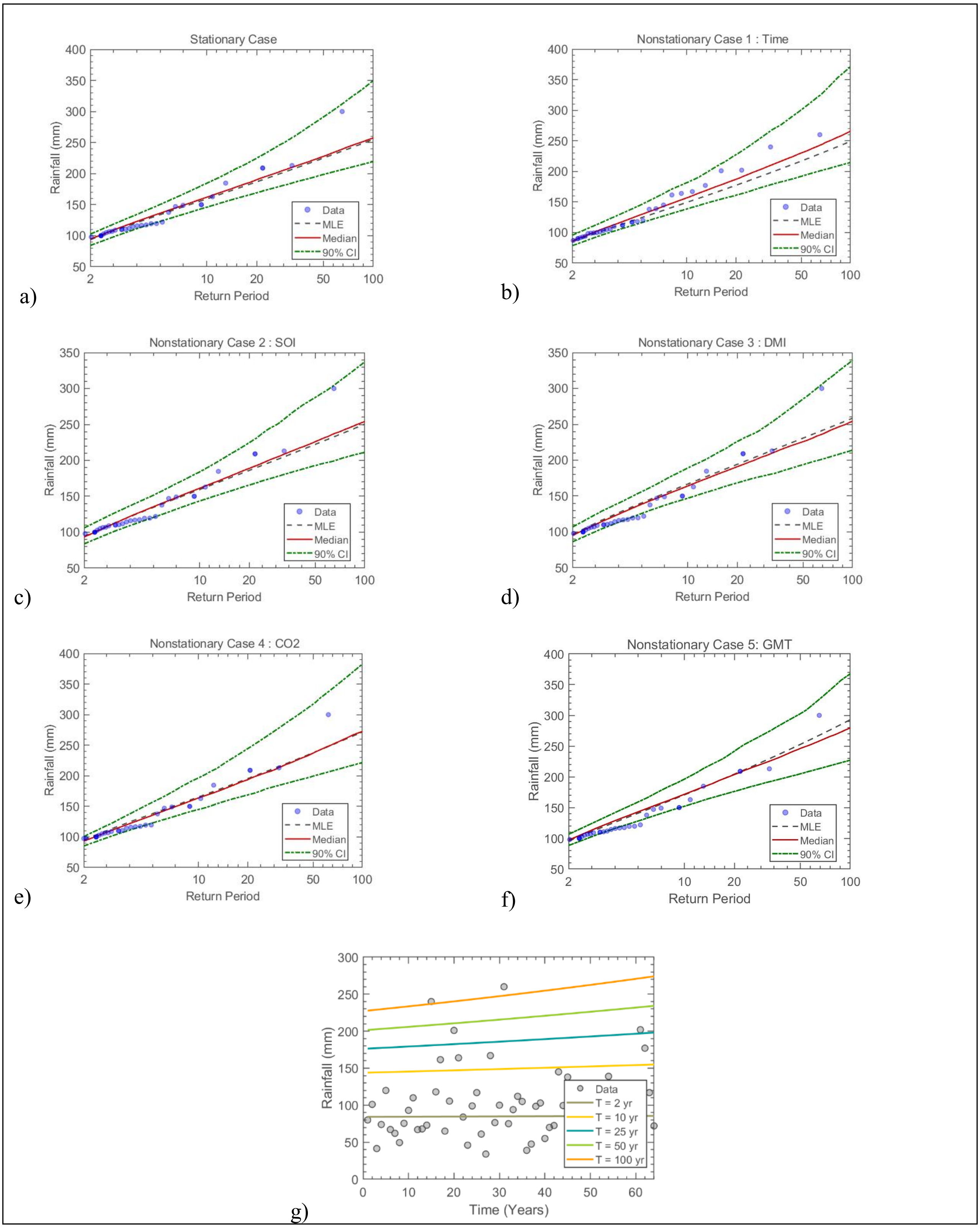

Figure 7.36 The GEV (a) stationary model, (b) non-stationary model considering time as a covariate, (c) non-stationary model considering SOI as a covariate, (d) non-stationary model considering DMI as a covariate, (e) non-stationary model considering CO_2 as a covariate, (f) non-stationary model considering GMT as a covariate and (g) effective return period as a function of time for Station 149: Kwambonambi – Mondi Forestry

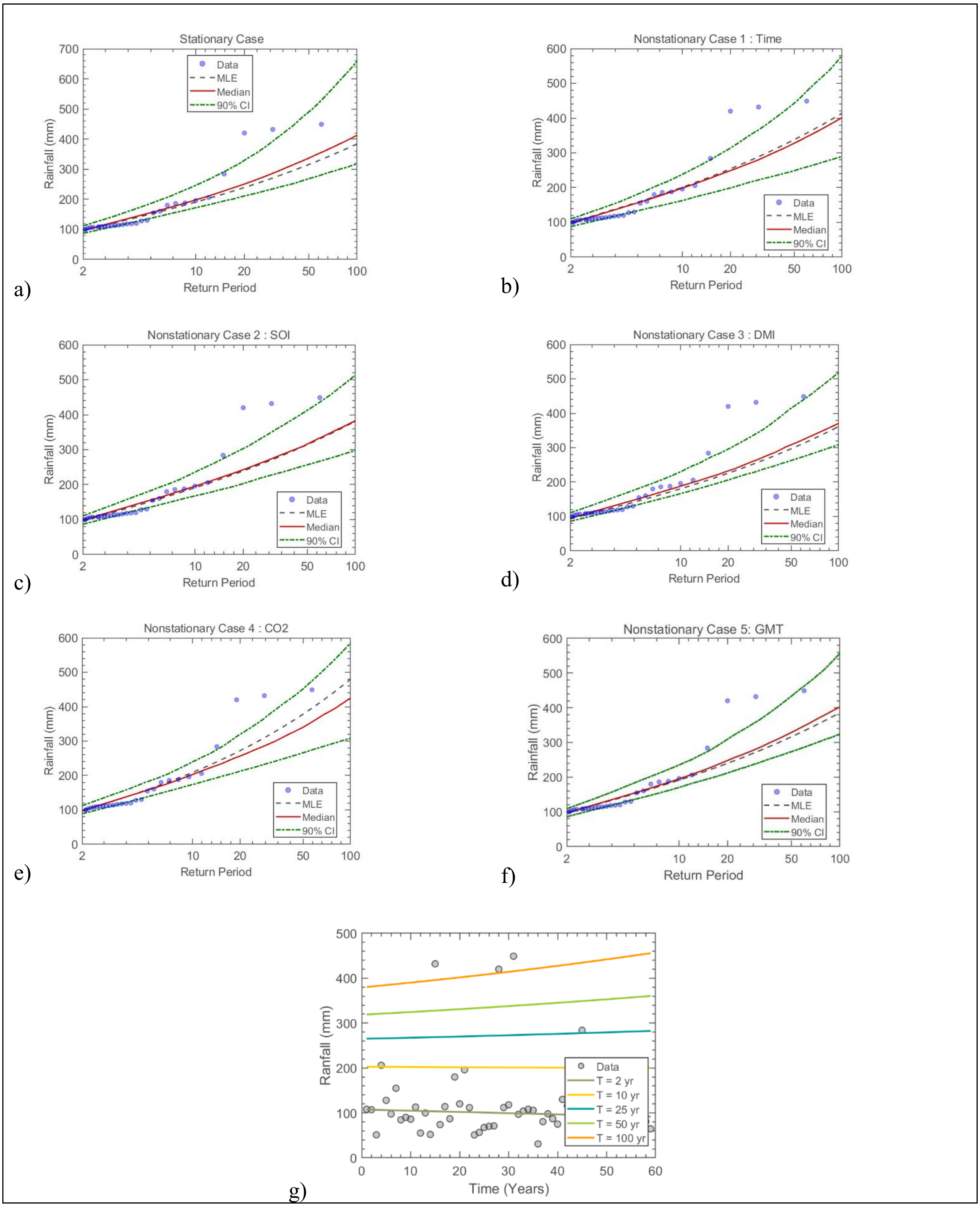

Figure 7.37 The GEV (a) stationary model, (b) non-stationary model considering time as a covariate, (c) non-stationary model considering SOI as a covariate, (d) non-stationary model considering DMI as a covariate, (e) non-stationary model considering CO_2 as a covariate, (f) non-stationary model considering GMT as a covariate and (g) effective return period as a function of time for Station 151: ULOA – Mark & Ross Sugar Estate

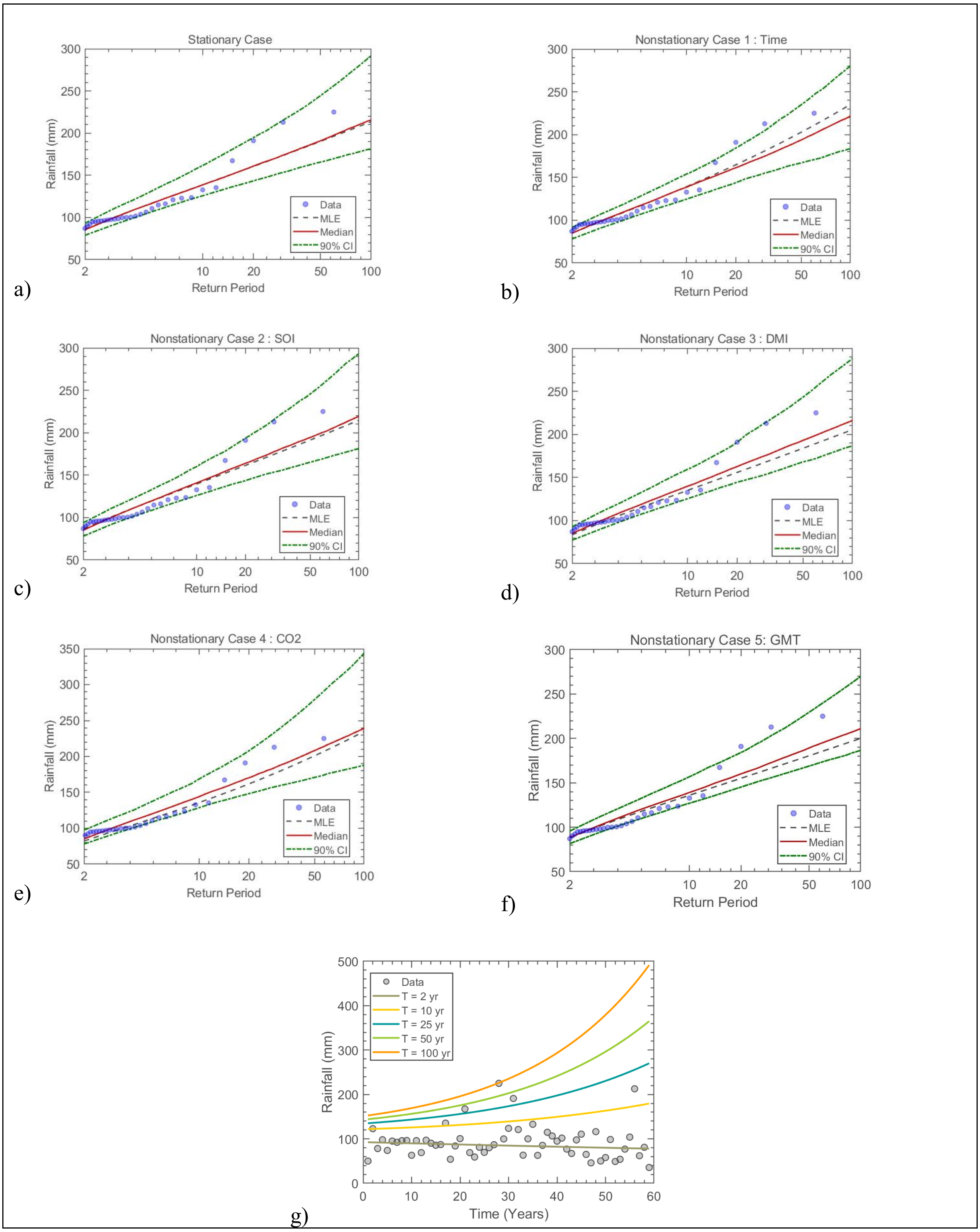

Figure 7.38 The GEV (a) stationary model, (b) non-stationary model considering time as a covariate, (c) non-stationary model considering SOI as a covariate, (d) non-stationary model considering DMI as a covariate, (e) non-stationary model considering CO_2 as a covariate, (f) non-stationary model considering GMT as a covariate and (g) effective return period as a function of time for Station 152: Mtubatuba – Nyalazi River

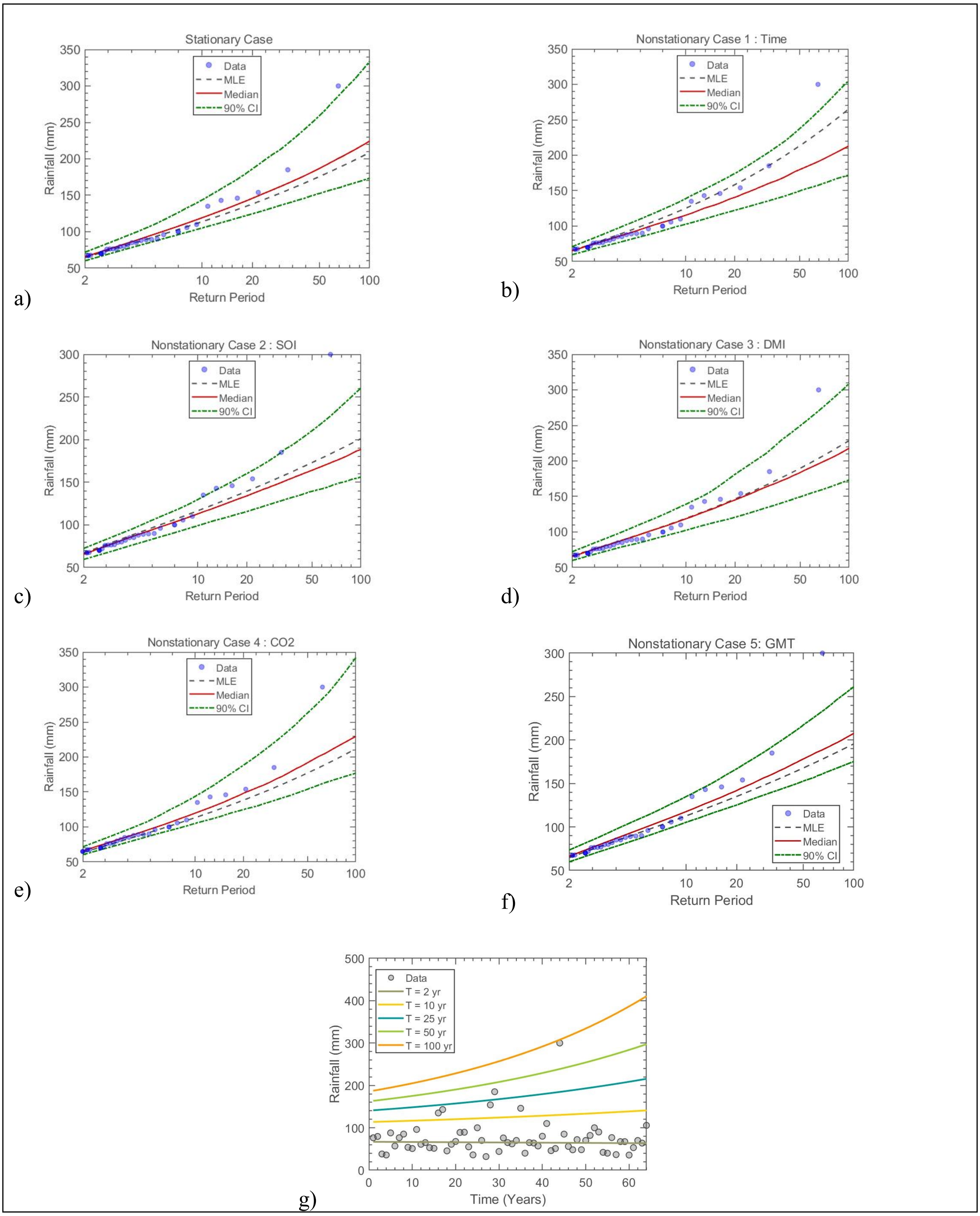

Figure 7.39 The GEV (a) stationary model, (b) non-stationary model considering time as a covariate, (c) non-stationary model considering SOI as a covariate, (d) non-stationary model considering DMI as a covariate, (e) non-stationary model considering CO_2 as a covariate, (f) non-stationary model considering GMT as a covariate and (g) effective return period as a function of time for Station 154: Mkuze – Mkuze Estate

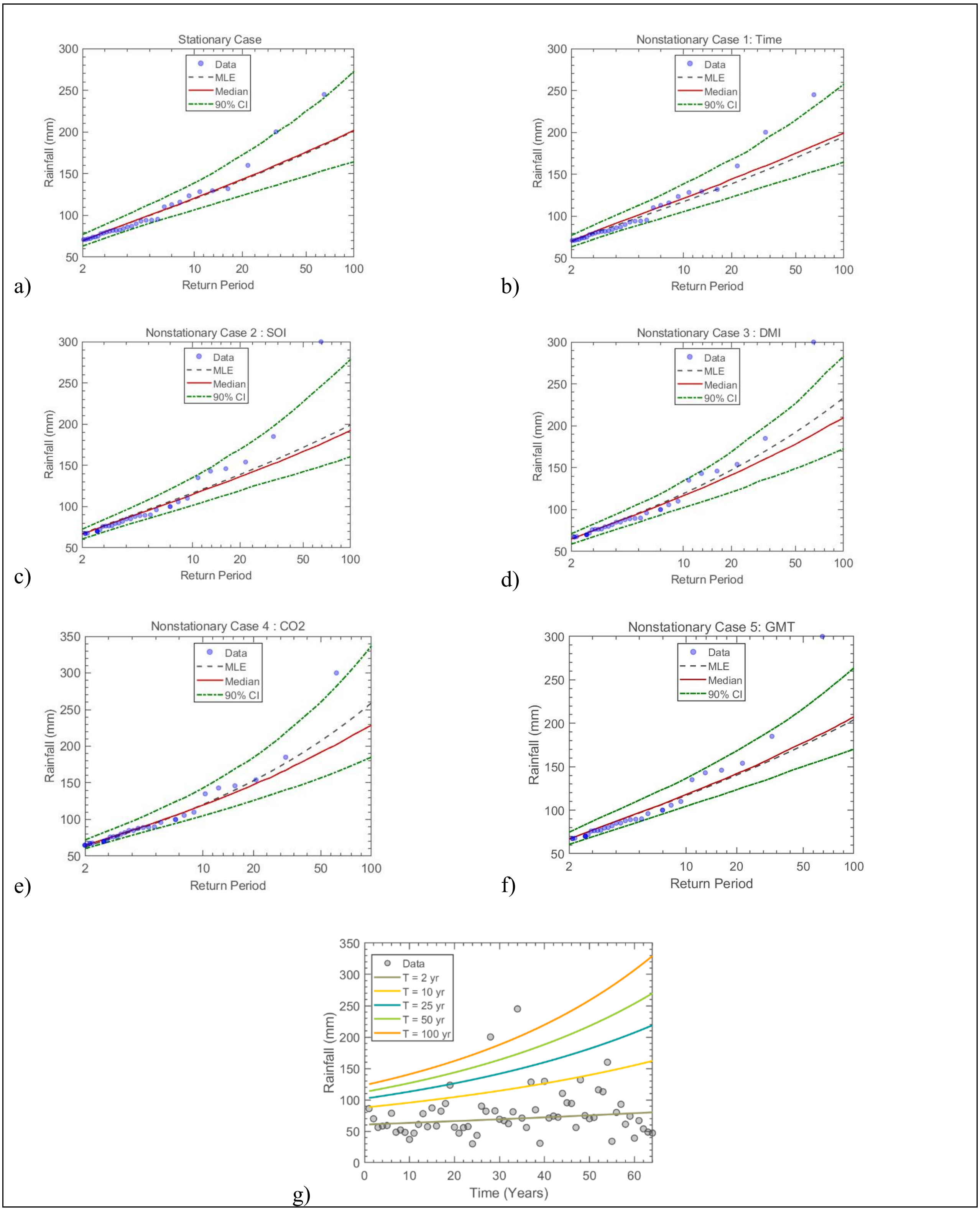

Figure 7.40 The GEV (a) stationary model, (b) non-stationary model considering time as a covariate, (c) non-stationary model considering SOI as a covariate, (d) non-stationary model considering DMI as a covariate, (e) non-stationary model considering CO_2 as a covariate, (f) non-stationary model considering GMT as a covariate and (g) effective return period as a function of time for Station 155: Pongola – Impala Irrigation Board

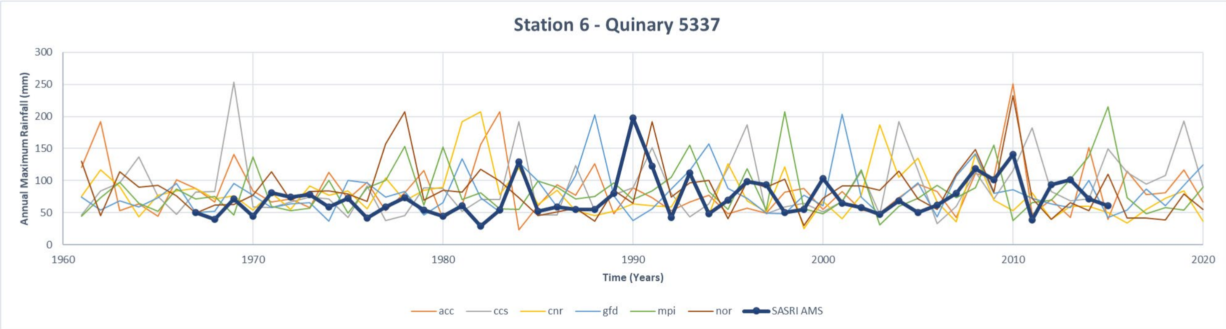

Figure 7.41 Time series of annual maximum rainfall for SASRI station 6 and 6 GCMs for corresponding years

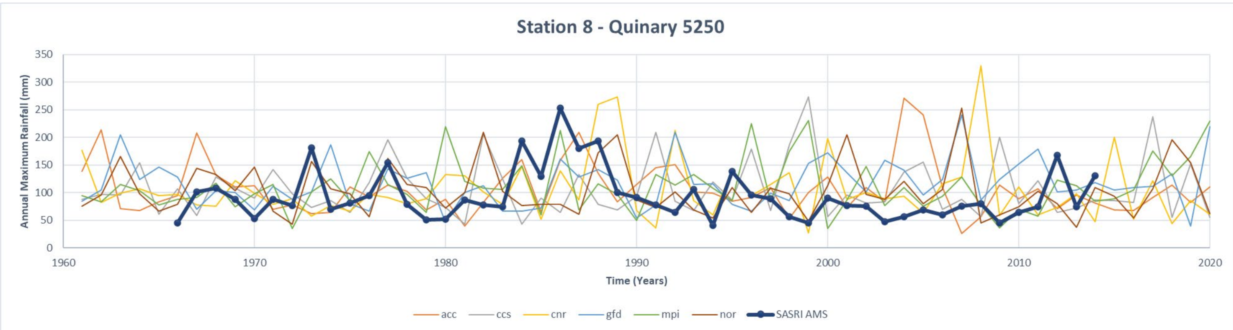

Figure 7.42 Time series of annual maximum rainfall for SASRI station 8 and 6 GCMs for corresponding years

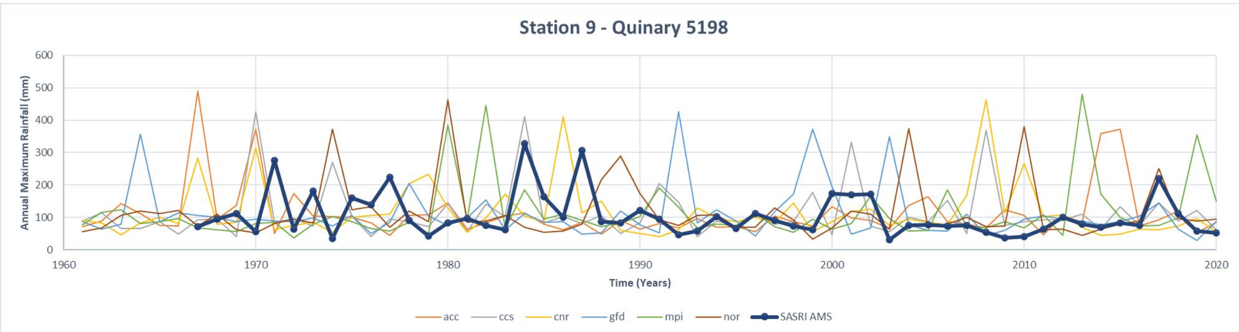

Figure 7.43 Time series of annual maximum rainfall for SASRI station 9 and 6 GCMs for corresponding years

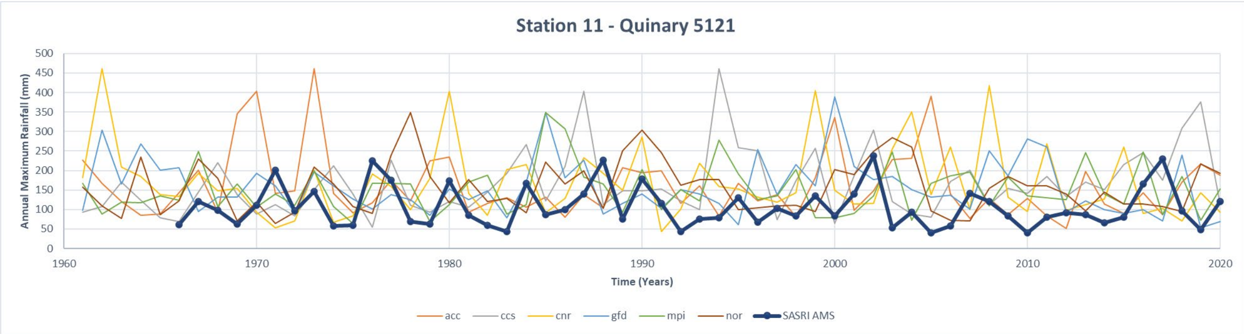

Figure 7.44 Time series of annual maximum rainfall for SASRI station 11 and 6 GCMs for corresponding years

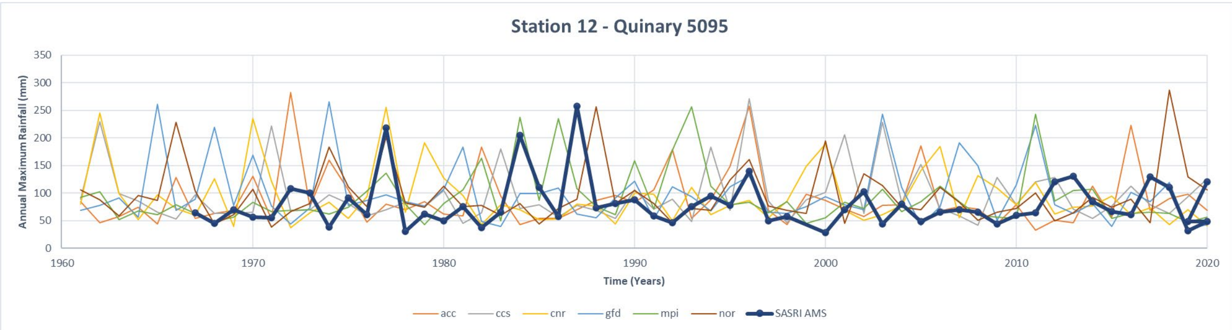

Figure 7.45 Time series of annual maximum rainfall for SASRI station 12 and 6 GCMs for corresponding years

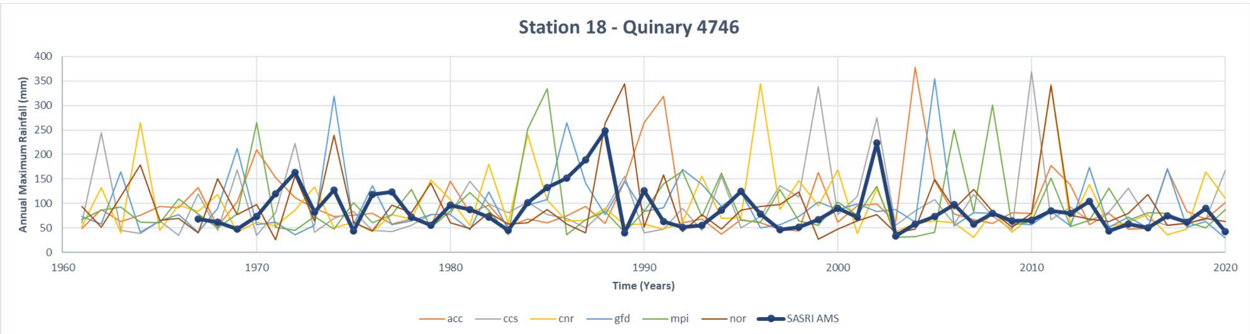

Figure 7.46 Time series of annual maximum rainfall for SASRI station 18 and 6 GCMs for corresponding years

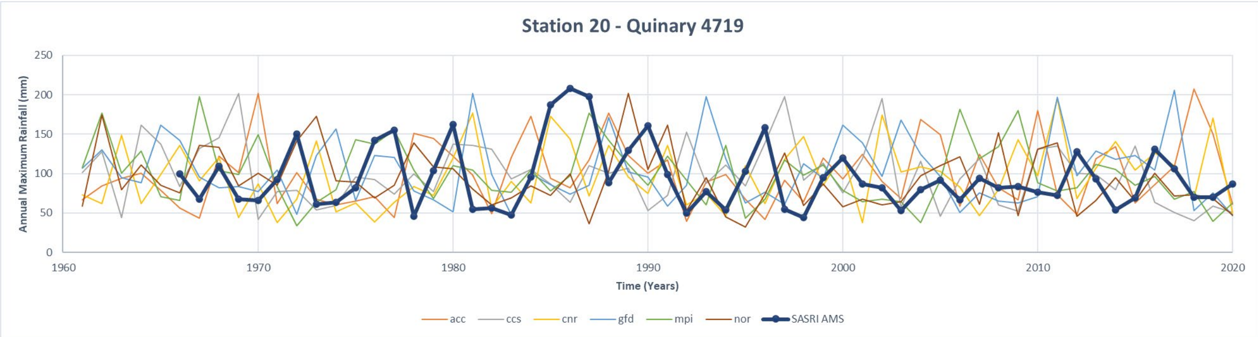

Figure 7.47 Time series of annual maximum rainfall for SASRI station 20 and 6 GCMs for corresponding years

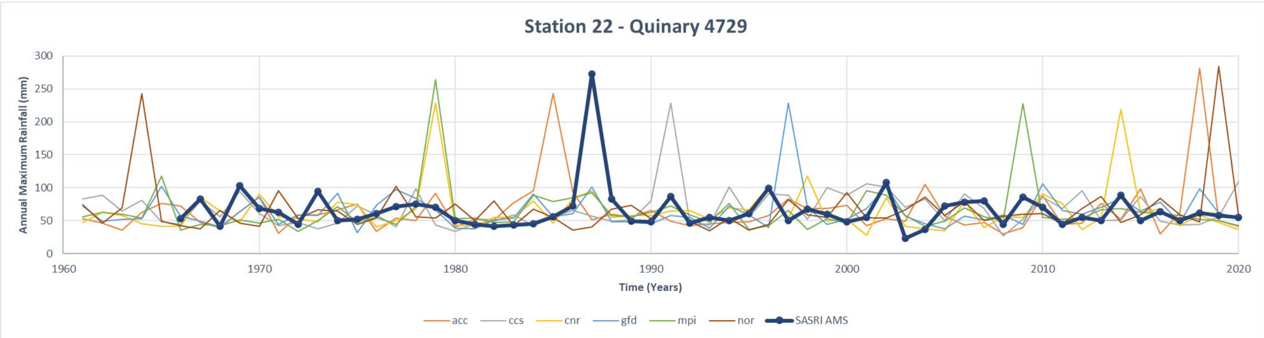

Figure 7.48 Time series of annual maximum rainfall for SASRI station 22 and 6 GCMs for corresponding years

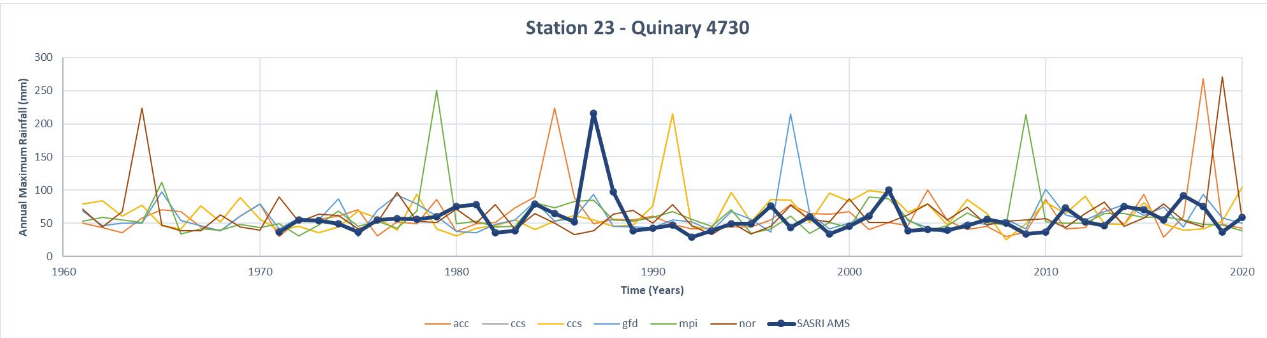

Figure 7.49 Time series of annual maximum rainfall for SASRI station 23 and 6 GCMs for corresponding years

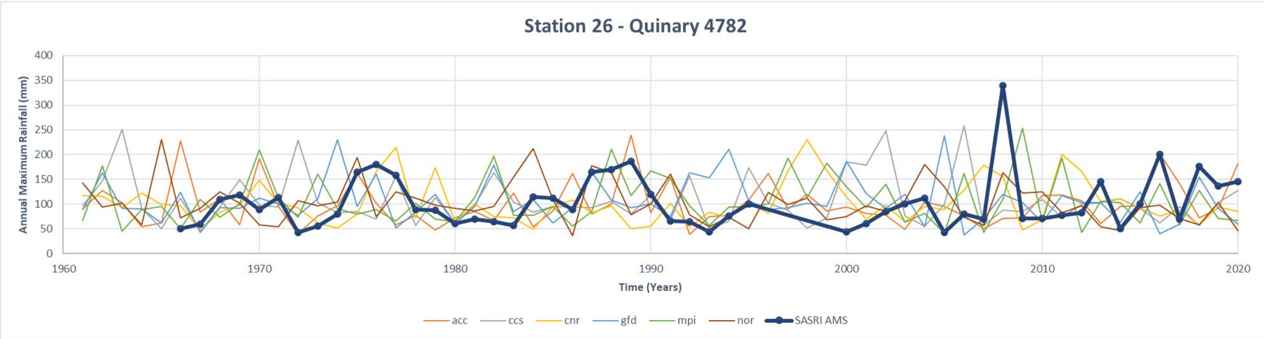

Figure 7.50 Time series of annual maximum rainfall for SASRI station 26 and 6 GCMs for corresponding years

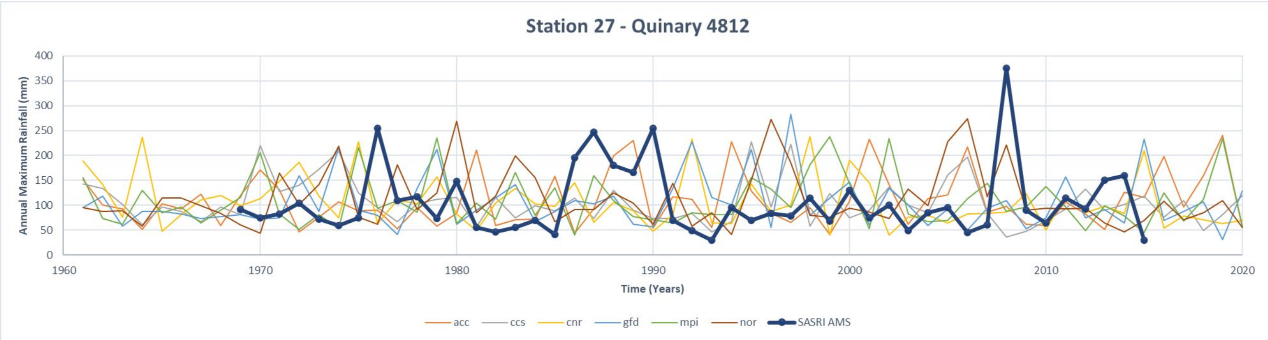

Figure 7.51 Time series of annual maximum rainfall for SASRI station 27 and 6 GCMs for corresponding years

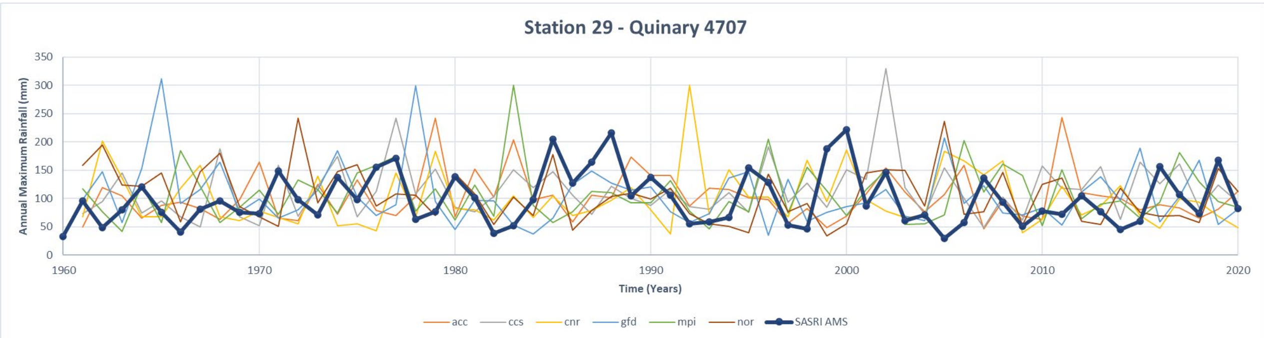

Figure 7.52 Time series of annual maximum rainfall for SASRI station 29 and 6 GCMs for corresponding years

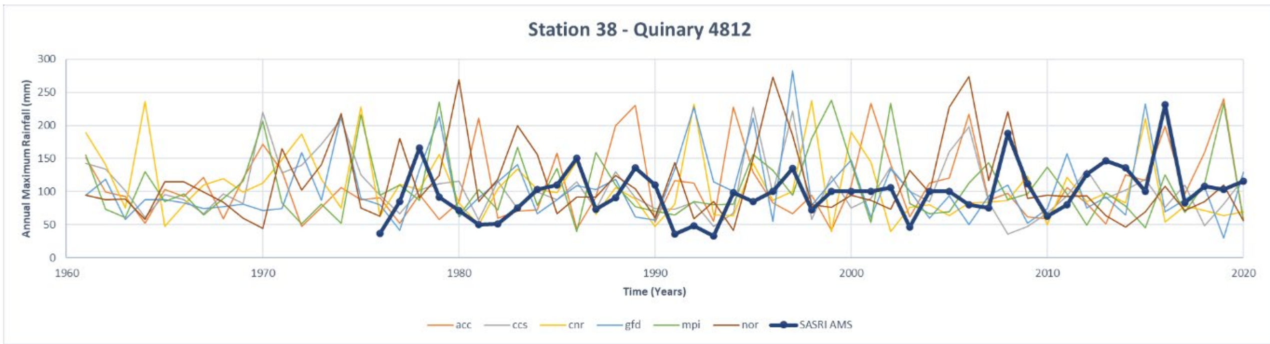

Figure 7.53 Time series of annual maximum rainfall for SASRI station 38 and 6 GCMs for corresponding years

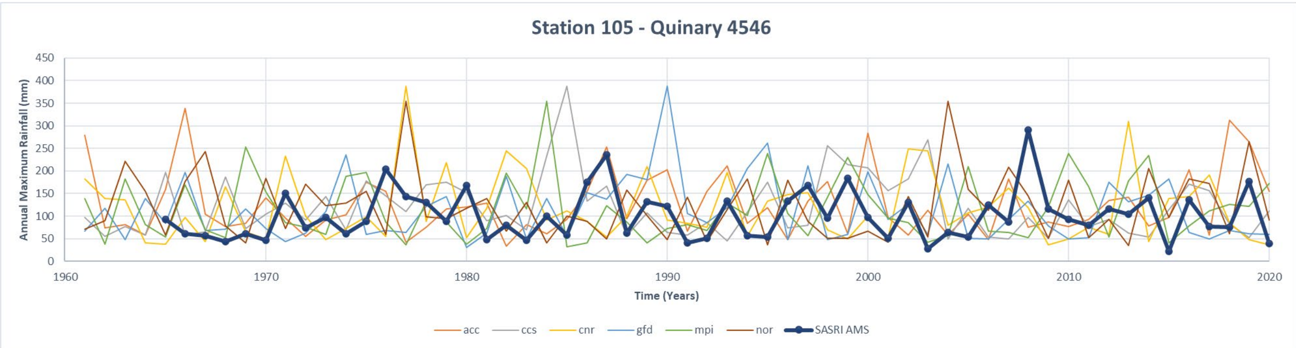

Figure 7.54 Time series of annual maximum rainfall for SASRI station 105 and 6 GCMs for corresponding years

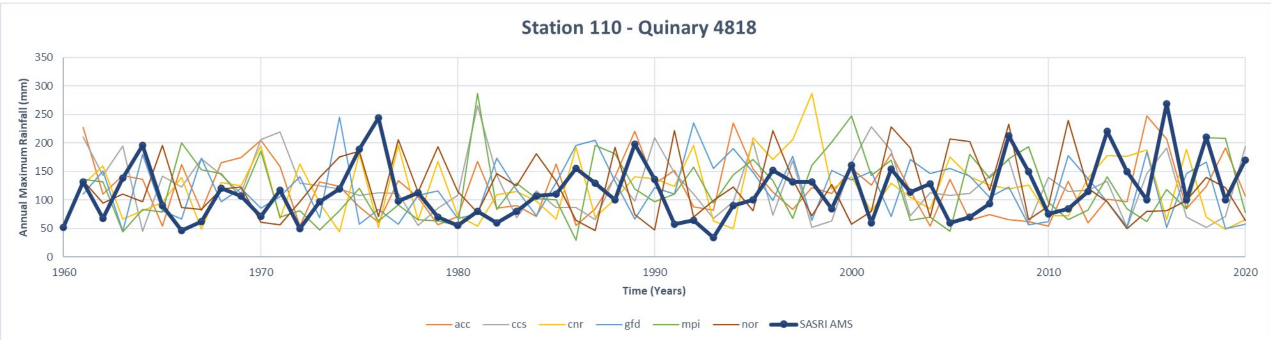

Figure 7.55 Time series of annual maximum rainfall for SASRI station 110 and 6 GCMs for corresponding years

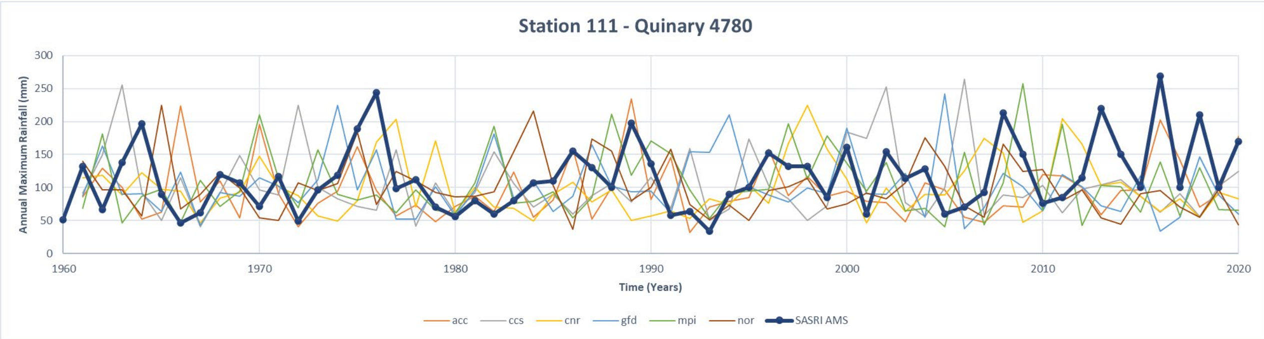

Figure 7.56 Time series of annual maximum rainfall for SASRI station 111 and 6 GCMs for corresponding years

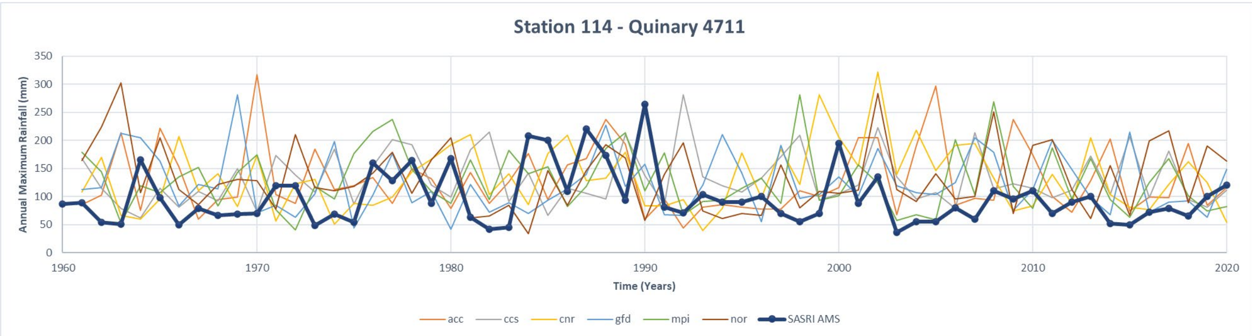

Figure 7.57 Time series of annual maximum rainfall for SASRI station 114 and 6 GCMs for corresponding years

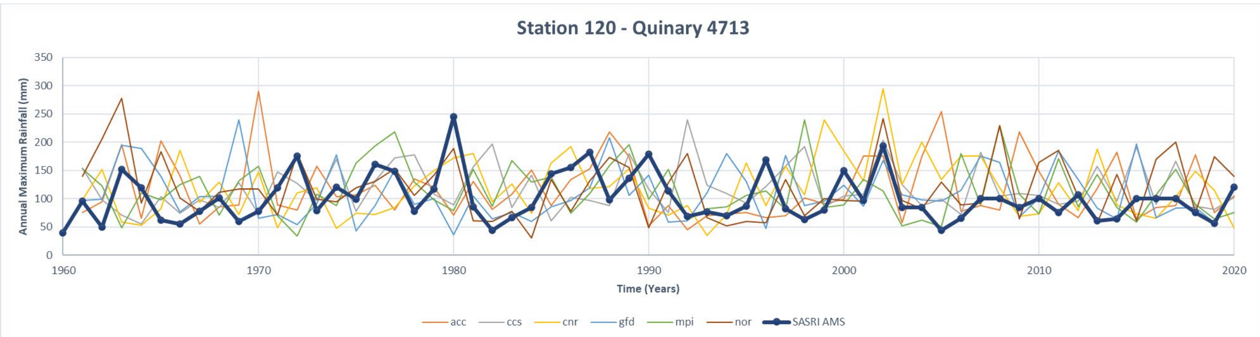

Figure 7.58 Time series of annual maximum rainfall for SASRI station 120 and 6 GCMs for corresponding years

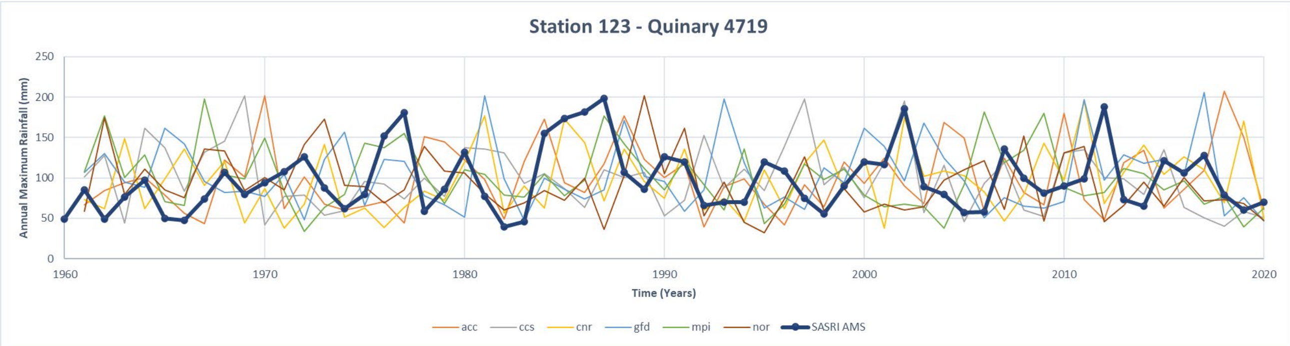

Figure 7.59 Time series of annual maximum rainfall for SASRI station 123 and 6 GCMs for corresponding years

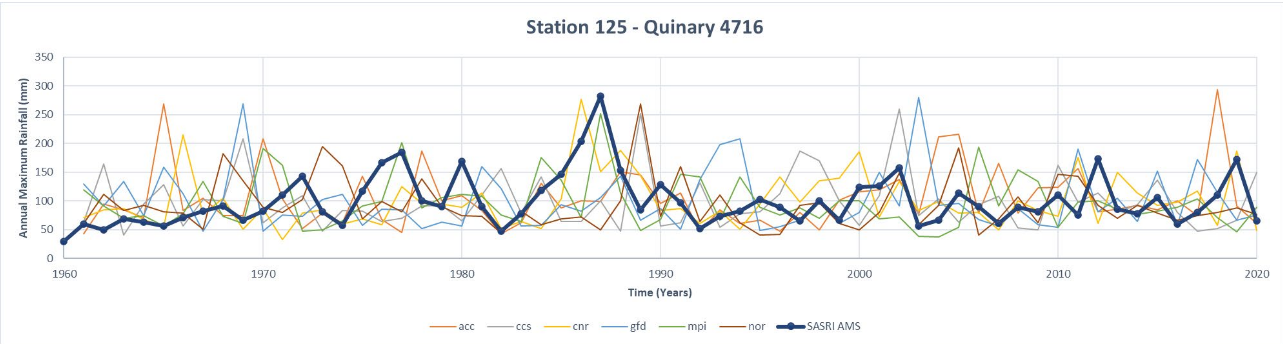

Figure 7.60 Time series of annual maximum rainfall for SASRI station 125 and 6 GCMs for corresponding years

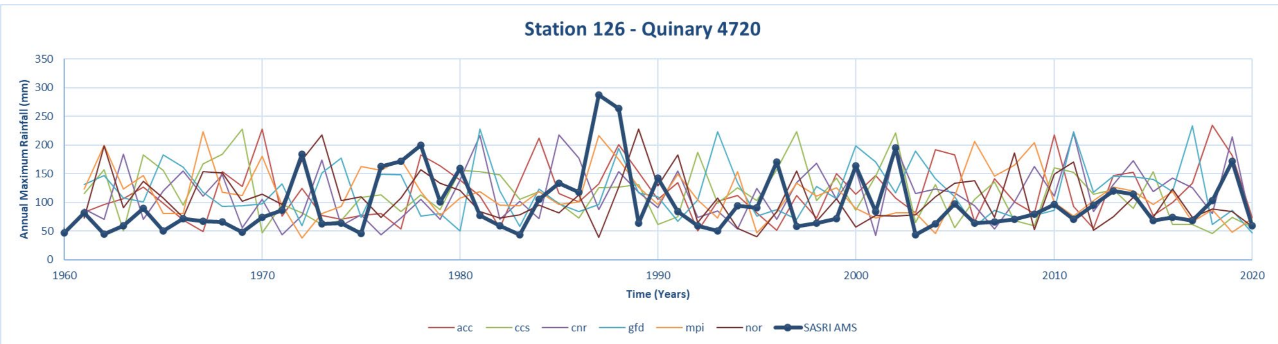

Figure 7.61 Time series of annual maximum rainfall for SASRI station 126 and 6 GCMs for corresponding years

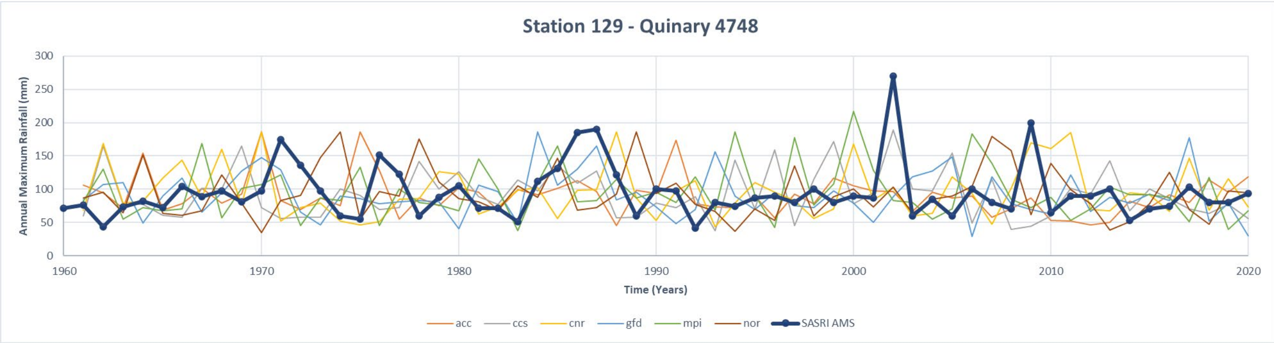

Figure 7.62 Time series of annual maximum rainfall for SASRI station 129 and 6 GCMs for corresponding years

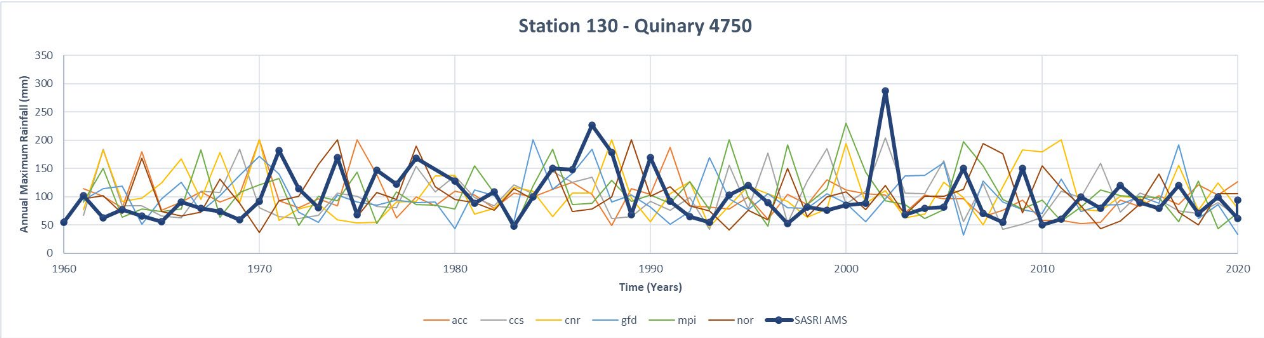

Figure 7.63 Time series of annual maximum rainfall for SASRI station 130 and 6 GCMs for corresponding years

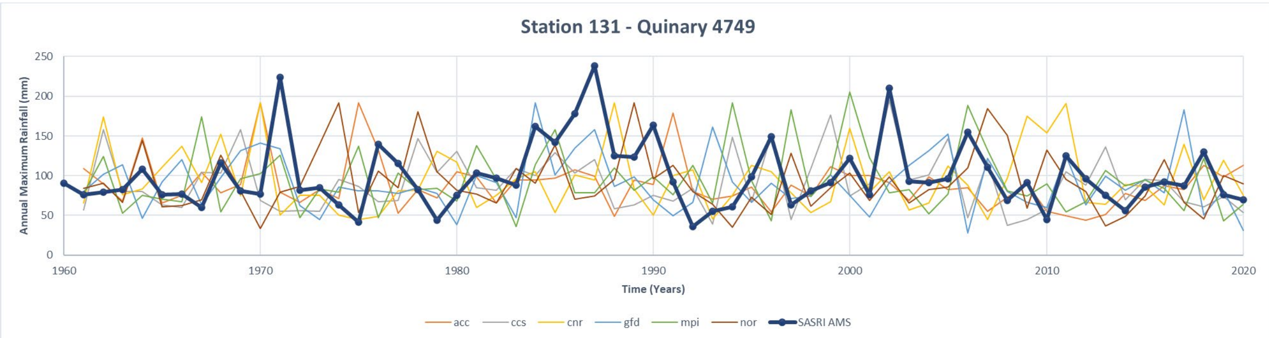

Figure 7.64 Time series of annual maximum rainfall for SASRI station 131 and 6 GCMs for corresponding years

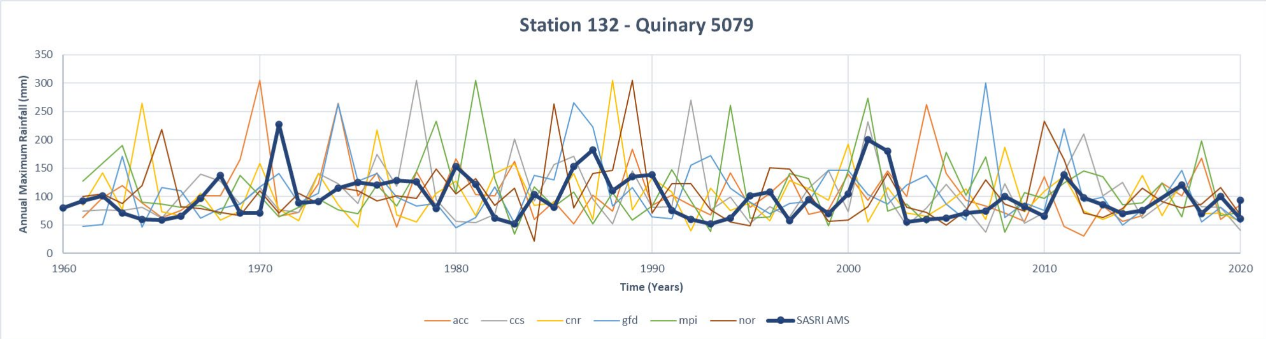

Figure 7.65 Time series of annual maximum rainfall for SASRI station 132 and 6 GCMs for corresponding years

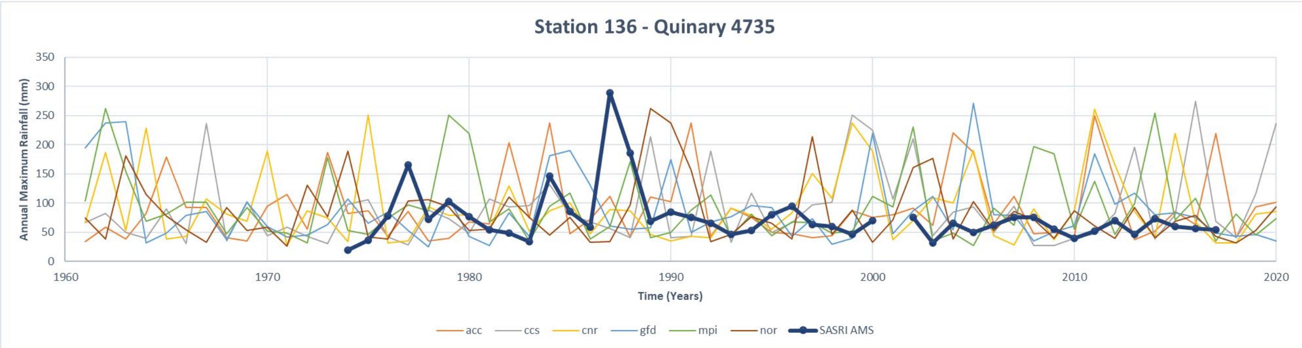

Figure 7.66 Time series of annual maximum rainfall for SASRI station 136 and 6 GCMs for corresponding years

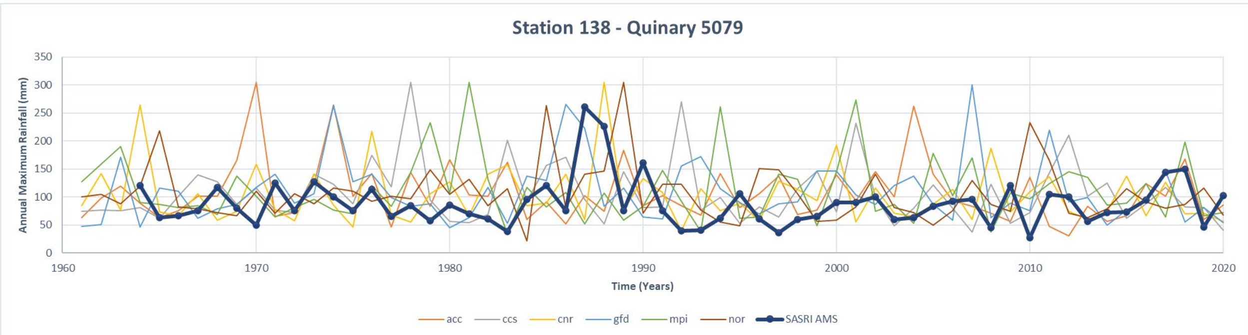

Figure 7.67 Time series of annual maximum rainfall for SASRI station 138 and 6 GCMs for corresponding years

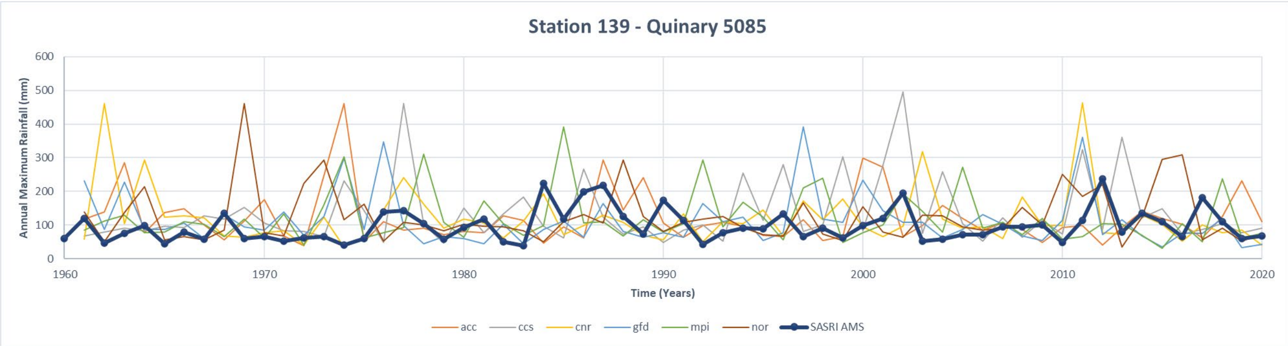

Figure 7.68 Time series of annual maximum rainfall for SASRI station 139 and 6 GCMs for corresponding years

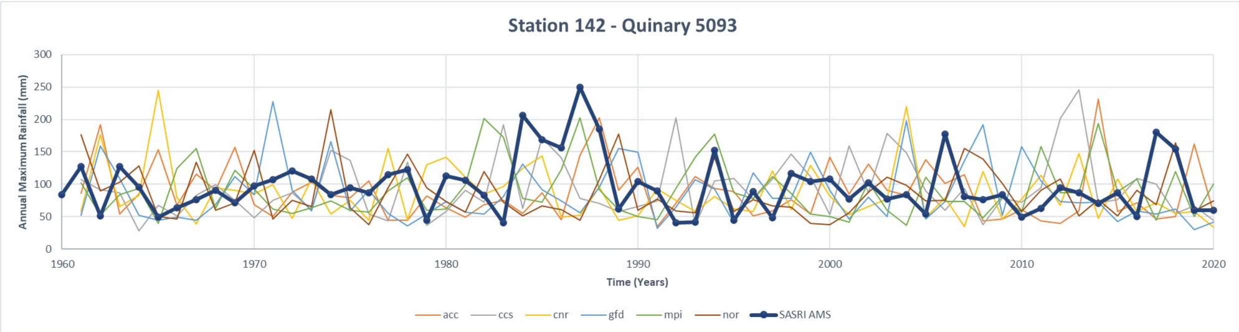

Figure 7.69 Time series of annual maximum rainfall for SASRI station 142 and 6 GCMs for corresponding years

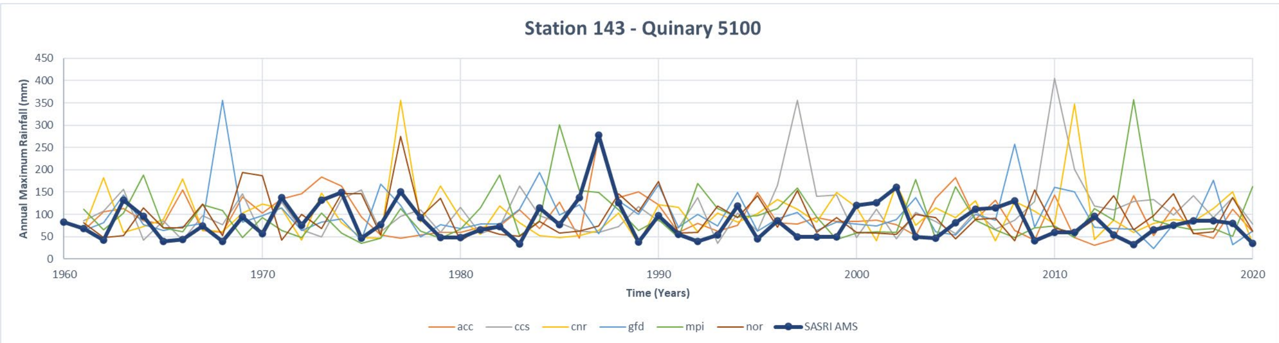

Figure 7.70 Time series of annual maximum rainfall for SASRI station 143 and 6 GCMs for corresponding years

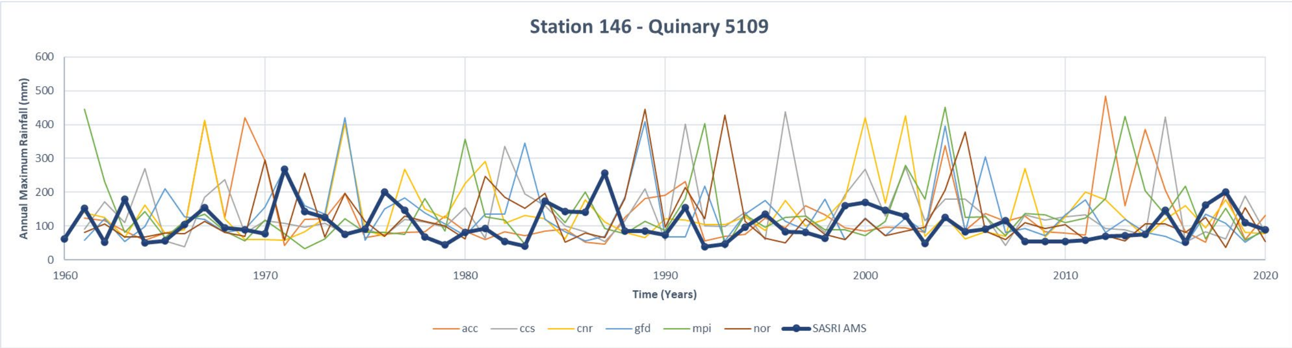

Figure 7.71 Time series of annual maximum rainfall for SASRI station 146 and 6 GCMs for corresponding years

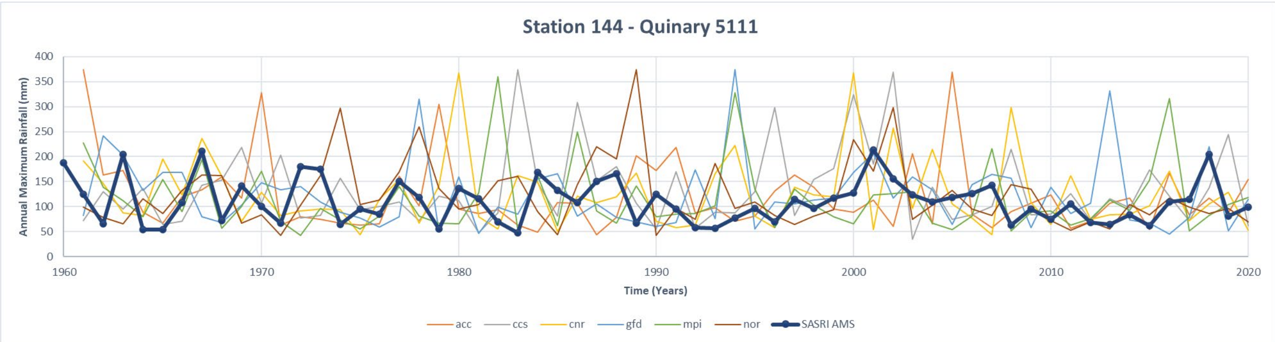

Figure 7.72 Time series of annual maximum rainfall for SASRI station 144 and 6 GCMs for corresponding years

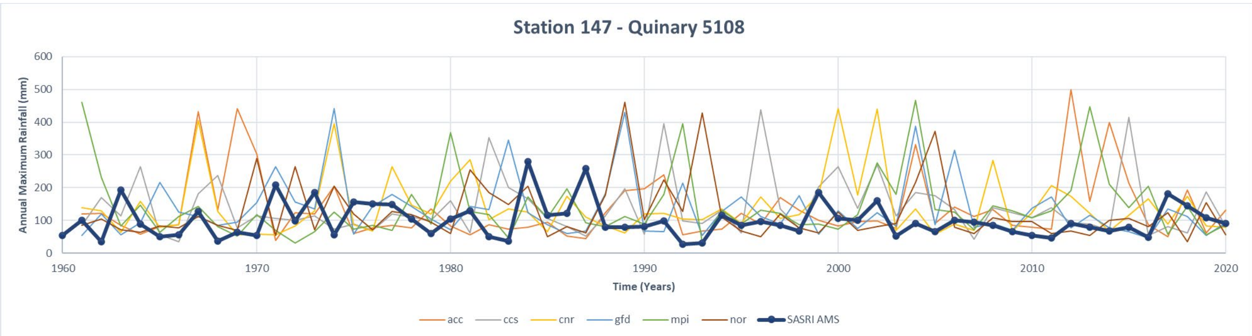

Figure 7.73 Time series of annual maximum rainfall for SASRI station 147 and 6 GCMs for corresponding years

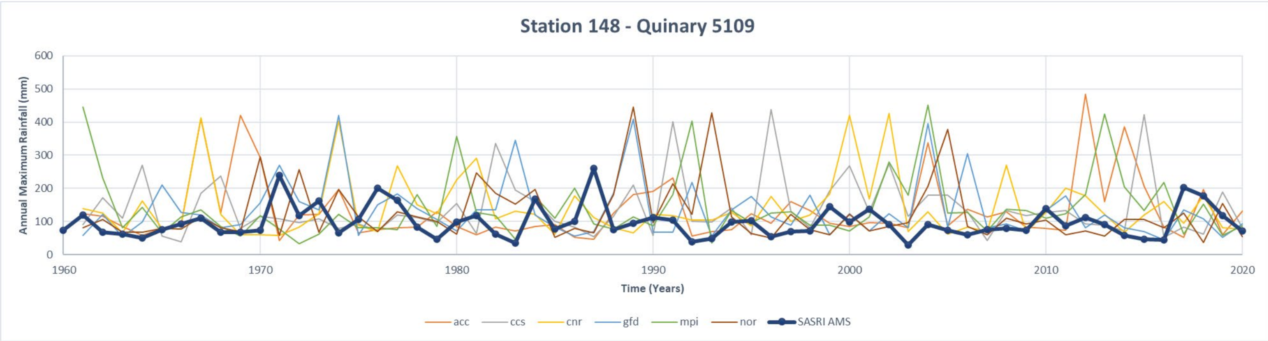

Figure 7.74 Time series of annual maximum rainfall for SASRI station 148 and 6 GCMs for corresponding years

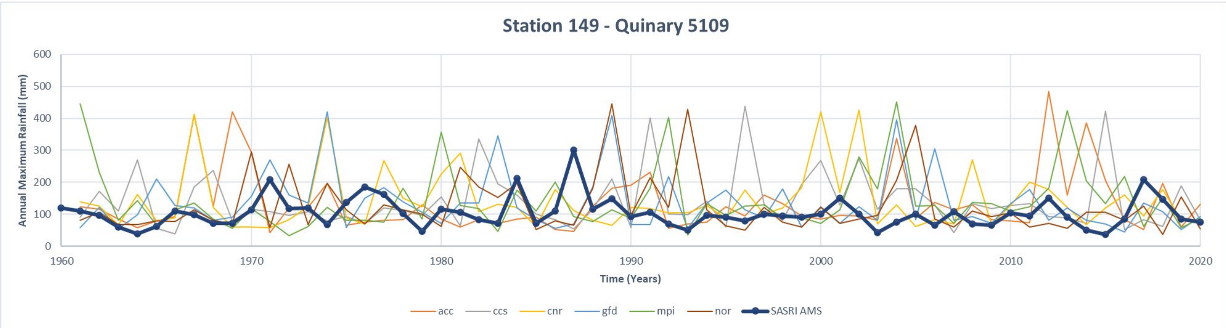

Figure 7.75 Time series of annual maximum rainfall for SASRI station 149 and 6 GCMs for corresponding years

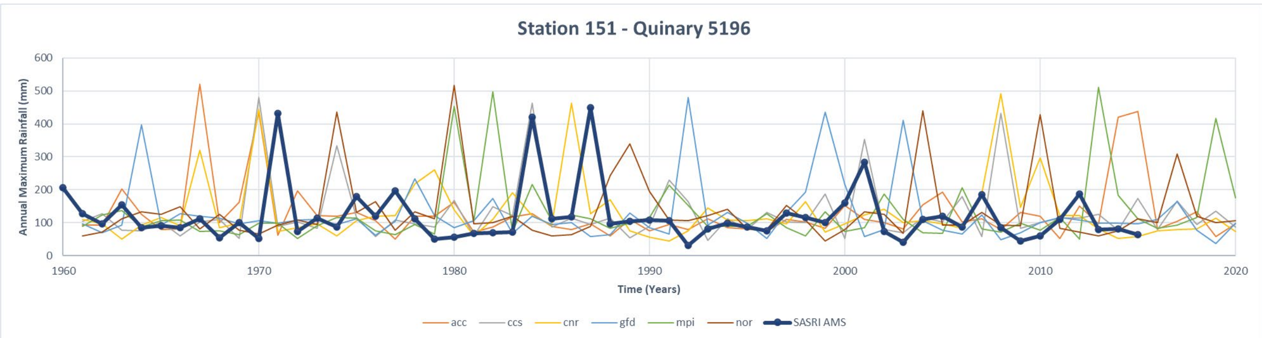

Figure 7.76 Time series of annual maximum rainfall for SASRI station 151 and 6 GCMs for corresponding years

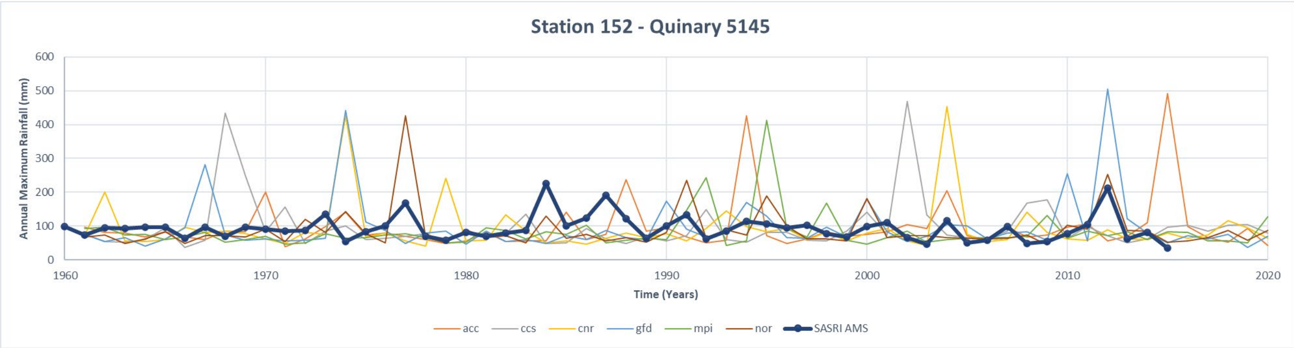

Figure 7.77 Time series of annual maximum rainfall for SASRI station 152 and 6 GCMs for corresponding years

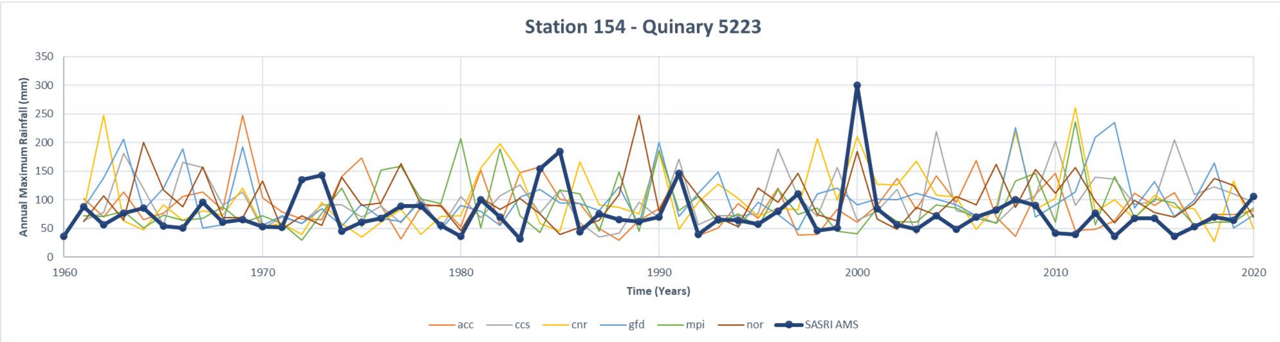

Figure 7.78 Time series of annual maximum rainfall for SASRI station 154 and 6 GCMs for corresponding years

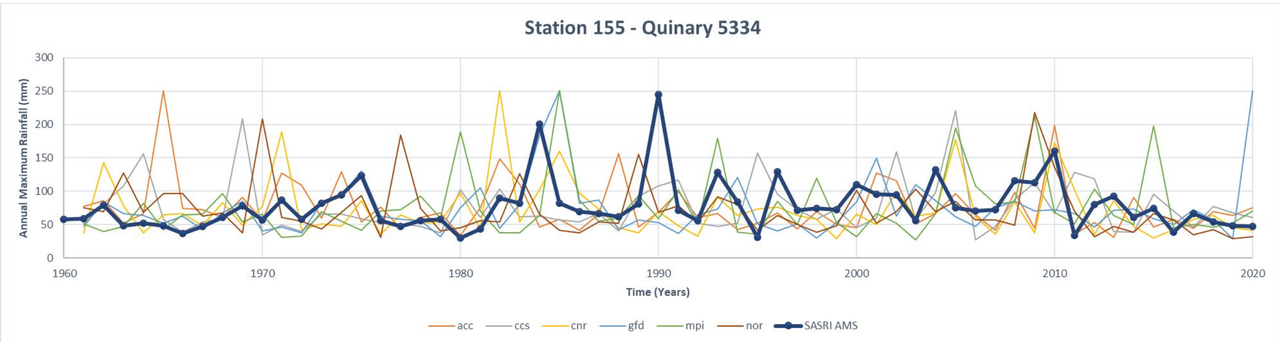

Figure 7.79 Time series of annual maximum rainfall for SASRI station 155 and 6 GCMs for corresponding years

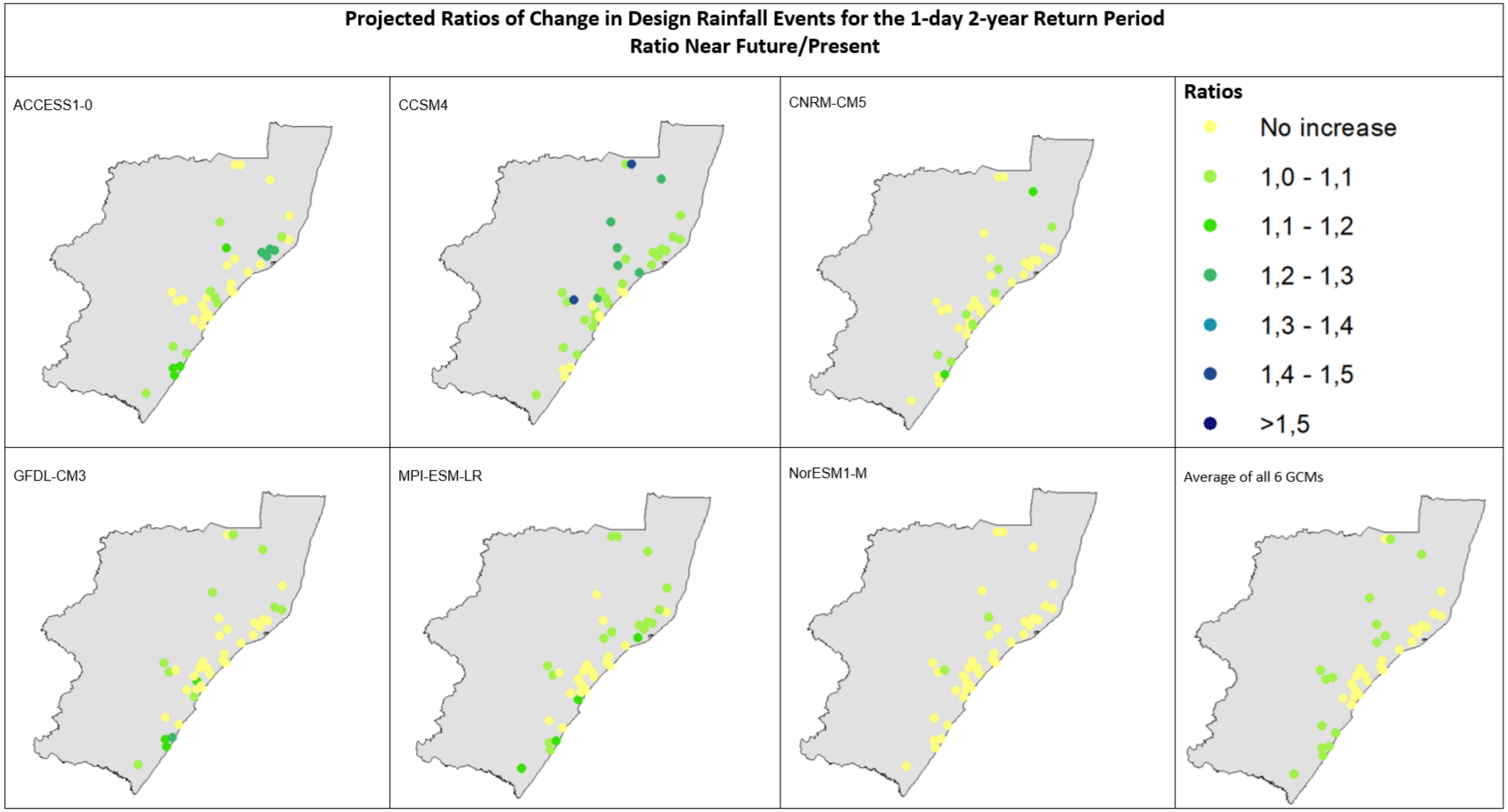

Figure 7.80 Projected changes from the present to the near future in design rainfalls for the 1-day 2-year Return Period derived from outputs from multiple GCMs

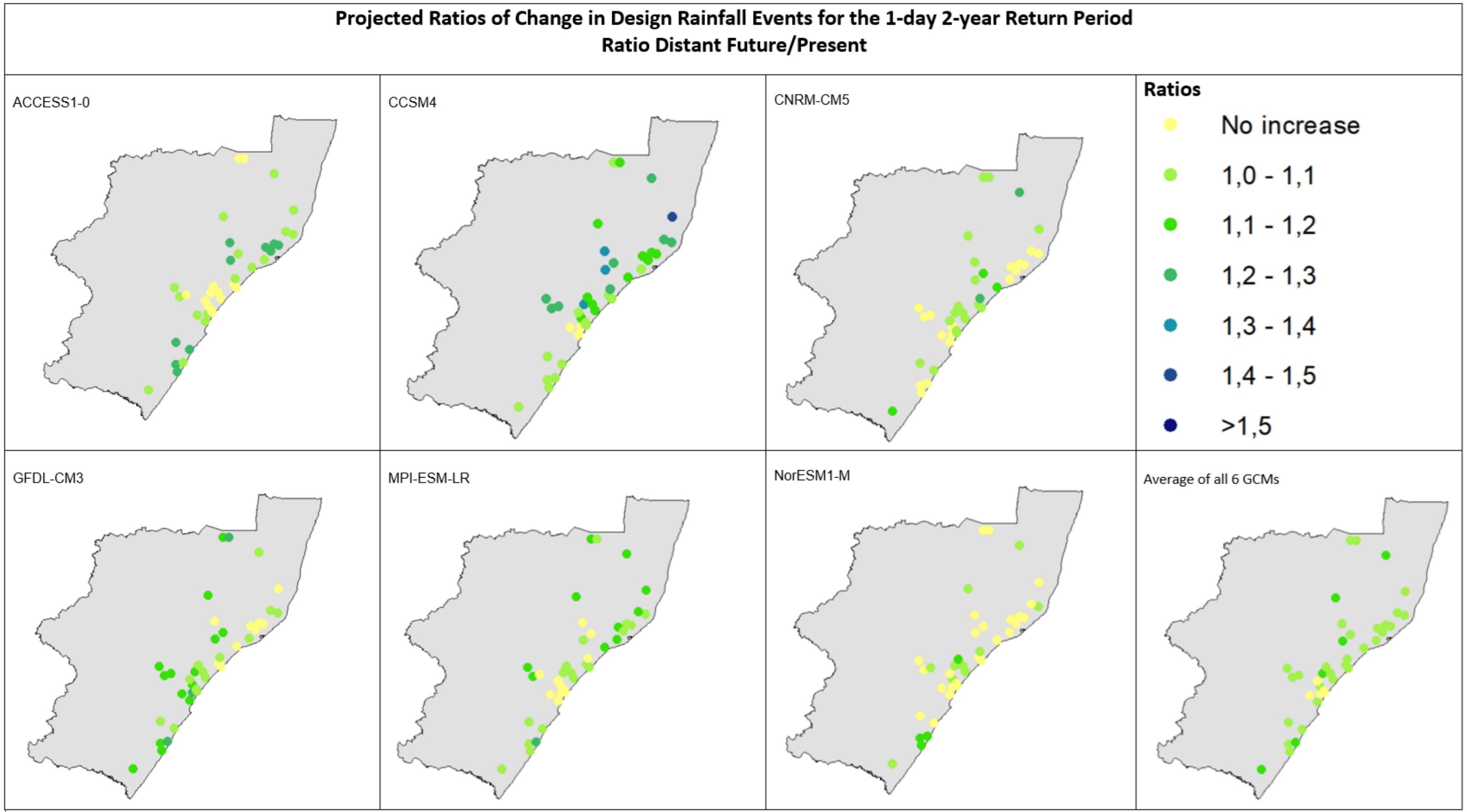

Figure 7.81 Projected changes from the present to the distant future in design rainfalls for the 1-day 2-year Return Period derived from outputs from multiple GCMs

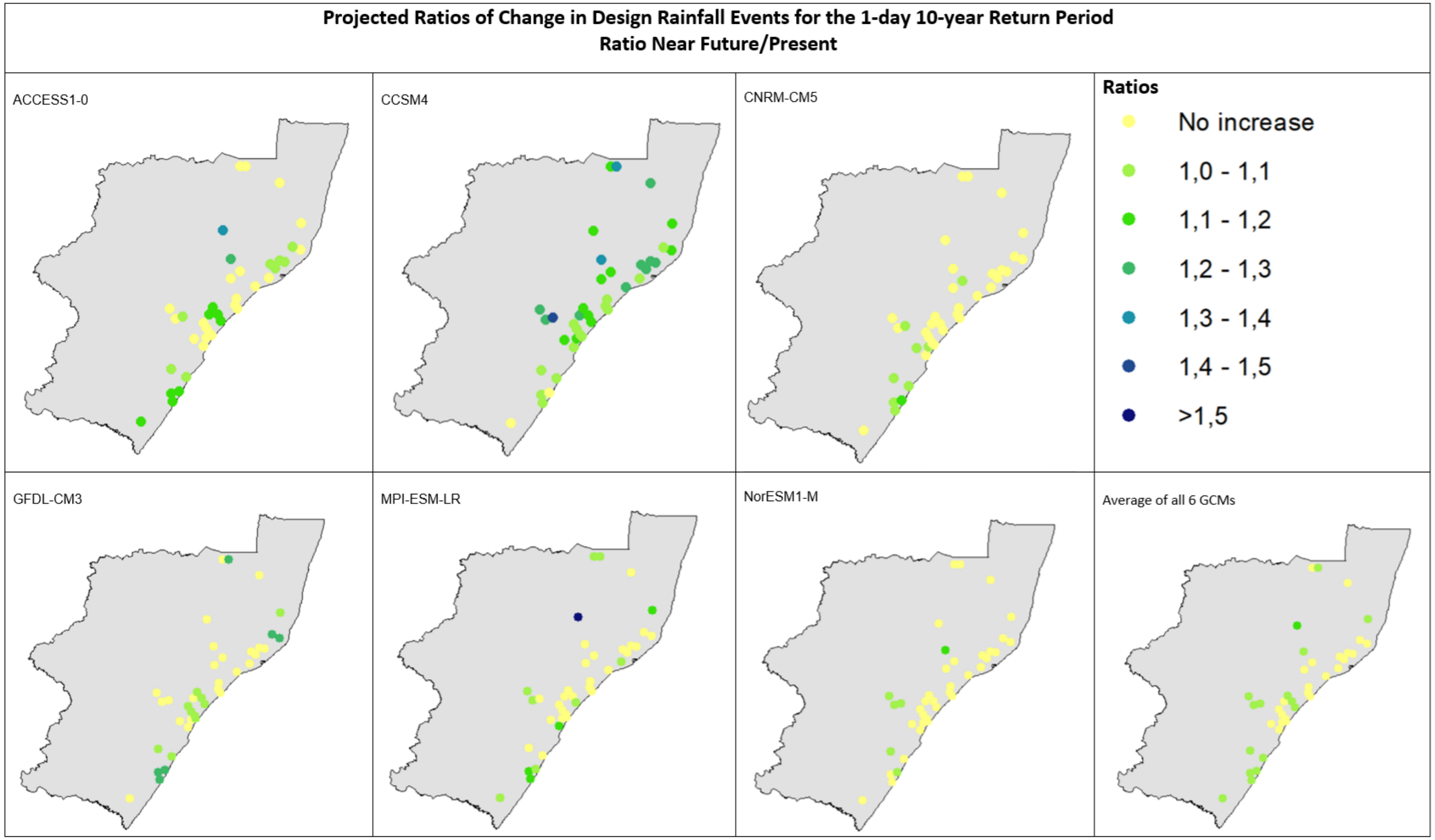

Figure 7.82 Projected changes from the present to the near future in design rainfalls for the 1-day 10-year Return Period derived from outputs from multiple GCMs

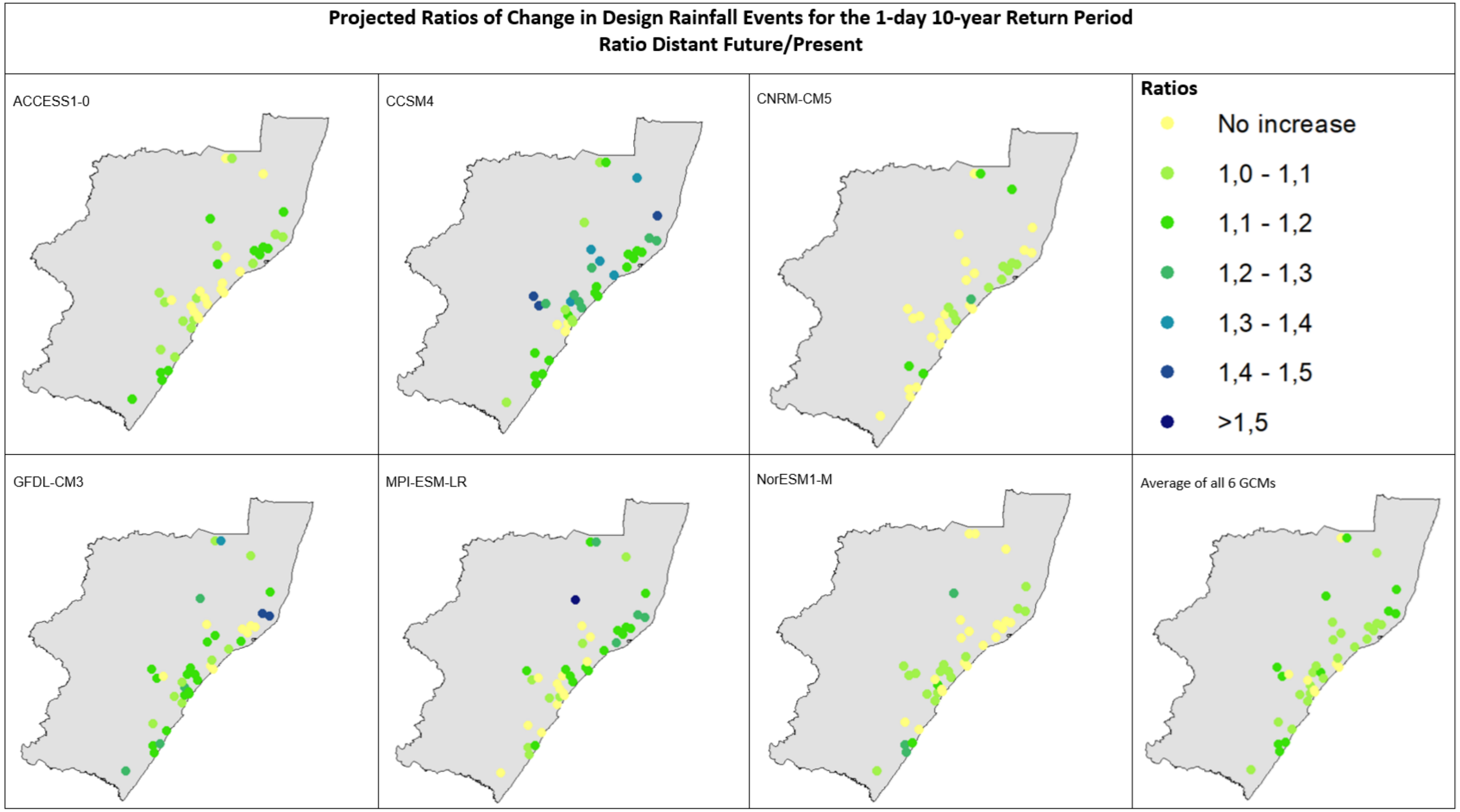

Figure 7.83 Projected changes from the present to the distant future in design rainfalls for the 1-day 10-year Return Period derived from outputs from multiple GCMs

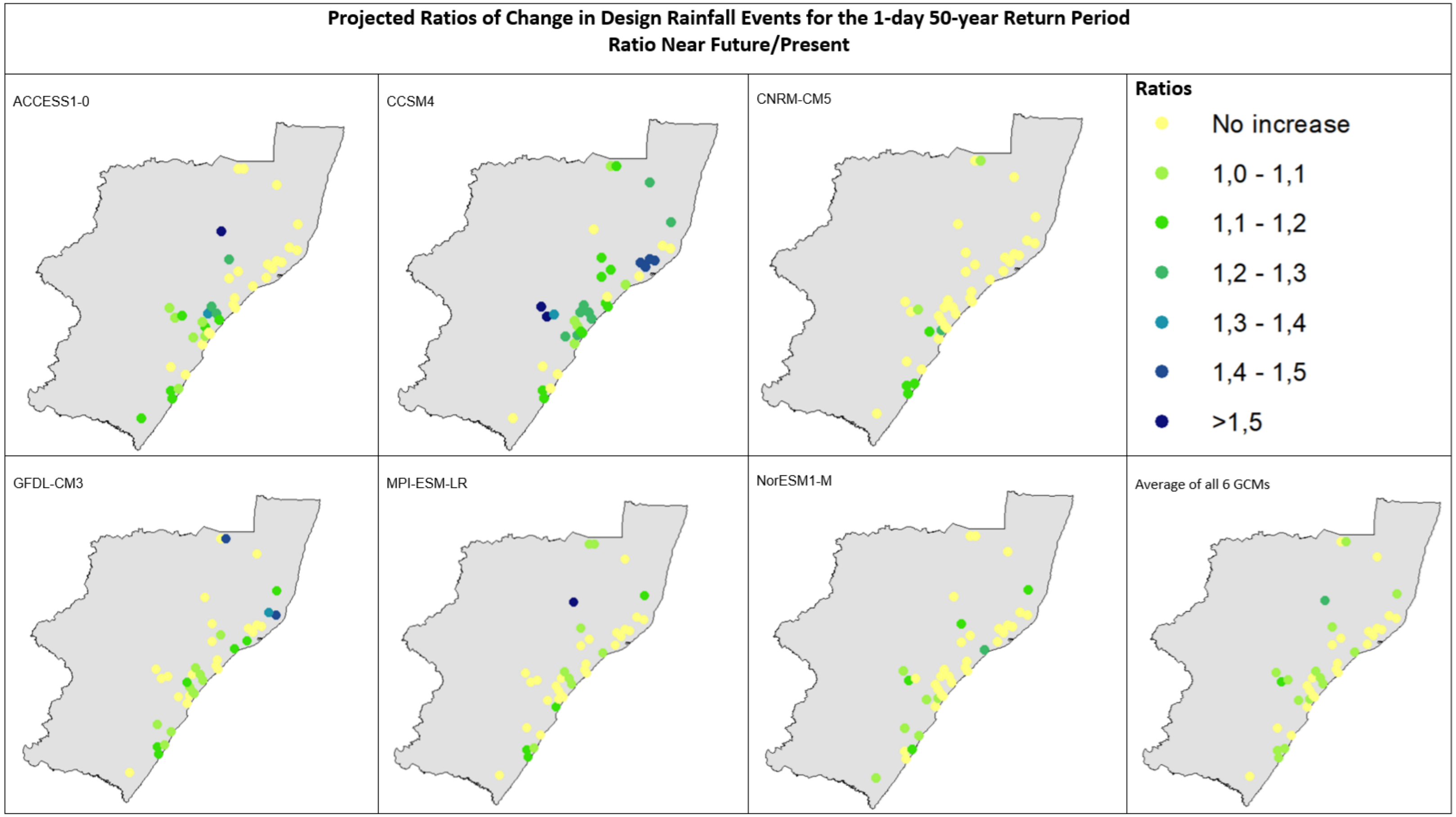

Figure 7.84 Projected changes from the present to the near future in design rainfalls for the 1-day 50-year Return Period derived from outputs from multiple GCMs

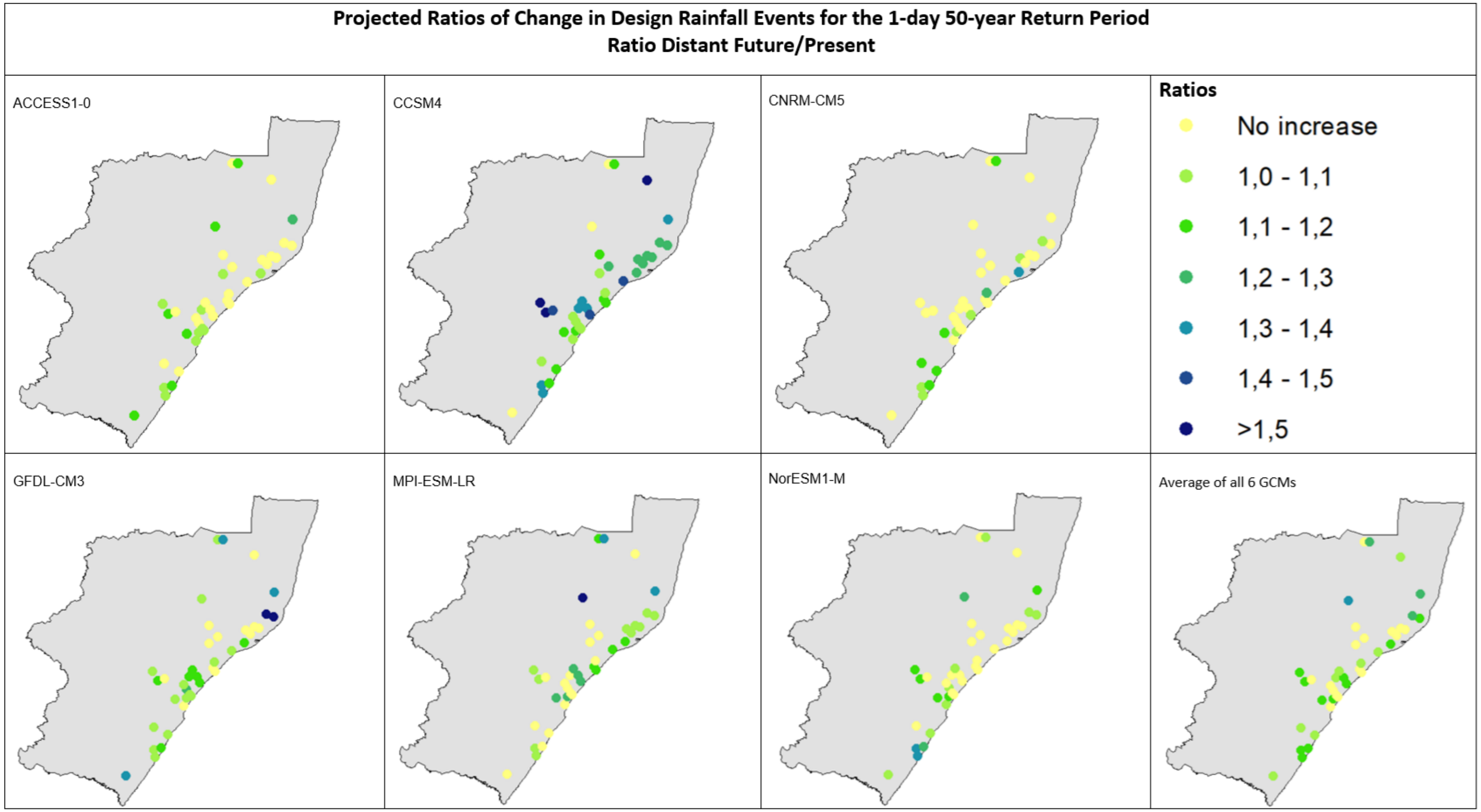

Figure 7.85 Projected changes from the present to the distant future in design rainfalls for the 1-day 50-year Return Period derived from outputs from multiple GCMs

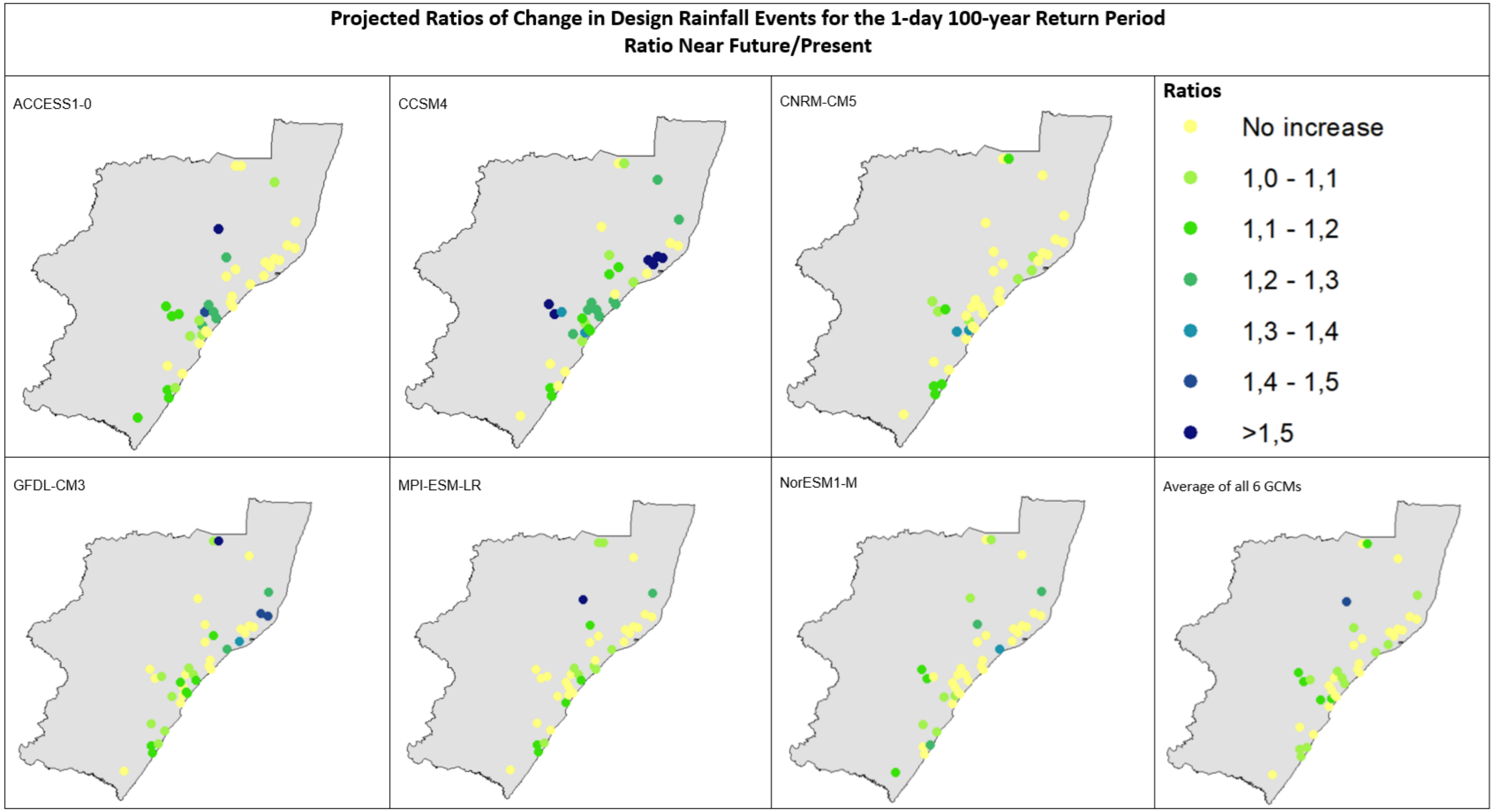

Figure 7.86 Projected changes from the present to the near future in design rainfalls for the 1-day 100-year Return Period derived from outputs from multiple GCMs

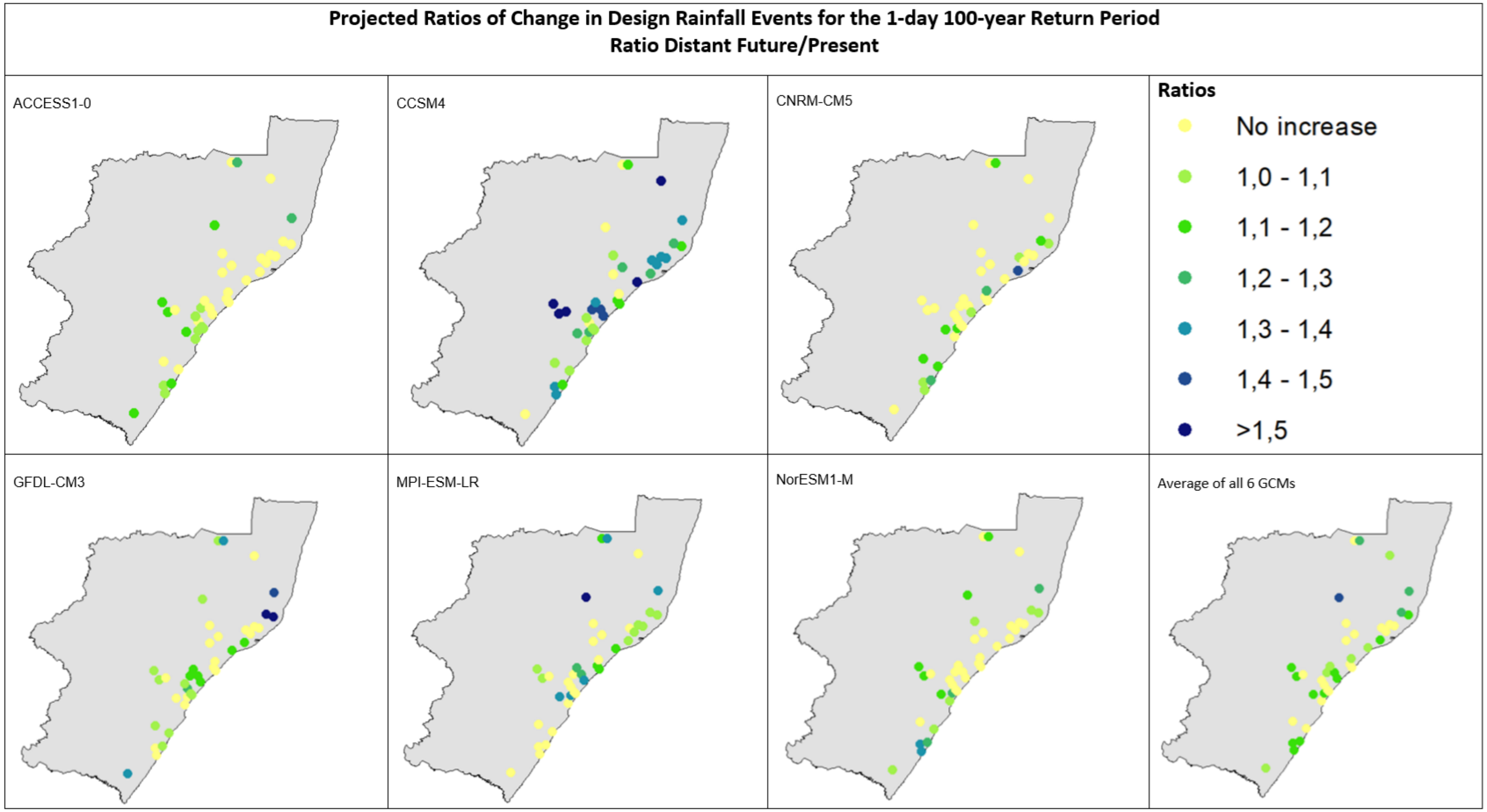

Figure 7.87 Projected changes from the present to the distant future in design rainfalls for the 1-day 100-year Return Period derived from outputs from multiple GCMs

8. APPENDIX B: Non-stationary Frequency Analysis of Extreme Floods in KwaZulu-Natal

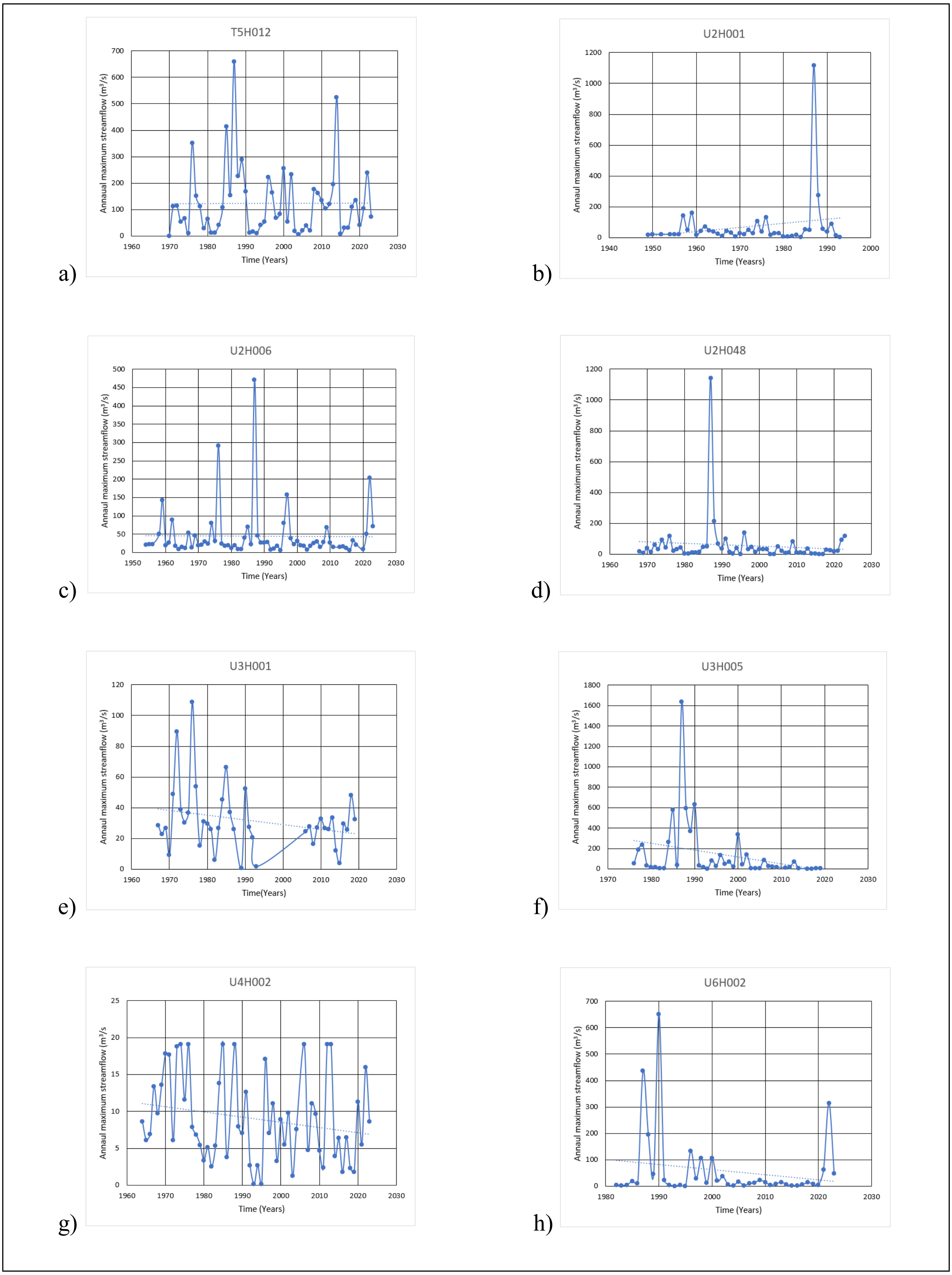
T5H012
Annaul maximum streamflow (m³/s)
Time (Years)
a)
U2H001
Annaul maximum streamflow (m³/s)
Time (Yeasrs)
b)
U2H006
Annaul maximum streamflow (m³/s)
Time (Years)
c)
U2H048
Annaul maximum streamflow (m³/s)
Time (Years)
d)
U3H001
Annaul maximum streamflow (m³/s)
Time(Years)
e)
U3H005
Annaul maximum streamflow (m³/s)
Time (Years)
f)
U4H002
Annaul maximum streamflow (m³/s)
Time (Years)
g)
U6H002
Annaul maximum streamflow (m³/s)
Time (Years)
h)

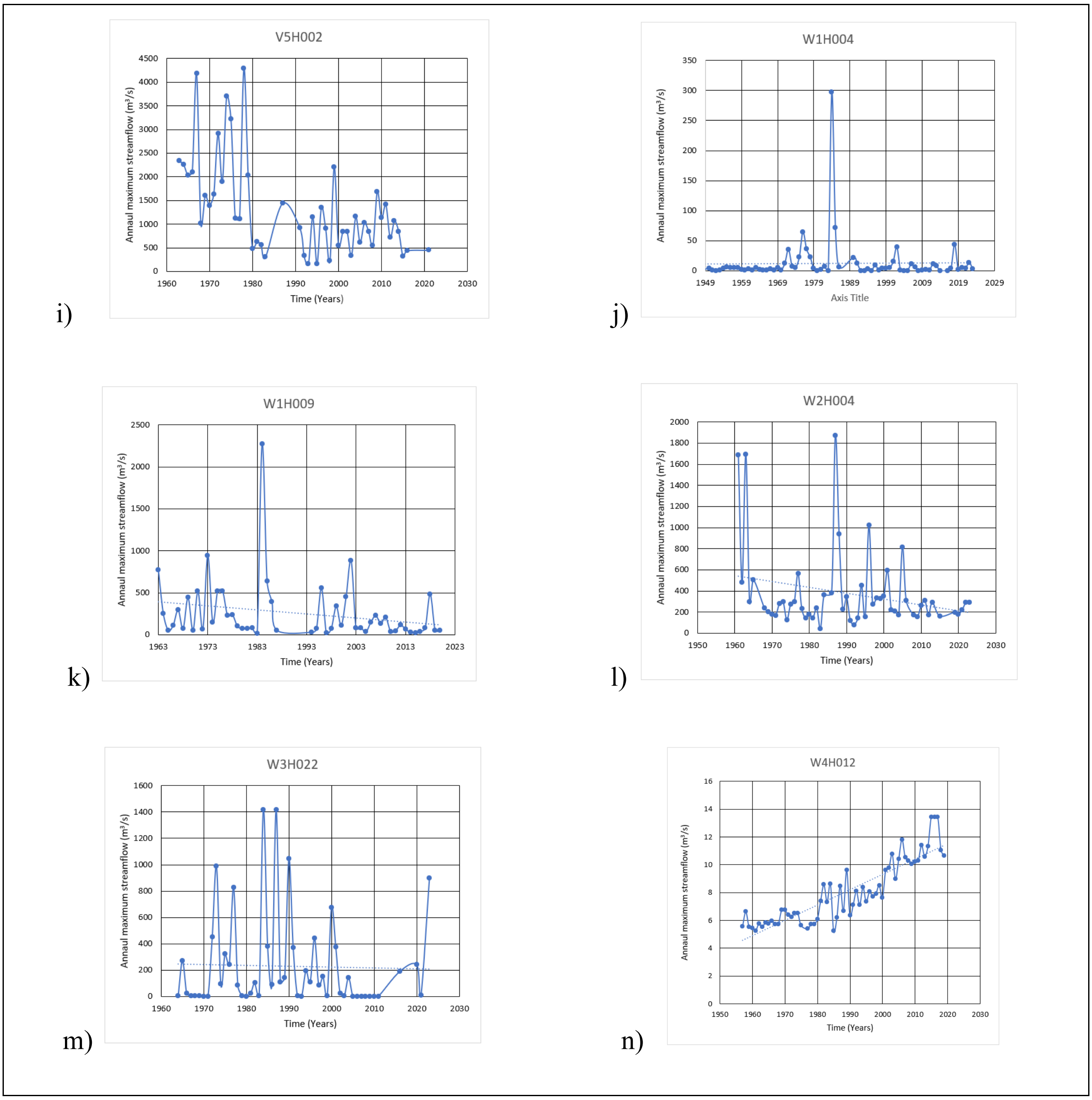

Figure 8.1 Time series of annual streamflows at stations along the East Coast of KwaZulu-Natal

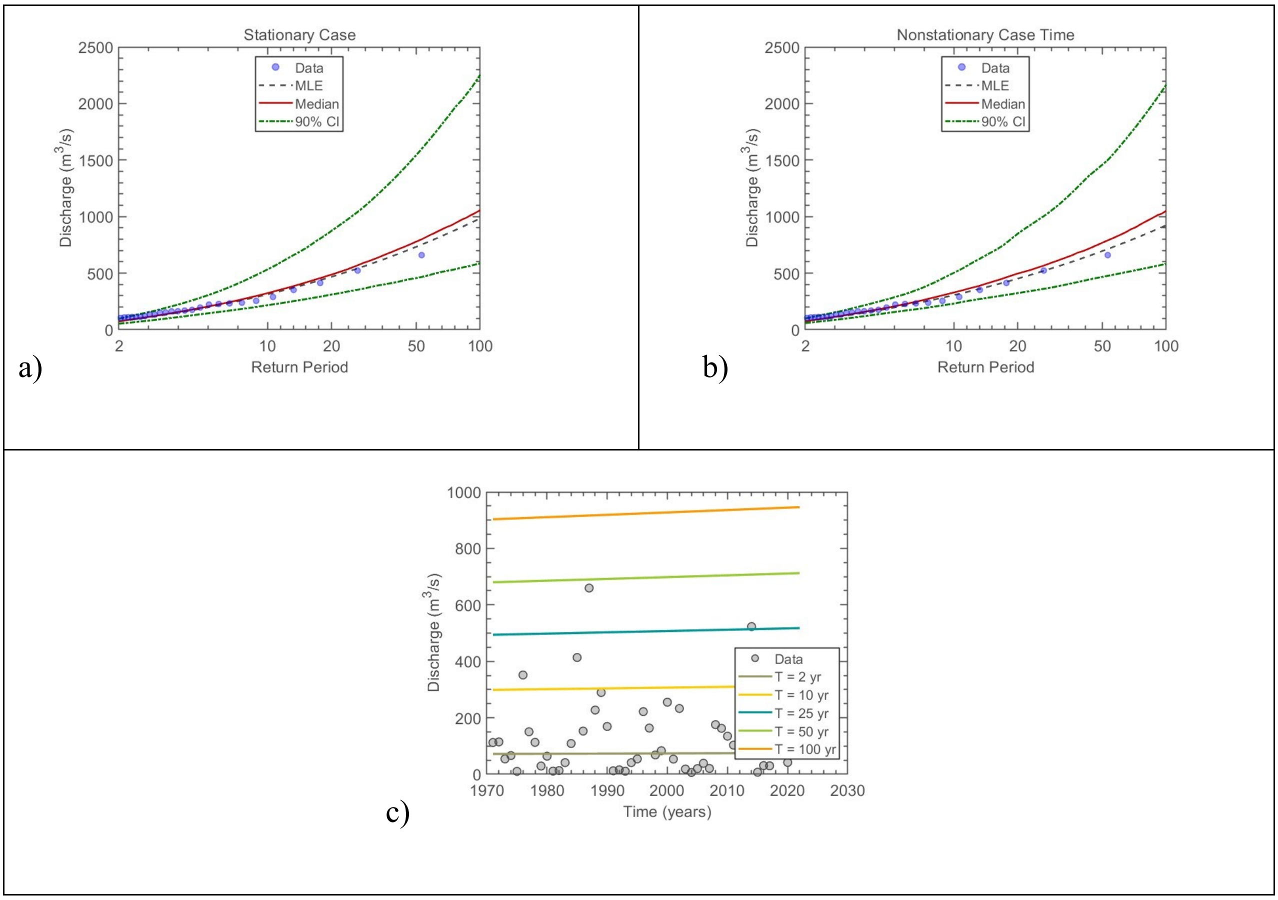

Figure 8.2 The LP3 (a) stationary model, (b) non-stationary model considering time as a covariate, and (c) effective return period as a function of time for Station: T5H012

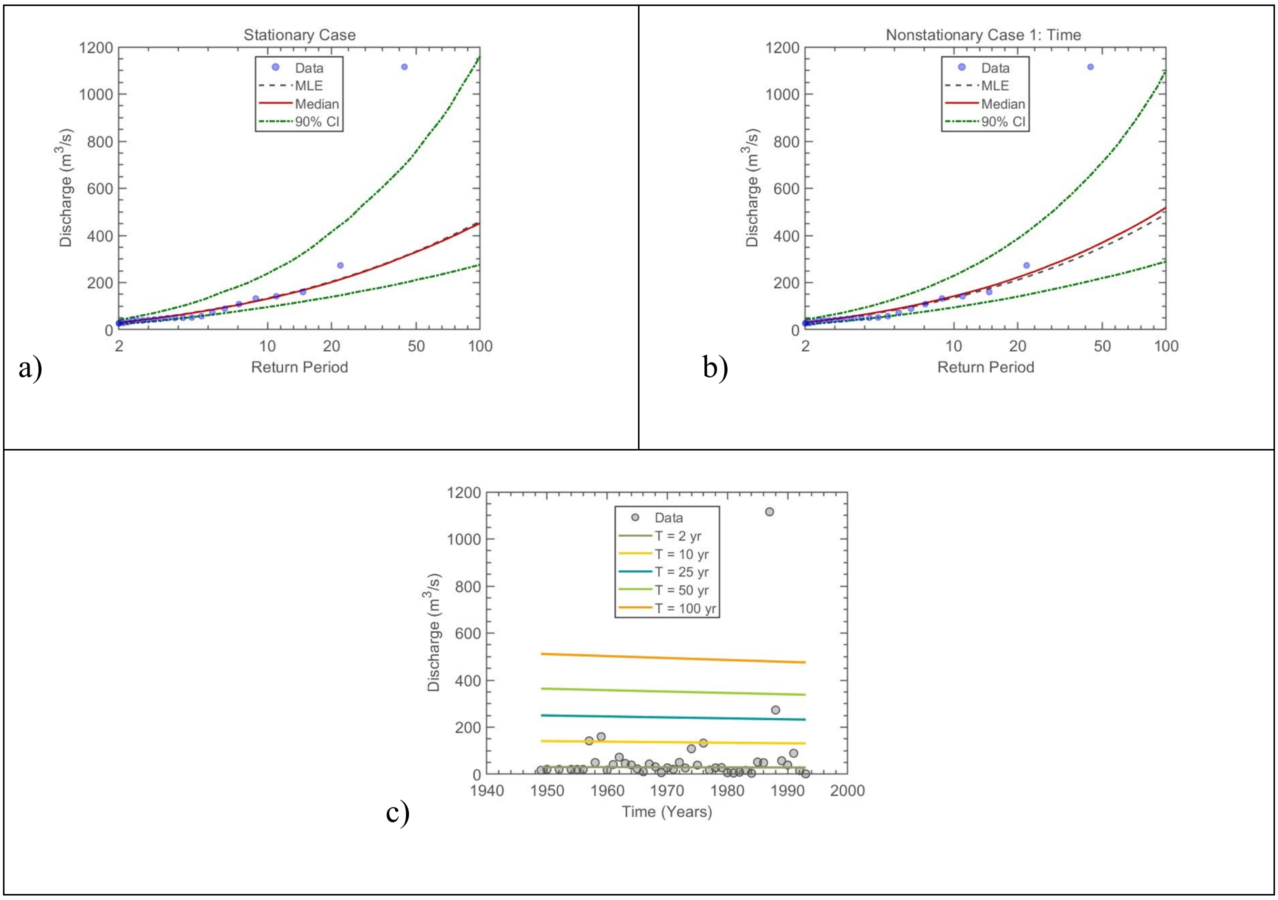

Figure 8.3 LP3 (a) stationary model, (b) non-stationary model considering time as a covariate, and (c) effective return period as a function of time for Station: U2H001

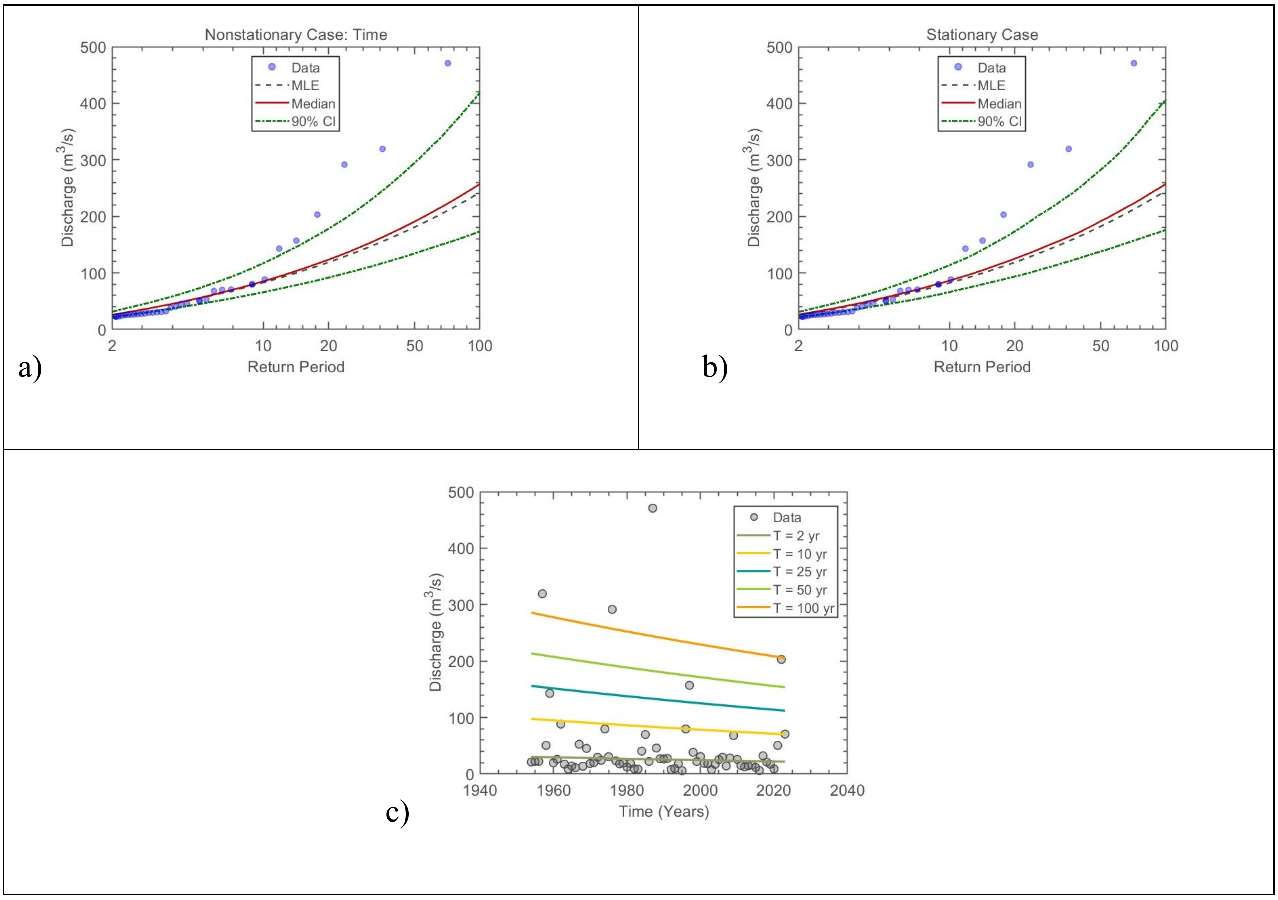

Figure 8.4 LP3 (a) stationary model, (b) non-stationary model considering time as a covariate, and (c) effective return period as a function of time for Station: U2H006

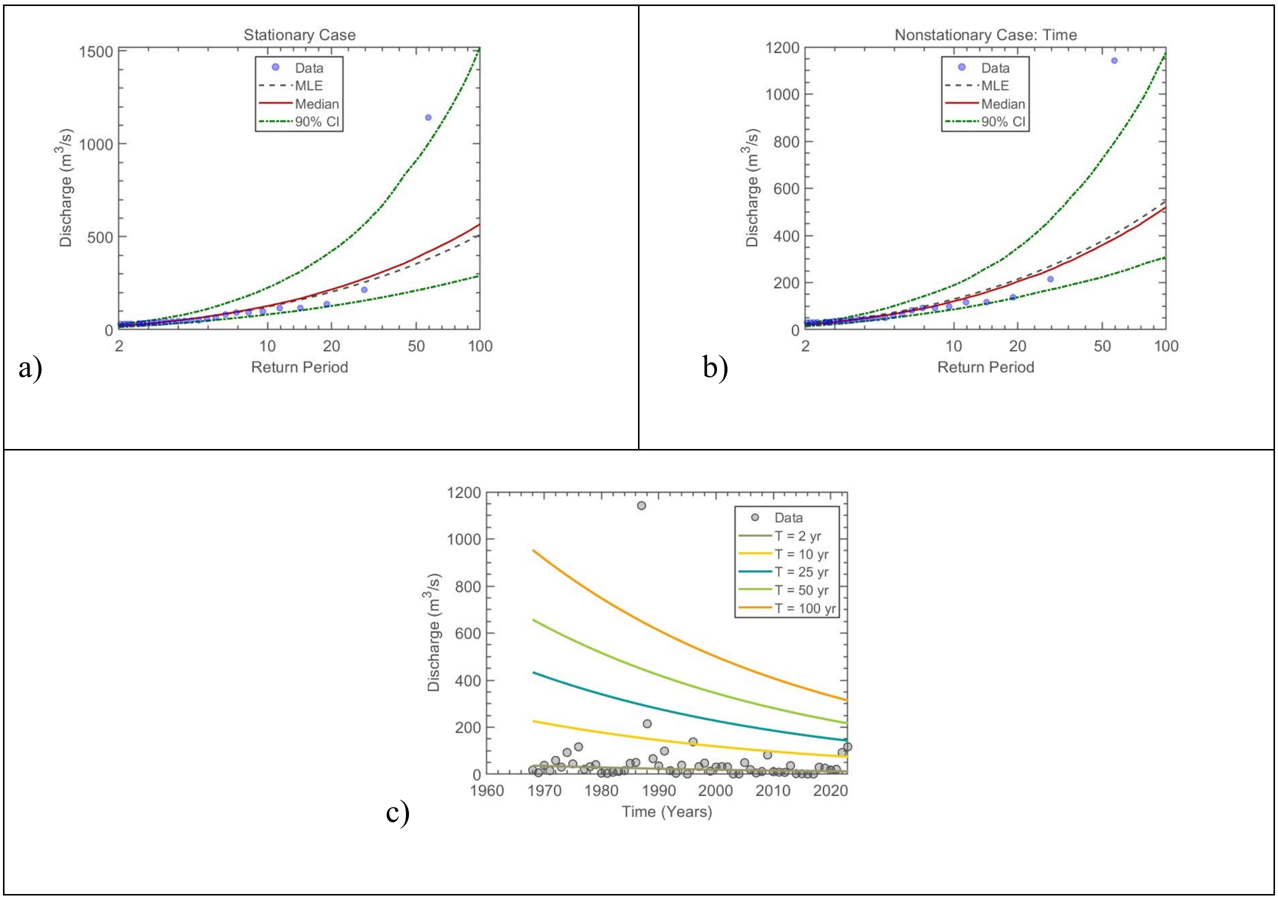

Figure 8.5 LP3 (a) stationary model, (b) non-stationary model considering time as a covariate, and (c) effective return period as a function of time for Station: U2H048

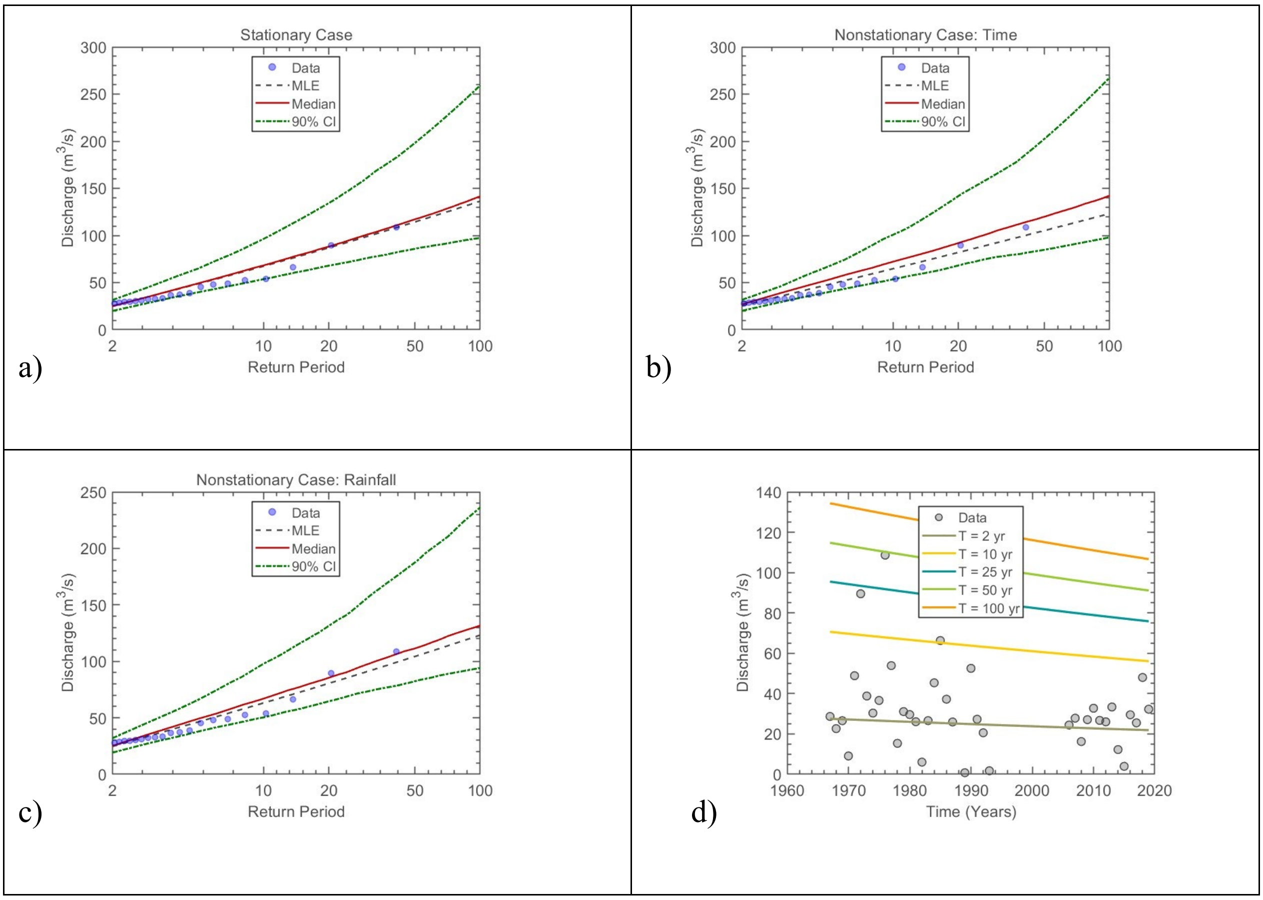

Figure 8.6 LP3 (a) stationary model, (b) non-stationary model considering time as a covariate, (c) non-stationary model considering rainfall as a covariate, and (d) effective return period as a function of time for Station:U3H001

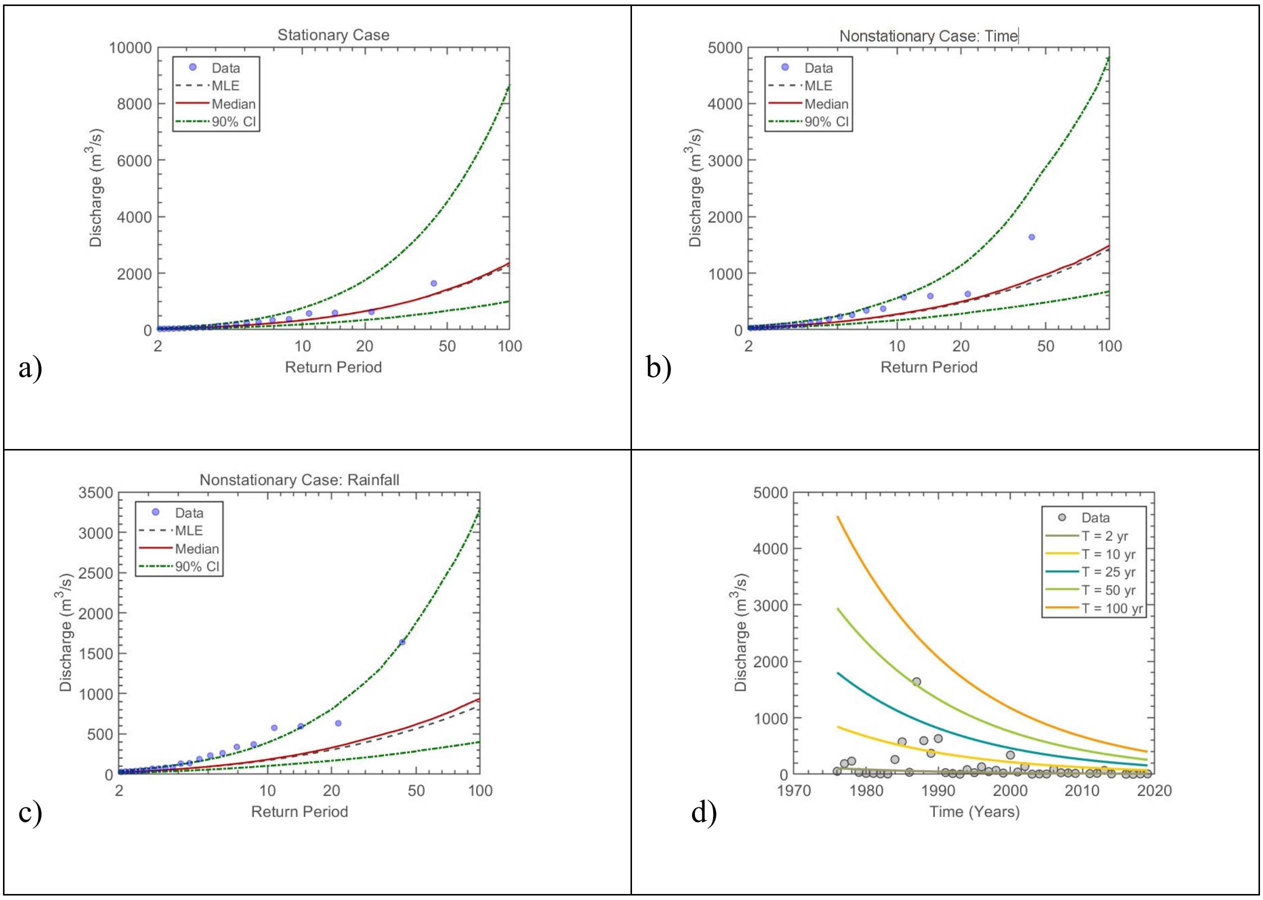

Figure 8.7 LP3 (a) stationary model, (b) non-stationary model considering time as a covariate, (c) non-stationary model considering rainfall as a covariate, and (d) effective return period as a function of time for Station:U3H005

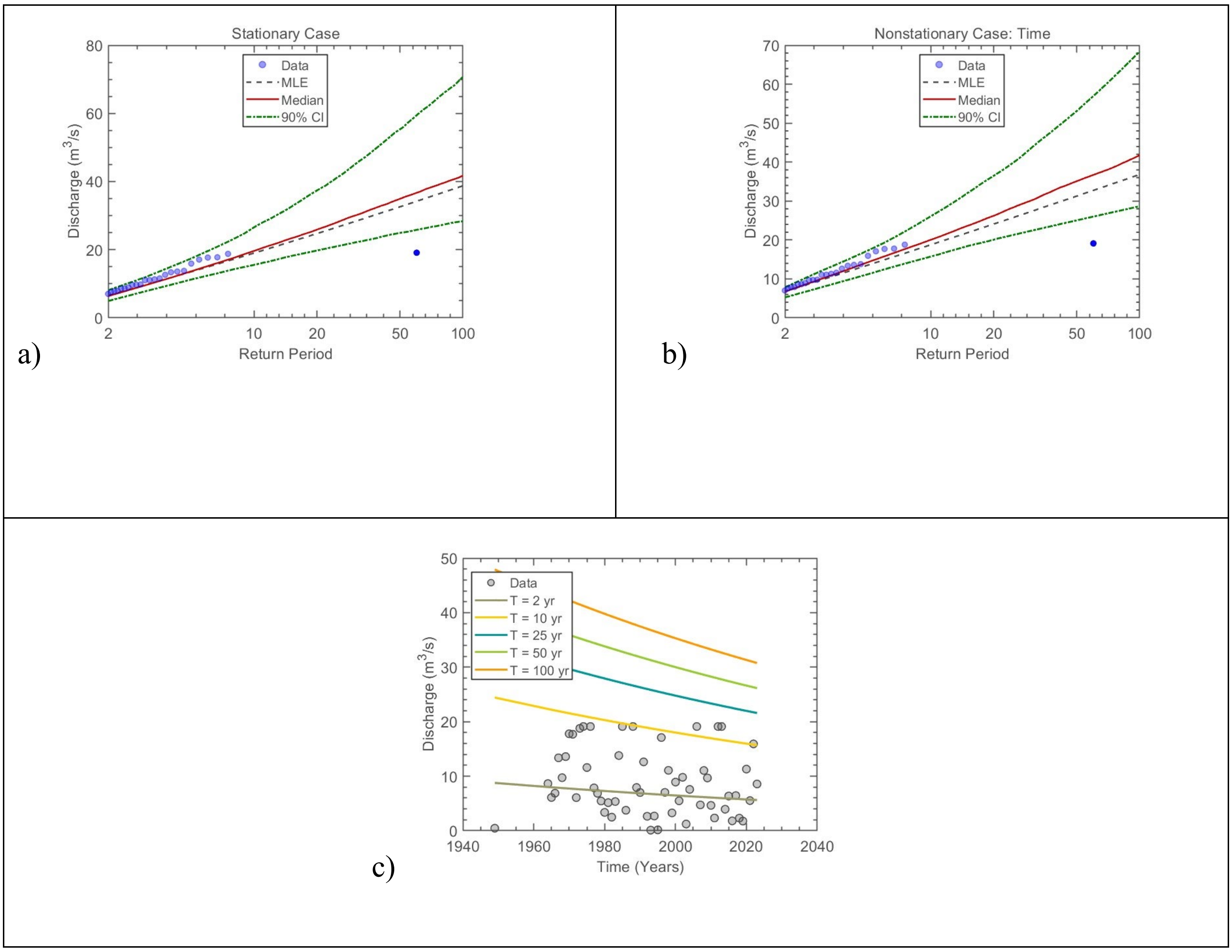

Figure 8.8 LP3 (a) stationary model, (b) non-stationary model considering time as a covariate, and (c) effective return period as a function of time for Station: U4H002

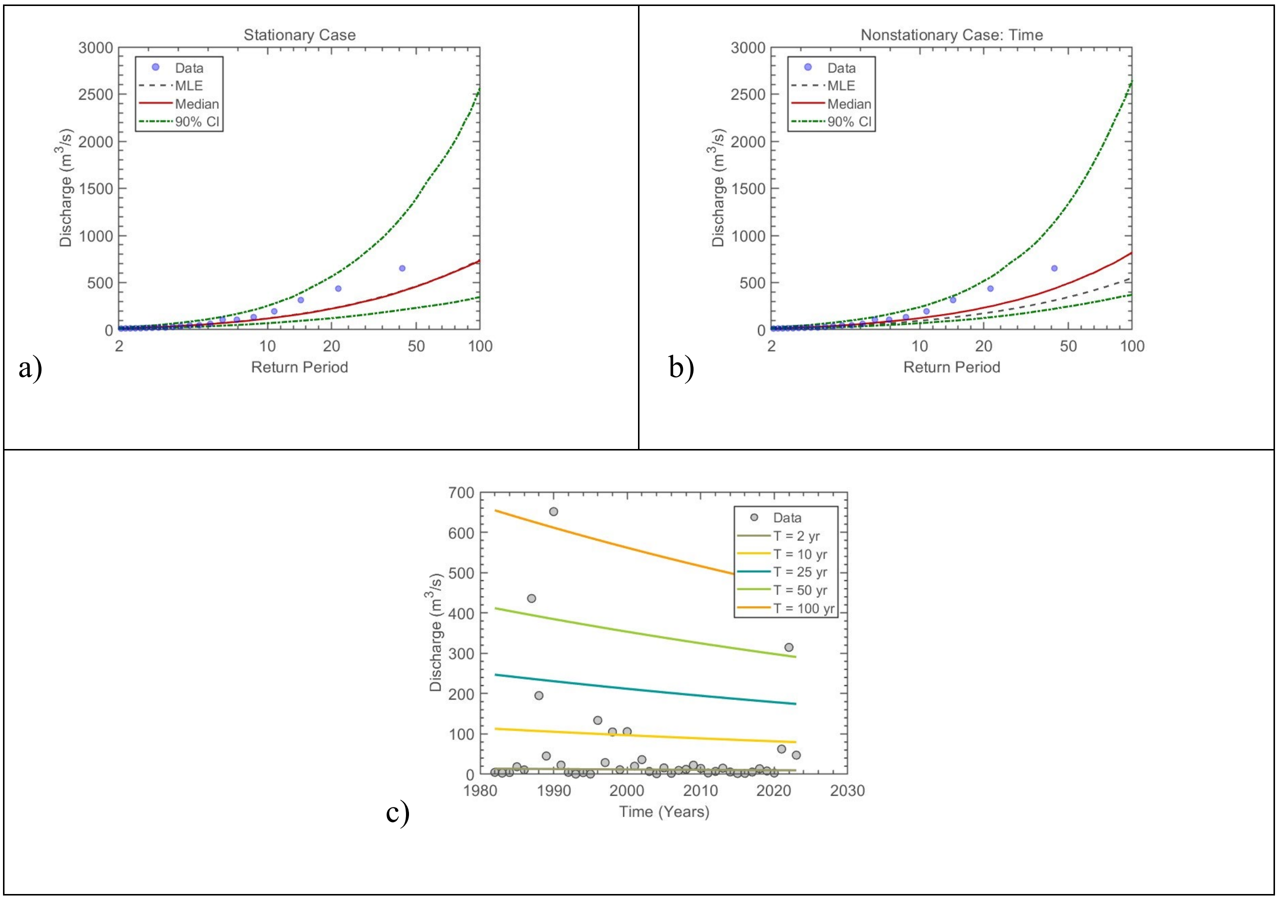

Figure 8.9 LP3 (a) stationary model, (b) non-stationary model considering time as a covariate, and (c) effective return period as a function of time for Station: U6H003

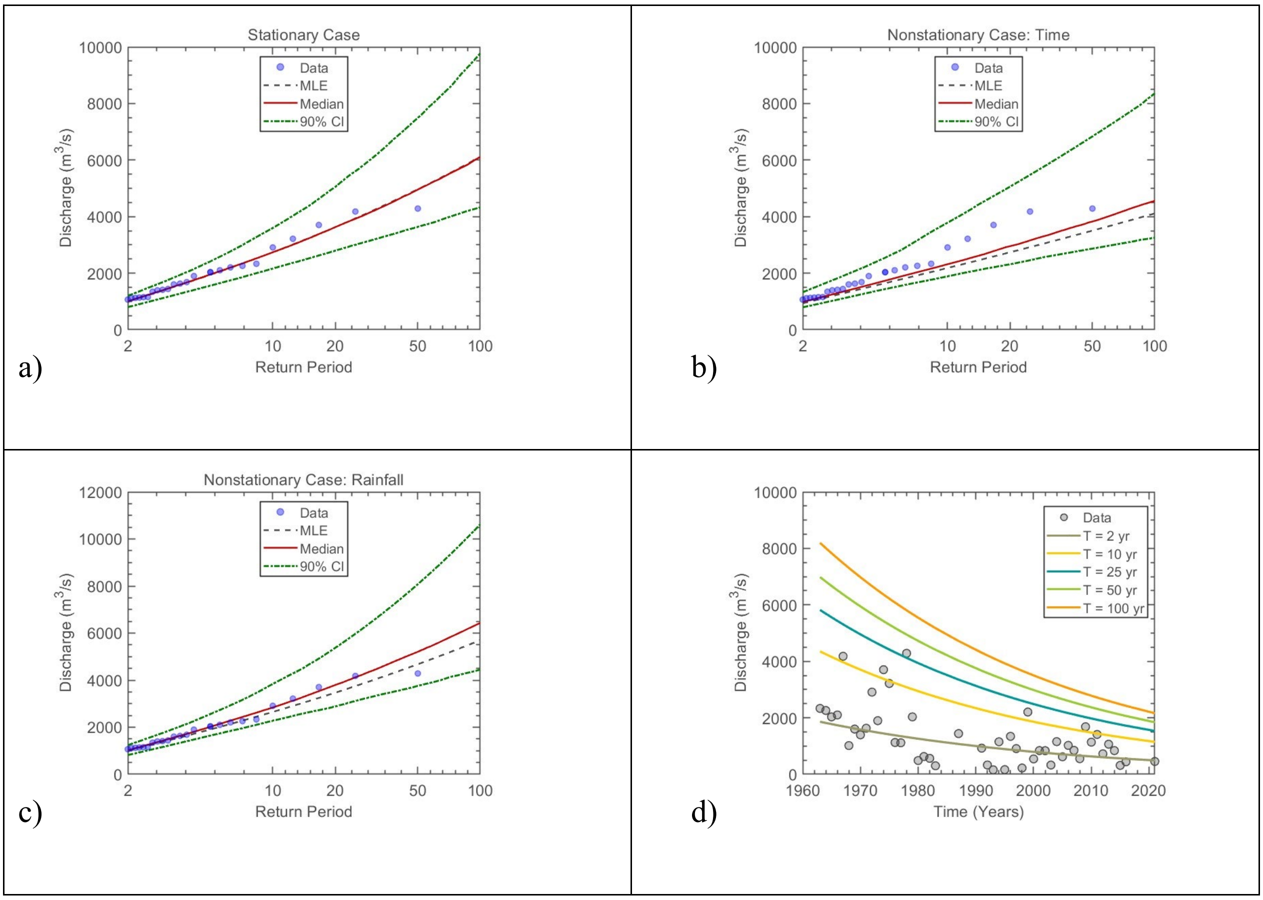

Figure 8.10 LP3 (a) stationary model, (b) non-stationary model considering time as a covariate, (c) non-stationary model considering rainfall as a covariate, and (d) effective return period as a function of time for Station:V5H002

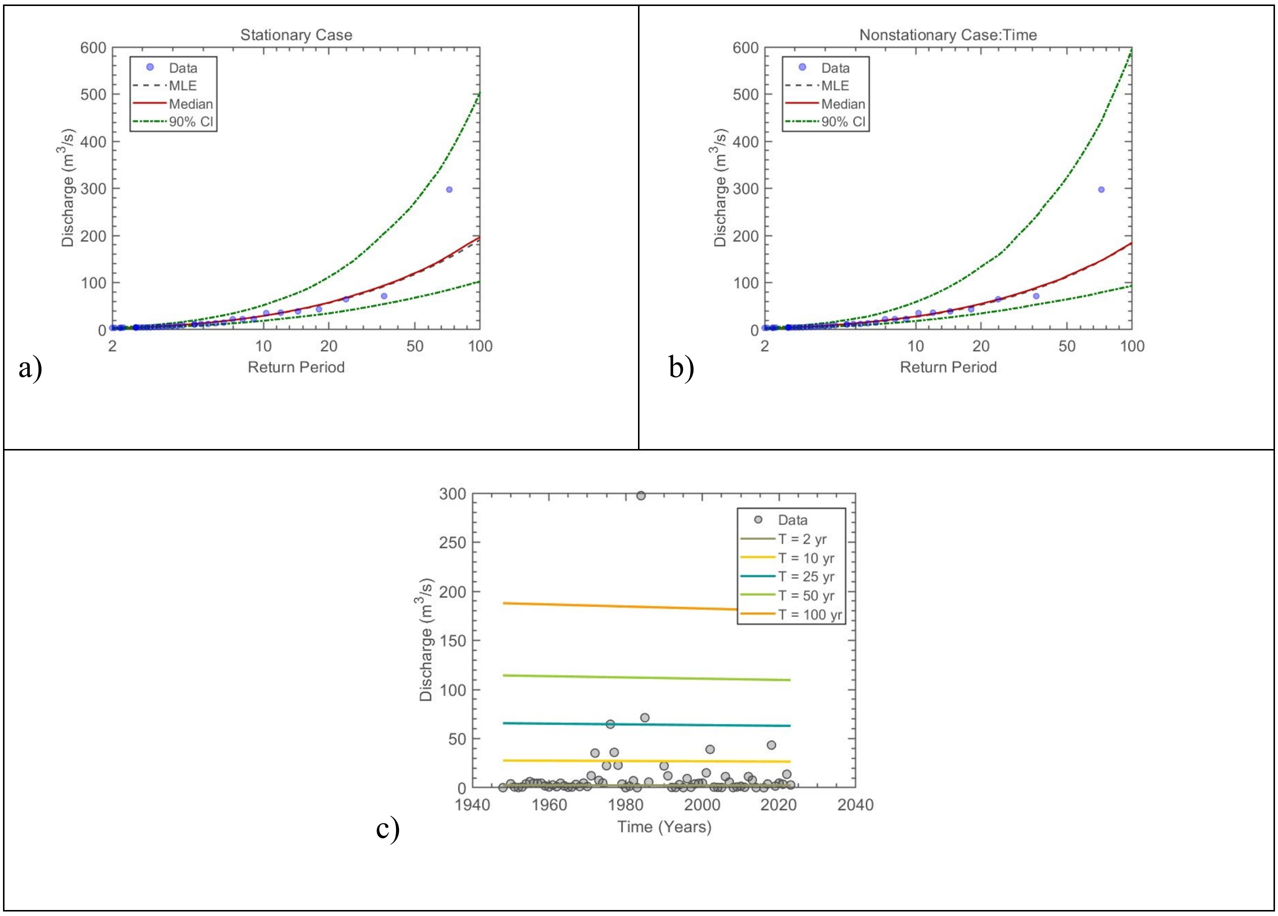

Figure 8.11 LP3 (a) stationary model, (b) non-stationary model considering time as a covariate, and (c) effective return period as a function of time for Station: W1H004

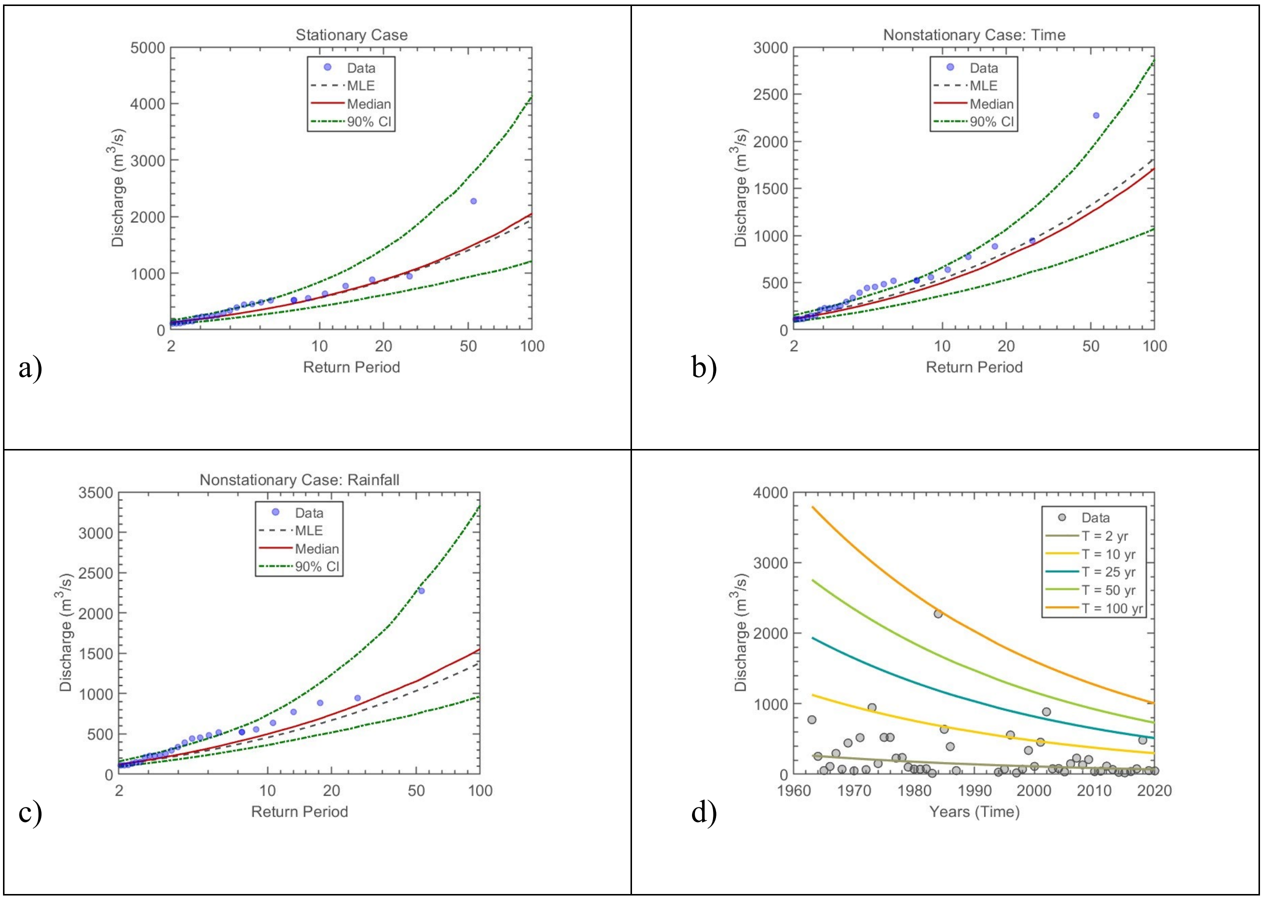

Figure 8.12 LP3 (a) stationary model, (b) non-stationary model considering time as a covariate, (c) non-stationary model considering rainfall as a covariate, and (d) effective return period as a function of time for Station:W1H009

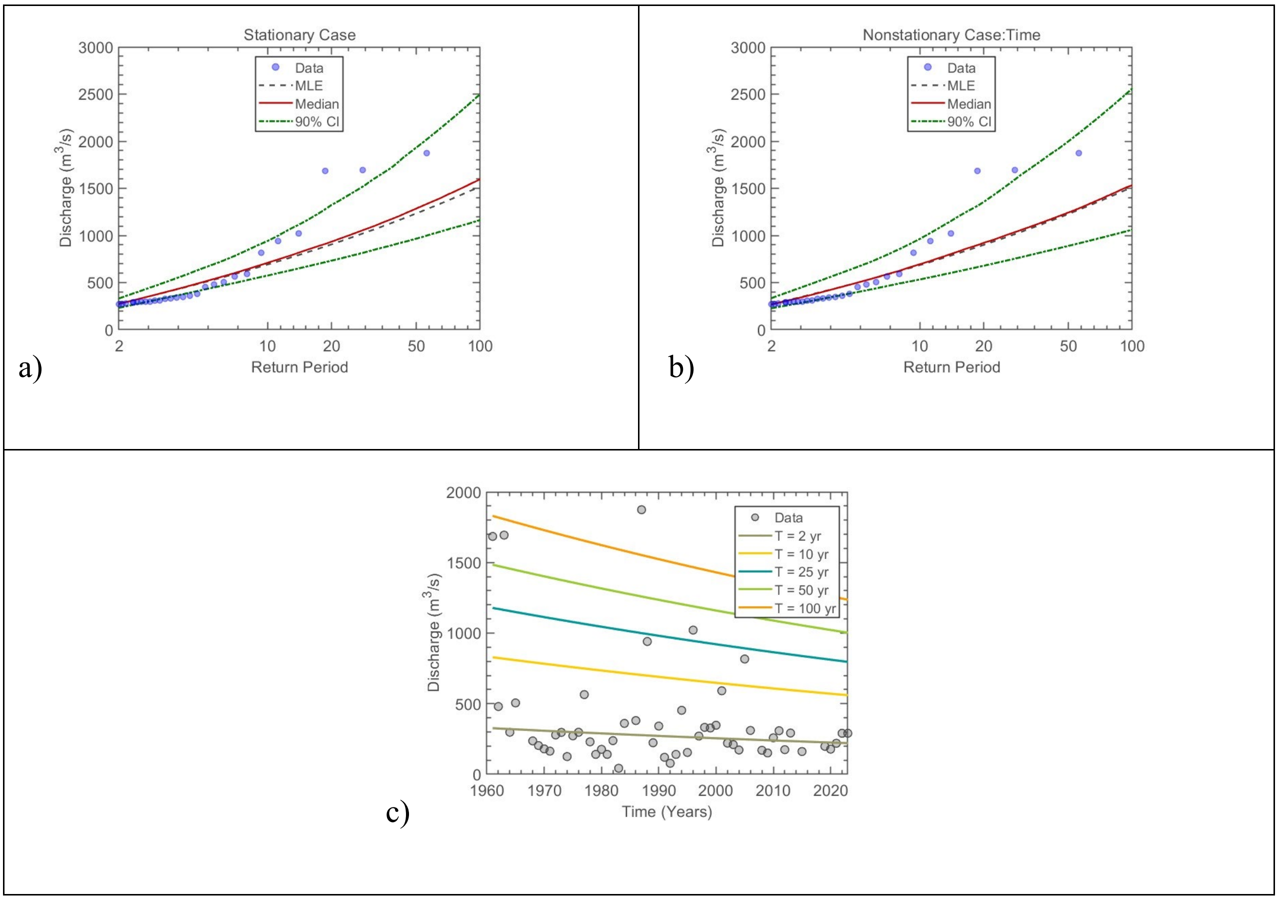

Figure 8.13 LP3 (a) stationary model, (b) non-stationary model considering time as a covariate, and (c) effective return period as a function of time for Station: W2H005

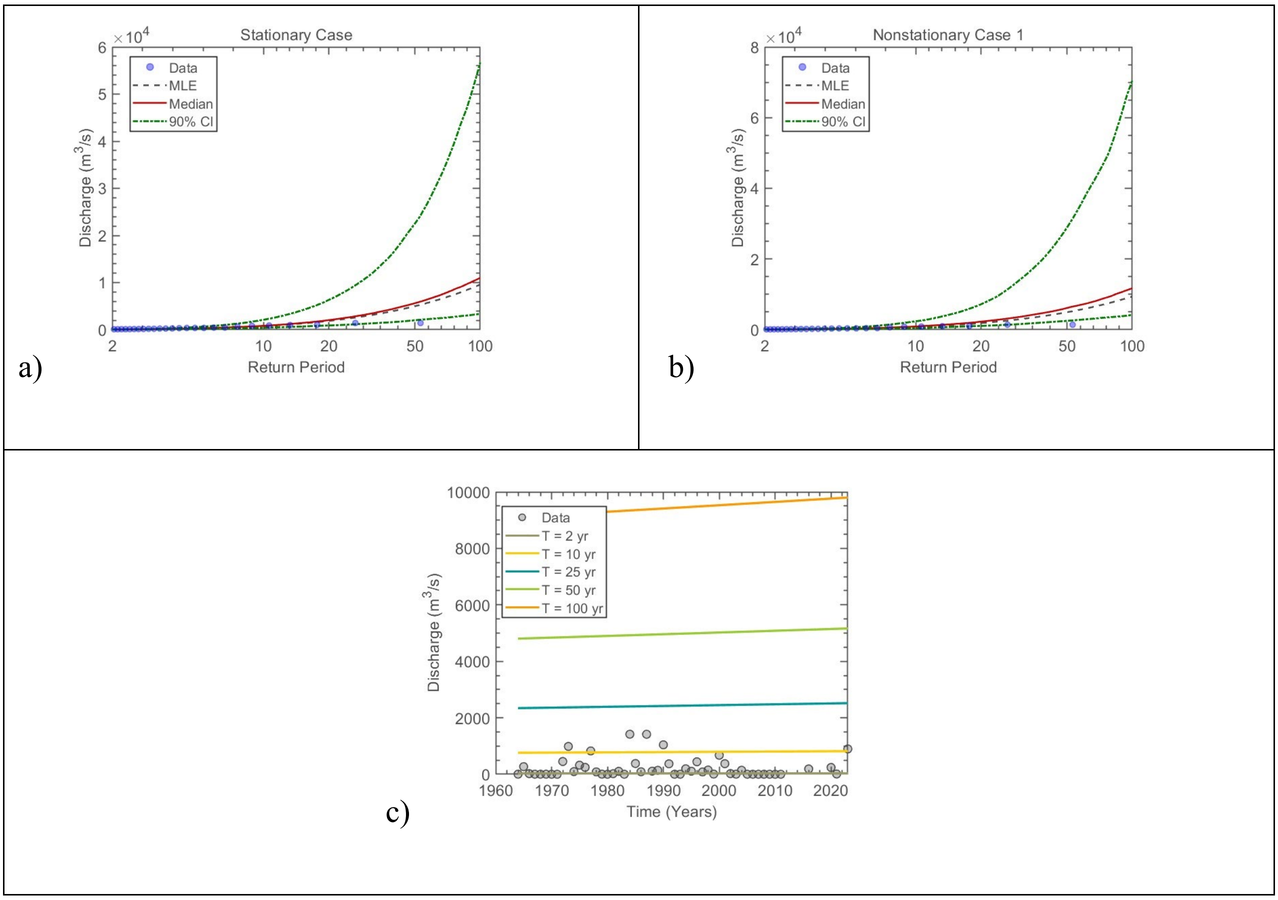

Figure 8.14 LP3 (a) stationary model, (b) non-stationary model considering time as a covariate, and (c) effective return period as a function of time for Station: W3H022

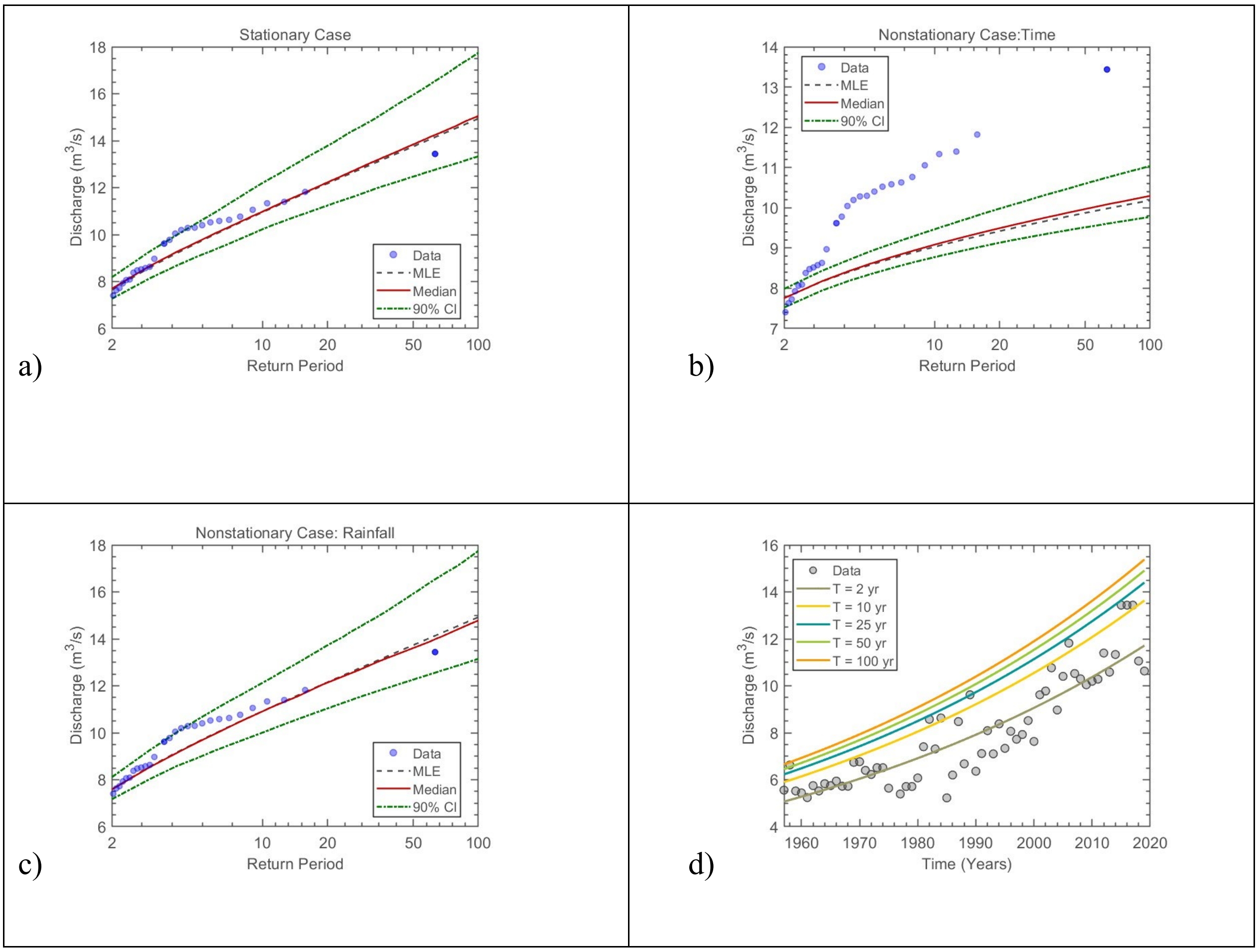

Figure 8.15 LP3 (a) stationary model, (b) non-stationary model considering time as a covariate, (c) non-stationary model considering rainfall as a covariate, and (d) effective return period as a function of time for Station:W4H012

Table 8.1 The LP3 statistical model performance criteria for all covariates

Station Number	**Stationary**			**Non-Stationary Time**			**Non-Stationary Rainfall**		
	AIC	**BIC**	**RMSE**	**AIC**	**BIC**	**RMSE**	**AIC**	**BIC**	**RMSE**
U3H001	107.06	**112.16***	19.71	**106.37***	113.12	**15.17***	107.83	114.59	20.74
U3H005	176.15	181.37	9782.30	168.51	175.45	404.24	**167.43***	**174.27***	**27.42***
V5H002	122.90	128.58	29.43	**108.19***	**115.76***	**11.72***	124.78	132.35	22.34
W1H009	168.59	174.44	32.37	164.98	172.80	**25.28***	**163.32***	**171.12***	641.57
W4H012	19.89	26.28	**22.27***	**-78.60***	**-70.09***	32.32	21.39	29.87	23.42

***Better performing model**